



2016

# Use Of Laboratory Geophysical And Geotechnical Investigation Methods To Characterize Gypsum Rich Soils

Raghava A. Bhamidipati

University of Kentucky, jones.kgp@gmail.com

Digital Object Identifier: <http://dx.doi.org/10.13023/ETD.2016.391>

**[Click here to let us know how access to this document benefits you.](#)**

---

## Recommended Citation

Bhamidipati, Raghava A., "Use Of Laboratory Geophysical And Geotechnical Investigation Methods To Characterize Gypsum Rich Soils" (2016). *Theses and Dissertations--Civil Engineering*. 45.  
[https://uknowledge.uky.edu/ce\\_etds/45](https://uknowledge.uky.edu/ce_etds/45)

This Doctoral Dissertation is brought to you for free and open access by the Civil Engineering at UKnowledge. It has been accepted for inclusion in Theses and Dissertations--Civil Engineering by an authorized administrator of UKnowledge. For more information, please contact [UKnowledge@lsv.uky.edu](mailto:UKnowledge@lsv.uky.edu).

**STUDENT AGREEMENT:**

I represent that my thesis or dissertation and abstract are my original work. Proper attribution has been given to all outside sources. I understand that I am solely responsible for obtaining any needed copyright permissions. I have obtained needed written permission statement(s) from the owner(s) of each third-party copyrighted matter to be included in my work, allowing electronic distribution (if such use is not permitted by the fair use doctrine) which will be submitted to UKnowledge as Additional File.

I hereby grant to The University of Kentucky and its agents the irrevocable, non-exclusive, and royalty-free license to archive and make accessible my work in whole or in part in all forms of media, now or hereafter known. I agree that the document mentioned above may be made available immediately for worldwide access unless an embargo applies.

I retain all other ownership rights to the copyright of my work. I also retain the right to use in future works (such as articles or books) all or part of my work. I understand that I am free to register the copyright to my work.

**REVIEW, APPROVAL AND ACCEPTANCE**

The document mentioned above has been reviewed and accepted by the student's advisor, on behalf of the advisory committee, and by the Director of Graduate Studies (DGS), on behalf of the program; we verify that this is the final, approved version of the student's thesis including all changes required by the advisory committee. The undersigned agree to abide by the statements above.

Raghava A. Bhamidipati, Student

Dr. Michael E. Kalinski, Major Professor

Dr. Yi-Tin Wang, Director of Graduate Studies

---

USE OF LABORATORY GEOPHYSICAL AND GEOTECHNICAL  
INVESTIGATION METHODS TO CHARACTERIZE GYPSUM RICH SOILS

---

DISSERTATION

---

A dissertation submitted in partial fulfillment of the requirements for the  
degree of Doctor of Philosophy in the College of Engineering at the  
University of Kentucky

By

Raghava A. Bhamidipati

Lexington, Kentucky

Director: Dr. Michael E. Kalinski, Ph.D., P.E, Professor of Civil Engineering

Lexington, Kentucky

Copyright © Raghava A. Bhamidipati 2016

## ABSTRACT OF DISSERTATION

### USE OF LABORATORY GEOPHYSICAL AND GEOTECHNICAL INVESTIGATION METHODS TO CHARACTERIZE GYPSUM RICH SOILS

Gypsum rich soils are found in many parts of the world, particularly in arid and semi-arid regions. Most gypsum occurs in the form of evaporites, which are minerals that precipitate out of water due to a high rate of evaporation and a high mineral concentration. Gypsum rich soils make good foundation material under dry conditions but pose major engineering hazards when exposed to water. Gypsum acts as a weak cementing material and has a moderate solubility of about 2.5 g/liter. The dissolution of gypsum causes the soils to undergo unpredictable collapse settlement leading to severe structural damages. The damages incur heavy financial losses every year.

The objective of this research was to use geophysical methods such as free-free resonant column testing and electrical resistivity testing to characterize gypsum rich soils based on the shear wave velocity and electrical resistivity values. The geophysical testing methods could provide quick, non-intrusive and cost-effective methodologies to screen sites known to contain gypsum deposits. Reconstituted specimens of ground gypsum and quartz sand were prepared in the laboratory with varying amounts of gypsum and tested. Additionally geotechnical tests such as direct shear strength tests and consolidation tests were conducted to estimate the shear strength parameters (drained friction angle and cohesion) and the collapse potential of the soils.

The effect of gypsum content on the geophysical and geotechnical parameters of soil was of particular interest. It was found that gypsum content had an influence on the shear wave velocity but had minimal effect on electrical resistivity. The collapsibility and friction angle of the soil increased with increase in gypsum. The information derived from the geophysical and geotechnical tests was used to develop statistical design equations and correlations to estimate gypsum content and soil collapse potential.

KEYWORDS: gypsum, shear wave velocity, electrical resistivity, collapse potential, friction angle

Raghava A. Bhamidipati

August 12, 2016

USE OF LABORATORY GEOPHYSICAL AND GEOTECHNICAL  
INVESTIGATION METHODS TO CHARACTERIZE GYPSUM RICH SOILS

By

Raghava A. Bhamidipati

Dr. Michael E. Kalinski

*Director of Dissertation*

Dr. Yi-Tin Wang

*Director of Graduate Studies*

August 12, 2016

## ACKNOWLEDGEMENTS

This doctoral research was only possible due the support of many different individuals during my years as a graduate student. Firstly, I like to acknowledge my supervisor Dr. Michael E. Kalinski for his guidance throughout my research. He has always been very supportive and believed in my work, also giving me an opportunity to pursue my ideas. Taking his graduate level courses such as ‘geotechnical aspects of landfill design’ and ‘groundwater and seepage’ was a positive experience during my initial days at the University of Kentucky. I very much admired his style of teaching and interaction with the students. I am also very grateful to him for appointing me as a teaching assistant for the undergraduate soil mechanics laboratory, a task which really served to enhance my skills in soil mechanics. I also thank Dr. L. Sebastian Bryson. He has been a great teacher of geotechnical engineering and has always been very helpful both inside and outside the laboratory. I thank Dr. Edward Woolery for serving on my doctoral committee and for introducing me to geophysics. Along with Dr. Kalinski, Dr. Woolery has sparked in me an interest in geophysics leading me to pursue the topic further for doctoral research. I also thank Dr. Gabe Dadi, Dr. Ole Wendroth and Dr. Kyle Perry for serving on my doctoral committee and providing valuable suggestions and inputs for my dissertation.

I sincerely thank Mr. Robert Day and Mr. Jim Norvell for providing technical assistance for my research on several occasions. Teaching the undergraduate soil mechanics lab would not have been possible without their constant help and presence. A special thanks to Ms. Shelia Williams and Ms. Suzy Wampler for being

very helpful through my stay as a graduate student and answering my countless queries. My fellow graduate students Alfred Susilo, Wisam Muttarshar, Ryan Ortiz, Yuxia Ji (Delbert) and Ehsan Jafari have all been highly supportive and friendly. I also thank Mr. Eric Green and Mr. Tony Fields at the Kentucky Transportation Center (KTC), for giving me an opportunity to work during the summers. In addition to keeping my payroll running, working with KTC has helped me travel to many different locations all across Kentucky, an experience that was thoroughly enriching. Lastly and most importantly, I thank my parents for everything that I am today. I dedicate this work to them.



## TABLE OF CONTENTS

ACKNOWLEDGEMENTS .....	iii
LIST OF TABLES .....	ix
LIST OF FIGURES .....	x
1. Introduction.....	1
1.1 Background .....	1
1.2 Gypsiferous soils and rocks.....	5
1.3 Gypsum soils in agriculture.....	9
1.4 Engineering and geological considerations of gypsum soils and rocks .....	11
1.4.1 Subsidence due to dissolution of gypsum .....	11
1.4.2 Volume change .....	18
1.4.3 Corrosion of Concrete .....	19
1.4.4 Formation of Ettringite and Thaumassite.....	19
1.4.5 Miscellaneous problems .....	21
1.5 Research objectives.....	22
1.6 Scope of research .....	23
2. Overview of Research Methods.....	26
2.1 Introduction .....	26
2.2 Geotechnical methods .....	27
2.2.1 Direct shear strength test (ASTM D3080).....	27
2.2.2 One-Dimensional Consolidation Test (ASTM D2435).....	30
2.2.3 Specific Gravity Test (ASTM D854) .....	33
2.3 Geophysical laboratory methods.....	34
2.3.1 Seismic tests .....	34
2.3.2 Electrical Resistivity Testing.....	40
2.4 Conclusion.....	43
3. Electrical Resistivity Testing of Reconstituted Gypsum Rich Soils.....	44
3.1 Background .....	44
3.2 Testing methodology.....	46

3.2.1 Two-electrode soil box method (ASTM G187) .....	47
3.2.2 Four-electrode soil box method (ASTM G57) .....	50
3.3 Relationship between resistivity and moisture content .....	52
3.4 Relationship between resistivity and gypsum content .....	56
3.5 Observations and inferences.....	60
3.6 Relationship between resistivity and porosity.....	63
3.7 Observations and inferences.....	66
3.8 Conclusion.....	68
4. Estimating the Stiffness of Gypsum Rich Soils using Free-free Resonant Column	
Testing.....	69
4.1 Introduction .....	69
4.2 Test Setup .....	70
4.3 Methodology .....	74
4.4 Testing procedure .....	76
4.4.1 Dry soil testing using cell pressure.....	76
4.4.2 Tests on moist soils.....	82
4.4.3 Testing moist soils using cell pressure .....	87
4.5 Results .....	89
4.6 Conclusion.....	93
5. Laboratory Geotechnical Tests on Reconstituted Gypsum Soils.....	97
5.1 Introduction .....	97
5.2 Direct shear strength test setup.....	99
5.3 Results and observations .....	102
5.4 Inferences .....	109
5.5 Specific gravity test (ASTM D854) .....	112
5.6 Grain size analysis (ASTM D422).....	114
5.7 Conclusion.....	116
6. Consolidation and Collapse Potential Testing of Gypsum Soils .....	118
6.1 Introduction .....	118
6.2. Collapsibility tests using Geocomp direct shear machine.....	122
6.2.1 Collapse potential with change in gypsum content .....	124

6.2.2 Vertical strain with change in water content .....	126
6.2.3 Vertical strain with dissolution and time .....	130
6.3 Collapsibility tests using consolidation load frame.....	134
6.3.1 Collapse potential with gypsum content.....	135
6.3.2 Collapse potential with time .....	138
6.4 Inferences and conclusion .....	139
7. Statistical analysis of test results and estimation of gypsum content .....	142
7.1 Introduction .....	142
7.2 Regression Analysis .....	143
7.3 Statistical analysis of shear wave velocity data .....	144
7.4 Statistical analysis of electrical resistivity data.....	153
7.5 Statistical analysis of direct shear strength test data .....	159
7.6 Statistical analysis of collapse potential data .....	162
7.7 Estimating gypsum content using geophysical methods.....	166
7.8 Conclusion.....	170
8. Conclusion .....	173
8.1 Summary .....	173
8.2 Observations and Inferences .....	174
8.3 Limitations of the research.....	177
8.4 Suggestions for future research.....	178
Appendix A. Using the Function Generator and Dynamic Signal Analyzer in the Free-Free Resonant Column testing.....	181
A.1 Function Generator and Amplifier .....	181
A.2 Dynamic Signal Analyzer and EDM software .....	183
Appendix B. Multiple variable regression Outputs .....	188
B.1 Shear wave velocity as a function of gypsum content, effective stress and degree of saturation .....	188
B.2 Shear wave velocity as a function of gypsum content and effective stress .....	189
B.3 Electrical resistivity as a function of gypsum content, volumetric water content and dry density .....	190
B.4 Vertical strain as a function of gypsum content and time .....	191
Appendix C. Alternative laboratory geophysical methods for soil investigation.....	192

C.1. Bender Element Testing .....	192
C.2. Four-probe resistivity cell.....	194
References.....	196
Vita.....	201

## LIST OF TABLES

Table 1.1 Major gypsum producing countries and their annual output	3
Table 1.2 Some physical properties of gypsum and anhydrite	8
Table 3.1 Pore-water resistivity of soils with different gypsum contents	59
Table 3.2. Gypsum soil samples and their Archie's Law parameters	67
Table 4.1. Gypsum-sand mixtures used in testing	70
Table 4.2. Polar moments of inertia of the components of a typical test specimen	75
Table 5.1 Specifications of the shear box for a typical specimen	100
Table 5.2 Measured specific gravity values of the soils	112
Table 5.3 Sieve sizes used in grain size analysis of quartz and gypsum	114
Table 6.1 Severity of collapse based on CP values	120
Table 6.2 Electrical conductivity and salinity of effluent water	133
Table 6.3 Dimensions of a test sample	134
Table 6.4 Loading steps in the collapse potential test	136
Table 7.1 Regression outputs of $v_s$ modeled as a function of GC, $\sigma'$ and $w$ %.	145
Table 7.2 Regression outputs of $v_s$ modeled as a function of GC and $\sigma'$	146
Table 7.3 Pore water resistivity of gypsum soil specimens	154
Table 7.4 Regression outputs of resistivity modeled as a function of GC%, vol. water content and dry density	156
Table 7.5 Regression outputs of strain modeled as a function of GC and time (mins.)	165
Table 7.6 Average rate of change of $v_s$ between 10%-35% degree of saturation	167

## LIST OF FIGURES

Figure 1.1 Satin spar gypsum	2
Figure 1.2 Distribution of gypsum rocks and soil across the world	4
Figure 1.3 Gypsiferous soil distribution in northeast Africa, southern Europe and southwest Asia.	4
Figure 1.4 SEM image of sulfate-rich soil in Texas	8
Figure 1.5 Pinkish gypsum strata outcropping west of Abu Dhabi, United Arab Emirates	9
Figure 1.6 Development of a sinkhole in limestone karst	14
Figure 1.7 Example of subsidence in gypsum karst in Ripon, England	16
Figure 1.8 A picture of the damaged St. Francis dam in Los Angeles, 1928	17
Figure 1.9 The Mosul dam in Iraq, built on a bed of gypsum rock	17
Figure 2.1 Geocomp Direct Shear Machine (Shear Trac II) used for this study	27
Figure 2.2 Mohr-Coulomb failure envelope	29
Figure 2.3 Soil response to shear loading	30
Figure 2.4 Consolidation cell test setup	31
Figure 2.5 A typical e-log $\sigma'$ curve	32
Figure 2.6 Specific gravity test setup	34
Figure 2.7 Block-diagram of a fixed-free resonant column test	37
Figure 2.8 Block diagram of a free-free resonant column test	39
Figure 2.9 Two-electrode soil box test	41
Figure 2.10. Four-electrode soil box test	42
Figure 3.1 Typical electrical resistivity range of earth materials	45
Figure 3.2 –electrode soil box test arrangement	48
Figure 3.3 Resistivity versus volumetric water content using 2-electrode resistivity box method	49
Figure 3.4. Wenner 4-electrode configuration	50
Figure 3.5. Four-electrode soil box test configuration	51
Figure 3.6. Four-electrode soil box test setup in lab	51

Figure 3.7 Resistivity versus vol. moisture content for 0% gypsum	53
Figure 3.8 Resistivity versus vol. moisture content for 10% gypsum	53
Figure 3.9 Resistivity versus vol. moisture content for 20% gypsum	54
Figure 3.10 Resistivity versus vol. moisture content for 40% gypsum	54
Figure 3.11 Resistivity versus vol. moisture content for 60% gypsum	55
Figure 3.12 Composite resistivity versus $\theta$ profiles using of the five soil samples	55
Figure 3.13 Resistivity plotted against gypsum content at $S = 100\%$	57
Figure 3.14 Resistivity plotted against gypsum content at $S = 100\%$	58
Figure 3.15. Measuring pore-water resistivity using Extech-400 conductivity meter	59
Figure 3.16. Comparison of pore water resistivity with soil resistivity	60
Figure 3.17. Resistivity versus porosity for 0% gypsum sand (saturated)	65
Figure 3.18 Resistivity versus porosity for 20% gypsum sand (saturated)	66
Figure 3.19 Resistivity versus porosity for 50% gypsum sand (saturated)	66
Figure 4.1 Soil M30 (sand with 30 % gypsum)	71
Figure 4.2 End caps of the specimen with their respective attachments	72
Figure 4.3. FFRC testing configuration	73
Figure 4.4 Lab test setup	73
Figure 4.5. Dynamic signal analyzer showing the a) Time-domain b) Frequency domain spectra	77
Figure 4.6 plot of $v_s$ versus $\sigma_o'$ for M0 (0 % gypsum), dry	78
Figure 4.7 plot of $v_s$ versus $\sigma_o'$ for M10 (10% gypsum), dry	78
Figure 4.8 plot of $v_s$ versus $\sigma_o'$ for M20 (20% gypsum), dry	79
Figure 4.9 plot of $v_s$ versus $\sigma_o'$ for M30 (30% gypsum), dry	79
Figure 4.10 plot of $v_s$ versus $\sigma_o'$ for M40 (40% gypsum), dry	80
Figure 4.11 plot of $v_s$ versus $\sigma_o'$ for M50 (50% gypsum), dry	80
Figure 4.12 plot of $v_s$ versus $\text{Log } \sigma_o'$ for M100 (100% gypsum), dry	81
Figure 4.13 Comprehensive plot showing the best-fit $v_s$ versus $\sigma_o'$ curves for all the soils	81

Figure 4.14 Assembly to saturate the soil specimens	82
Figure 4.15 Plot of $v_s$ versus degree of saturation (S) for M0 (0 % gypsum) at 58 kPa	84
Figure 4.16 Plot of $v_s$ versus degree of saturation (S) for M10 (10% gypsum) at 58 kPa	84
Figure 4.17 Plot of $v_s$ versus degree of saturation (S) for M20 (20% gypsum) at 58 kPa	85
Figure 4.18 Plot of $v_s$ versus degree of saturation (S) for M30 (30% gypsum) at 58 kPa	85
Figure 4.19 Plot of $v_s$ versus degree of saturation (S) for M40 (40% gypsum) at 58 kPa	86
Figure 4.20 Plot of $v_s$ versus degree of saturation (S) for M60 (60% gypsum) at 58 kPa	86
Figure 4.21 Comprehensive $v_s$ versus S plot for all soils tested at 58 Kpa	87
Figure 4.22 Plot of $v_s$ versus S for 0% gypsum specimen at two different confining stresses	88
Figure 4.23 Plot of $v_s$ versus S for 30% gypsum specimen at two different confining stresses	89
Figure 4.24 Comprehensive plot of $v_s$ versus $\sigma_o'$ curves for the dry soils tested without cell-pressure	92
Figure 4.25 Dismantled specimen with 60% gypsum content	93
Figure 4.26. Comparison of $v_s$ versus $\sigma_o'$ between Ottawa sand and 20% gypsum sand	94
Figure 5.1 Geocomp Shear Trac II direct shear machine used for this study	100
Figure 5.2 Typical <i>SHEAR</i> plot for $\tau$ versus $\Delta H$ .	102
Figure 5.3 Plot of $\tau_f$ versus $\sigma$ 10% gypsum (dry)	103
Figure 5.4 Plot of $\tau_f$ versus $\sigma$ for 20% gypsum (dry)	103
Figure 5.5 Plot of $\tau_f$ versus $\sigma$ for 30% gypsum (dry)	104
Figure 5.6 Plot of $\tau_f$ versus $\sigma$ for 60% gypsum (dry)	105



Figure 5.7 Plot of $\tau_f$ versus $\sigma$ for 10% gypsum (cemented)	105
Figure 5.8 Plot of $\tau_f$ versus $\sigma$ for 20% gypsum (cemented)	106
Figure 5.9 Plot of $\tau_f$ versus $\sigma$ for 40% gypsum (cemented)	106
Figure 5.10 Plot of $\tau_f$ versus $\sigma$ for 60% gypsum (cemented).	107
Figure 5.11 Friction angle versus gypsum content for the specimens tested	108
Figure 5.12 Cohesion versus gypsum content for the specimens tested	108
Figure 5.13 Void ratio versus normal stress	110
Figure 5.14 Specific gravity plotted against gypsum content	113
Figure 5.15 Gradation curves for quartz sand and gypsum	115
Figure 6.1. Plot showing the typical result from a CP test	120
Figure 6.2 Consolidation load frame	122
Figure 6.3 Consolidation versus time plot using SHEAR	124
Figure 6.4 Vertical strain versus gypsum content at 200 kPa	125
Figure 6.5 Collapse potential versus soil gypsum content at 200 kPa	125
Figure 6.6 strain versus initial w% for 20% gypsum at 200 kPa	127
Figure 6.7 strain versus initial w% for 30% gypsum at 200 kPa	127
Figure 6.8 strain versus initial w% for 50% gypsum at 200 kPa	128
Figure 6.9 strain versus initial w% for 70% gypsum at 200 kPa	128
Figure 6.10 strain versus initial w% plot for all soils tested	129
Figure 6.11 strain versus gypsum content at 200 kPa	130
Figure 6.12 test arrangement for gypsum dissolution	131
Figure 6.13. The Extech 400 conductivity meter in use	131
Figure 6.14 Vertical strain versus soaking time at 200 kPa	132
Figure 6.15 Collapse potential versus gypsum content (1 hour collapse step)	136
Figure 6.16 Collapse potential versus gypsum content (24 hours collapse step)	137
Figure 6.17 strain versus vertical load for all the soils tested	137
Figure 6.18 Creep deformation of three soil samples over 72 hours	138
Figure 6.20 Collapse potential test results of three soil samples	140
Figure 7.1 Comparison of predicted vs actual shear wave velocities	146

Figure 7.2 regression coefficient C vs gypsum content	147
Figure 7.3 Normalised shear wave velocity versus soil gypsum content	148
Figure 7.4. Normalised shear wave velocity versus gypsum content for specimens with less than 50% gypsum	149
Figure 7.5 Normalised shear wave velocity versus soil gypsum content ( tested without cell pressure)	150
Figure 7.6 Normalised shear wave velocity versus gypsum content for specimens containing up to 50% gypsum (tested without cell pressure)	151
Figure 7.7. Normalised shear wave velocity versus degree of saturation	152
Figure 7.8 Normalized electrical resistivity versus volumetric water content	154
Figure 7.9 Normalized electrical resistivity vs dry density	155
Figure 7.10 Normalized resistivity versus volumetric water content	157
Figure 7.11 Friction angle versus gypsum content of dry gypsum sand mixtures	160
Figure 7.12 Predicted versus actual shear strength values of dry gypsum sand specimens	161
Figure 7.13 Collapse potential versus gypsum content	163
Figure 7.14 Vertical strain versus moisture content	164
Figure 7.15 Collapse settlement of gypsum soils versus time	164
Figure 7.16. Shear-wave velocity versus degree of saturation for five gypsum soils	166
Figure 7.17. An approach to estimating gypsum content of soil using geophysical methods	169

## **1. Introduction**

### **1.1 Background**

Gypsum is a sulfate mineral made up of hydrated calcium sulfate,  $\text{CaSO}_4 \cdot 2\text{H}_2\text{O}$ . It is a very soft mineral with a Moh's scale hardness of 1.5-2.0 and can be easily scratched with a finger nail. Gypsum is naturally found in various forms such as alabastrine, crystalline and fibrous. It is known to occur in shades of white, pink, red, yellow and brown and is sometimes translucent. Alabastrine gypsum or alabaster is the most widely occurring form. It is composed of secondary crystals of gypsum which can measure up to a few centimeters. The fibrous variety, also known as satin spar, is the most easily recognizable form of gypsum. It is generally white in color and contains gypsum fibers (Figure 1.1). The crystalline form occurs in crystals of varying sizes. The larger crystals are usually about 1 m long and possess fan or blade-like shapes.

Gypsum consists of about 21% water by weight and 50% water by volume (Cooper & Calow, 1998). Heating of gypsum causes it to lose three-fourths of its water and form calcium-sulfate hemihydrate ( $(2\text{CaSO}_4 \cdot \text{H}_2\text{O})$ ) which is commonly known as plaster of Paris. This material is mixed with water to form a paste that dries and sets to form a hard material. Due to its abundance and physical and chemical properties, gypsum is widely used as a construction material in many parts of the world.

Anhydrite ( $\text{CaSO}_4$ ) is a mineral produced by the dehydration of primary gypsum. The dehydration process takes place when gypsum gets buried at great depths. Anhydrite is typically found at a depth of 100-500 m. It is harder and denser than gypsum. The Mohs scale hardness of Anhydrite is about 3.0 -3.5 and it can be scratched using a piece of

annealed copper. Anhydrite generally assumes a laminated or the chicken wire-mesh structure (Cooper & Calow, 1998).



Figure 1.1 Satin spar gypsum (Jones, 2013)

Gypsum is present throughout the world in many geological periods ranging from Cambrian to recent. Most gypsum deposits are found in arid and semi-arid regions of the world. Although it is difficult to establish the extent of soils containing gypsum in the world, Eswaran and Zi-Tong (1991) estimated 207 million hectares of soils with gypsum horizons (Herrero & Porta, 2000). Most gypsum occurs in the form of evaporites. Evaporites are defined as minerals that precipitate out of water due to high mineral concentrations or a high rate of evaporation. Gypsum is frequently associated with dolomite and salt deposits. Gypsum is also associated with limestone, mudstone and sandstone sequences deposited in lakes and basins. Some places such as the Persian Gulf States which are known to have recent coastal deposits, also contain gypsum.

Gypsum is present in substantial amounts all over the world, but only a fraction of it is exploited. In a broad sense, gypsum occurs predominantly in Southern and Eastern Europe, Middle Eastern countries, parts of North Africa and the United States. In the United States, gypsum is found in significant quantities in New Mexico, Texas, Arizona, California, Utah, Nevada, Wyoming and Utah. In some places such as Southern New Mexico near Alamogordo, gypsum is the main component of the soil. This region is well known for the White Sands National Monument, which is comprised of gypsum sand dunes.

Gypsum is extensively used as a fertilizer for crops and as a building material. The major gypsum producing countries and the annual production rate in thousand metric tons is shown in Table 1.1 (Founie, 2007). In the USA, commercially useful Gypsum deposits are found in a number of states. The distribution of gypsum soil and rock across the world is shown in Figure 1.2. Figure 1.3 shows the distribution of gypsiferous soils in North-East Africa, Southern Europe and South-west Asia.

Table 1.1 Major gypsum producing countries and their annual output (Founie, 2007)

<b>Country</b>	<b>Gypsum production (thousand metric tons)</b>
United States	21,000
Spain	13,200
Iran	13,000
Canada	9,500
Thailand	8,335
China	7,500
Mexico	7,000
Japan	5,950
France	4,800
Australia	4,000

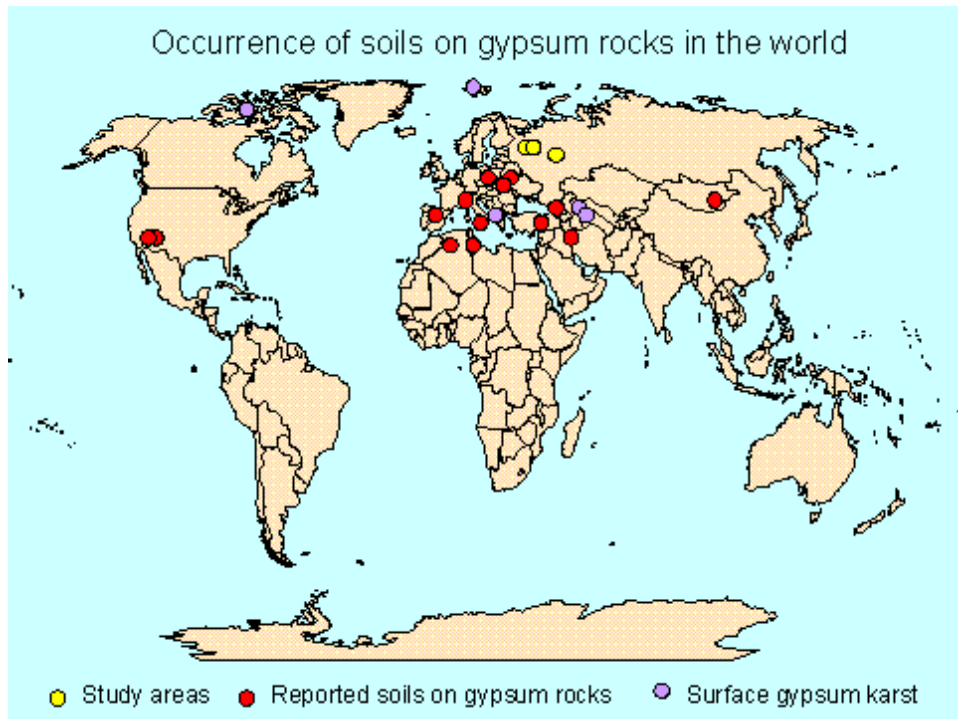


Figure 1.2 Distribution of gypsum rocks and soil across the world (Cooper & Calow, 1998)

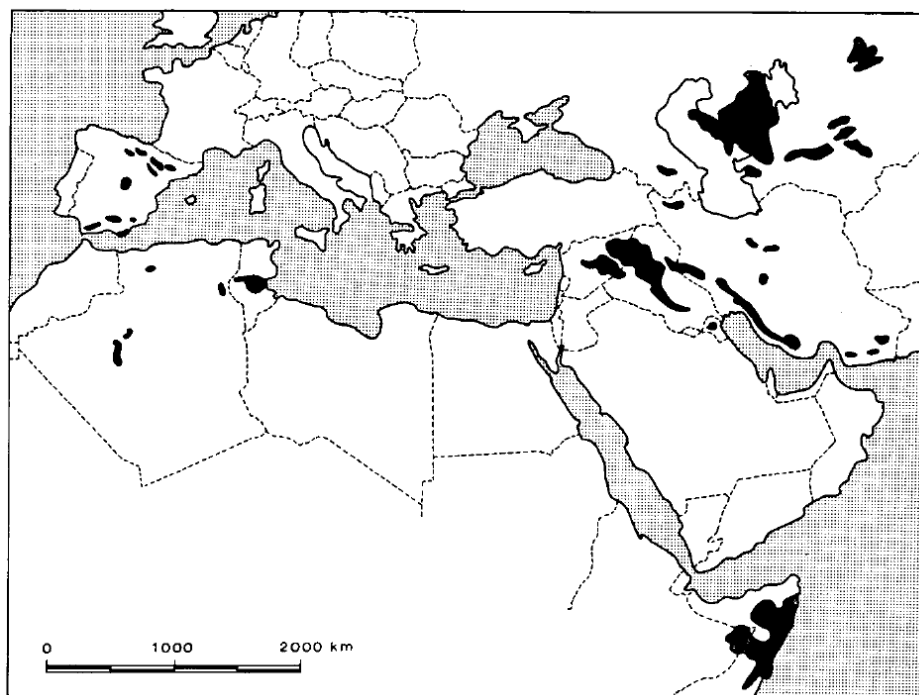


Figure 1.3 Gypsiferous soil distribution in northeast Africa, southern Europe and southwest Asia. (Alphen & Rios Romero, 1971)

## 1.2 Gypsiferous soils and rocks

Gypsum rich soils around the world are commonly described using the terms ‘gypsiferous’ or ‘gypseous’. According to Herrero and Porta (2000), the term ‘gypsiferous’ should be used for those soils which are ‘gypsum bearing’ or contain some gypsum, but where gypsum is not the dominant soil component. Likewise, ‘gypseous’ should be used to describe those soils which contain a significant amount of gypsum and the physical and chemical properties of the soil are attributed to the gypsum. However ‘gypsiferous’ is the more generic term which has commonly been used to define soils containing gypsum.

Gypsum is more common in soils of arid regions than soils of humid regions. Arid regions are generally known to have vast amounts of sand and the soil is mostly poorly graded. In these regions, extensive saline flats known as ‘sabkhas’ develop in low lying coastal areas or inland plains with shallow water tables. These plains are underlain by sand, silt or clay and contain salt. Gypsum along with dolomite, calcite, anhydrite, magnesite etc., is a common mineral in such regions (Bell, 2007). Due to scant precipitation there is very little downward leaching and salts such as gypsum precipitate in the pores surface deposits of soils. The gypsum sands are typically characterized by low strength and low density. The low bulk density is attributed to the low specific gravity of gypsum which is around 2.3. The sands are often cemented to a certain extent by salts like halite, calcite and gypsum. These types of soils pose a number of engineering problems related to permeability, deformability and low strength. The properties of gypsiferous soils depend upon several factors, such as the origin of the gypsum deposit, depth of the soil layer and effects of weathering and evapotranspiration. Gypsum is easily

transported by water. Based on the size of the gypsum crystals, gypsum soil layers can have a powdery or a sandy appearance (Alphen & Rios Romero, 1971).

A commonly occurring feature of soils in arid regions is the formation of crusts or cretes. This is brought about by the cementation of minerals which takes place when mineral salts get precipitated from groundwater. Temperature and humidity conditions also influence the formation of cretes. Calcium carbonate generally precipitates in this manner, when the concentration exceeds 60%, to form 'calcrete'. Cretes are hard material with hardness varying with depth. Gypcrete is a similar crustal formation which occurs in many places (Bell, 2007).

The soil survey staff, USA (1960), define 'gypsic horizon' as a layer secondarily enriched with calcium sulfate. Furthermore, it should have a thickness of at least 15 cm and a minimum of 5% or more gypsum than underlying layer. The product of the layer thickness in cm and gypsum percentage should be more than 150 (Alphen & Romero, 1971).

The geotechnical properties of gypsum rich soils are characterized by their Atterberg limits, grain size distribution, strength, cohesion, angle of internal friction, compressibility, collapsibility, hydraulic conductivity etc. These properties vary considerably from place to place and are largely dependent on the local soil mineralogy. Studies have shown that in most places, gypsic subsoils do not contain more than 15% clay (Alphen & Rios Romero, 1971). For a majority of gypsiferous soils, the drainage varies from moderate to rapid. The drainage may however decrease if a gypsum incrustated layer is present. A great variation in hydraulic conductivity has been observed, the values ranging from  $5.7E-05$  cm/s to about  $9.3E-03$  cm/s. Hydraulic conductivity is an important



soil property that quantifies the rate of flow of water through soil. Based on the data collected from soils in Azerbaijan, Spain and Syria it was found that usually there is more than 35% gypsum present in subsurface layers and 5% or less gypsum is present in the surface layers. Exceptions can however occur if the surface profiles are highly eroded.

Gypsum rocks consist of gypsum or anhydrite, usually in one or more forms of alabaster. Anhydrite rock is stronger than gypsum rock. Papadopolpos et al. (1994) investigated the influence of crystal size on the geotechnical properties of gypsum. They conducted point load tests and unconfined compression tests on samples of gypsum rocks and found that fine grained material like alabaster had the highest strength, followed by large crystals such as selenite (Bell, 2007). Medium sized crystals showed the lowest strength. The presence of impurities in the calcium sulfate rock also showed to increase the strength of the rock by decreasing the size of the crystals (Skinner, 1959; Bell, 2007). Bell (1994) conducted tensile strength tests on samples of anhydrite and gypsum and found that anhydrite had a very high tensile strength whereas gypsum had a medium to high tensile strength. The solubility of gypsum varies from 2.1-2.6 g/l which is relatively high among minerals. This often leads to the formation of caverns and sinkholes in thick beds of gypsum. A summary of the different physical properties of gypsum and anhydrite rocks is shown in Table 1.2. Alabaster is quite often wrongly identified as limestone, which causes a number of engineering hazards (Cooper & Calow, 1998). Figure 1.4 shows scanning electron microscope image of sulfate rich soil in Texas (Harris et al., 2004). Figure 1.5 shows gypsum strata outcropping in United Arab Emirates.

Table 1.2 Some physical properties of gypsum and anhydrite

Property	Gypsum	Anhydrite
Specific gravity, $G_s$	2.3-2.4	2.9-3.0
Moh's scale hardness	1.5-2.0	3.0-3.5
color	White, grey, pink, yellowish-brown	Grey and pale bluish grey
Porosity, $n$	Around 4-7 %	Around 3%
Unconfined compressive strength, $S_u$	24-35 MPa	66-123 Mpa
Tensile strength	2.2-3.6 Mpa	7.1-8.2 Mpa
Schmidt hammer hardness (ASTM D5873)	8-23	35-37
Young's modulus, $E$	15-36 GPa	56-87 GPa

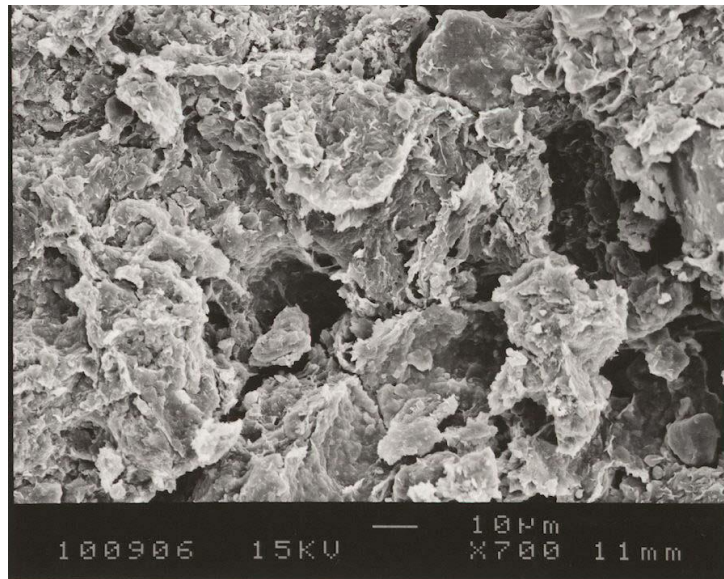


Figure 1.4 SEM image of sulfate-rich soil in Texas (Harris et al., 2004)



Figure 1.5 Pinkish gypsum strata outcropping west of Abu Dhabi, United Arab Emirates (Shahid & Abdelfattah, 2009).

### **1.3 Gypsum soils in agriculture**

The presence of a limited amount of gypsum in soils in arid regions is helpful for plant growth. Gypsum prevents alkali formation in soils when the land is irrigated under conditions of inadequate drainage. At low concentrations gypsum is known to be a soil amending agent. Gypsum provides calcium and sulfur nutrients to soil and has been used as a fertilizer. It sometimes reduces the toxicity of soils by moving into the soil and displacing ions like  $Al^{3+}$ . It is also known to improve the structure of the soil in the capacity of a binding or a flocculating agent where it holds the soil particles together. This in turn addresses problems such as erosion and water logging and enables root penetration through soils.

Higher concentrations of gypsum may however prove detrimental to plant growth. Alphen and Romero (1971) reported that soils with more than 25% gypsum content caused

reduction in crop yields. At higher concentrations, cementation takes place between the soil and gypsum, the layer becomes hard and makes it difficult for roots to grow deeper into the soil. Nevertheless, if the gypsum layer around the root zone is granular or powdery, then it does not pose a major problem. Excess gypsum in soil may also interfere with the nutrient intake of plants, specifically, potassium and magnesium by decreasing amount of exchangeable cations from the soil. Nitrogen and phosphate content in soils is also low in gypsiferous surface layers. This leads to a decrease in crop-yield and calls for the use of fertilizers. Alfalfa, wheat, maize, barley, cotton and apricots are examples of some of the major crops that are cultivated on gypsiferous soils.

The depth of gypsic layer is of special concern as it affects the water-holding capacity of the soil. Studies have shown that, if a gypsic layer occurs at a depth of less than 60 cm, then it reduces the water holding capacity in the root zone (Alphen & Rios Romero, 1971). When the gypsum layers is present at a depth of more than 1 meter, then the soil is deemed safe for irrigation and cultivation. Gypsum soils pose the risk of moderate to high ground subsidence due to the dissolution of gypsum and increased percolation. This aspect is a major engineering hazard while constructing irrigational facilities such as canals in gypsiferous soils and will be discussed in detail in subsequent sections of this dissertation.

## 1.4 Engineering and geological considerations of gypsum soils and rocks

Gypsum is a widespread mineral occurring in numerous places around the world. The unique physical and chemical properties of gypsum lend some peculiar properties to gypsiferous soils which are often very problematic. Gypsum rich soils are known to cause a number of engineering and geological hazards which incur heavy financial losses every year. Some of the most significant engineering hazards of gypsiferous soils are discussed in the following section.

### 1.4.1 Subsidence due to dissolution of gypsum

Geological disasters due to gypsum dissolution and subsidence have been occurring throughout the world and are well documented. Many places like northern England, Lithuania, Germany, France, Turkey, Russia, the Shanxi and Hebei coalfields of China and the United States, have suffered significant losses due to subsidence caused by gypsum (Cooper & Calow, 1998).

The rapid dissolution of gypsum poses a major threat to any development at sites with gypsiferous soils. The solubility of gypsum is about 2100 mg/l which is considerably higher than the solubility of limestone (400 mg/l). It gets easily dissolved even in non-saline waters. The reaction is very rapid as long as the groundwater is not saturated with gypsum. In spite of seemingly high solubility among minerals, gypsum belongs to the class of sparingly soluble salts and as such solutions attain equilibrium concentrations at low gypsum concentrations. Upon dissolution in water gypsum liberates  $\text{Ca}^{2+}$  and  $\text{SO}_4^{2-}$  ions according to the equation:



Flowing water often dissolves more gypsum than still water because the former is usually unsaturated with respect to calcium sulfate and saturation does not occur. Moderate river action can annually dissolve up to 1 meter of gypsum and the dissolution rates are similar even underground (Bell, 2007). The volume change characteristics of soil due to dissolution of calcium sulphate (anhydrite) were studied by Al-Amoudi and Abduljauwad (1994) using conventional and modified odometer tests. From their experiments it was found that in the conventional odometer test, the void ratio of calcium sulphate samples showed a marked increase when permeated with distilled water and brine. This high difference in void ratios shows the compressibility of the soil matrix (Azam, 2000).

Alabastrine, the most commonly occurring form of gypsum is often misidentified as limestone at many sites which leads to serious engineering problems. Alabastrine is weaker than limestone and consequently has lesser arching potential. This causes gypsum karsts to collapse more easily than limestone. These features cause rapid development and expansion of underground caves and cavities. Sinkholes and caves develop readily in thick beds of gypsum which are responsible for massive cracking and subsidence on the ground surface at many places. Sometimes extended periods of rainfall in certain places have caused collapse of soils in a very short span of time (Bell, 2007). In some places where gypsum beds reach the ground surface, the dissolution of gypsum can be detected by the appearance of funnel shaped sinkholes formed by the collapse of the overlying seams. The rate of subsidence depends on factors such as the dimensions of the cavity and the physical and geotechnical properties of the overlying deposit.

The presence of joints and cracks in rocks and aquifers propagate the development of underground caves in many gypsum outcrops. Gypsum karst is often characterized by collapse passages. The dissolution of gypsum is higher at the joints and large cavities grow and develop in these zones. As these cavities increase in size, they tend to become unstable and collapse. Once the roof of the cavity collapses, the cavity starts moving upwards towards the surface. In this process brecciated rock columns are left below, which are termed as breccia pipes or collapse columns. The nature of the rock overlying gypsum determines the size of the collapsed area. If competent rock is present, the breccias pipes and collapse areas are usually 10-30 m in diameter, whereas in the presence of soft mudstone, the collapse areas are about 3-5 m in diameter. The amount of gypsum removed and the bulking factor of the collapsed material are the factors which govern the depth of the holes. In Lithuania and Germany the holes are about 10-20 m deep. When the dissolution of gypsum takes place on the top surface rock, which is in contact with an overlying water bearing deposit, the outcome is not necessarily a cave system. This kind of dissolution has been observed extensively near Zaragoza in Spain. In such cases, most of the dissolution takes place at the interface of the overlying deposit and gypsum. If thick unconsolidated fluvial deposits are resting on top of gypsum, they might fail and collapse into the cavities inside the rock (Cooper & Calow, 1998). Ripon in Yorkshire, England, is one of the places worst affected by subsidence caused by gypsum dissolution (Figure 1.7). Several major collapses have occurred here within a century and more such collapses are likely. It is not unusual to find collapse hollows of 80 m diameter and 30 m depth in this region. Figure 1.6 shows the development of a subsidence sinkhole underneath a soil

deposit on limestone karst, following a pattern similar to that of sinkholes in gypsum karst.

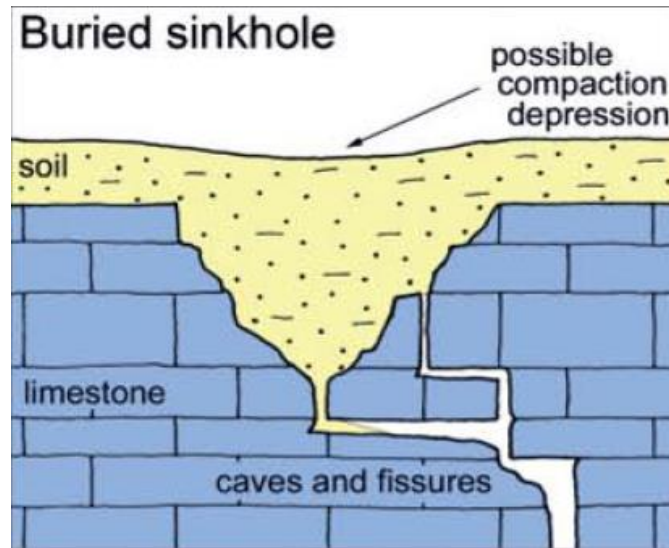


Figure 1.6 Development of a sinkhole in limestone karst (Waltham, 2008)

Development of sinkholes and caverns in beds of gypsum located below reservoirs is a major engineering hazard. They grow and develop very rapidly within a few years. Considerable amounts of leakage and water losses occur at some reservoir beds due to the presence of limestone and gypsum karst. Tremendous amounts of seepage forces keep getting built up due to the dissolution of gypsum in reservoir beds which leads to leakage. The unwarranted subsidence and leakage from caves have caused many dams and reservoirs to be abandoned and rendered useless. As of 1998, 24 dam sites have been known to be seriously impacted by gypsum dissolution, 14 of which are within the United States. The catastrophic failure of the St. Francis Dam in Los Angeles, California, in 1928 is one the biggest engineering disasters to have occurred, resulting in the death of 400 people (Yilmaz, 2001) (Figure 1.8). The failure was brought about by the dissolution of gypsum cement and conglomerate in the left abutment of the dam. The Mosul Dam in



Iraq, constructed on the Tigris River, is facing a serious threat of a disastrous failure because of the constant dissolution and erosion of gypsum rock lying underneath the dam (Fig. 1.9). The failure of the dam could lead to severe losses of lives and infrastructure on the downstream side (Martin, 2016).

When dry gypsum rich soil comes in contact with water it becomes collapsible and hazardous, posing major engineering challenges for geotechnical engineers. Structures like irrigation canals and dams have been reported to show major deformations and failures. Many such instances have been reported in Iraq. Additionally, phenomenon such as uneven settlement and excessive deformation of structures result when gypsiferous soils are exposed to water. This occurs primarily due to the dissolution of salts and loss of cementing material present leading to an increase in void ratio. This leads to a loss of stability in the soil and grains re-arrange into a denser configuration. The soil in such cases is known to be 'collapsible' and is characterized by its 'collapse potential'. Numerous researchers have tried to study collapsible soils in the Middle East, especially in Iraq, and assess the collapse potential of the soils. Many structures constructed on gypsum soils in Iraq were reported to having developed crack patterns and uneven deformations when the supporting soil came in contact with water (Al-Saoudi et al., 2013). Several researchers have conducted extensive investigations on the engineering and collapse properties of gypsum soils in different regions of Iraq. Jennings and Knight (1975) gave the most widely used criteria for establishing the hazard level of collapsible soils based on collapse potential. In Ebro Valley, Spain, hydraulic structures built on loess deposits had undergone major deformations even when the soil contained just 3.5%

gypsum. Alphen and Romero (1971) stated that any gypsiferous soil containing more than 2% gypsum is unsuitable for foundations.



Figure 1.7 Example of subsidence in gypsum karst in Ripon, England (Cooper & Calow, 1998)



Figure 1.8 A picture of the damaged St. Francis dam in Los Angeles, 1928 (Rogers, 2007)



Figure 1.9 The Mosul dam in Iraq, built on a bed of gypsum rock (Hanchey, 2016)

### 1.4.2 Volume change

The relative stability of gypsum and anhydrite is dependent on temperature, moisture and pressure conditions. Considerable volume change occurs when anhydrite is hydrated to form gypsum. Gypsification of anhydrite causes catastrophic problems like heaving of floors in tunnels and uplift in dams. Other significant damage includes cracking of concrete and other structural members, uplifting of slabs and heave of pavements. Likewise the dehydration of gypsum results in volume shrinkage and fracture due to settlement. The distress in soil increases considerably if the moisture content keeps varying from time to time (Bell, 2007). Azam (2003) investigated the influence of calcium sulfate mineralogy on swelling and consolidation of soils in eastern Saudi Arabia. Gypsum is usually stable at temperatures below 38 ° C and anhydrite is stable above 58 ° C and pressure of around 100 kPa. The hydration of anhydrite into gypsum is shown in the reaction below:



Conventional or modified oedometer tests have been used to study the heaving characteristics of calcium sulfate rich soils. Some studies have found that it expands about one-fourth as much as clay. Anhydrite ( $\text{CaSO}_4$ ) transforms to bassanite ( $\text{CaSO}_4 \cdot 0.5\text{H}_2\text{O}$ ) before getting converted to gypsum ( $\text{CaSO}_4 \cdot 2\text{H}_2\text{O}$ ). The volume changes, which are about 30-60 % generate pressures in the range of 2 to 69 MPa. Humidity and local weather condition play a major role in this transformation. Gypsification does not depend much on temperature but it takes place at a relative humidity of 100 % (Azam, 2003). Likewise the dehydration of gypsum can bring about a decrease in volume of up to 38.5%. In both

the hydration and dehydration reaction, the crystalline structures of gypsum and anhydrite are affected.

The process of hydration does not require much time. It could occur at any depth depending upon the location of anhydrite. If anhydrite occurs at shallow depths, the hydration process is gradual and is followed by gypsum removal from the solution. On the other hand, if it occurs at greater depths, anhydrite gets confined and the process of hydration leads to a gradual buildup of a huge amount of pressure which sometimes gets liberated in a sudden and a rapid fashion (Bell, 2007).

### **1.4.3 Corrosion of Concrete**

The presence of gypsum in soil often causes corrosion of concrete, when the sulphate component of gypsum reacts with the free quicklime (CaO) in concrete. What takes place is an acid-base reaction whose rate depends on the texture of the soil and the relative strengths of the acid ( $\text{SO}_4^{2-}$ ) and base (CaO) groups. The reaction is responsible for weakening of concrete. Corrosion of concrete is a common phenomenon in areas experiencing frequent wetting and drying cycles as well as those areas where the gypsum content in soil is more than 1%. In arid regions where the concentration of evaporates is high, other sulphates in the soil such as magnesium sulphate and sodium sulphate also result in the weakening of concrete due to corrosion (Muckel, 2004).

### **1.4.4 Formation of Ettringite and Thaumasite**

In the presence of Sulphate rich compounds like gypsum in soil, the occurrence of calcium oxide and a high pH favour the formation of ettringite and thaumasite, two expansive minerals. This usually happens after the application of calcium-based stabilizers to soil. Calcium based stabilizers are added to soils to improve or modify some

of their engineering properties like strength and workability, but the formation of ettringite and thaumasite may cause serious distresses and damage to structures due to heaving. The scale of damage and distress caused by the formation of ettringite and thaumasite depend upon the strength of the soil and the spatial distribution of ettringite or thaumasite in the soil matrix. Often the cost of reconstruction is much higher than the original cost of soil stabilization (Little & Nair, 2009).

Ettringite is a hydrous calcium alumino-sulphate mineral ( $\text{Ca}_6[\text{Al}(\text{OH})_6]_2(\text{SO}_4)_3 \cdot 26\text{H}_2\text{O}$ ) which gets precipitated in highly alkaline conditions in soils and concrete with abundant amounts of sulphate. Thaumasite is a complex compound often found in the presence of ettringite. It is essentially a calcium carbonate silicate sulphate hydrate mineral represented by the structural formula ( $\text{Ca}_6[\text{Si}(\text{OH})_6]_2(\text{CO}_3)_2(\text{SO}_4)_2 \cdot 24\text{H}_2\text{O}$ ). Thaumasite is assumed to be formed due to the alteration of ettringite in the presence of carbonates and silica

Ettringite formation is followed by expansion in volume of the soil matrix the magnitude dictated by the amount of fines in the soil. The presence of water aids the reaction by partly dissolving the gypsum and thus making more sulphate ions available for reaction. The Molar volume of ettringite formed by external hydration is 1.37 times the volume of the original reactants. Unlike ettringite, the final volume of thaumasite is only about 0.45 times the volume of the initially present ettringite. Thaumasite formation reduces the overall size of the matrix and results in degradation or crumbling of the matrix, a fact that has been verified from field observations.

#### **1.4.5 Miscellaneous problems**

Sand dunes are common geological features of many arid regions where the sand originates from weathering of rocks or from unconsolidated deposits. One of the biggest problems associated with gypsum dunes in arid regions is the destabilization of inactive dunes by construction activity. The disturbed dune tends to get re-activated, starts to migrate and buries the structures which come in its way. Another major problem is the contamination of groundwater from waste water disposal facilities built on gypsum dunes. The absence of fines in the soil leaves no scope for filtration of the effluent before it touches the ground water table. The roughly uniform size of the sand grains provides a good medium for the easy movement of effluent into the groundwater. Since gypsum gets dissolved without much difficulty, it adds more to the problem of groundwater contamination (Mulvey, 1992). Gypsum aquifers yield very hard water and their rate of pollutant transmission is comparable to that of rivers (Alphen & Rios Romero, 1971). Soils in arid regions, especially the sabkha soils often have little strength. In some cases, normally and slightly overconsolidated clays are found to be very sensitive. The low strength of the soils is due to the concentrated solutions of salts such as gypsum.

## **1.5 Research objectives**

The various challenges and problems associated with gypsum soils have been briefly described in this chapter. The engineering hazards posed by gypsum soils affect not only lives of people but also cause heavy economic losses every year. The geological hazards of gypsum have been known to people for quite some time and most of the major engineering disasters have been documented. As countries keep growing and economies keep developing, there is a need to develop the residential, energy and infrastructural sectors accordingly. Over a period of time one simply cannot avoid construction in a region because of the presence of gypsum. In lieu of these aspects, there is an increasing demand for establishing quicker cost-effective techniques to identify and assess sites with gypsum rich soils and predict any potential hazards that might be associated with the engineering properties of the soil. Researchers have studied collapsible soils for several years and many empirical relationships have been proposed by them. Often these relationships are specific to a region and may not always work in other regions of the world. Geotechnical investigations, which include both in-situ and laboratory based tests are generally laborious and time consuming. Also the information derived from these are much localized. They do not give a broad picture of the site conditions, spread out across an area.

Geophysical testing methods may address these issues by offering quick and inexpensive ground investigation techniques and being non-destructive and non-intrusive in nature. These methods primarily include seismic testing, electrical resistivity testing, micro-gravity and electromagnetic methods. While some of these tests are better suited for in-situ investigations, some tests can be conducted both on a laboratory scale as well



as a field scale. These days, geophysical methods are playing an increasingly important role in civil engineering. The methods may also be specifically applied to characterize and assess proposed construction sites in regions known to contain gypsum soils. The results from these tests may be interpreted directly or indirectly using correlations. Geophysical parameters are usually proxies to geotechnical spatial variables such as density, moisture, void ratio etc., and accordingly offer valuable site information at a bulk level.

The main objective of this research was to use some geophysical testing methods to investigate gypsum soils and develop certain criteria to estimate the geotechnical parameters that are responsible for causing collapse settlement. These include factors such as gypsum content, moisture content, density etc. The effect of gypsum content on soil behavior was of particular interest.

### **1.6 Scope of research**

This research aims at using a combination of laboratory scale geophysical and geotechnical tests to study gypsum rich soils and characterize them based on the test results. The geophysical methods serve as non-intrusive soil testing methods which are both rapid and inexpensive. The study also proposes to see if the information derived from the geophysical tests could be correlated to known geotechnical parameters of soil. The soils used for this research are reconstituted gypsum and quartz sand mixtures mixed at different proportions. Research work was broadly divided into three phases, the first involving laboratory geophysical testing and the second phase consisting of geotechnical tests. The geophysical tests included free-free resonant column (FFRC) testing to study gypsum soils based on shear wave velocity data and electrical resistivity testing to study

gypsum soils based on resistivity trends. Geotechnical tests consisted of direct shear strength tests and consolidation tests, which were used to measure the shear strength properties and collapse potential respectively. Specific gravity tests and grain size analysis was performed in addition to these tests.

Lastly, statistical analysis of these results was conducted and some predictive equations were developed to estimate the soil parameters that influence the collapse settlement of gypsum soils. A flowchart was developed to predict gypsum content of the soils in field using geophysical techniques. Each chapter in the dissertation is a presentation of the different phases of research:

- Chapter 2: Overview of research methods: Discusses the main research methodologies that were considered for the research which include both geophysical and geotechnical laboratory methods.
- Chapter 3: Electrical resistivity testing : This chapter describes the different tests conducted to study the variation in resistivity with change in moisture content, gypsum content and dry density, along with the results and interpretations.
- Chapter 4: Free-free resonant column testing: Describes the variation in stiffness of gypsiferous soils with change in gypsum content, effective stress and moisture content. This is followed with a discussion of the results and interpretation.
- Chapter 5: Laboratory geotechnical testing: This chapter details the examinations of some geotechnical properties of the sandy gypsum soils considered for the research. These include the friction angle, cohesion, specific gravity and grain size distribution of the soils.

- Chapter 6: Consolidation and collapse potential testing: This chapter contains a discussion of laboratory investigations conducted to look into the collapse settlement problem associated with gypsum soils. Collapsibility of gypsum sands is studied under varying conditions of gypsum content, moisture content and time of loading.
- Chapter 7. Statistical analysis of test results and estimation of gypsum content: Single and multiple variable regression analysis is performed on the test data to develop relationships between the soil variables. Additionally, a methodology is proposed to estimate the gypsum content of the soils in the field, based on the geophysical test results.
- Chapter 8. Conclusion: Summarizes the main outcomes of the research and its uses. It also describes some limitations of the research and offers suggestions for future research.

## 2. Overview of Research Methods

### 2.1 Introduction

A set of geophysical and geotechnical tests were used to conduct this research. This chapter gives a brief overview of the common testing methods that could be used for studying gypsiferous soils in a laboratory setup. The geotechnical properties of the soils that could be investigated were the friction angle ( $\phi$ ), cohesion, specific gravity, dry density, collapsibility and hydraulic conductivity, whereas electrical resistivity and stiffness (quantified by shear wave velocity,  $v_s$ ) were the geophysical properties. The soils chosen for research were reconstituted soils made up of quartz sand and ground gypsum. Soil samples were prepared by mixing quartz sand and gypsum in different proportions of gypsum by weight, with gypsum content ranging from 0- 100%. Throughout the research ‘gypsum content’ represents the percentage of the mass of gypsum with respect to the mass of the soil sample.

$$\text{Gypsum Content (GC)} = (\text{mass of gypsum} / \text{mass of soil}) \times 100\% \quad (2.1)$$

Some tests required the use of samples made up entirely of quartz sand or gypsum. The use of reconstituted gypsum sand mixtures in the absence of actual field samples could be justified by the fact that gypsiferous soils in arid regions are primarily sandy soils.

## 2.2 Geotechnical methods

### 2.2.1 Direct shear strength test (ASTM D3080)

Direct shear strength testing (ASTM D3080) is used to estimate the shear strength properties of granular soils under drained conditions. It is one of the oldest and widely used tests in soil mechanics. In this test, a soil specimen is typically placed in a square or a circular box, which is divided horizontally into two halves. The two halves can be moved relative to each other under the presence of a vertical (normal) load, thus causing shearing of the soil specimen. The split between the two halves of the box defines the failure plane of the soil specimen. The box is placed in a shear machine which is operated either manually or using a computer (Fig 2.1).

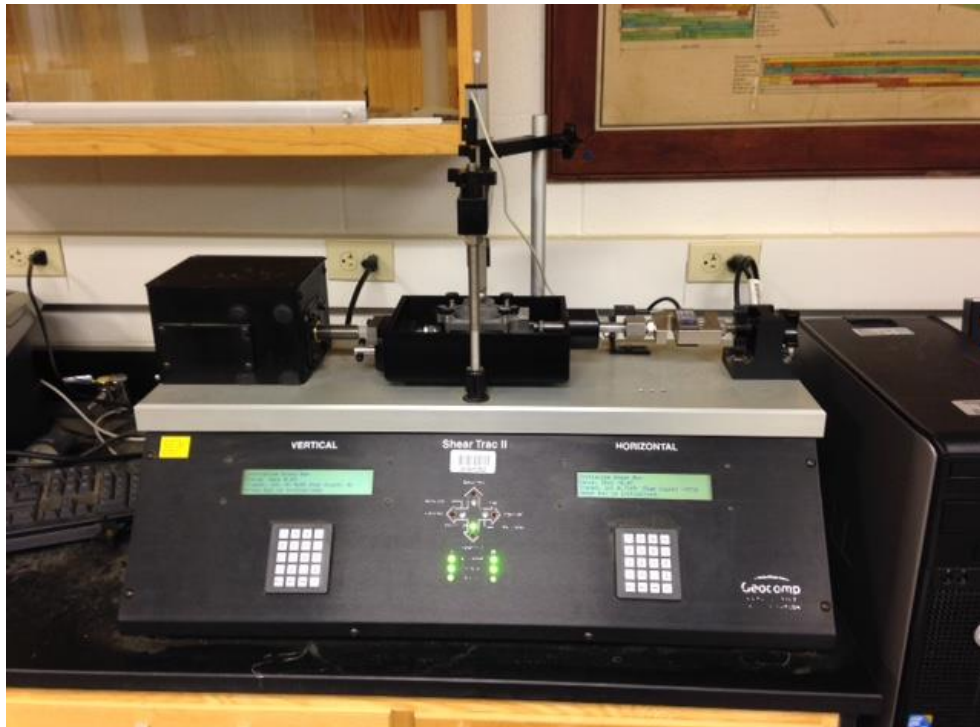


Figure 2.1 Geocomp Direct Shear Machine (Shear Trac II) used for this study

For this research we use a circular metal shear box with a diameter of 2.5 in. and depth of 1 in. Normal and horizontal loads were applied pneumatically and measured using load cells, so the maximum allowable load depends on the capacity of the load cell. There are two possible ways in which the specimen can be tested, namely, a stress-controlled test and a strain-controlled test. In the former test, horizontal force is incrementally applied to the specimen in discrete amounts until failure is reached. This test is more representative of field conditions. In a strain-controlled test, the specimen is displaced horizontally at a constant displacement rate until the specimen fails. The constant displacement is applied on one half of the specimen using a motor. This test has the advantage of measuring both the peak shear strength and the ultimate residual shear strength of the soil. In both tests, the horizontal and vertical displacements of the specimen are measured using analog or digital gauges.

The test can be used to measure both drained cohesion ( $c$ ) and friction angle ( $\phi$ ) of a coarse-grained soil specimen. This is done by performing the test using different normal loads and plotting the Mohr-Coulomb failure envelope for the particular soil type (Fig 2.2). The slope of the failure envelope is the tangent of the friction angle and the y-intercept represents the cohesion. The shear stress and normal stress are related using the expression:

$$\tau_f = c + \sigma \tan \phi \quad (2.2)$$

Where  $\tau_f$  is the shear stress at failure and  $\sigma$  is the normal stress acting on the soil.

The shear force versus displacement plots for soils show two unique responses (Fig. 2.3). Dense soils show a distinct peak shear strength, which is identified as the failure shear strength, followed by an ultimate residual or critical state shear strength. In the case

of loose soils, the shear strength increases with displacement till a constant or critical state shear strength is reached. This value is identified as the failure shear stress and is typically defined at a threshold strain (e.g. 5%). The test is discussed in detail in Chapter 5.

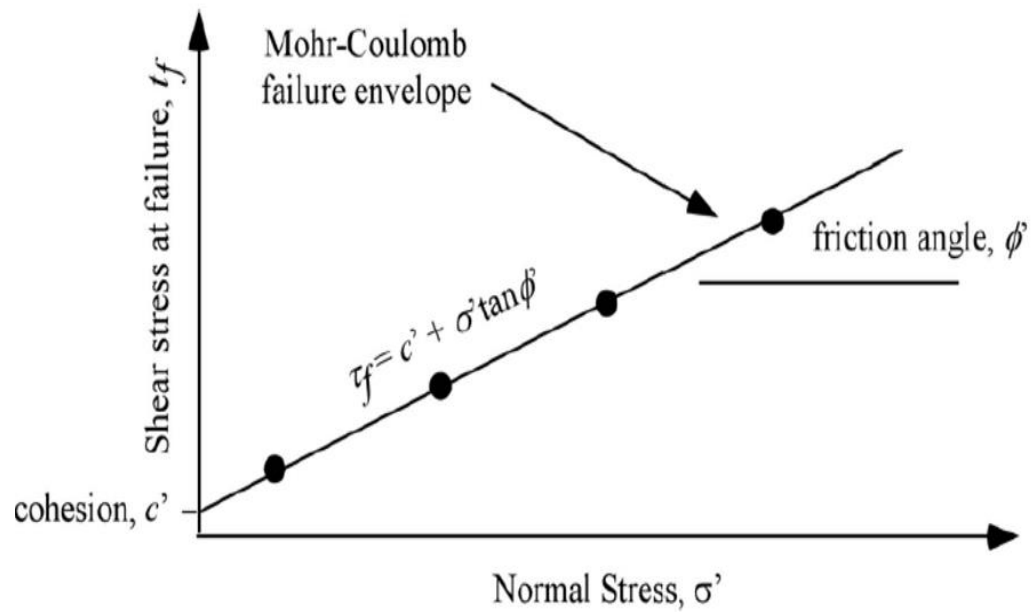


Figure 2.2 Mohr-Coulomb failure envelope (Kalinski, 2006)

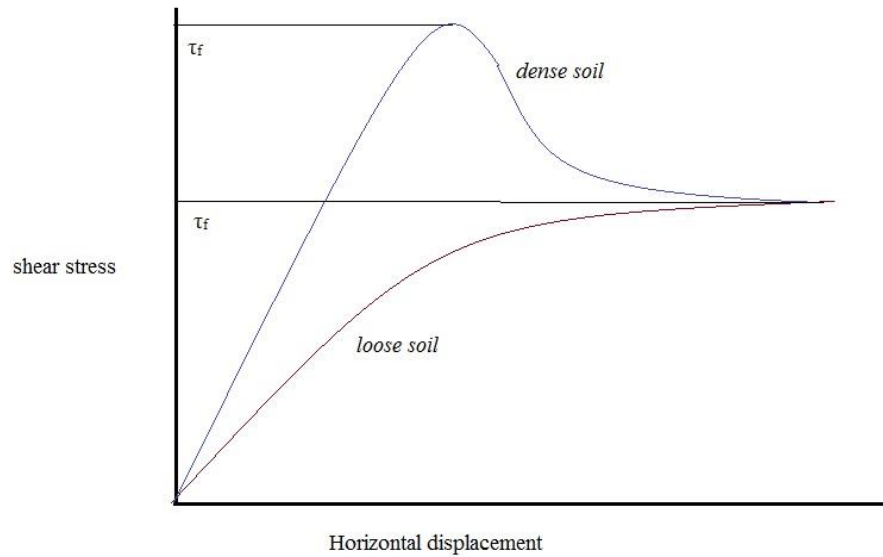


Figure 2.3 Soil response to shear loading

### 2.2.2 One-Dimensional Consolidation Test (ASTM D2435)

Consolidation is the time dependent dissipation of excess pore water pressure in a fine grained soil specimen subjected to loading and the accompanying decrease in void ratio. This test is used to measure the long-term settlement and the change in void ratio of a fine grained specimen. Both the time rate of settlement and the ultimate settlement of soil can be estimated using this test and the field behavior of the soil can be predicted. The excess pore water pressure generated in the soil due to increase in effective stress is slowly dissipated, and the rate of dissipation is governed by the hydraulic conductivity of the soil.

The test is performed using a consolidation load frame or an oedometer on a cohesive circular soil specimen that is typically 2.5 in. in diameter and approximately 0.75 inches in thickness. The specimen is placed in a metal ring and is placed between two porous stones, one at the top and one at the bottom (Fig 2.4). The whole arrangement is



placed in a consolidation load cell which is filled with water to keep the specimen saturated. The specimen is loaded using a lever arm on which calibrated loads are placed. An analog or digital displacement gauge is used to measure the vertical deformation of the specimen under the applied load. Each load is placed for 24 hours and deformation measurements are taken at various time intervals. These data are used to plot the time-settlement plots which are used to evaluate the initial, primary and secondary stages of consolidation under an applied normal load. The parameters derived from this plot are the coefficient of vertical consolidation,  $c_v$ , and the settlement corresponding to 100% degree of primary consolidation,  $d_{100}$ .

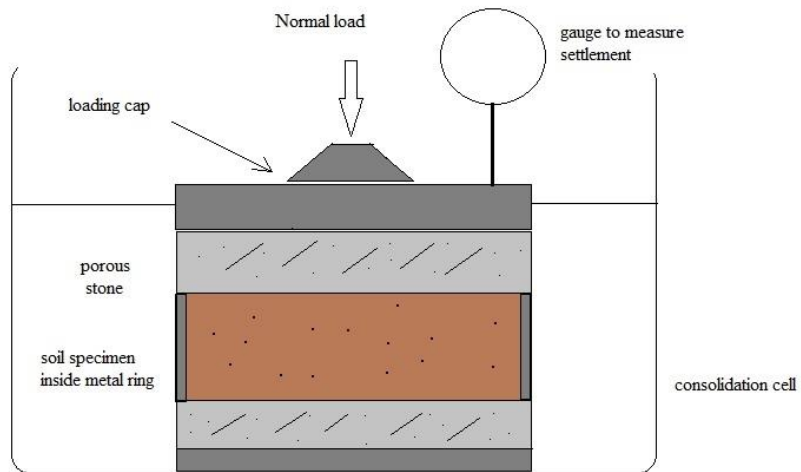


Figure 2.4 Consolidation cell test setup

After every 24 hours, the load on the specimen is increased and the settlement is continued. The cell is dismantled at the end of the test and soil sample is taken out and its dry mass is measured. The changes in void ratio of the specimen are back-calculated using the test data and a void ratio versus effective stress plot (popularly known as the e-log  $\sigma'$  curve) is constructed (Fig. 2.5). This curve is used to evaluate parameters such as maximum past pressure ( $\sigma'_{max}$ ), coefficient of compression ( $c_c$ ) and coefficient of recompression ( $c_r$ ). These parameters are vital for the assessment of the field performance of the particular soil under long term loading. This test is discussed in further detail in Chapter 6.

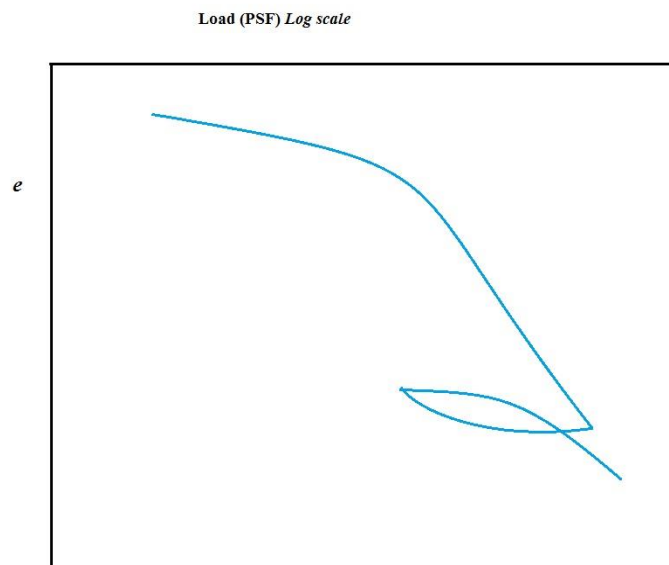


Figure 2.5 A typical e-log  $\sigma'$  curve

### 2.2.3 Specific Gravity Test (ASTM D854)

Specific gravity ( $G_s$ ) is a measure of the mass density of soil solids normalized relative to the mass density of water. Specific gravity depends on the mineralogy of a soil and consequently varies with soil types. Sands generally have  $G_s$  around 2.65 whereas clayey or silty soils have  $G_s$  in the range of 2.7-2.85. It is an important parameter to consider when studying gypsum rich soils since gypsum has a low specific gravity among minerals. Likewise, gypsum rich soils have a lower specific gravity than pure quartz or clay, the value depending on the gypsum content.

This test is performed using a specific gravity bottle, calibrated to measure 500 ml of water (Fig. 2.6). A certain mass of oven dried soil sample is taken ( $M_1$ ). The mass of the volume of water displaced in the flask by this soil is measured ( $M_2$ ). Specific gravity of the soil is then calculated by the relation:

$$G_s = M_1 / M_2 \quad (2.3)$$

The soil and the water in the flask are ideally vacuumed for 2-4 hours to remove any air from the system which might otherwise affect the mass calculations. Specific gravity is often adjusted using a temperature correction factor 'K' and specific gravity at 20° C is reported.

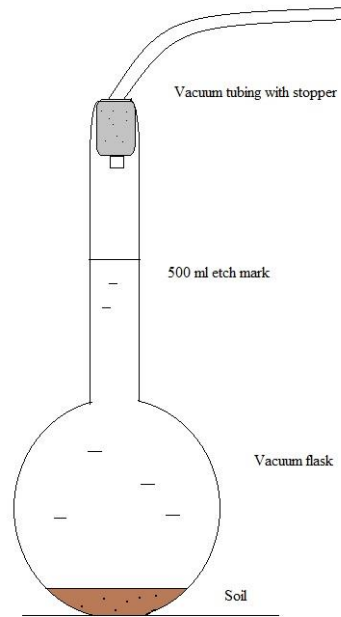


Figure 2.6 Specific gravity test setup

## 2.3 Geophysical laboratory methods

### 2.3.1 Seismic tests

Low strain seismic testing refers to those tests in which the dynamic shear stresses induced on soil specimens are less than 0.001% and are essentially based on propagation of waves through the soil matrix. In this strain range, stiffness is independent of strain and the material behaves in an elastic manner. These are one of the most widely used geophysical tests and are specifically meant to identify the dynamic properties of soil used in solving problems associated with geotechnical earthquake engineering and soil dynamics. Low-strain tests also offer the advantage of testing the sample in a relatively undisturbed state, which helps in maintaining in-situ conditions of the soil specimens. Dynamic soil properties are determined from both field and laboratory seismic tests. Laboratory tests are conducted on smaller specimens, regarded as ‘elements’ or ‘models’.

These specimens serve to represent field soils and the tests conditions are created to mimic actual field conditions (Kramer, 1996). Soil stiffness and damping are the most extensively used parameters that are derived from these tests. Stiffness parameters include shear-wave velocity ( $v_s$ ) and small-strain shear modulus ( $G_{max}$ ) which are related as:

$$G_{max} = \rho v_s^2 \quad (2.4)$$

Where  $\rho$  is the mass density of the soil and  $G_{max}$  is the small strain shear modulus.

Low strain seismic tests are based on the premise of creation of a wave pulse which produces a combination of P-waves, S-waves and surface waves. The arrival times of these waves at a distant location are recorded and analyzed. The arrival time is in turn used to calculate wave velocity as the energy travels through the soil media. It is a common practice to average the time-records from a number of impulses, to increase the signal to noise ratio. This helps in reducing the random noise and strengthening the original signal. P-waves have the highest velocity among all the waves generated.

### **2.3.1.1 Fixed-free resonant column testing (ASTM D4015)**

Resonant column testing is a widely used laboratory test to measure the dynamic properties of soil. Cylindrical specimens of soils with a typical length /diameter ratio of 2:1 are subjected to small strain harmonic loading in the axial or torsional mode using an electromagnetic loading assembly (Kramer, 1996). Cohesive soil specimens used for the test are generally 1.5 in. in diameter and 3.0 in.in length. Some researchers have also conducted the test by using impulse loading and random noise loading. The base of the specimen is fixed to a pedestal and the top is free to rotate. The test is therefore commonly known as the ‘Fixed-free resonant column test’. Specimens are often put inside a confining

chamber to simulate in-situ stress conditions. Typically undisturbed specimens are obtained from Shelby tubes and are consolidated prior to loading. Larger specimens are generally used for testing coarse grained soils. For this research, reconstituted gypsum sand specimens with 4.0 in. (10.2 cm) diameter and 9.0 in. (22.9 cm) length were used.

The loading system for the fixed-free configuration consists of four coils and magnets positioned diametrically across the circular cap (Fig 2.7). These magnets respond to the electromagnetic field induced by the harmonic voltage pulse in the coils and impart torsional excitation to the specimen. The frequency and amplitude of the harmonic loading can be controlled. A function generator is used to produce a harmonic voltage pulse, used for loading the specimen from the top. The strain-response of the specimen is detected by accelerometers attached to the loading cap and recorded in the form of a time history. Response amplitude is analyzed as a function of frequency. After subjecting the specimen to loading, the ‘resonant frequency’ ( $f_n$ ) of the specimen is identified as the frequency at which the strain-amplitude of the specimen is a maximum. It is dependent on the physical characteristics of the specimen such as its density, geometry, stiffness and confining stress.

For a specimen of height ‘ $h$ ’, polar moment of inertia ‘ $I$ ’ and a top loading system with polar moment of inertia ‘ $I_o$ ’, the fundamental angular frequency of the specimen derived from the test ( $\omega_n$ ), can be used to calculate the  $v_s$  using the relationship:

$$I/I_o = (\omega_n h / v_s) \tan (\omega_n h / v_s), \quad (2.5)$$

where  $\omega_n = 2 \pi f_n$

When the top loading system is very light in comparison to the specimen, the above equation simplifies to:

$$v_s = 4 f_n h \quad (2.6)$$

From the derived value of  $v_s$ , shear modulus can be estimated using Eqn. 2.4.

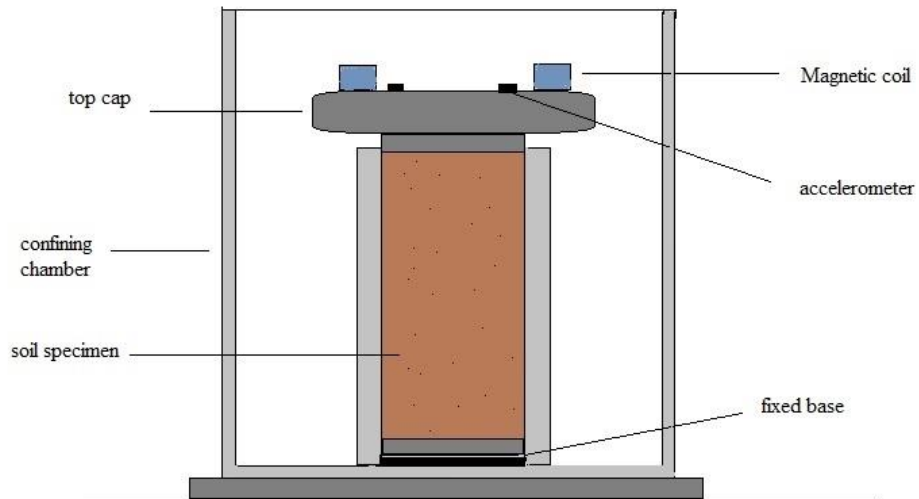


Figure 2.7 Block-diagram of a fixed-free resonant column test

### 2.3.1.2 Free-Free Resonant column testing

Free-free resonant column testing (FFRC) is a simpler alternative to the conventional fixed-free resonant column test (Kalinski & Thummaluru, 2005). The Free-Free Resonant Column testing is used for measuring small-strain shear modulus ( $G_{max}$ ) and small-strain material damping ( $D_{min}$ ) to predict the dynamic response of a soil site to earthquake shaking. Soil stiffness can be estimated from this test by measuring shear-wave velocity ( $v_s$ ) or small-strain shear modulus ( $G_{max}$ ). Like the fixed-free resonant column test, this test makes use of a cylindrical soil specimen. The specimens is suspended horizontally

from two supporting rods in such a way that both the ends are free to rotate (Fig. 2.8). Each end of the specimen has a light plastic end cap attached. One end is glued to a device like a solenoid, which can impart torsional excitation to the specimen. Accelerometers are attached to the other end, which detect the strain response of the specimen, which is recorded as a time history or frequency spectra. The ‘resonant frequency’ ( $f_n$ ) of the specimen is identified as described in the fixed-free resonant column test. If both the end caps and the attachments are made of very light material, then they will have minimal impact on the rotational inertia of the system and the shear wave velocity,  $v_s$ , is calculated by using the expression:

$$v_s = 2 f_n L \quad (2.7)$$

Where  $L$  is the length of the specimen. This test was used to measure the stiffness of gypsum soil specimens and is discussed in detail in Chapter 4 of this dissertation. By using a combination of vacuum and cell pressure, the test can be performed by simulating stresses comparable to those of in-situ soils.



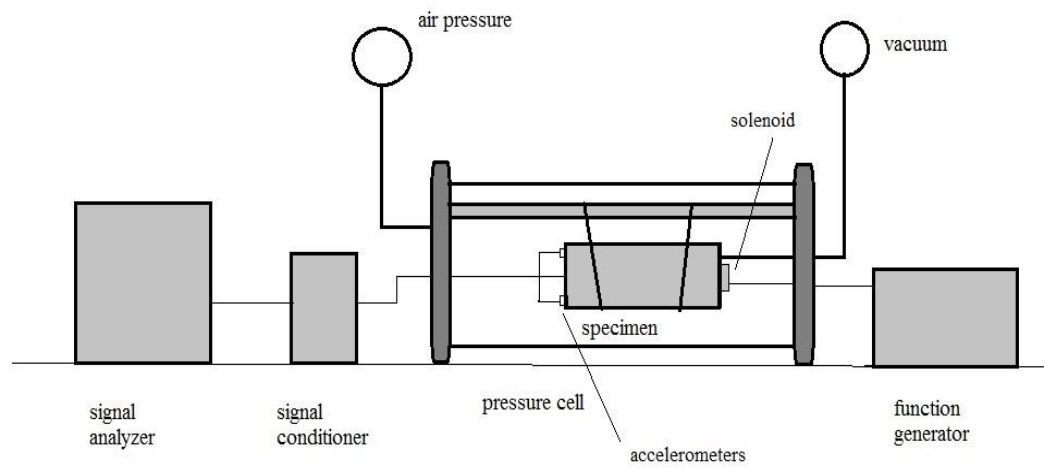


Figure 2.8 Block diagram of a free-free resonant column test

### 2.3.2 Electrical Resistivity Testing

Soils and rocks exhibit a wide range of electrical resistivity based on their mineralogical composition and the water content in their pores. Most minerals are generally insulators and their electrical conductivity is primarily due to the water present in the pores. Resistivity testing methods involve introduction of an electric current into the ground using two current electrodes and measuring the potential difference between two potential electrodes. The resistance measured in Ohms is converted to apparent resistivity (Ohm-m) based on the electrode configuration and geometry. Electrical resistivity (ER) of soil is affected by numerous parameters such as water content, fines content, temperature, density, mineralogy and salinity of pore-fluid. Resistivity measurements can thus provide an insight into these physical and chemical parameters of soil and their variation. The non-destructive and non-intrusive nature of the test makes it an attractive alternative for geotechnical investigations. Apart from engineering and geological studies, the ER technique is also widely used to assess soil conditions for agricultural purposes.

For a cylindrical soil body of cross sectional area  $A$  and length  $L$ , the electrical resistivity  $\rho$  in Ohm-m is given as:

$$\rho = R (A/L) \quad (2.9)$$

where  $R$  is the measured resistance in Ohms

For a potential drop of ( $V$ ) Volts and a measured electric current of ( $I$ ) Amperes, resistance (Ohms) is calculated using Ohms Law:

$$R = V/I \quad (2.10)$$

### 2.3.2.1 Resistivity measurement using two-electrode soil box method (ASTM G187)

This test is used for laboratory measurement of electrical resistivity of soil samples. It is used to assess the corrosion potential of soils in foundations, which may be very detrimental for the life of underground structures. The test apparatus consists of a rectangular soil box constructed out of insulating material (Fig 2.9). Two metal end-plate electrodes are fitted at the opposite ends of the box. A soil sample is placed in the box such that it lies between the two end electrodes. A commercial resistance meter is used to measure the resistance of the soil. Resistance is directly measured across the two end plate electrodes in Ohms and is converted to apparent resistivity (Eqn. 2.9). The ratio ' $A/L$ ' is known as the soil box factor or geometry factor  $k$ . This test is relatively simple to conduct as is often used to complement the four-electrode soil box method (ASTM G57).

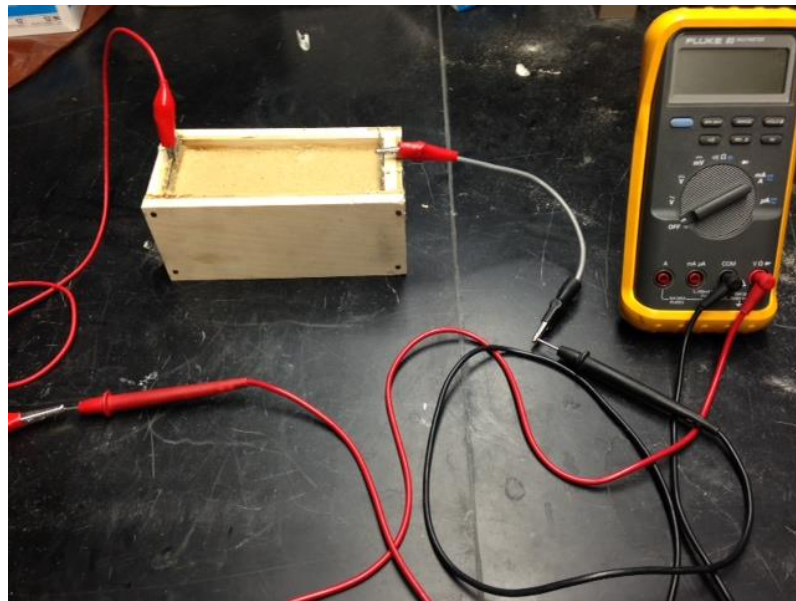


Figure 2.9 Two-electrode soil box test

### 2.3.2.2 Resistivity measurement using four-electrode soil box method (ASTM G57)

This is another popular laboratory method to measure the electrical resistivity of soil samples. Like the two-electrode soil box test, this test finds extensive application in estimating the corrosion potential of soils which might be hazardous for the life of underground structures. Testing apparatus is made up of a rectangular box made of insulating material and is commercially available as the ‘Miller soil box’ (Fig. 2.10). The box has two end-plate metal electrodes through which electric current is passed through the soil. It also has two metal pins acting as inner electrodes across which the voltage drop is measured. Resistance is calculated as the measured voltage drop divided by the electric current. Current is measured by attaching an Ammeter in series with the circuit and potential drop between the inner electrodes is measured by connecting a voltmeter parallel to the circuit. The test uses the ‘Wenner electrode configuration’ in which all the electrodes are equally spaced. For a box with a cross sectional area  $A$ , electrode spacing  $l$ , and measured resistance  $R$  (Ohms), resistivity in Ohm-m is calculated as:

$$\rho = R (A/l) \quad (2.11)$$

The relationship is also expressed as:

$$\rho = k R \quad (2.12)$$

Where  $k = A/l$  is calculated as the soil box factor or geometry factor.

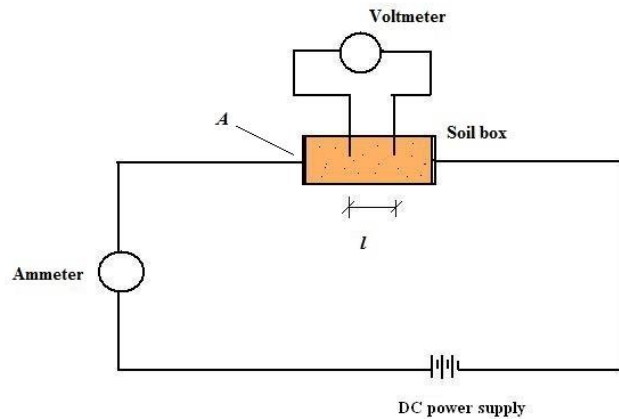


Figure 2.10. Four-electrode soil box test

## 2.4 Conclusion

This chapter describes the geotechnical and geophysical laboratory tests that were considered for the research. In this research, resonant column tests and ER tests were conducted first, followed by geotechnical tests. Some tests were modified or used in an alternative manner to suit the needs of the research. All the tests were conducted on reconstituted specimens of gypsum sand mixtures. Tests were repeated on several samples by varying one or more parameters such as gypsum content, moisture content, confining stress or dry density. There were a few more tests such as constant hydraulic conductivity test which were proposed for testing the soils, but was later deemed unsuitable for the research based on the information gathered from literature survey. Some alternative geophysical tests can be used in the laboratory to characterize soils. These methods have been described in Appendix C of the dissertation.

### **3. Electrical Resistivity Testing of Reconstituted Gypsum Rich Soils**

#### **3.1 Background**

Electrical resistivity profiling is a widely used non-invasive geophysical method for sub-surface investigations. The method was first developed by Schlumberger in the early 20<sup>th</sup> century to characterize subsurface features of rocks and was subsequently applied by oil companies to locate potential petroleum reserves underground (Samouelian et al., 2005). Many properties of soil and rock show a good correlation with electrical resistivity. The basic principle involves introduction of a direct current or an alternating current into the ground and measuring the resulting potential difference between two points. Figure 3.1 shows the typical electrical resistivity range of some common earth materials. There is a wide range of electrical resistivity for soils, ranging from  $10^0$  -  $10^5$  Ohm-m. Numerous factors dictate the electrical properties of earth materials, the most important ones being soil water content, mineralogy, fraction of fines, grain size, salinity, pore-fluid, bulk density and temperature.

Resistivity tests can also be used to monitor the temporal variations in these soil properties. In addition to being a widely used site investigation method, resistivity testing also finds great use in agriculture (to monitor salinity levels of soils), studies involving the chemistry of groundwater and estimating the corrosion of underground structures. For this research, the electrical resistivity technique has been used as a possible alternative for characterization of gypsum rich soils on a laboratory scale.

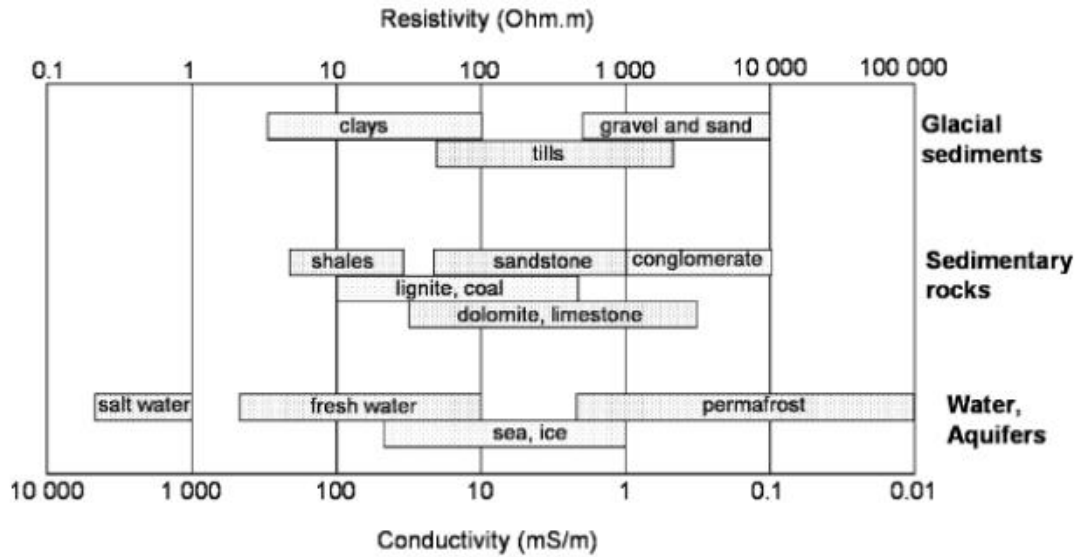


Figure 3.1 Typical electrical resistivity range of earth materials (Samouelian et al., 2005)

Several researchers studied the relationships between soil properties and their geoelectrical characteristics. Rhoades et al. (1976) and Rhoades et al. (1977) developed a relationship correlating bulk soil electrical conductivity with pore-water electrical conductivity, volumetric water content and soil surface conductivity (Samouelian et al., 2005). Gupta and Hanks (1972) proposed a linear relationship between soil resistivity and water content. Archie (1942) proposed an empirical method for correlating electrical resistivity of clay-free granular soils with pore-water resistivity and porosity. Kalinski and Kelly (1993) estimated the volumetric water content of soils containing 20% clay. They also developed a circular four-probe resistivity cell as an alternative to the Miller soil box for laboratory measurements of soil resistivity. Guinea et al. (2010) described how laboratory measurements, theoretical models and field data can be used to identify commercial useful gypsum rock deposits in north-eastern Spain. Bhatt et al. (2014) used

a statistical approach to establish a correlation between electrical resistivity and water content of sand in a laboratory setup.

The two-electrode soil box method (ASTM G187) and four-electrode soil box method (ASTM G57) were used for the study. In the two-electrode method, the resistivity of the soil is calculated by directly measuring the resistance of the soil across the length of the box using a standard multimeter. This particular test was based on the premise of Kalinski and Vemuri (2005), wherein, the effect of degree of saturation, compaction effort and volumetric moisture content on the electrical conductivity of clay were studied. In the four-electrode soil box method, current from a steady DC source is applied across the ends of the box and the potential drop between the two inner electrodes is measured. Resistivity is calculated as  $K$  times the ratio of voltage by current, where  $K$  is the calibration constant of the box.

### 3.2 Testing methodology

A wooden soil testing box with inner dimensions 15.0 cm x 6.0 cm x 6.0 cm was used for conducting the tests along with two rectangular electrodes placed at either ends of the box. The box was filled with a moist mixture of sand and gypsum. Knowing the weight and volume of the box, and the weight of dry soil, the volumetric water content ( $\theta$ ) could be calculated. Resistivity ( $\rho$ ) was computed as:

$$\rho = R (A/l) = R(K) \quad (3.1)$$

Where  $A/l$ , the ratio of cross-sectional area to length, is the calibration constant. The soil resistance  $R$  is measured using a multimeter. Resistance of a mixture was measured and



plotted over a range of moisture content. The test was repeated for mixtures with varying proportions of gypsum and a comparison was made.

### **3.2.1 Two-electrode soil box method (ASTM G187)**

A saturated mixture of gypsum and sand was placed in the box and lightly compacted until it was spread evenly in the box ( $e_o = 0.62$ ) to the top (Fig 3.2). The two electrodes at either ends of the box, made of wire mesh and aluminum foil, were connected to the two probes of a fluke multimeter and resistance was measured in  $k\Omega$ . Measurements were taken twice by reversing the polarity of the probes. The internal resistance of the multimeter was found to be  $0.3\Omega$ , which is negligible compared to the resistance of the soil. Also the box constant ( $k$ ) was determined to be 2.48. Tap water was used for conducting these tests instead of de-ionized water because the objective was to make a relative comparison between soils with different gypsum percentages. The electrical conductivity of tap water typically ranged from  $450 \mu\text{S}/\text{cm}$  to  $700 \mu\text{S}/\text{cm}$  during the entire duration of research. This corresponds to an average resistivity of  $17.4 \text{ Ohm}\cdot\text{m}$ .

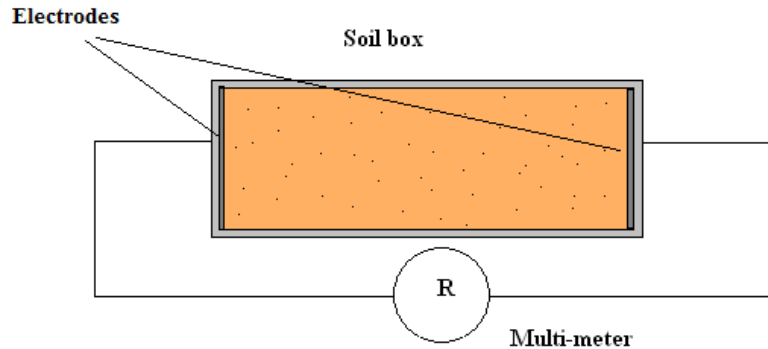


Figure 3.2 -electrode soil box test arrangement

The mixture when initially placed in the box was saturated at a moisture content of approximately 25%. The soil was allowed to sit and desiccate over a period of 5 to 6 days. During this time, resistance was measured at regular intervals. As water content decreased, the weight of the soil box also decreased. The change in weight at each point was recorded. Finally, when no further change in weight was observed, the final measurement was taken and the soil sample was removed from the box. To obtain a reasonably accurate dry weight of the soil sample, the soil was transferred into an oven safe container and the dried for several hours in an oven. The oven was set to 60° C per the ASTM standard to prevent the breakdown of gypsum into anhydrite or bassanite.

This method yielded profiles characteristic of those of typical resistivity versus water content plots (Fig 3.3). Resistivity was at the lowest when the mixture was close to saturation and increased as the water content decreased. The resistivity was also within the typical range of resistivities for quartz and feldspar. However this method had some major limitations. The resistance readings had a lot of fluctuation. To ensure a reasonable

recording, a number of measurements had to be taken and averaged. The other major disadvantage was that of directional variation of resistance. When the polarity of the multimeter probes was switched, there was a substantial difference in resistance reading. The difference was even more pronounced at lower moisture contents. In lieu of these limitations and uncertainties, the two-electrode soil box method was discarded after testing two soil samples.

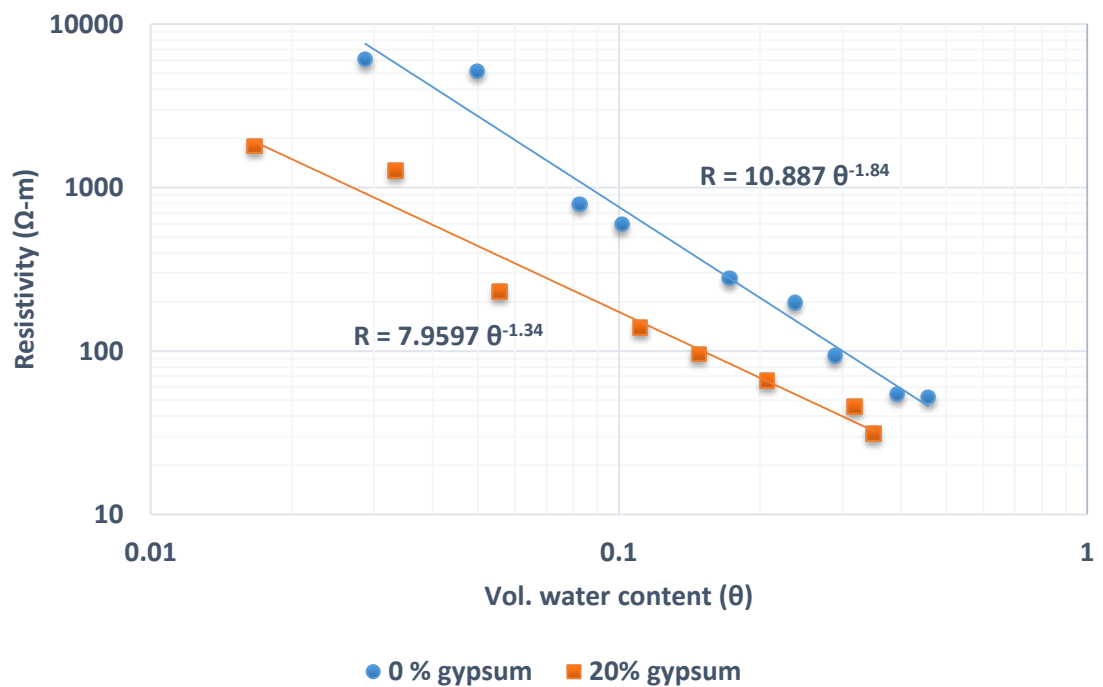


Figure 3.3 Resistivity versus volumetric water content using 2-electrode resistivity box method

### 3.2.2 Four-electrode soil box method (ASTM G57)

Due to the shortcomings of the two-electrode soil box method, a four-electrode testing scheme was implemented. The test was based on the *Wenner configuration* (Fig 3.4) in which 4 electrodes are placed in a straight line with equal spacing. As such, the separation between the electrodes was 5.0 cm. The same wooden box was used for this test (Figs 3.5, 3.6). It had a cross sectional area of 36.0 cm<sup>2</sup> and a length of 15.0 cm.

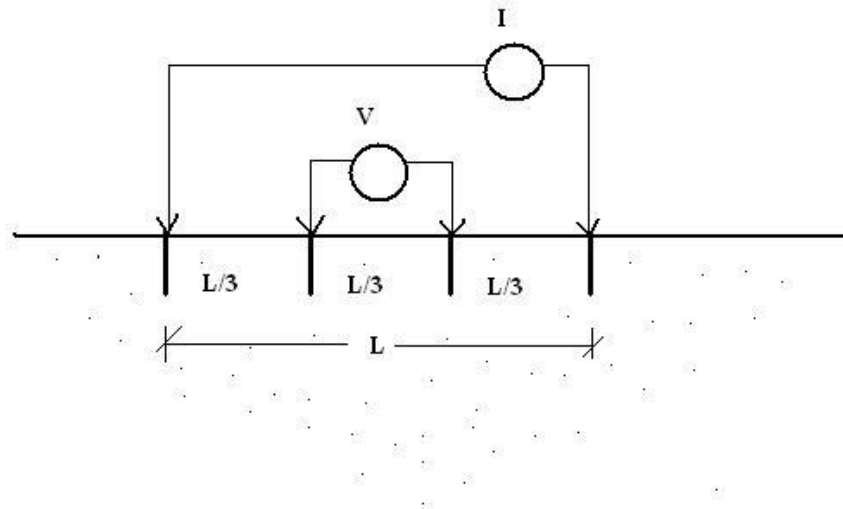


Figure 3.4. Wenner 4-electrode configuration

A Steady DC power source from an Agilent E3620A power supply was used to maintain a steady current flow across the outer electrodes. It was set to supply 6.0 V DC. The current flow ( $i$ ) through the box was measured using a multimeter connected in series with the soil box. Two stainless steel electrodes were placed in the middle to measure the voltage drop ( $V$ ). Another multimeter was connected in parallel with the soil box to measure the voltage drop across the two inner electrodes. The arrangement is illustrated in

Figs 3.5 and 3.6. In this configuration, Resistance ( $R$ ) was calculated as  $V/I$  and resistivity of the soil ( $\rho$ ) was calculated as:

$$\rho = K(R) \tag{3.2}$$

Where  $K$  is the calibration constant of the box. Considering a cross sectional area ( $A$ ) of  $33 \text{ cm}^2$  and an electrode spacing ( $l$ ) of  $5.0 \text{ cm}$ ,  $K$  was determined to be  $6.6 \text{ cm}$ .

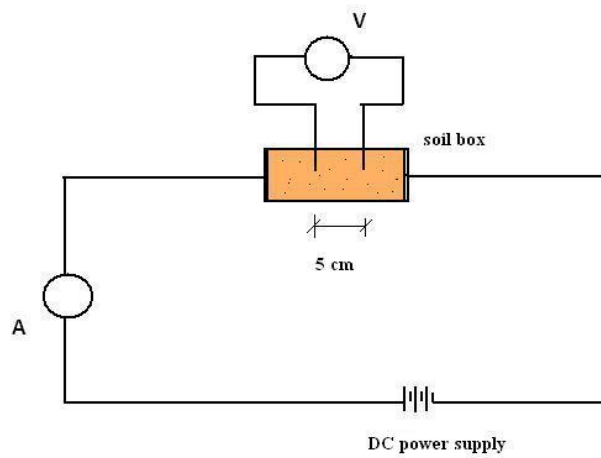


Figure 3.5. Four-electrode soil box test configuration

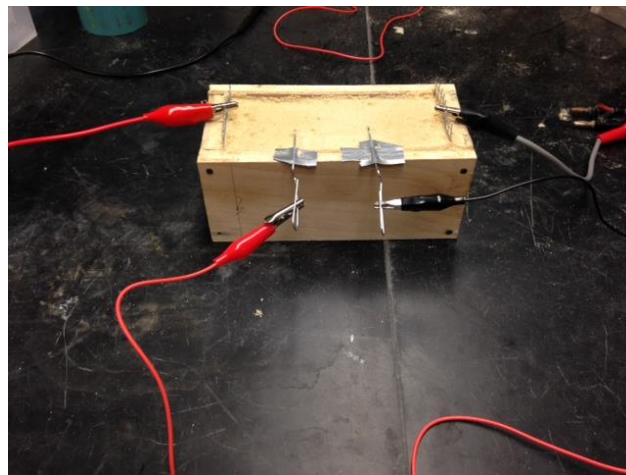


Figure 3.6. Four-electrode soil box test setup in lab

### 3.3 Relationship between resistivity and moisture content

In the first part of the testing, resistivity was measured and plotted against volumetric moisture content ( $\theta$ ). A moist sample of soil was taken and filled into the box. It was lightly compacted to ensure uniform distribution across the box ( $e_o \sim 0.6$ ). Once the soil was filled and leveled, the DC power source was turned on to introduce current into the circuit. Using the ammeter and voltmeter components of the two multimeters, the current in the system and the voltage drop across the two inner electrodes could be read simultaneously.

Measurements were taken twice a day and the mixture was allowed to dry naturally. The change in the weight of the box was used to estimate the change in moisture content. After about five days, when no further weight change was seen, the sample would be dismantled and the final moisture content of the soil would be found.

A major advantage of this method was that current and voltage varied proportionately, keeping  $R$  stable. Also, reversing the direction of current did not show any appreciable change in resistance of the soil. Therefore this method was deemed more suitable to measure resistivity. Five different sands were tested and their results were plotted in Figs 3.7-3.12.

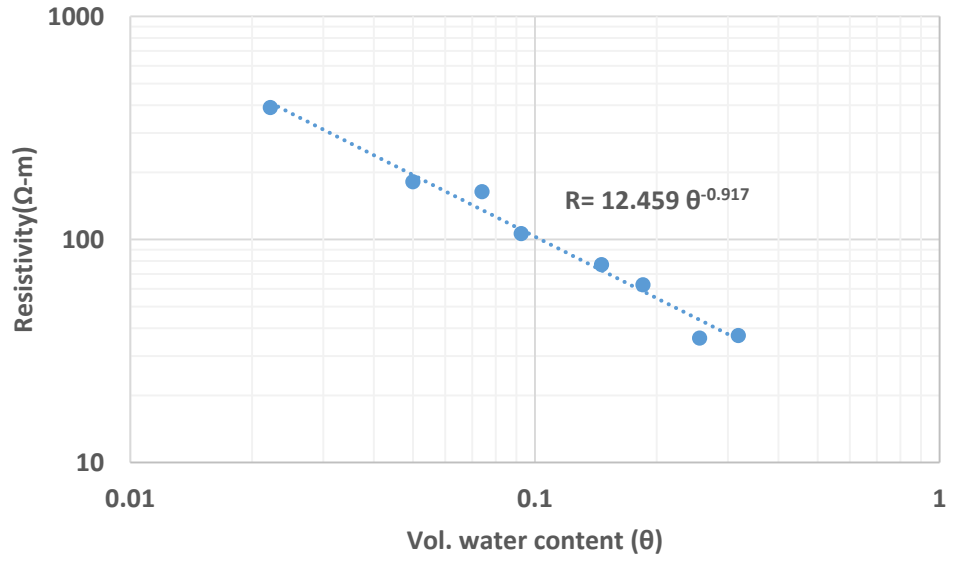


Figure 3.7 Resistivity versus vol. moisture content for 0% gypsum

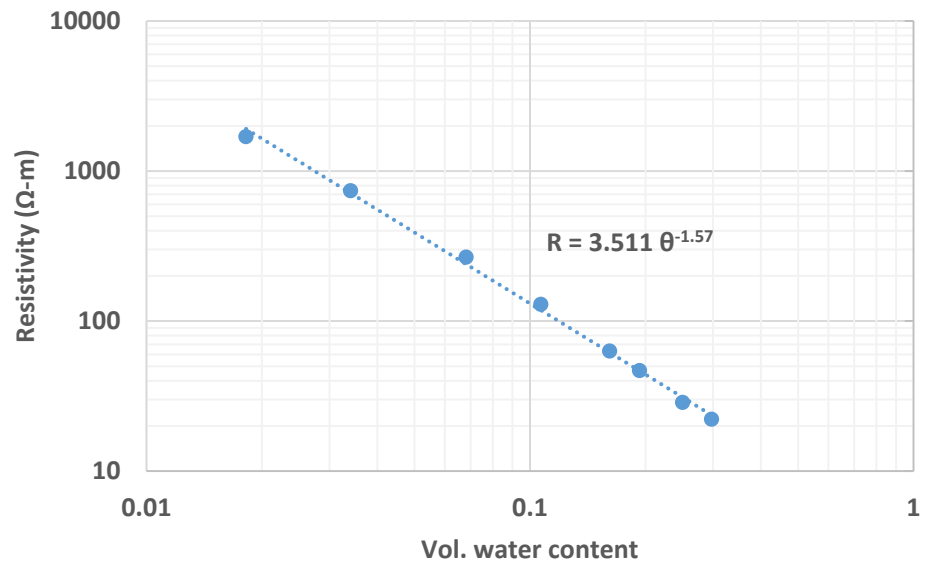


Figure 3.8 Resistivity versus vol. moisture content for 10% gypsum

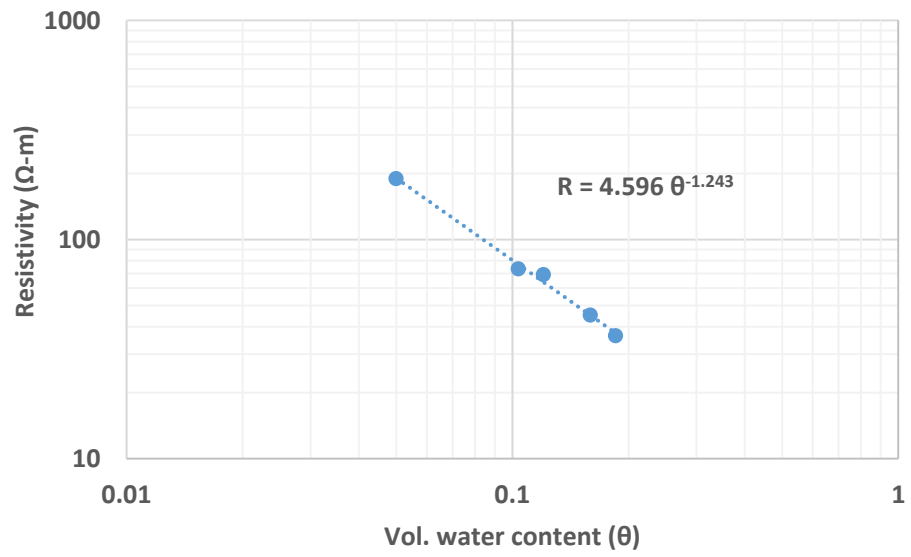


Figure 3.9 Resistivity versus vol. moisture content for 20% gypsum

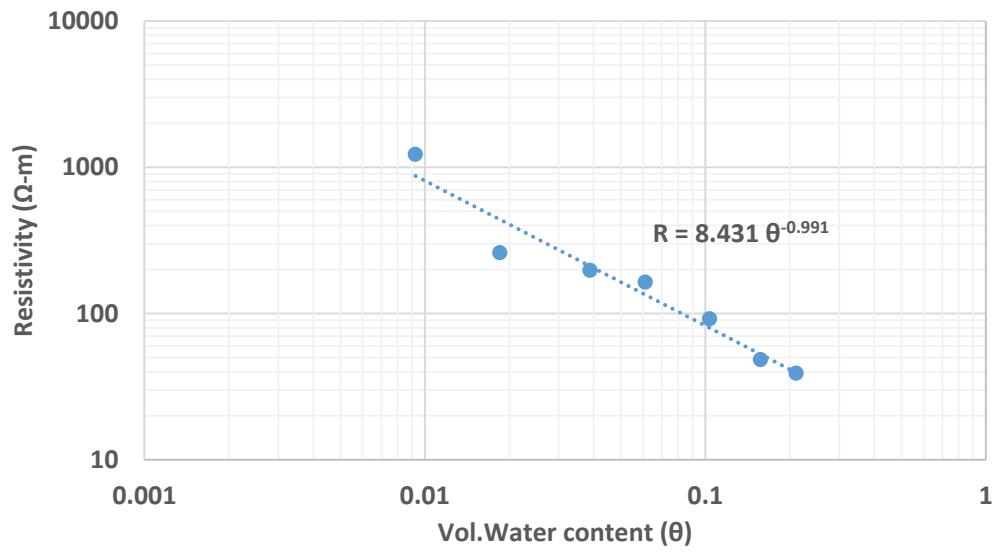


Figure 3.10 Resistivity versus vol. moisture content for 40% gypsum



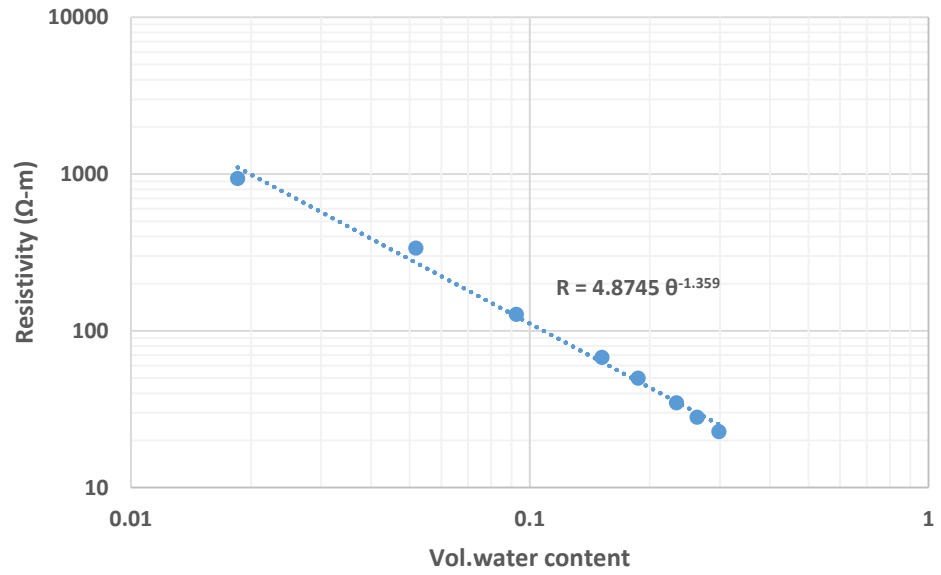


Figure 3.11 Resistivity versus vol. moisture content for 60% gypsum

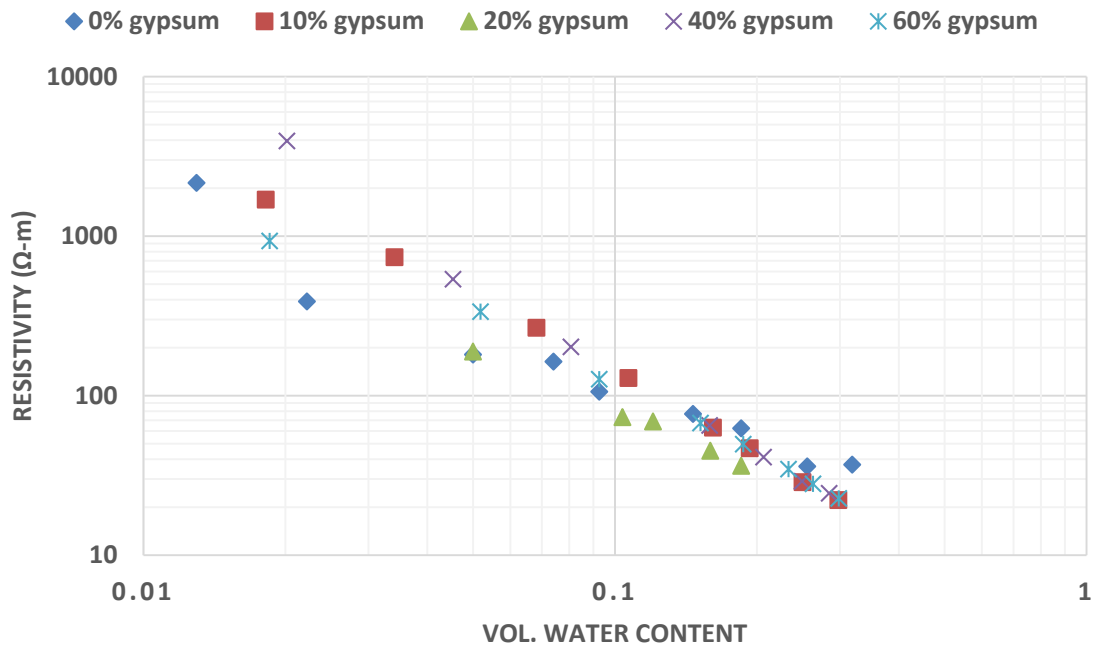


Figure 3.12 Composite resistivity versus  $\theta$  profiles using of the five soil samples

### **3.4 Relationship between resistivity and gypsum content**

A set of tests were performed to see the effect of gypsum content on the bulk resistivity of gypsum-sand mixtures saturated with water. Mixtures were prepared with 25% water content. After being hydrated for about an hour, they were put in soil box and compacted lightly to ensure a uniform distribution. In all cases, void ratio of sands was kept close to 0.6. Next the voltage electrodes were inserted into the soil box and the apparatus was ready for testing.

The DC power source was set to 4V to supply a current for the circuit. The resulting current through the soil and potential drop between the inner electrodes were measured. Fifteen tests were performed in this manner on a number of mixtures, some of them being repeated multiple times. The resistivity at saturation was graphed against the gypsum content in the sands. The resulting plot is shown in Figure 3.13.

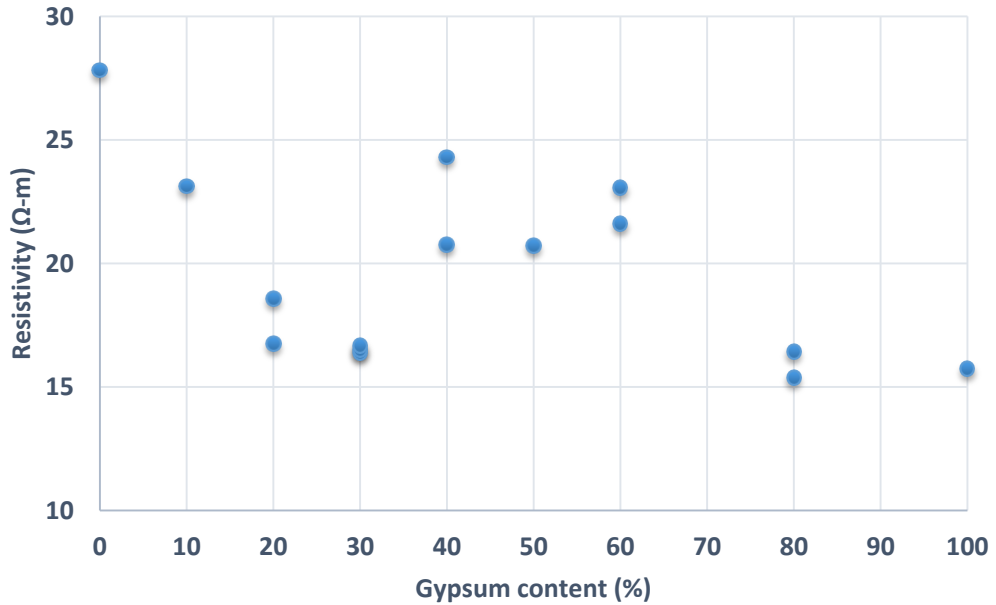


Figure 3.13 Resistivity plotted against gypsum content at  $S = 100\%$ , using the wooden soil box

The testing scheme was repeated after a few months using a new acrylic soil box to validate this data. The box had the same inner and outer dimensions as the wooden box. Unlike the wooden box, the acrylic box was resistant to decay caused by prolonged contact with moist soil. Select mixtures were tested and the water content and compaction were carefully controlled to avoid any significant scatter in the data. All specimens were prepared at a dry density of approximately  $1.5 \text{ g/cm}^3$ . The relatively small size of the test specimens ensured that the dry density values were comparable. Required amount of water to saturate the specimen was estimated. Again the resistivity was graphed against gypsum content, which yielded a plot as shown in figure 3.14. The two datasets compare favorably.

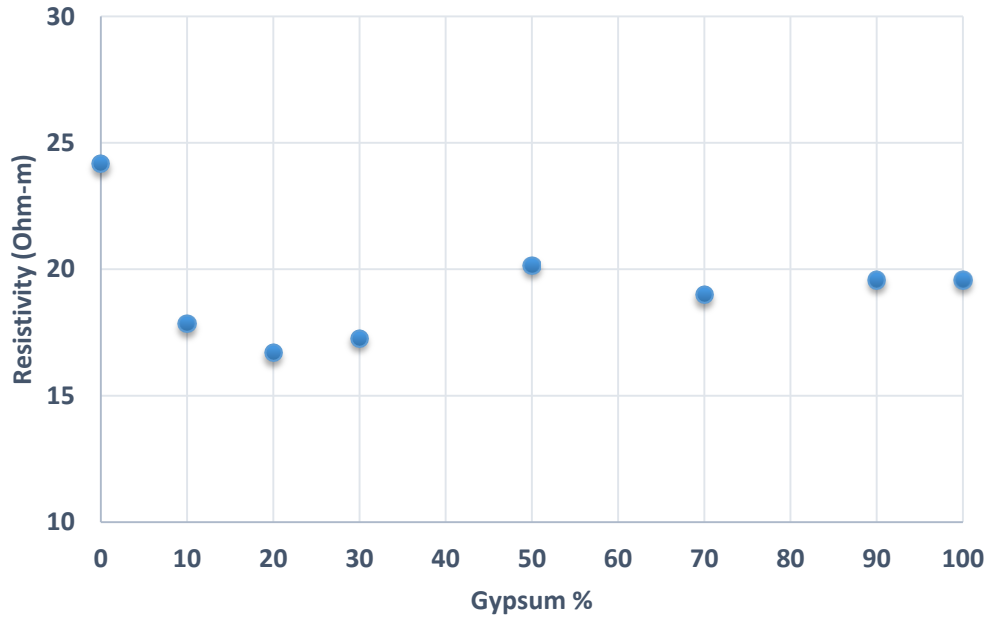


Figure 3.14 Resistivity plotted against gypsum content at S = 100%, using the plastic soil box

The excess water collected on top of some soil samples was decanted and set for pore water resistivity measurements. Pore water resistivity was measured using an Extech 400 conductivity meter at 20° C (Fig. 3.15). The device can measure electrical conductivity, salinity and the total dissolved solids (TDS) in any solution. However only the conductivity values were recorded and converted to resistivity. Table 3.1 shows the pore water resistivity measurements obtained from the different soil samples. Figure 3.16 compares the pore water resistivity values with those of soil resistivity.

Table 3.1 Pore-water resistivity of soils with different gypsum contents

Gypsum %	Electrical resistivity ( $\Omega\text{-m}$ )
0	9.34
10	2.85
20	2.70
30	3.09
40	3.32
50	3.22
60	3.46



Figure 3.15. Measuring pore-water resistivity using Extech-400 conductivity meter

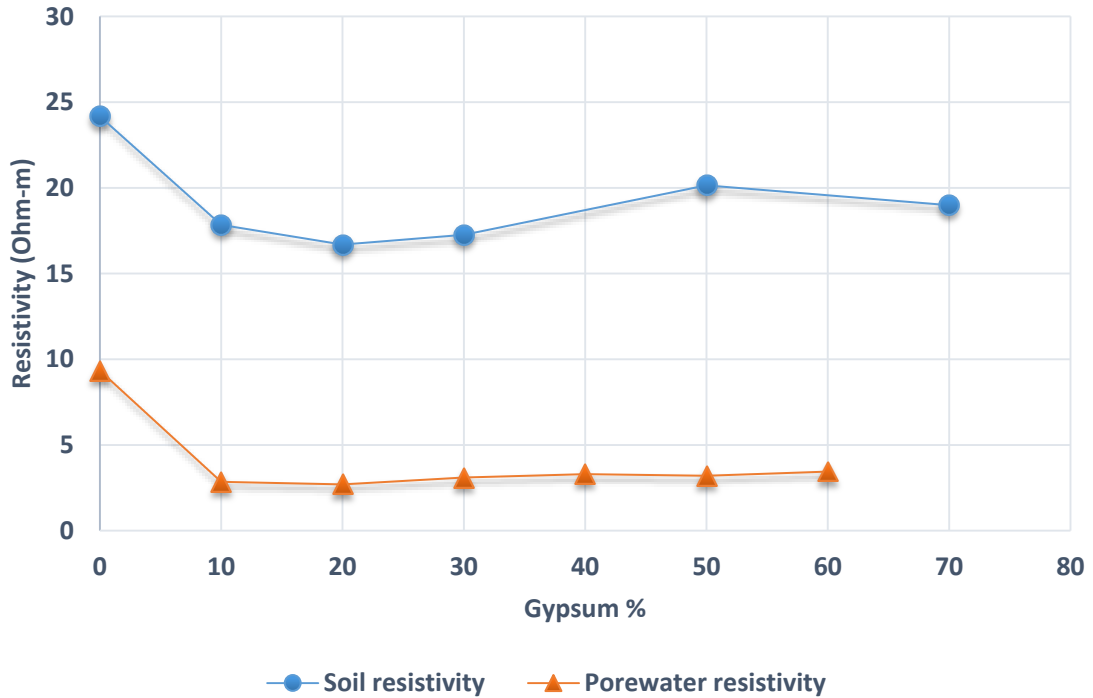


Figure 3.16. Comparison of pore water resistivity with soil resistivity

### 3.5 Observations and inferences

Both sand (quartz) and gypsum are poor conductors of electricity and are essentially insulators at low moisture contents. In both the 2-electrode and 4-electrode soil box tests, it was seen that the change in resistivity was mainly related to the change in water content of the soil. Resistivity is found to decrease with an increase in volumetric water content. The general relationship between resistivity and water content was akin to  $y=a*x^{-b}$ , where  $a$  ranged from 0.4 to 1.3 and  $b$  ranged from 0.9 to 1.4. This relationship can be seen in Figures 3.7-3.10. The correlation was fairly good, yielding an R-squared value of 0.94 – 0.99. The relationship can be compared to the empirical relation proposed by Archie (Samouelian et al., 2005):

$$R = R_w a S^{-n} \phi^m \quad (3.3)$$

Where  $R$  is the soil resistivity,  $R_w$  is the pore water resistivity,  $S$  is the degree of saturation,  $\phi$  is the porosity and  $a$ ,  $n$  and  $m$  are empirical constants. Since the test is performed on a same sample throughout, the porosity would remain constant leaving saturation the only variable. The equation then changes to:

$$R = R_w a S^{-n} \quad (3.4)$$

When dry, both gypsum and quartz are very good insulators. Under saturated conditions there is an increase in conductivity of gypsiferous soils, due to the liberation of  $\text{Ca}^{2+}$  and  $\text{SO}_4^{2-}$  ions by gypsum. These liberated ions are partially dissolved in the water and partially adsorbed on the soil surface. After testing several mixtures at saturation, a general trend was observed where resistivity was at a maximum when there was no gypsum in the sample. It then dropped rapidly with increase in gypsum content, reaching minima at about 30% gypsum. Thereafter resistivity increased, and remained fairly constant up to about 70% gypsum. At very high gypsum concentrations, (>70%), the trend was a little ambiguous. One set of tests suggested a decrease in resistivity whereas the second set of tests maintained a fairly constant resistivity beyond 50% gypsum.

Literature suggests that, soil surface acts as surface for adsorbent for  $\text{Ca}^{2+}$  and  $\text{SO}_4^{2-}$  ions liberated in the presence of water (Bolan et al., 1991). As such, the dissolution of gypsum is more in saturated soil than in water itself. This explains the decrease in resistivity with increase of gypsum. But gypsum is known to be a sparingly soluble salt (2.0 – 2.6 g/l) (Adiku et al., 1992). This results in the pore-water attaining a saturation concentration at relatively small gypsum concentrations. Beyond this amount, no further gypsum can be dissolved and addition of gypsum could only result in

precipitation. This explains why there is no change in resistivity beyond a certain concentration of gypsum in the soil. It is the dissolved gypsum that causes the increase in conductivity. The conductivity of porewater measured at 20°C varied between 3.05-3.7 mmho/cm. These values correspond to a resistivity range of 2.7 - 3.3  $\Omega$ -m, as shown in Table 3.1.

The ambiguity in resistivity at higher gypsum concentrations may be a result of higher settlement for the same compaction effort. From the consolidation tests it was found that settlement generally increased with increase in gypsum. Varying dry density affects the tortuosity of the soil which might ultimately affect the observed resistivity.

To address this aspect, another set of tests were conducted to study the change in resistivity with density (porosity). Archie's Law could again be applied to saturated sands to predict the resistivity of soils over a range of porosities. Unlike the previous testing regime, saturation would be kept constant in this case and the density is varied. The details of these tests and results will be discussed in the following sections.

Even though there is not a very significant variation in resistivity of saturated sands with the addition of gypsum, this method could still be applied to characterize sites with gypsiferous soils. Electrical resistivity testing can be used with other site investigation methods in sites with low to moderate amounts of gypsum.



### 3.6 Relationship between resistivity and porosity

A series of tests was conducted to see the effect of soil density on electrical resistivity. The test was again based on the premise of Archie's Law which states that bulk soil resistivity in rocks and granular soils is proportional to pore-water resistivity, degree of saturation and porosity. Since sample density can be varied by soil compaction, it is possible to perform the resistivity tests across a range of porosity.

Three mixtures were tested with gypsum contents of 0%, 20% and 50%. The choice of mixtures was based on the results of the prior resistivity tests, which indicated a dip in resistivity at 20% gypsum content and a subsequent increase and stabilization. From the different tests, it was also found that sand could be packed to greater densities with increasing gypsum content. Based on all these results, it was expected that the mixtures might show specific resistivity trends based on the gypsum concentration and porosity. The effect of gypsum on the cementation exponent 'm' of the Archie's Law was of particular interest.

To perform this test, the four-electrode soil box was again used. Sand was the poured into the box. Initially sand was poured loosely to maintain a higher void ratio. In each subsequent test it was compacted more and more till the point where void ratio could not be reduced any further. The optimum amount of water required to saturate the specimen was estimated, based on the sample specific gravity and void ratio:

$$G_s w = S e \quad (3.5)$$

At saturation,  $S = 1$ , so the required water content was approximated using the expression:

$$w = e / G_s \quad (3.6)$$

The calculated amount of tap water was added to the specimen in small amounts until complete saturation was attained. The tap water had an average resistivity of 16.6 Ohm-m at 22° C. The soil was then left to hydrate for fifteen minutes. After hydration, the ammeter and the voltmeter were connected to the box in the Wenner configuration and a DC current was passed at 4V using the Agilent E3620A DC power source.

Measurements were taken at different values of porosity. Resistance values (KOhm) were converted to Resistivity (Ohm-m) using a conversion factor of 57.5. The factor was calculated based on the geometry of the box and electrode spacing. The resistivity was then plotted against porosity. A best fit curve was fitted through these points. Pore-water was collected from the loosely packed sands by compacting them and decanting the water collected on top. The electrical conductivity of porewater was measured using an Extech 400 conductivity meter in mmho/cm. Conductivity was converted to resistivity (Ohm-m). The pore-water resistivity values for the three specimens are shown in Table 3.2. The results are shown in Figures 3.17-3.19.

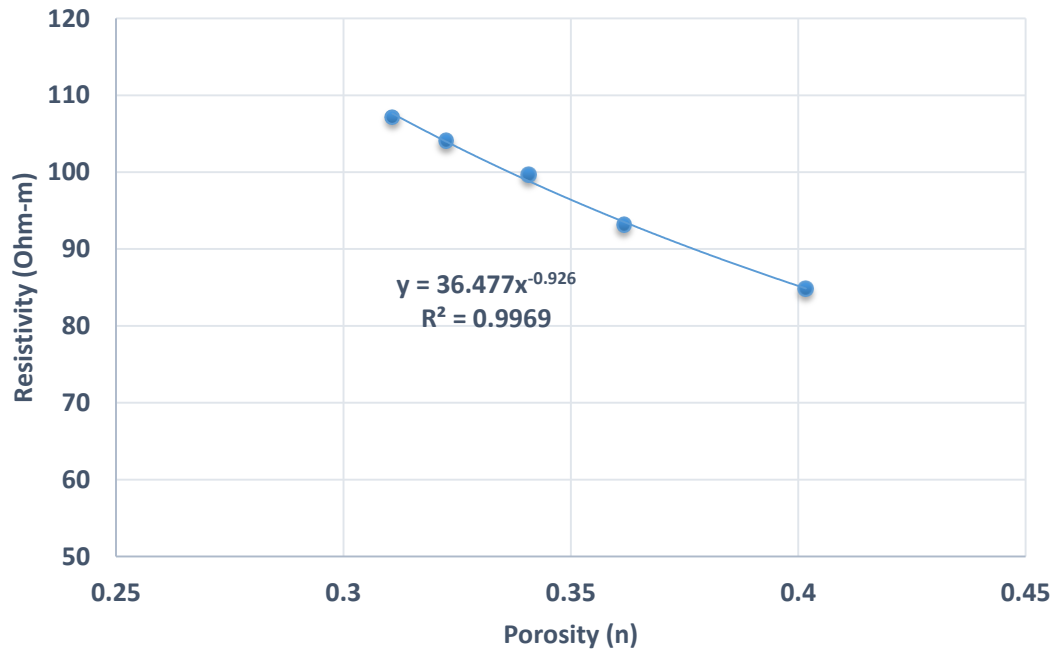


Figure 3.17. Resistivity versus porosity for 0% gypsum sand (saturated)

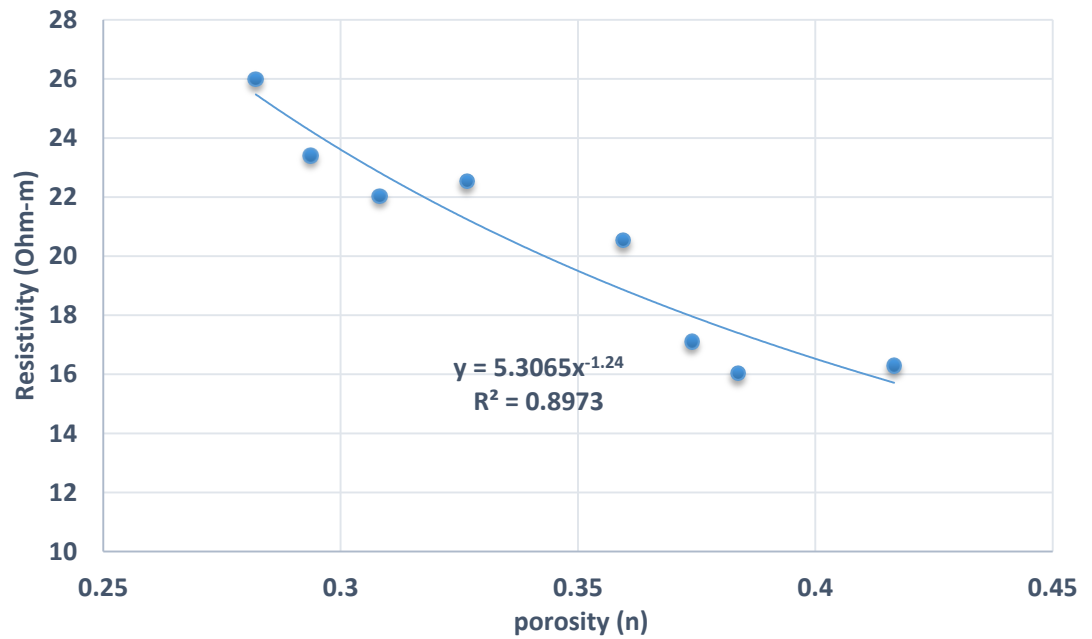


Figure 3.18 Resistivity versus porosity for 20% gypsum sand (saturated)

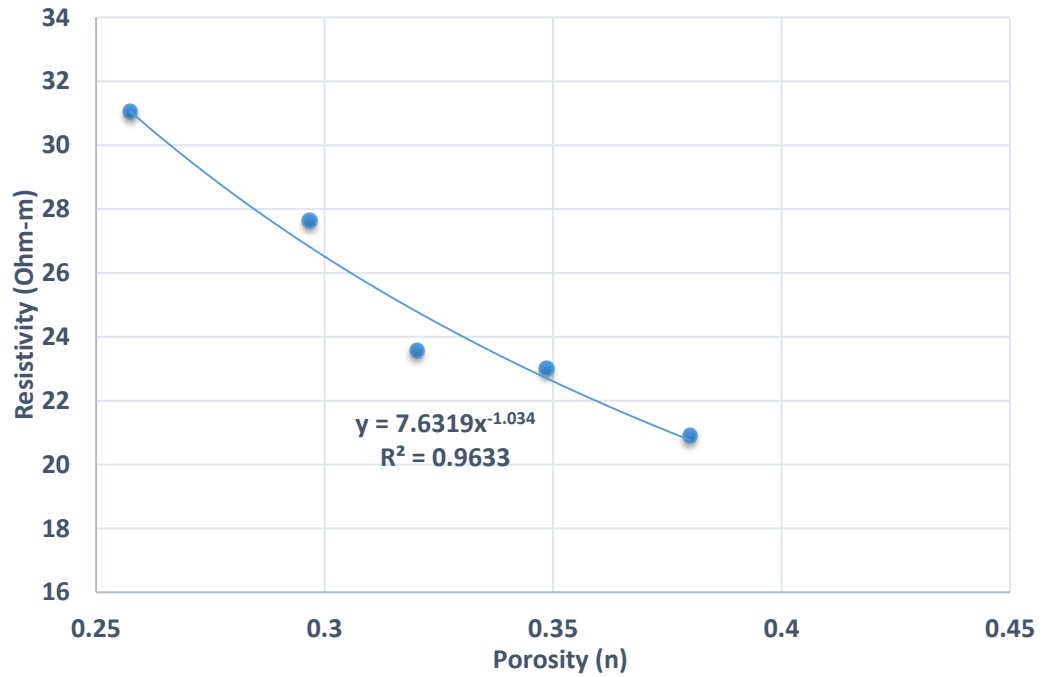


Figure 3.19 Resistivity versus porosity for 50% gypsum sand (saturated)

### 3.7 Observations and inferences

For a given soil mixture, electrical resistivity showed a good correlation with porosity. It was observed that electrical resistivity decreased with increasing porosity. The R-squared values fell in the range of 0.91 to 0.99. The best fit curve exponential curve was expected to have a form similar to that of Archie's Law expression. The expression was again of the form  $y = a R_w x^m$ , where ' $m$ ' is the cementation exponent, ' $a$ ' is a constant and  $R_w$  is the pore-water resistivity. As all the specimens were tested at  $S = 100\%$ , the saturation coefficient becomes unity.

Of the three mixtures tested, sand with 20% gypsum showed the largest value of  $m$ . Higher  $m$  values usually represent a greater degree of cementation within a given soil fabric. Pure sand (with no gypsum) yielded the smallest value of  $m$  and sand with 50%

gypsum had an intermediate value. Table 3.2 lists the mixtures and their corresponding  $m$  values from the resistivity-porosity plots.

Table 3.2. Gypsum soil samples and their Archie's Law parameters

Soil	Pore water resistivity (Ohm-m)	$m$
0% gypsum	9.34	0.926
20% gypsum	2.70	1.28
50 % gypsum	3.22	1.03

The size of the box was a limitation in the test. Since the volume of the box was not very large (450 cm<sup>3</sup>), the range of void ratios at which soil could be placed and compacted was limited. This resulted in corresponding limited porosity range. For most cases, porosity could only be varied in the range of 0.28-0.40. This could also have impacted the parameter ' $m$ ' which is normally higher for rocks and subsurface soil formations. Typical  $m$  values range from 1.3 to 2.5 (Engler, 2012).

Another observation which was verified from this test was the increase in compaction with increase in gypsum. In other words, sand with a greater proportion of gypsum could be compacted to lower porosities. This behavior could be explained by the fact that gypsum is a soft material. The application of greater compaction effort serves to crush gypsum, compressing the soil to a smaller volume.

### **3.8 Conclusion**

Electrical resistivity of gypsum soils shows a good correlation with volumetric moisture content. It however does not have a unique relationship with gypsum content. In other words, the electrical resistivity of gypsiferous soils is fairly independent of gypsum content. The pore water resistivity measurements from the different specimens confirmed this observation. Electrical resistivity of the soils also varies with the porosity of the specimens. Due to the small size of the specimen, porosity only varied over a narrow range and correspondingly, the variation in resistivity was small. It was also observed that among the three variables: moisture content, gypsum content and porosity, change in moisture content had the most significant impact on electrical resistivity. The information derived from the electrical resistivity testing was used to develop statistical models which can be used for predictive analysis. These relationships and models are described in Chapter 7 of this dissertation.

## 4. Estimating the Stiffness of Gypsum Rich Soils using Free-free Resonant Column

### Testing

#### 4.1 Introduction

Gypsiferous soils across the world are susceptible to numerous engineering hazards, annually incurring losses of the order of millions of dollars. The unique properties of the mineral gypsum ( $\text{CaSO}_4 \cdot 2\text{H}_2\text{O}$ ), such as softness, moderate solubility and reactivity are responsible for rendering soils hazardous for new or existing constructions (Cooper & Calow, 1998). Gypsum is often found in arid regions of the world along with calcite and dolomite in the form of evaporites. Gypsum rich soils have a high permeability, low unit weight and are predisposed to settlement. The problem of subsidence is especially widespread and catastrophic.

There is a great need for developing non-destructive and non-intrusive tests to rapidly screen sites with gypsiferous soils. Geophysical testing methods such as seismic tests are known to be very effective for such analysis. Conventionally, fixed-free resonant column testing or the bender element testing methods (BE) have been in use for performing small-strain dynamic tests on soils (shear strains in the range of  $10^{-3}$  to  $10^{-4}$ ). The technique used in this study is known as the free-free resonant column testing (FFRC), a simpler alternative to the conventional fixed-free resonant column test (Kalinski & Thummaluru, 2005). It has an advantage over bender element testing, wherein small strain material damping can also be estimated ( $D_{min}$ ). The interpretation of bender element data is also somewhat subjective. Free-free resonant column testing is used for measuring small-strain shear modulus ( $G_{max}$ ) and small-strain material damping ( $D_{min}$ ) to predict the response of a site to earthquake shaking. Small-strain shear modulus represents the largest value of shear

modulus of any given soil found at low strain amplitudes. Soil stiffness can be estimated from this test by measuring shear-wave velocity ( $v_s$ ). By using a combination of vacuum and cell pressure, the test can be performed over a range of comparable to those of in-situ soils.

#### 4.2 Test Setup

The term ‘gypsiferous’ is broadly used to describe soils having a significant amount of gypsum, but not exceeding 50 % by proportion (Herrero & Porta, 2000). The natural gypsum content of soils in many gypsum affected areas of the world is typically within this range, although it could occasionally be exceptionally high in some locations. Gypsum is also usually found in arid regions, where soils generally have substantial coarse-grained fractions. Considering these aspect, mixtures of fine quartz (minus # 40 fractions) and ground gypsum were prepared in the laboratory with different percentages of gypsum by weight (Fig. 4.1). Table 4.1 shows the soils used for the tests and their respective gypsum percentages.

Table 4.1. Gypsum-sand mixtures used in testing

<b>Soil type</b>	<b>Percentage of gypsum</b>
M0	0
M10	10
M20	20
M30	30
M40	40
M50	50
M100	100





Figure 4.1 Soil M30 (sand with 30 % gypsum)

The mixtures were reconstituted into cylindrical specimens with an aspect ratio of 2:1 using a latex membrane and two end caps. A rotary solenoid (Ledex 500, model No. H-1079-032) was attached to one end of the specimen and a pair of PCB accelerometers (PCB 353B16) was attached to the other end across the diameter. The accelerometers have a sensitivity of 10 mv/g and an operating frequency of 0.7 – 20,000 Hz (Kalinski & Thummaluru, 2005). The usage of two accelerometers oriented in the same direction ensures that the recorded motion is predominantly torsional. The resonant frequency ( $f_n$ ) of the specimen was identified as the frequency which produces the maximum torsional amplification. The solenoid, which is connected to a function generator, excites the specimen in the torsional mode by imparting a transient pulse. Figure 4.2 shows the end caps with the positioning of the accelerometers and the solenoid. The torsional excitation of the specimen was measured by the accelerometers as a function of frequency. The summed voltage output from the accelerometers was passed through a PCB signal

conditioner (Model no. 482A22) and recorded by a dynamic signal analyzer (Coco-80). The Coco-80 dynamic signal analyzer has a dynamic input range of 150 dB, 8 input channels and a maximum sampling rate of 102.4 kHz. It also has an output feature with an SMB connector and 100 dB dynamic range

Vacuum was applied to one end of the specimen to provide positive effective stress. The specimen was then mounted in a free-free configuration on an assembly of two end plates and supporting rods. An acrylic tube is placed between the end plates. This arrangement represents a pressure cell and it is connected to an air pressure system (Figs. 4.3, 4.4). The effective confining stress ( $\sigma_o'$ ) is measured as the sum of the vacuum and applied cell pressure.

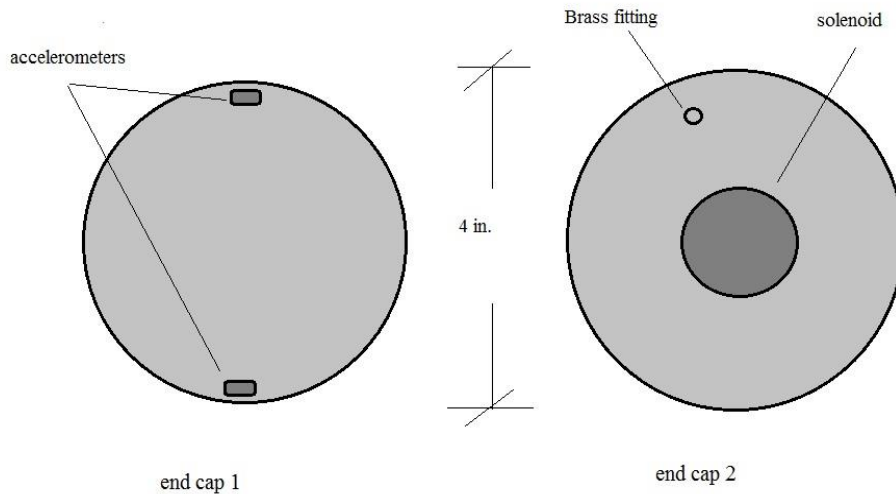


Figure 4.2 End caps of the specimen with their respective attachments

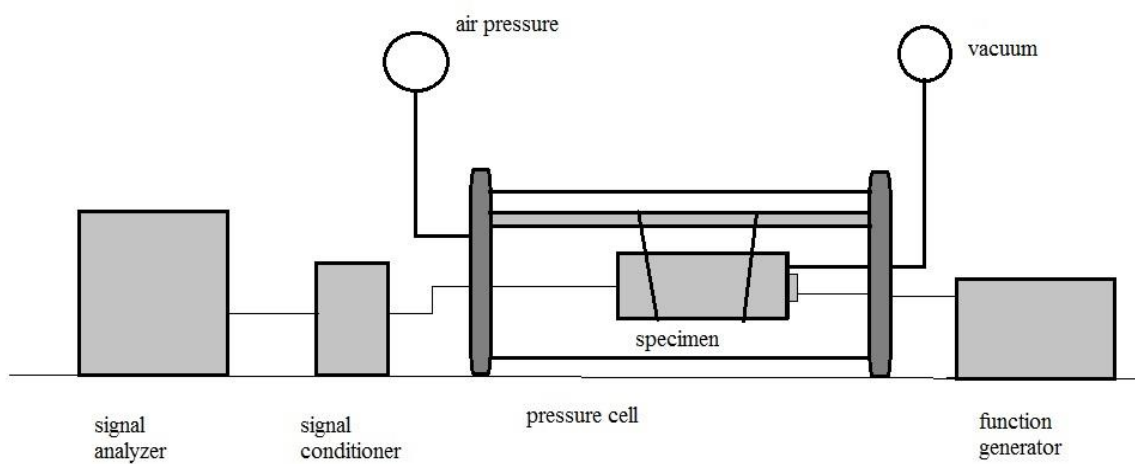


Figure 4.3. FFRC testing configuration

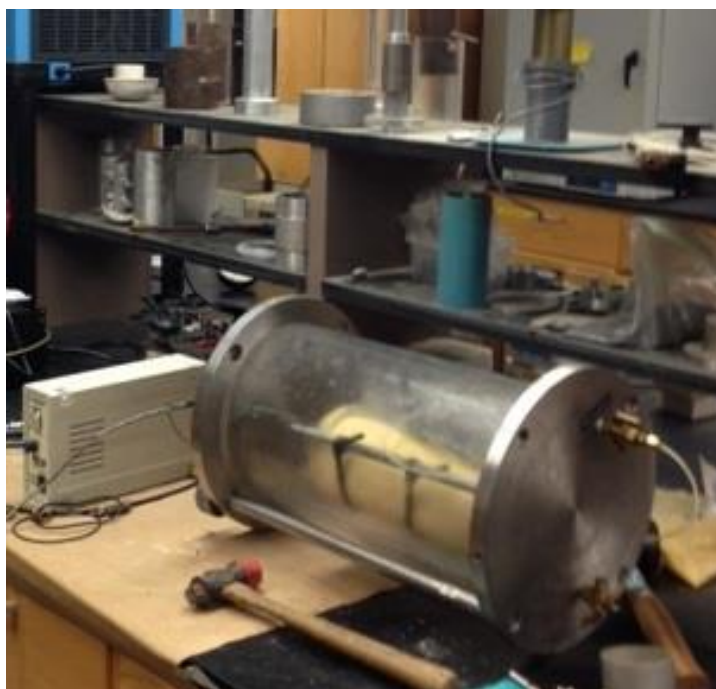


Figure 4.4 Lab test setup

### 4.3 Methodology

Kramer (1996) gave the following relationships between the length of the specimen ( $L$ ) and the polar moment of inertia of the Specimen ( $I$ ):

$$I / I_o = \beta \tan \beta, \quad (4.1)$$

And

$$\beta = 2\pi f_n L / V_s, \quad (4.2)$$

where  $I_o$  is the polar moment of inertia of the loading cap and the instruments attached to it.

For the free-free condition,

$$\tan \beta = (\mu_1 + \mu_2) \beta / (\mu_1 \mu_2 \beta^2 - 1) \quad (4.3)$$

Where,  $\mu_1 = I_1 / I$

and  $\mu_2 = I_2 / I$

And  $I_1$  and  $I_2$  are the polar moments of inertia of the masses attached to the ends of the specimen. Equation 4.3 is an implicit equation and can be solved iteratively to obtain  $\beta$ .

Unless  $I_1$  and  $I_2$  are not very small as compared to  $I$ , the observed resonant frequency of the specimen may be affected. For this reason, the end caps, porous stones and the electrical and torsional arrangement attached to them should be made of light material (Kalinski & Thummaluru, 2005). Assuming an average specimen mass of 3200 g, length ( $L$ ) of 22.86 cm and a specimen diameter of 4 in ( 10.16 cm ), the values of the polar moments of inertia

of the specimen ( $I$ ), end cap with accelerometers and porous stone ( $I_1$ ) and end cap with solenoid and porous stone ( $I_2$ ) have been calculated and presented in Table 4.2.

Table 4.2. Polar moments of inertia of the components of a typical test specimen

Object	Moment of inertia about the center of specimen (g-cm <sup>2</sup> )
End with accelerometers	2946.0
End with solenoid	2867.0
Soil specimen	41290.2

In this context,  $I_1$  and  $I_2$  are very small compared in comparison to  $I$ . From trial and error, Equation 4.3 is solved and the value of  $\beta$  comes out to be 2.76. Shear wave velocity is then determined by rearranging Eqn. 4.2:

$$v_s = 2 \pi f_n L / 2.76 \quad (4.4)$$

If the end cap assembly was sufficiently light then  $\beta$  would tend to  $\pi$  and Eqn. 4.2 would be simplified to:

$$v_s = 2 f_n L \quad (4.5)$$

In this particular testing scheme,  $f_n$  of the specimens under different stress levels is recorded and is used to compute  $v_s$  using Eqn. 4.4. The dynamic response of a site is characterized by stiffness of the soil which is measured by the small-strain shear wave velocity ( $v_s$ ) and small-strain shear modulus ( $G_{max}$ ). The relationship between these parameters is given by:

$$G_{max} = \rho V_s^2 \quad , \quad (4.6)$$

where  $\rho$  is the mass density of soil .

Shear-wave velocity is known to increase with effective confining stress ( $\sigma'_o$ ) and is roughly proportional to the fourth root of  $\sigma'_o$ . The variation in  $v_s$  for the all the mixtures was studied over a pressure range of 17 kPa to 300 kPa. The test results could thus represent the shear-wave velocities of in-situ gypsiferous soils.

#### **4.4 Testing procedure**

##### **4.4.1 Dry soil testing using cell pressure**

Once a specimen was prepared, a vacuum of 17 kPa was applied to support the system. It was then mounted on the rods between the end plates. The acrylic cell was then introduced between the end plates and the arrangement was made air-tight by using o-rings and vacuum grease. At this point, the specimens were ready to be tested. Using the manual trigger operation of the function generator, a voltage pulse was sent to the solenoid. The torsional excitation of the specimen measured by the accelerometers was recorded as a time-domain signal using the Coco-80 dynamic signal analyzer. The analyzer converted the time-domain signal into a frequency domain signal or auto-power spectra (APS) using Fourier analysis (Fig. 4.5). The resonant frequency ( $f_n$ ) was identified from the APS. The setup and configurations of the function generator and dynamic signal analyzer required for conducting the tests are given in Appendix A.

Initial tests were performed using only vacuum and  $f_n$  was identified at 17 kPa, 34 kPa and 58 kPa. As it was not possible to attain a vacuum greater than 58 kPa, pressurized air was introduced into the cell to create confining pressure. As such, the effective stress acting on the specimen would be the sum of vacuum and confining pressure (Kalinski & Thummaluru, 2005). After the application of cell pressure,  $f_n$  was measured at the following effective stresses: 85kPa, 105 kPa, 130 kPa, 160 kPa, 200 kPa, 230 kPa, 260kPa and 300

kPa. Once tested at a particular stress, the pressure was increased gradually to the next level and the specimen was allowed to stand for five to ten minutes before measurement was performed. This was done in order to ensure a uniform distribution of stress. To be consistent, the void ratio of all the specimens was kept close to 0.55. A typical soil specimen was 4.0 inches in diameter, 9.0 inches in length and weigh around 3200 g. Figures 4.6-4.13 show the  $v_s$  of the different soils plotted against  $\sigma'_o$ . Seven different soils were set for testing.

After testing a particular soil, the air pressure was gradually reduced and turned off. The acrylic cell was removed and the specimen was dismantled after removing the vacuum. The membrane was changed every time before starting the test with a different mixture.

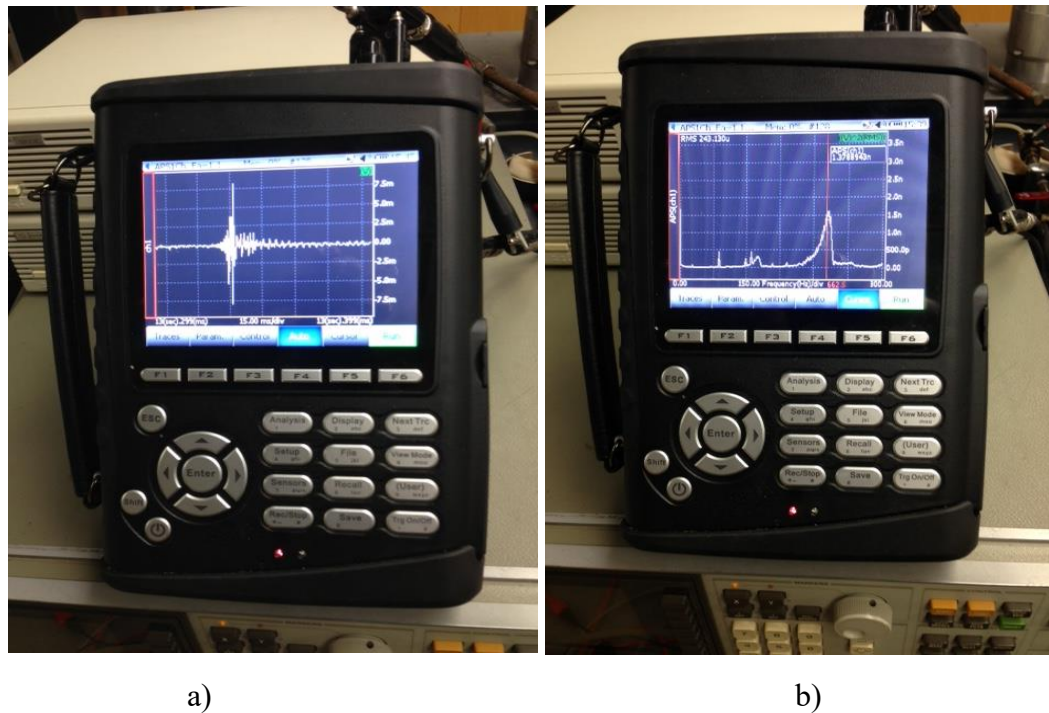


Figure 4.5. Dynamic signal analyzer showing the a) time-domain b) frequency domain spectra

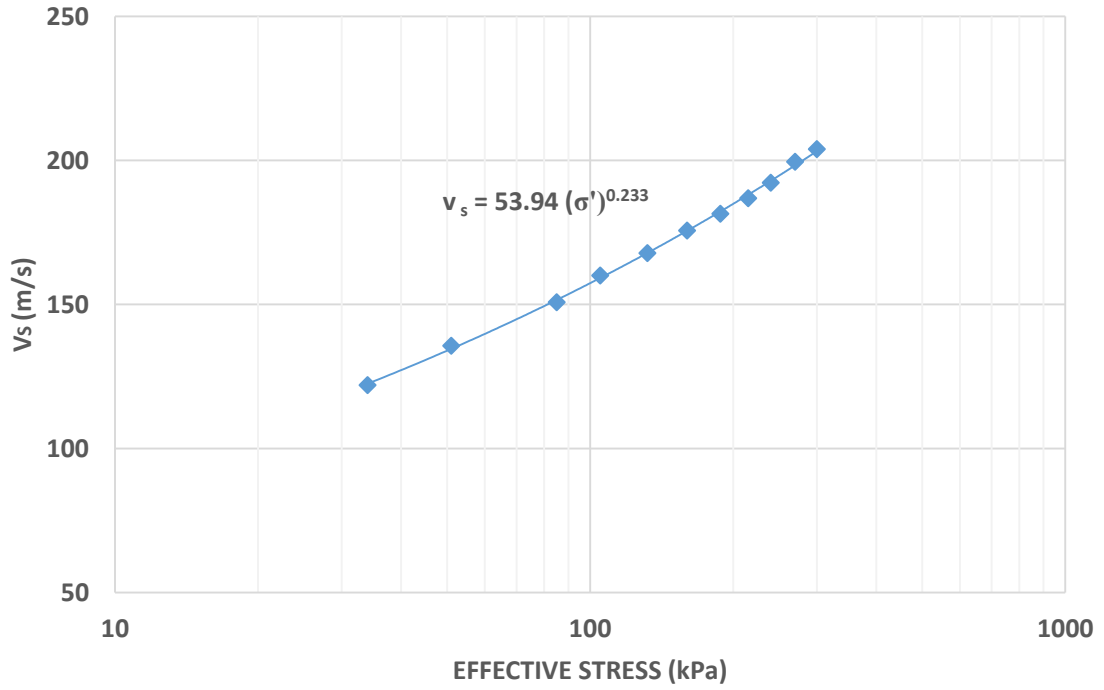


Figure 4.6 plot of  $v_s$  versus  $\sigma'_o$  for M0 (0 % gypsum), dry

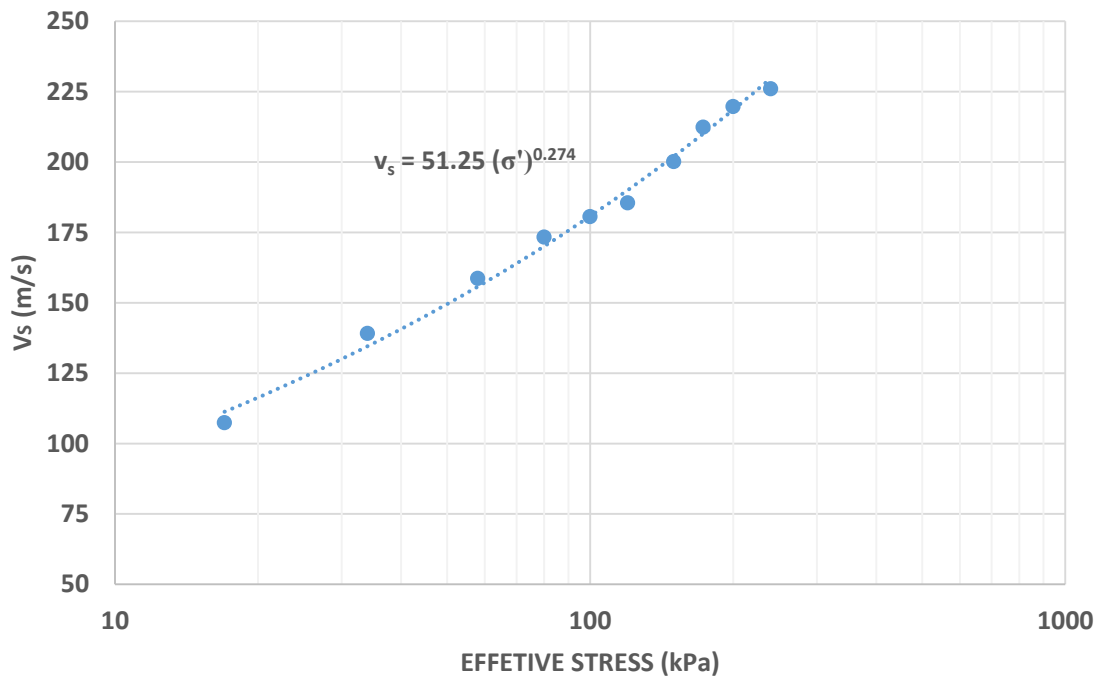


Figure 4.7 plot of  $v_s$  versus  $\sigma'_o$  for M10 (10% gypsum), dry



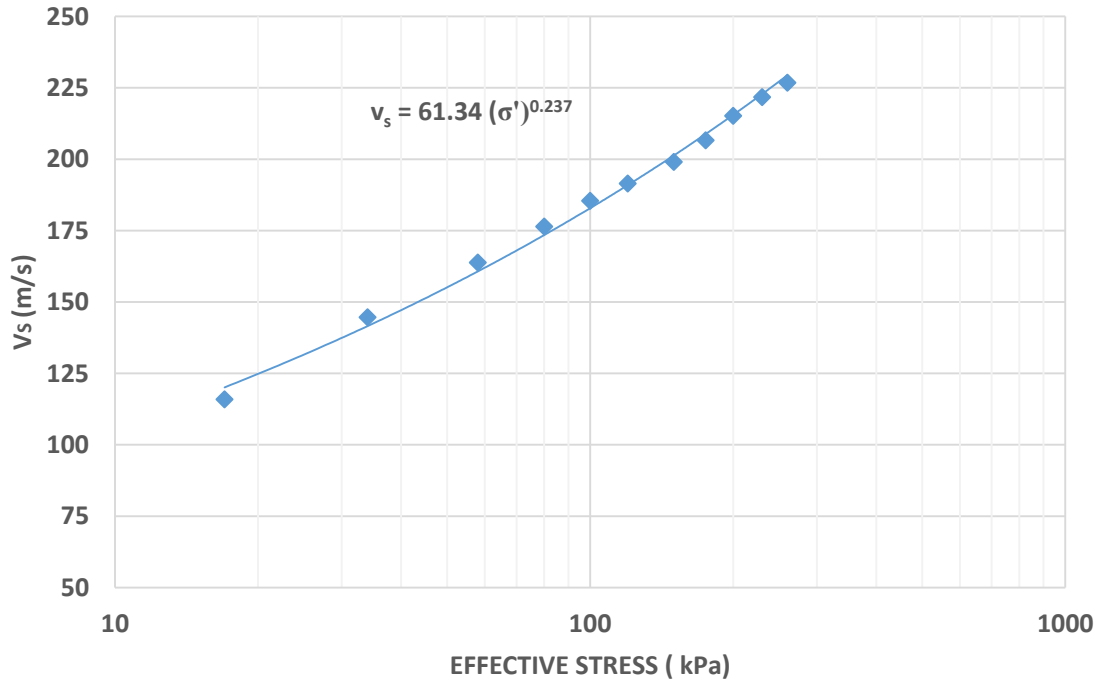


Figure 4.8 plot of  $v_s$  versus  $\sigma'_o$  for M20 (20% gypsum), dry

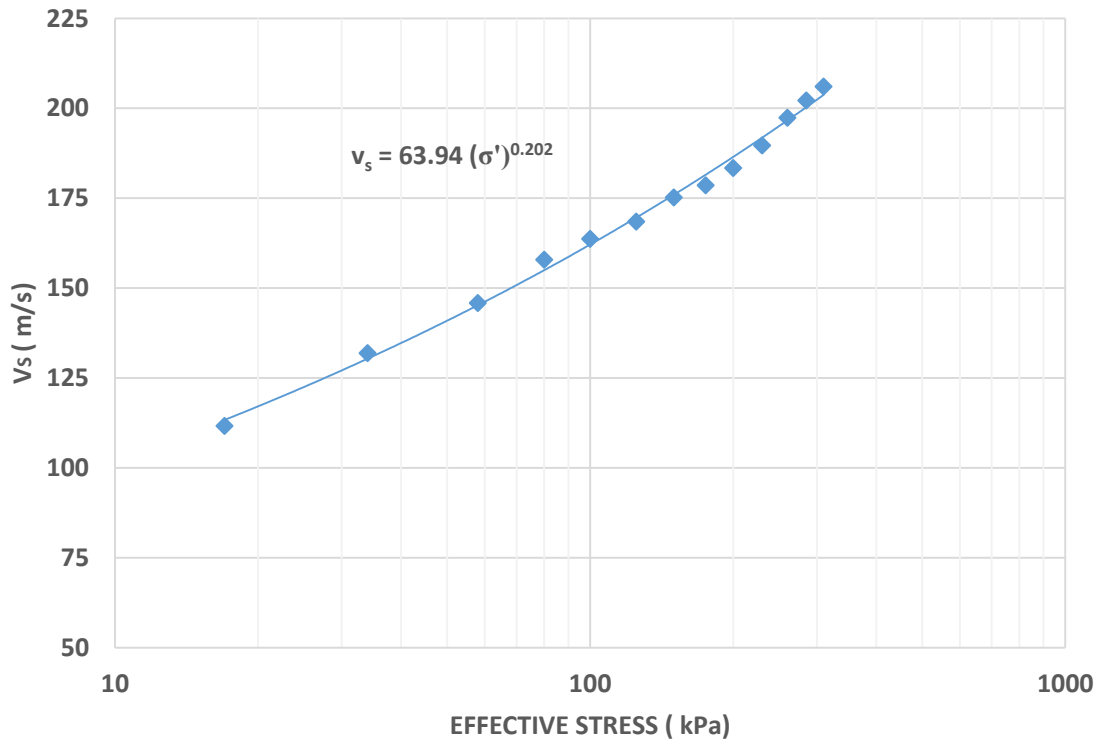


Figure 4.9 plot of  $v_s$  versus  $\sigma'_o$  for M30 (30% gypsum), dry

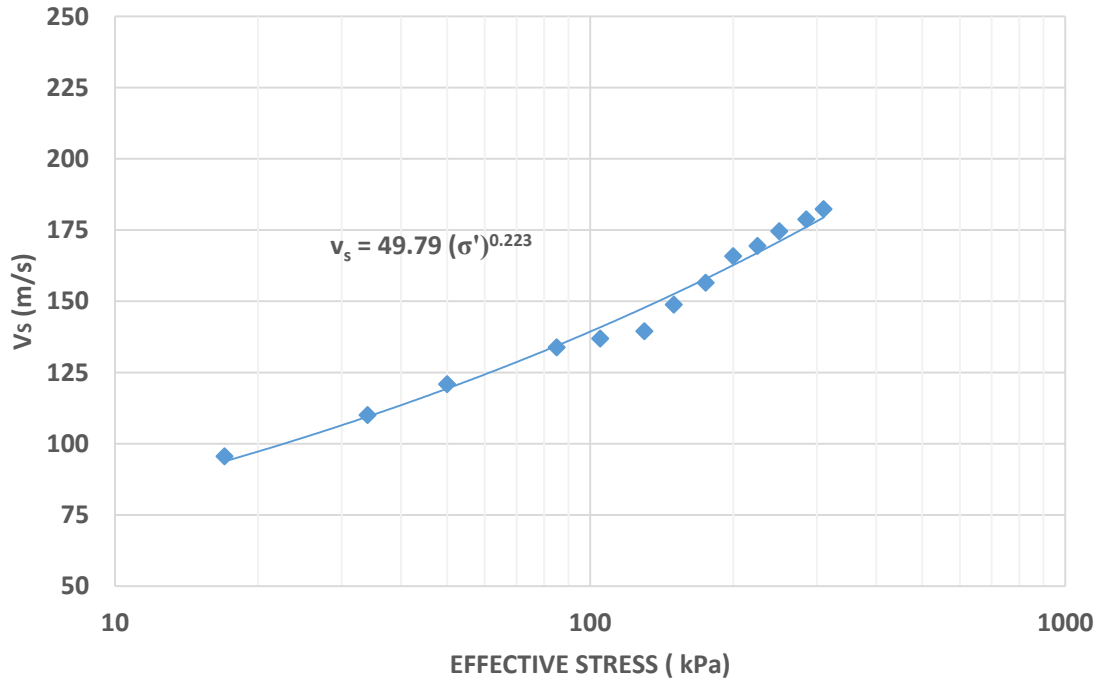


Figure 4.10 plot of  $v_s$  versus  $\sigma'_o$  for M40 (40% gypsum), dry

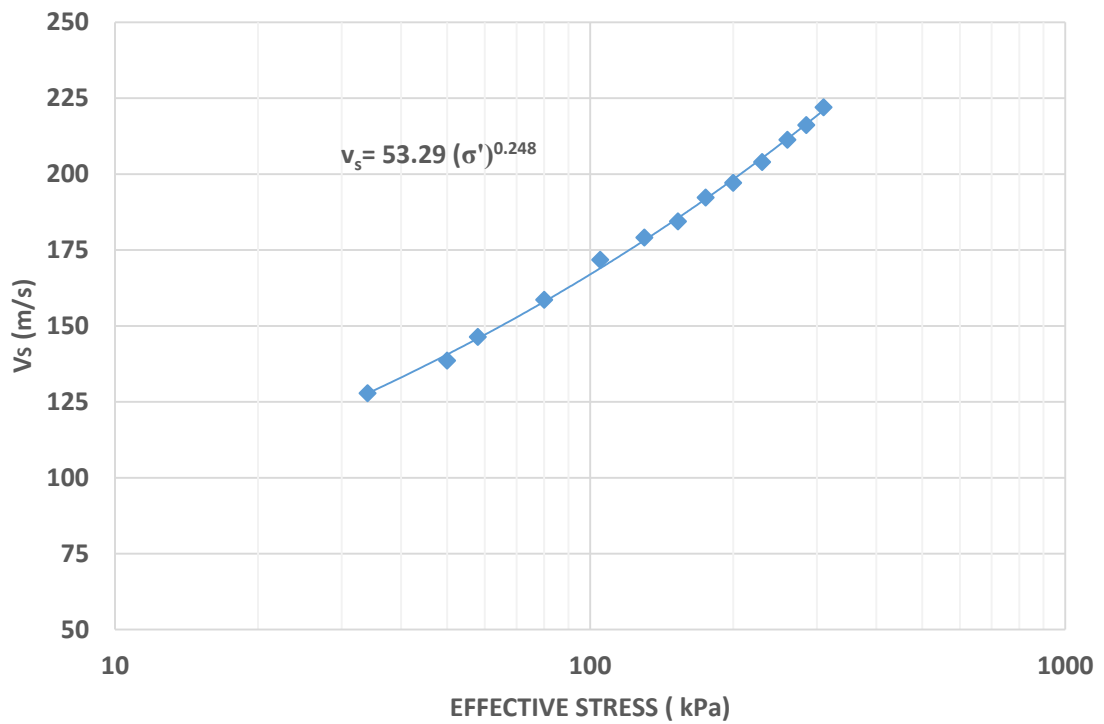


Figure 4.11 plot of  $v_s$  versus  $\sigma'_o$  for M50 (50% gypsum), dry

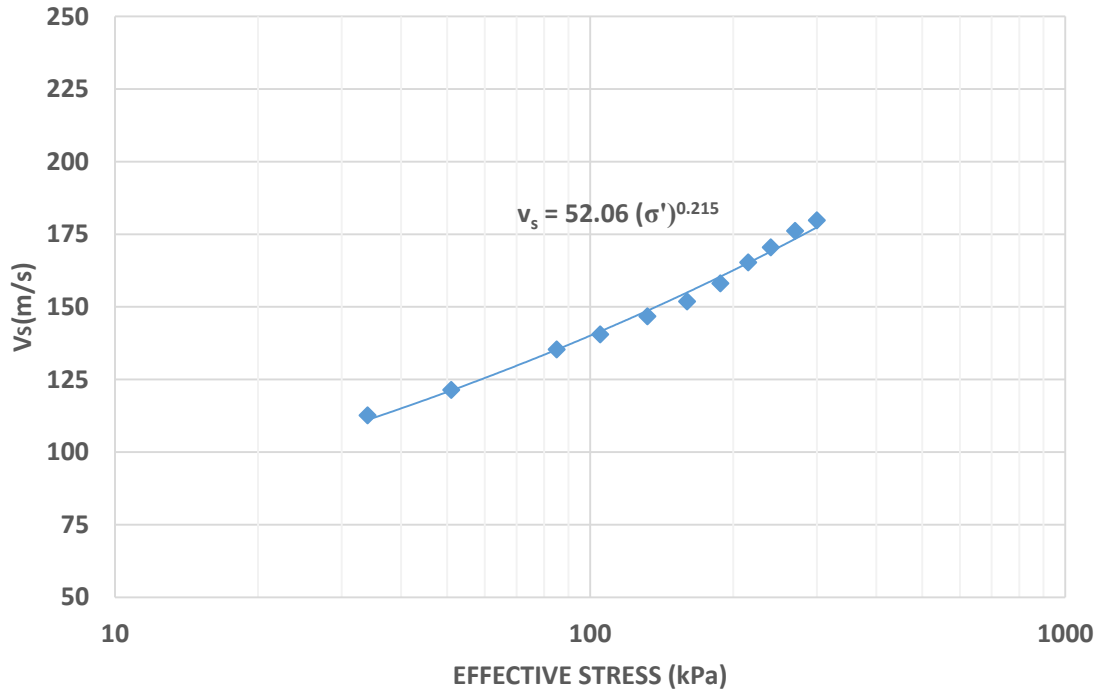


Figure 4.12 plot of  $v_s$  versus  $\text{Log } \sigma'_o$  for M100 (100% gypsum), dry

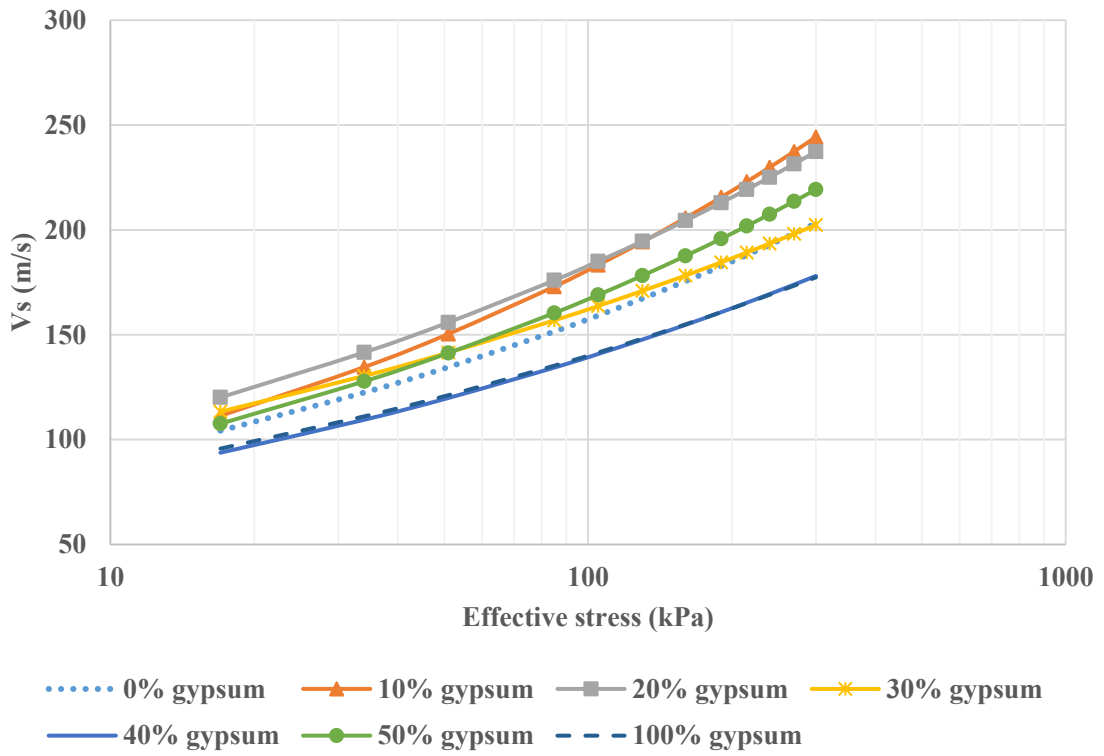


Figure 4.13 Comprehensive plot showing the best-fit  $v_s$  versus  $\sigma'_o$  curves for all the soils

#### 4.4.2 Tests on moist soils

After conducting free-free resonant column tests on dry gypsum soils, a series of tests was conducted to study the effect of moisture on the stiffness of gypsum sands and cementation effects. Specimens were initially prepared in a manner identical to the previous testing regime. A 58 kPa vacuum was applied and the resonant frequency of the dry specimens was measured. Once the measurement was taken, the specimen was dismantled and the vacuum was reduced to 17 kPa. The specimens were still intact under the lower vacuum and were seated in an upright position. Under this arrangement, water was permeated through the bottom of the specimens. Figure 4.14 shows the arrangement for saturating the specimens. The vacuum pipe was passed through a vacuum trap to ensure that no water escapes into the system in the process of saturating the soil.

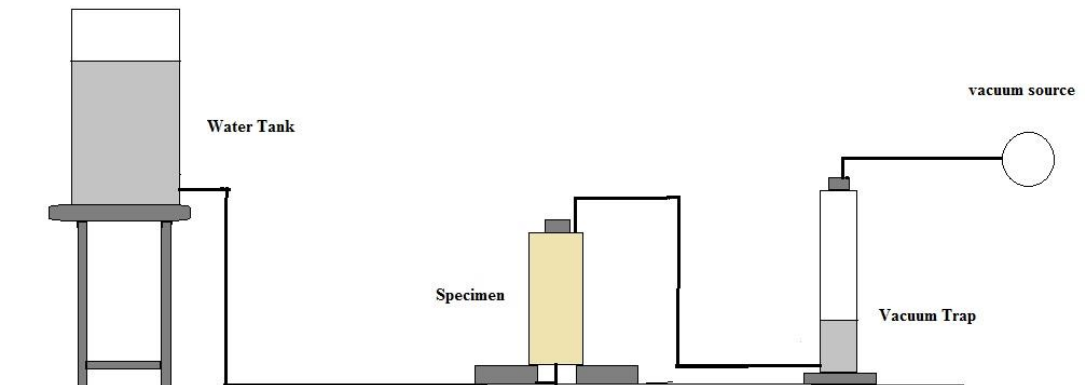


Figure 4.14 Assembly to saturate the soil specimens

Once no further increase in weight was observed, the specimen weight was noted and it was mounted back on the resonant column test apparatus. Degree of saturation,  $S$ , was estimated using the relation:

$$S = G_s w / e \quad (4.7)$$

Where  $w$  is the water content and  $e$  is the void ratio.

Five soils were tested with gypsum content ranging from 0% to 40%. No cell pressure was used in this test because of the difficulty in assembling the acrylic cell around the water pipes. As such, testing was carried out at 58 kPa gauge vacuum. The vacuum would draw water out of the specimen, also aiding the change in moisture content. Clear resonant peaks could be obtained from saturation level below 85%. As the saturation decreased, the resonant frequency of the specimens increased.

Measurements of resonant frequency were taken at varying degrees of saturation. The vacuum could only reduce the saturation to up to 50%. Beyond this point pressurized air was used to decrease the moisture content. The specimens would be dismounted and low pressure air (approx. 13 kPa) was passed through one end of the specimen while the other end would be kept open. This arrangement ensured the reduction of moisture content without disturbing the specimens. Decrease in saturation was calculated by change in weight of the specimen before each measurement. The shear wave velocity was plotted against the degree of saturation for each specimen. Five soil specimens with 0%, 10%, 20%, 30% and 40% gypsum were originally tested. Another soil sample with 60% gypsum was tested subsequently to validate some trends predicted from the previous tests. Figures 4.15 - 4.21 show  $v_s$  of the different soils plotted against  $S$ .

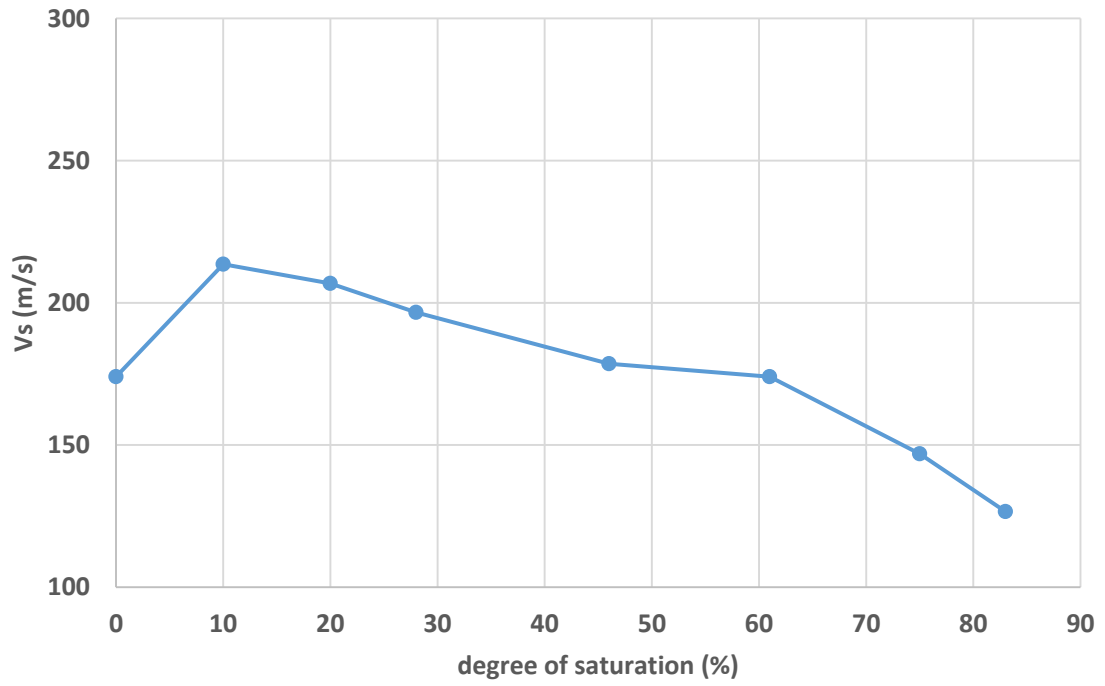


Figure 4.15 Plot of  $v_s$  versus degree of saturation (S) for M0 (0 % gypsum) at 58 kPa

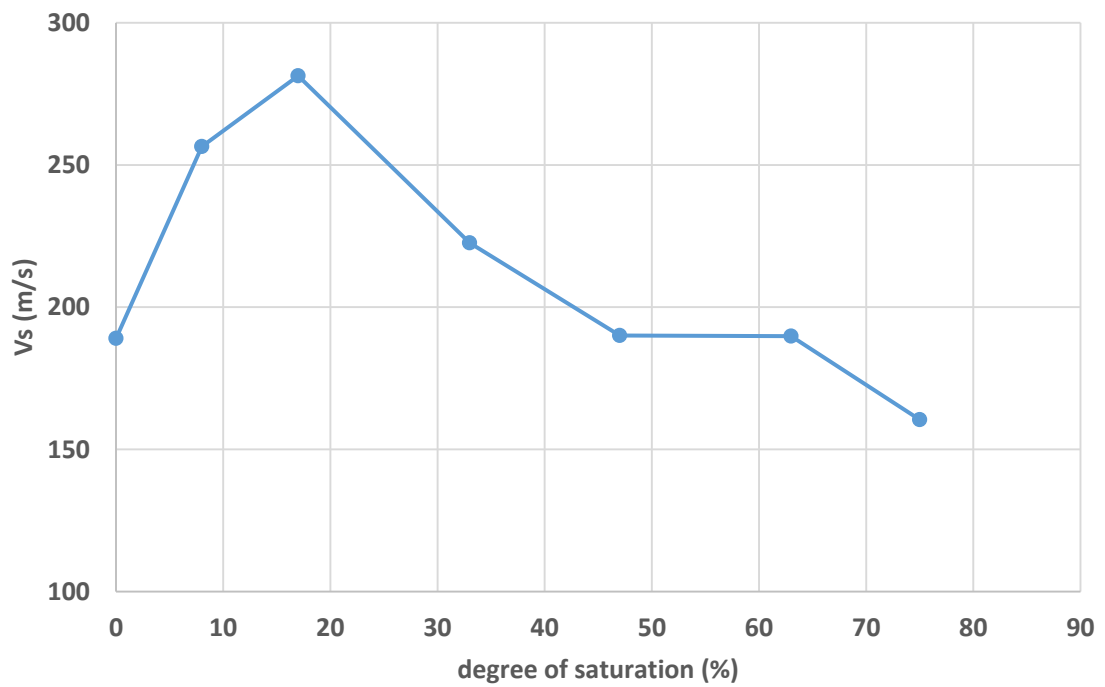


Figure 4.16 Plot of  $v_s$  versus degree of saturation (S) for M10 (10% gypsum) at 58 kPa

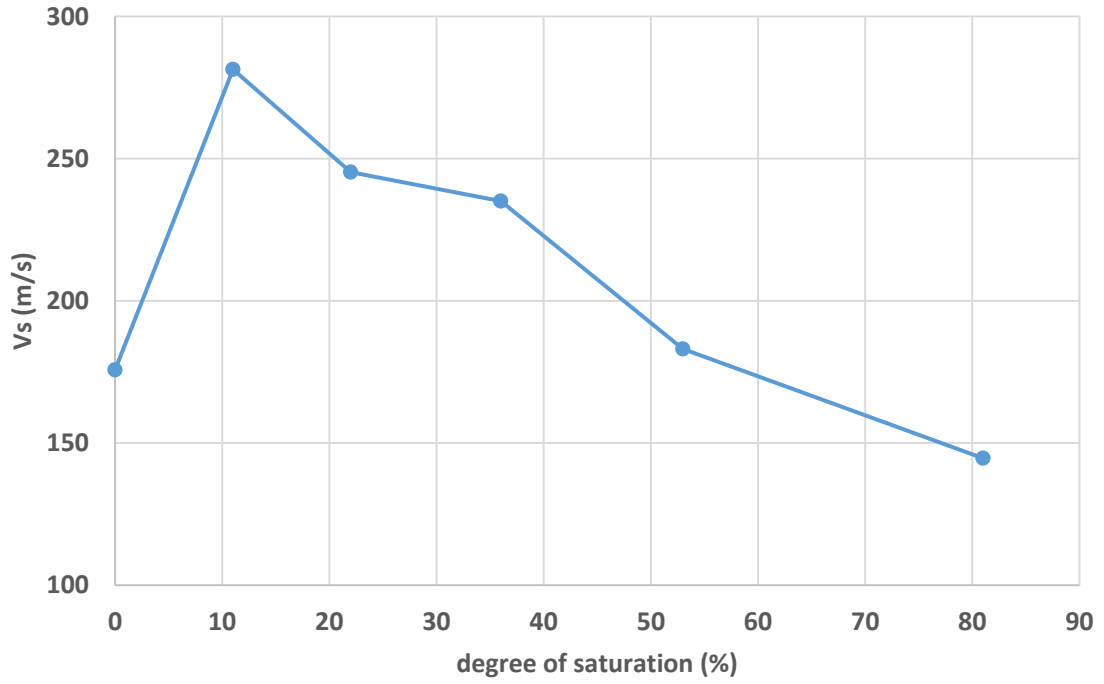


Figure 4.17 Plot of  $v_s$  versus degree of saturation (S) for M20 (20% gypsum) at 58 kPa

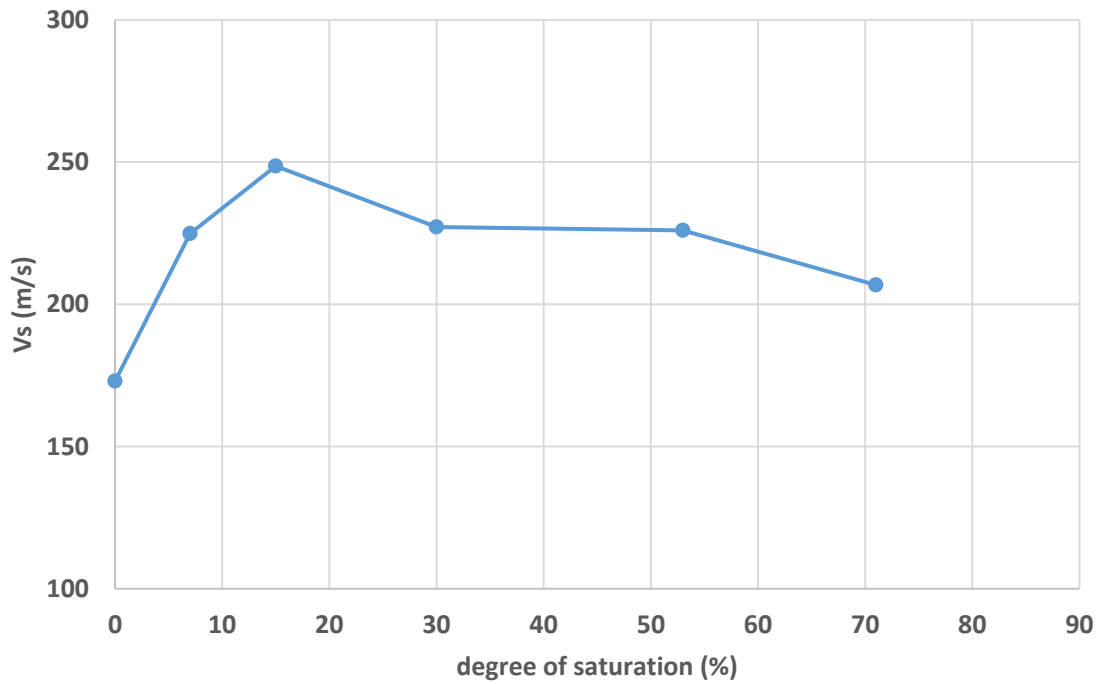


Figure 4.18 Plot of  $v_s$  versus degree of saturation (S) for M30 (30% gypsum) at 58 kPa

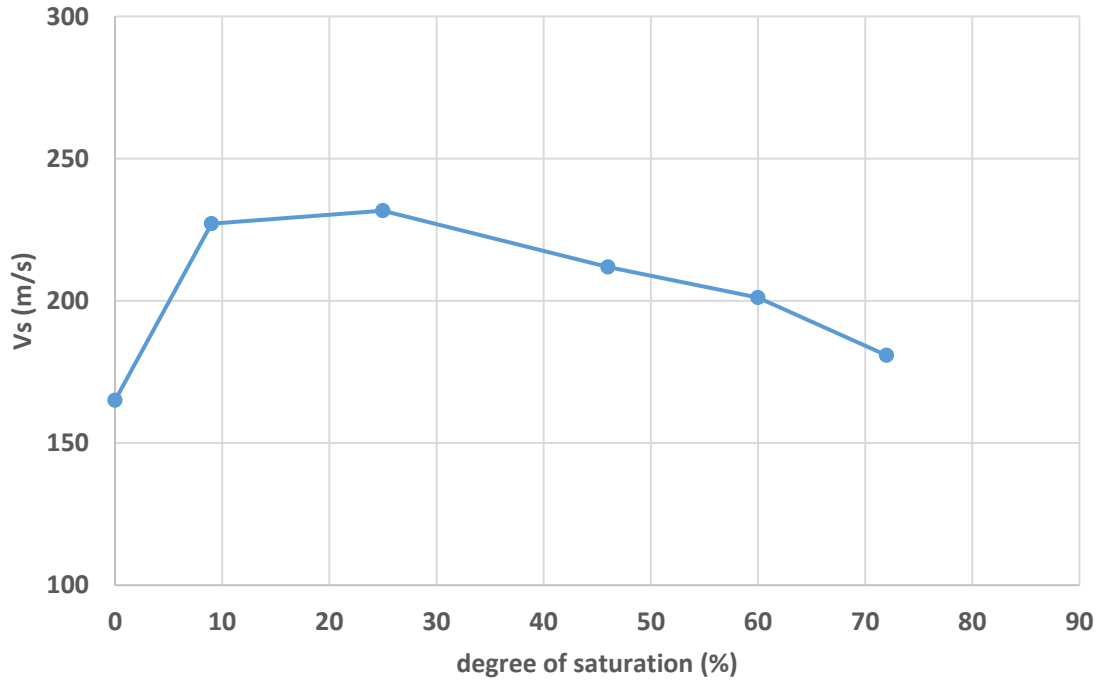


Figure 4.19 Plot of  $v_s$  versus degree of saturation (S) for M40 (40% gypsum) at 58 kPa

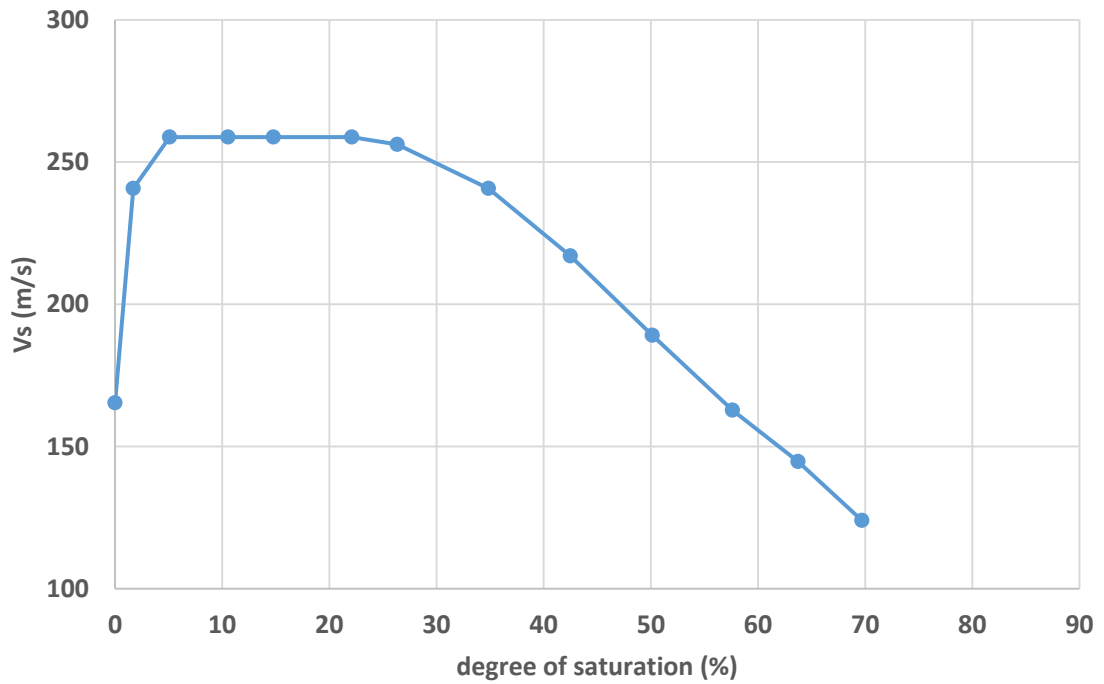


Figure 4.20 Plot of  $v_s$  versus degree of saturation (S) for M60 (60% gypsum) at 58 kPa



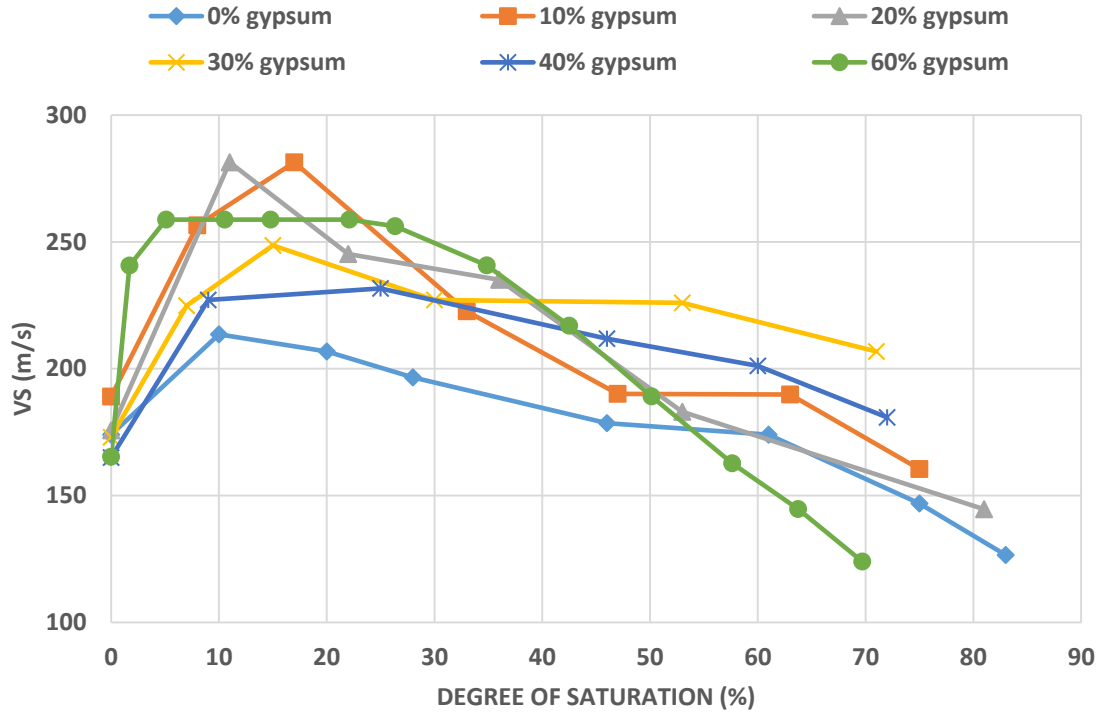


Figure 4.21 Comprehensive  $v_s$  versus  $S$  plot for all soils tested at 58 Kpa

#### 4.4.3 Testing moist soils using cell pressure

After performing resonant column tests on moist soils using 58 kPa of vacuum, two additional tests were performed on moist sands with the addition of cell pressure. These tests were performed in order to study the influence of cell pressure on the shear wave velocities of moist soils. In other words, the tests were carried out to verify whether an increase in effective stress would still yield similar looking  $v_s$  versus  $S$  profiles. In addition to the 58 kPa of vacuum a cell pressure of 69 kPa was used leading to an effective stress of 127 kPa. The same acrylic pressure cell arrangement was used as in the dry soil testing scheme.

This test however had two major limitations. First it was difficult to run a water tube through the pressure cell to wet the soil specimen. Degree of saturation would change

considerably in the process of assembling the pressure cell and making the pressure connections before the actual measurements could be taken. Secondly, the cell had to be dismantled once in a while to note the change in the weight of the specimen to estimate the degree of saturation. Because of these limitations, the test was discontinued after testing two specimens of soil specimens with 0% gypsum and 30% gypsum. A pair of measurements were taken each time, one at 127 kPa (with cell pressure) and one at 58 kPa (without cell pressure). Some meaningful results were however obtained from the two tests. Figures show the plots obtained from these tests. The figures show variations in  $V_s$  with  $S$  with and without using cell pressure.

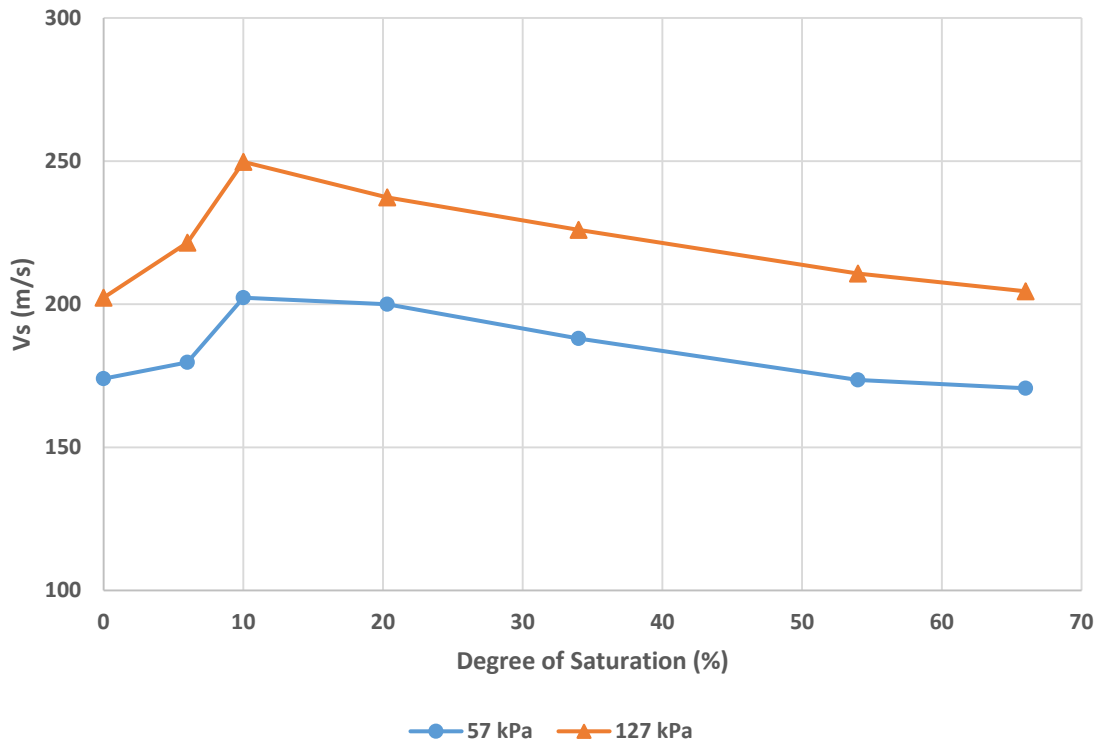


Figure 4.22 Plot of  $v_s$  versus  $S$  for 0% gypsum specimen at two different confining stresses

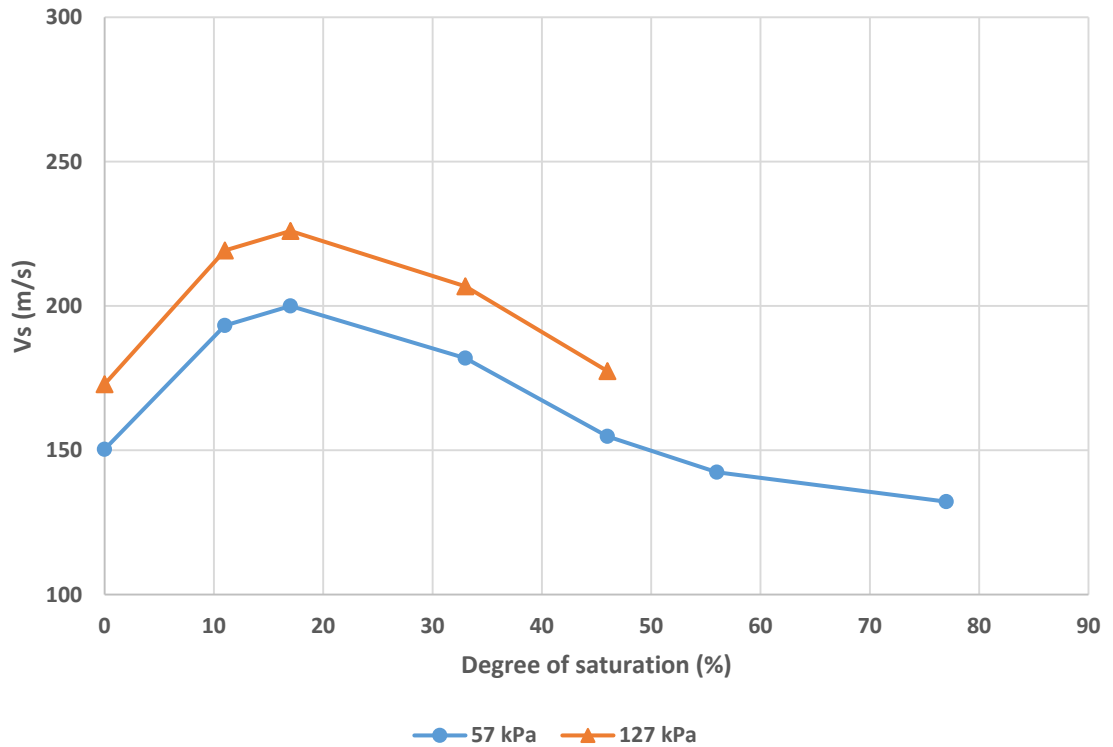


Figure 4.23 Plot of  $v_s$  versus  $S$  for 30% gypsum specimen at two different confining stresses

#### 4.5 Results

For the dry soil testing, mixtures M10-M50 were tested first, followed by M100 and finally M0. Each mixture was tested over a period of three to four days and the process involved specimen preparation, testing under vacuum, testing under cell pressure, dismantling and result analysis. The variation of  $v_s$  with  $\sigma_o'$  was plotted for each specimen. A power curve (with an  $R^2$  of almost 0.99) was fitted through the different data points. These plots are shown in Figures 4.6 - 4.13.

It was observed from the results that  $v_s$  initially increases very rapidly with stress and thereafter slows down beyond a certain stress level, for all the specimens tested. Mixtures M10 and M20 (with 10% and 20% gypsum content respectively) had the highest shear-wave velocities under the given testing conditions (ranging from 150 m/s to 210 m/s).

This showed that quartz sand with 10 to 20 percent gypsum content had the highest stiffness of all the mixtures tested. Shear wave velocity decreased as gypsum content increased beyond 30%. The stiffness of soil samples at higher gypsum contents was lower and the specimen made up 100% gypsum showed the lowest stiffness. Shear wave velocity of the specimens was found to be nearly proportional to the fourth root of  $\sigma'_o$  (the exponential term varying between 0.21 -0.25). To ascertain this trend of stiffness variation in gypsum soils, another set of tests was later performed on five soil samples with gypsum content ranging from 0%-75%. No cell pressure was used in these tests. The results of the test are shown in Fig. 4.24. The results of these tests were comparable to the earlier results and serve to confirm that stiffness of the specimens was higher at gypsum contents of 10%-30%.

It was also noticed that, with more gypsum content, the specimens could be compacted to slightly lower void ratios. This was due to the crushing of gypsum particles under the applied compaction effort. But the dry density and stiffness values still remained lower because of the lower specific gravity of gypsum as compared to quartz.

In the tests involving moist soils it was seen that  $v_s$  increased rapidly with decrease in saturation. Shear wave velocity was lowest at moisture levels close to saturation. This trend followed till a saturation of about 50% beyond which no further moisture could be removed by the vacuum system. Between saturations of 50%-30% the rate of increase in  $v_s$  was somewhat slow. It would then sharply increase peaking at saturations of 10%-20%. When the saturation was further lowered, the soil would start to break apart, disturbing the specimens significantly. The testing would thus be discontinued below  $S = 8\%$ . The plots

of  $v_s$  versus  $S$  for all the specimens tested is shown in Figures 4.15-4.21. Figure 4.21 shows the comprehensive  $v_s$  versus  $S$  plot for all five soils tested.

It was also observed that at low saturations, soils with 10% and 20% gypsum exhibited the highest  $v_s$ . Shear wave velocity as high as 290 m/s were measured at these specific moisture and gypsum combinations. The trends point towards an increase in stiffness of the specimens with decreasing moisture content. Matric suction is the main factor which contributes to the increase in stiffness of the soils at low moisture content. Cementation between the gypsum and quartz particles also enabled the increase in stiffness of the specimens as the water content was decreased. This aspect was observed in the dismantled specimens where the soil mass still maintained the cylindrical shape even after turning off the vacuum and drying the specimens. Both these factors tend to outweigh each other at different gypsum concentrations. Matric suction appeared to be the dominating factor at low gypsum contents as inferred by the distinct peaks in the curve. As the gypsum content was increased, cementation effect was more dominant and the peak became smaller and less distinct. To further verify this aspect, another specimen with 60% gypsum was tested at a later point. As predicted, it was found that below a certain moisture level, the soil stiffness was almost constant. Even at very low values of  $S$ , the specimen was steady and had a constant value of  $v_s$ . The specimen was very stiff even after dismantling (Fig. 4.25), pointing towards a high level of cementation and crete formation as described in Chapter 1.

Finally the tests on moist soils using cell pressure showed an increase in  $v_s$  with increase in effective stress. The trend was however identical to that obtained in the case of soils without cell pressure. Figures 4.22-4.23 illustrate this trend. It can be seen that the

profiles for both soil types are the same, the addition of cell pressure causing the original profile to shift upwards. This seems reasonable because of the fact that  $v_s$  increases with increase in effective stress.

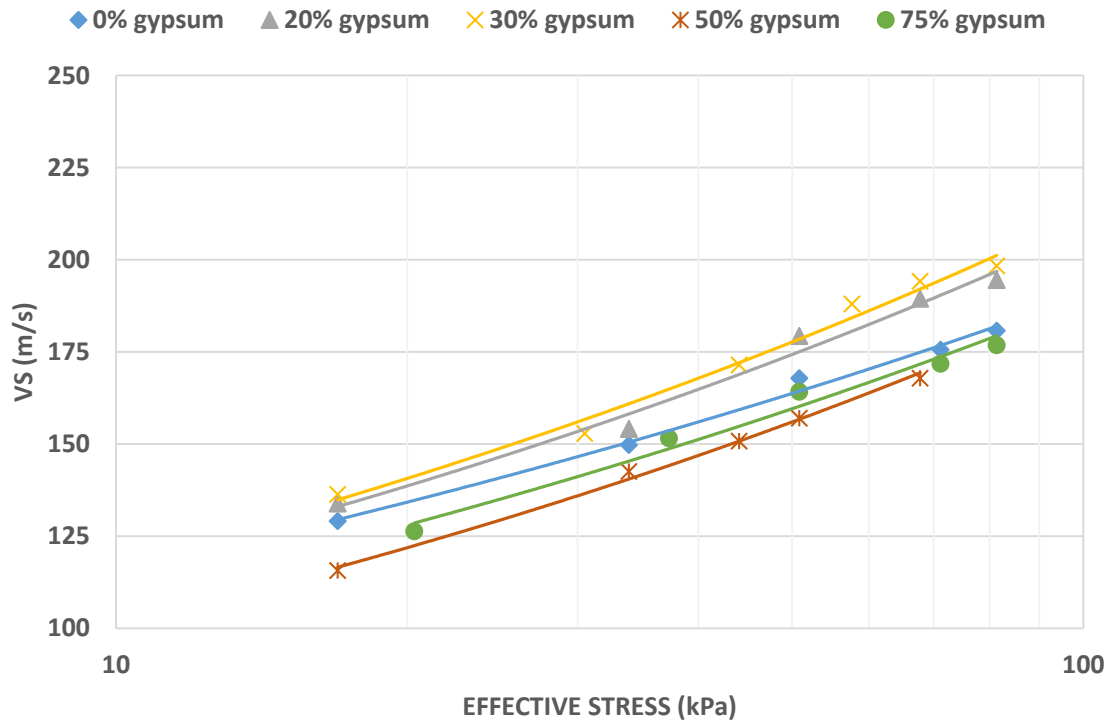


Figure 4.24 Comprehensive plot of  $v_s$  versus  $\sigma_o'$  curves for the dry soils tested without cell-pressure

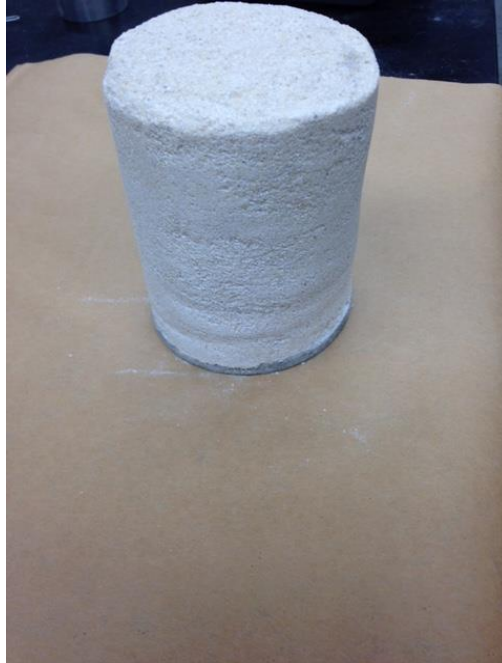


Figure 4.25 Dismantled specimen with 60% gypsum content

#### 4.6 Conclusion

Free-free resonant column testing on reconstituted gypsum soils led to some useful conclusions. The tests on dry soils using cell pressure showed that stiffness of gypsiferous sands ( $v_s$ ) increases with increasing confining stress. The increase in shear wave velocity was roughly proportional to the fourth root of confining pressure. This result was in agreement with the results of Kalinski and Thummaluru (2005), wherein free-free resonant column testing was used to measure the stiffness of dry Ottawa sand over a range of confining stresses. Figure 4.26 compares the results of Kalinski and Thummaluru (2005) with that of a soil specimen used in this research. The shear wave velocity values also compare with Cha and Cho (2007), where bender elements tests were used to estimate the shear wave velocity of sandy soils acquired from three different harbor construction sites in Korea, tested under varying void ratios.

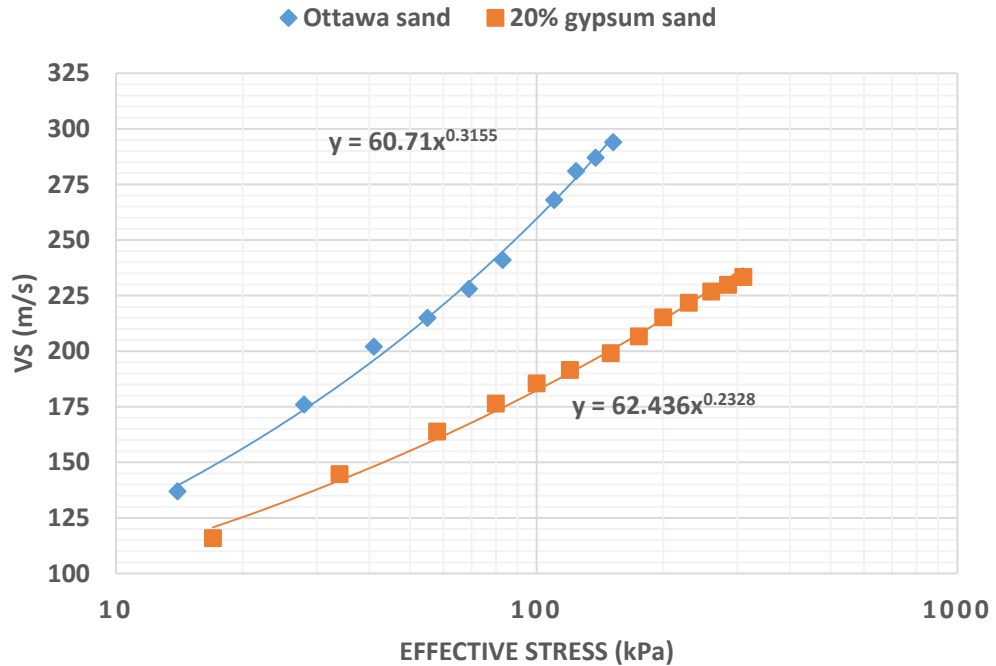


Figure 4.26. Comparison of  $v_s$  versus  $\sigma_o'$  between Ottawa sand (Kalinski & Thummaluru, 2005) and 20% gypsum sand

The test results indicate that quartz with 10-30% gypsum has the maximum stiffness, which is lost with increasing gypsum content. The observations are consistent with reported test results conducted on natural soils where the addition of about 10 to 30 percent gypsum increases the shear strength of soil (measured in terms of cohesion ( $c$ ) and angle of internal friction ( $\phi$ )) (Al-Marsoumi et al., 2006 ; Al-Marsoumi et al., 2008). This behavior could be attributed to the softness of gypsum and the contact between the quartz and gypsum particles. At lower gypsum contents, the quartz particles are still in contact with each other and gypsum occupies the interstitial void spaces and increases the overall stiffness of the material. As the gypsum content increases beyond a certain level (in this case, 30 %), the quartz particle contact starts reducing leading to a decrease in the material stiffness.



Gypsum has a lower specific gravity (2.32) than quartz (2.65). As such, when the proportion of gypsum in soils is high, the lower specific gravity of gypsum becomes a dominant factor and the soil stiffness would be lower. This aspect has been confirmed by testing a pure gypsum specimen which yielded the lowest  $v_s$  profiles among all the mixtures tested. The  $v_s$  values obtained for each of the specimens were representative of typical in-situ shear wave velocities of soils, which vary between 130 m/s to 400 m/s (SCDOT, 2008).

In the case of moist gypsum sands mixtures, the stiffness of the samples increased with decreasing moisture content. When the gypsum content was lower, matric suction becomes the primary factor which leads to an increase in stiffness of the samples. As such, soils with lower gypsum content were found to be the stiffest of all the soils tested at low degrees of saturation. At higher gypsum contents, matric suction was countered by cement hydration reaction brought about by the water, causing more gypsum particles to bond with quartz. The profiles of soils with 40% and 60% gypsum show that cementation becomes the dominating factor at higher gypsum concentrations and the influence of moisture and matric suction becomes insignificant. This behavior is explained by the apparent ‘plateauing’ of the  $v_s$  versus  $S$  curves for M40 and M60 at degrees of saturation below 35%. This was also verified from the fact that for the same effective stress (58kPa), the stiffness of the moist soils were much higher than those of dry soils. These results are in agreement with Qian et al. (1991) where it was shown that the shear modulus of partially saturated subrounded and angular sands was maximum at a degree of saturation of 10%-20%. The influence of matric suction on shear modulus was also more pronounced at lower confining stresses.

Lastly, the results from the two resonant column tests on moist specimens showed that stiffness of moist soils increased with increase in effective stress but the nature of the profile itself was not dependent on the confining stress. It is the amount of gypsum in the soil which determines the stiffness change of a soil under varying moisture levels. It can be concluded that 10%-20% is the optimum gypsum content to induce appreciable stiffness into the soil.

These results could be used as a basis for conducting non-destructive surface geophysical tests, to measure the in-situ  $v_s$  of soils in places where the engineering properties of gypsiferous soils are of concern. They can also be correlated with known geotechnical parameters of soils such as shear strength at places where adequate data or measurements are not available.

## **5. Laboratory Geotechnical Tests on Reconstituted Gypsum Soils**

### **5.1 Introduction**

Geotechnical testing of gypsum-sand mixtures was an important part of the research study. Gypsum soils are known to be complex engineering materials and it is essential to have a good understanding of the geotechnical properties of these soils in order to predict the engineering risks that might be associated with them in the field. The tests used in this research were mainly those which were applicable to coarse grained soils. These include direct shear strength test, grain size analysis, specific gravity tests, collapse potential testing and dissolution. The first three tests are discussed in this chapter whereas collapse potential tests and dissolution are described in the next chapter.

The direct shear strength test (ASTM D3080) is a very widely used method to determine the shear strength properties of granular soils. The test is specifically used to look at the friction angle ( $\phi$ ) and cohesion intercept ( $c$ ) of granular soils under conditions of drained loading. For granular soils, cohesion is typically very low. Due to the inherent difficulty in preparing specimens of cohesionless soils for triaxial testing, direct shear strength test is chosen as an alternative. Shear strength is used to estimate the bearing capacity of foundations and also used to assess the stability of earth slopes and retaining structures (Kalinski, 2006). The test was conducted for this study using a computer controlled direct shear machine (Geocomp Shear trac II) shown in Figure 5.1.

Gypsum is known to be a cementing agent in soil fabric. The cementing action comes into play when the soil comes in contact with water. In a typical cement hydration reaction, the calcium component of gypsum enables the formation of a calcium-silicate-

hydrate compound which is a strong amorphous material. It is usually present in cement rich materials like mortar and concrete. As such, in-situ gypsum soils can possess some degree of cohesion as opposed to pure quartz which has negligible cohesion.

Haeri et al. (2005) studied the mechanical properties of gypsum -cemented gravelly sand which was used to resemble alluvial soils of Tehran, Iran. The cement content varied from 1.5% to 6.0%. Triaxial tests were conducted on the soils and gypsum was used as the cementing agent. It was found that the cemented sands showed a brittle failure pattern indicating the brittle nature of gypsum as a cementing agent. They also noticed that friction angle increases slightly and the cohesion intercept increases significantly with an increase in cement content. A series of tests were conducted to see the impact of gypsum concentration on shear strength parameters of the test soils. Al-Marsoumi et al. (2008) investigated the mechanical properties of six gypsiferous sandy soil samples collected near Basrah in southern Iraq. Unconfined compression tests and triaxial tests were performed on these samples and it was found that both the cohesion and the internal friction angle increase with the addition of gypsum and attained a peak at a gypsum content of about 30%. This displays the dual role of gypsum as a cementing agent at lower concentrations and a dispersing agent at higher concentrations. Leaching contributes to loss of gypsum thereby decreasing the shear strength parameters.

The specific gravity of the gypsum-sand mixtures and grain size analysis were also additionally performed on the soil samples that were used for the research. Specific gravity ( $G_s$ ) determination is important in geotechnical engineering problems as it has a significant effect on the unit weight of soils. Grain size analysis helps in classification of soils and

helps predict their engineering characteristics like hydraulic conductivity, friction angle and cohesion.

Since gypsiferous soils are known to be susceptible to dissolution and collapse, hydraulic conductivity testing (ASTM D2434) was also considered as a part of the required geotechnical tests. Gypsum soils could be characterized based on their hydraulic conductivity values, but research shows that determination of hydraulic conductivity for gypsum soils is difficult (Al-Saoudi et al., 2013). This is because the rate of flow of water varies as gypsum dissolves in the permeameter and the soil particles rearrange themselves in the process of testing. Therefore the results generated are not very reliable. Due to this reason, hydraulic conductivity testing was not considered for this study.

## **5.2 Direct shear strength test setup**

The soil for the test is placed in a metal shear box which consists of two halves. Both the halves are connected with screws. Soil is poured gently into the box, using a funnel from a drop height of 1.0 inch (2.54 cm). It is tapped lightly to ensure a uniform distribution through the box. The box is 1.1 inches (2.8 cm) in depth and has a diameter of 2.5 inches (6.4 cm), yielding a total soil volume of approximately  $5.4 \text{ in}^3$  ( $90 \text{ cm}^3$ ). Porous stones are put at the top and the bottom of the box. Table 5.1 shows the details of a typical test specimen. Once the soil is filled, a loading cap is put on top of the box. Based on prior testing experience, it was assumed that the sand would belong to the category of loose soils.

Table 5.1 Specifications of the shear box for a typical specimen

Soil depth	1.1 in. (2.8cm)
Diameter	2.5 in. (6.4cm)
Cross-section area	4.9 in <sup>2</sup> (32.0 cm <sup>2</sup> )
Volume	5.4 in <sup>3</sup> (90 cm <sup>3</sup> )

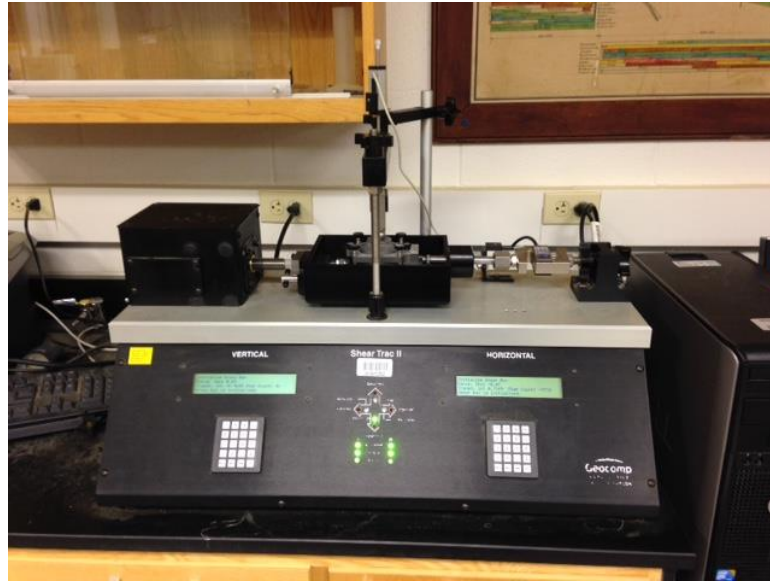


Figure 5.1 Geocomp Shear Trac II direct shear machine used for this study

The box is then put in the direct shear machine as shown in Fig 5.1. It has two load cells for horizontal and vertical loading and two LVDTs to read the corresponding deflections. The load cells and LVDTs are positioned and adjusted to fit snugly against each other and the loads are initially set to zero. The shear machine was operated using computer software named *SHEAR*. Soil parameters like specific gravity, specimen depth and diameter, moisture content and the required normal stress are entered into the software. Once the details are entered, the initial loads and deflections are zeroed and the test file is created.

The first part of the test involves consolidation of the soil specimen under the given normal load. For sands the primary and secondary consolidation are normally completed in about 3-4 minutes. After consolidation is complete, the locking pins are removed from the shear box and the shearing phase of the test is started. The software is configured in such a way that the test is 'strain controlled' i.e. the rate of shear displacement of the motors is constant. The horizontal deformation rate is set to 0.02 in./min. A maximum horizontal deformation of 0.3 in. is set to be the default end point of the test.

As the test progresses, the shear stress ( $\tau$ ) versus horizontal deformation ( $\Delta H$ ) plot increases rapidly and gradually decreases to a constant level. A typical test plot produced by *SHEAR* is shown in Fig. 5.2. When no further change in  $\tau$  is observed with  $\Delta H$ , the test is stopped. This value of  $\tau$  is known as the peak shear stress or  $\tau_f$  for loose soils. The value is recorded along with the vertical and horizontal displacements. For a given gypsiferous soil, the test is repeated at four different normal loads ( $N$ ) and  $\tau_f$  is noted for each test. The tests were conducted at  $N$  values of 15.0 psi, 30.0 psi, 45.0 psi and 60.0 psi (104 kPa, 207 kPa, 311 kPa and 414 kPa). The peak shear stresses are plotted against the corresponding normal stress and the 'Mohr-Coloumb failure envelope' for the particular gypsiferous sand is derived. The friction angle ( $\phi$ ) and cohesion ( $c$ ) of the soil are determined from this plot.

The first set of tests was conducted on dry soils. The second set of tests was conducted on saturated soil samples, kept moist for 1 hour post preparation. For most gypsiferous sands tested under dry conditions,  $\phi$  is generally between  $34^\circ$  to  $44^\circ$  and cohesion is nearly zero. Soaking the soils however gives rise to a finite value of cohesion because of the onset of cement-hydration reaction.

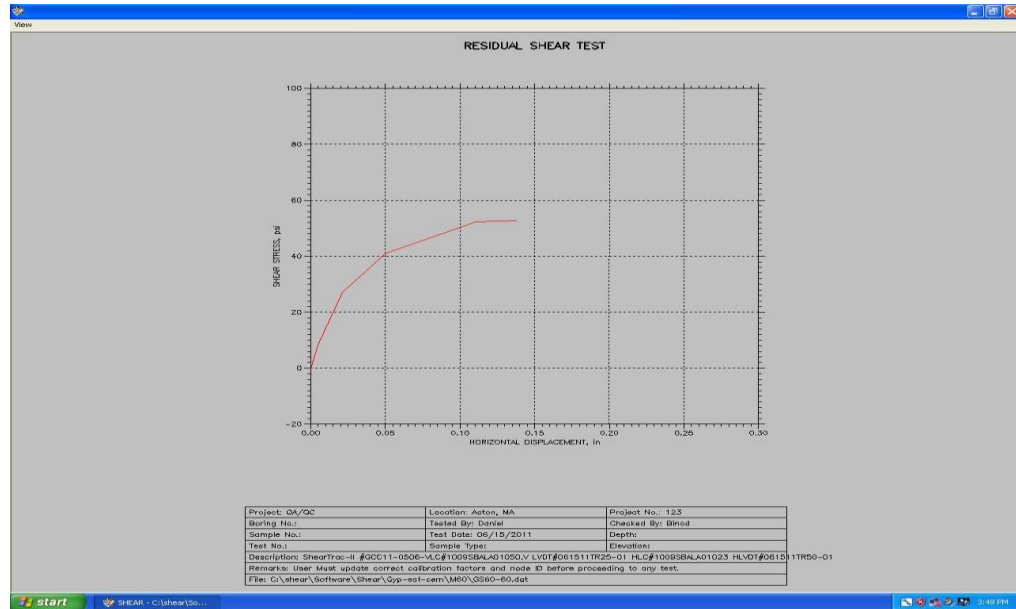


Figure 5.2 Typical *SHEAR* plot for  $\tau$  versus  $\Delta H$ .

### 5.3 Results and observations

The following plots show the Mohr-coulomb failure envelopes of the 10%, 20%, 30%, 40% and 60% gypsum-sand mixtures respectively. The soils were tested under dry conditions. The first two soils were tested at five normal stresses while the remaining were tested at four normal stresses. The plots (Figs. 5.3-5.6) showed unique friction angles for each soil type. Cohesion intercepts were generally very small.

In the next part of the test, the same mixtures were tested after each specimen was saturated and kept soaked for one hour. This was done in order to examine the possible effect of cement-hydration which might cause an increase in cohesion as compared to dry sands (Figs 5.7-5.10).



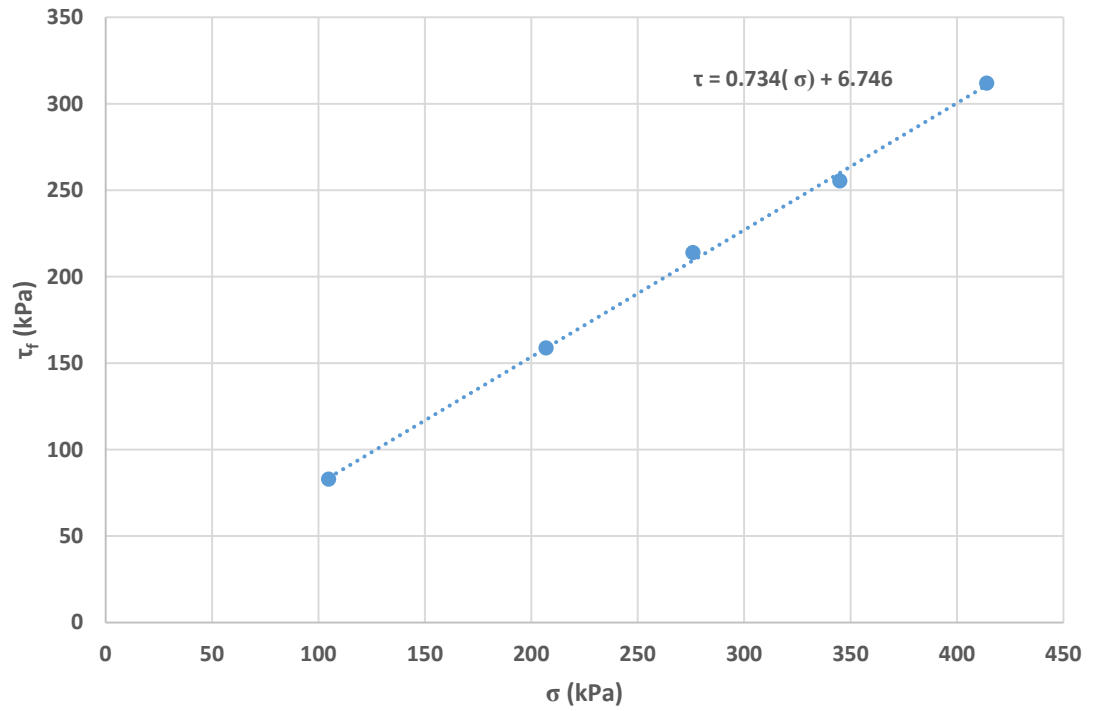


Figure 5.3 Plot of  $\tau_f$  versus  $\sigma$  10% gypsum (dry).

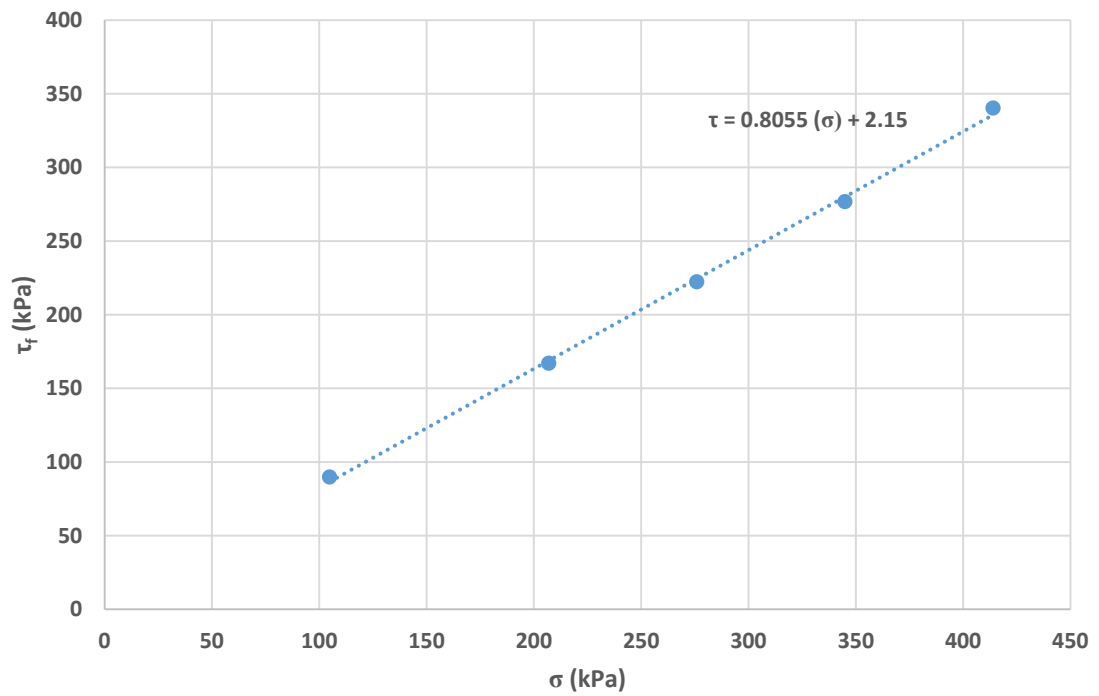


Figure 5.4 Plot of  $\tau_f$  versus  $\sigma$  for 20% gypsum (dry).

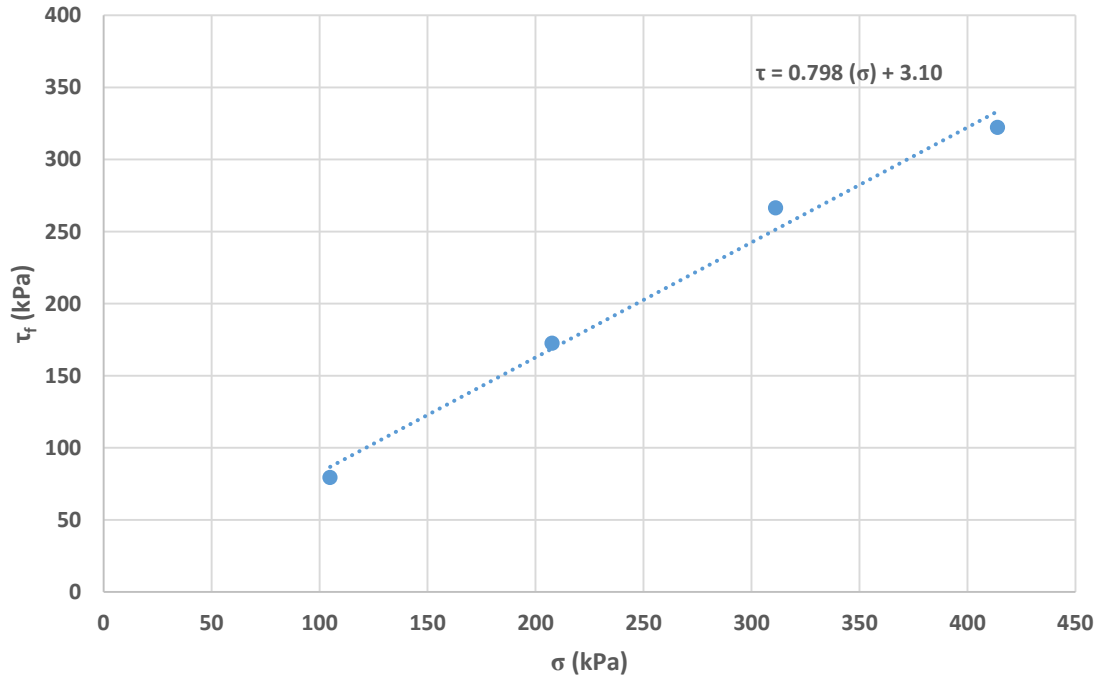


Figure 5.5 Plot of  $\tau_f$  versus  $\sigma$  for 30% gypsum (dry).

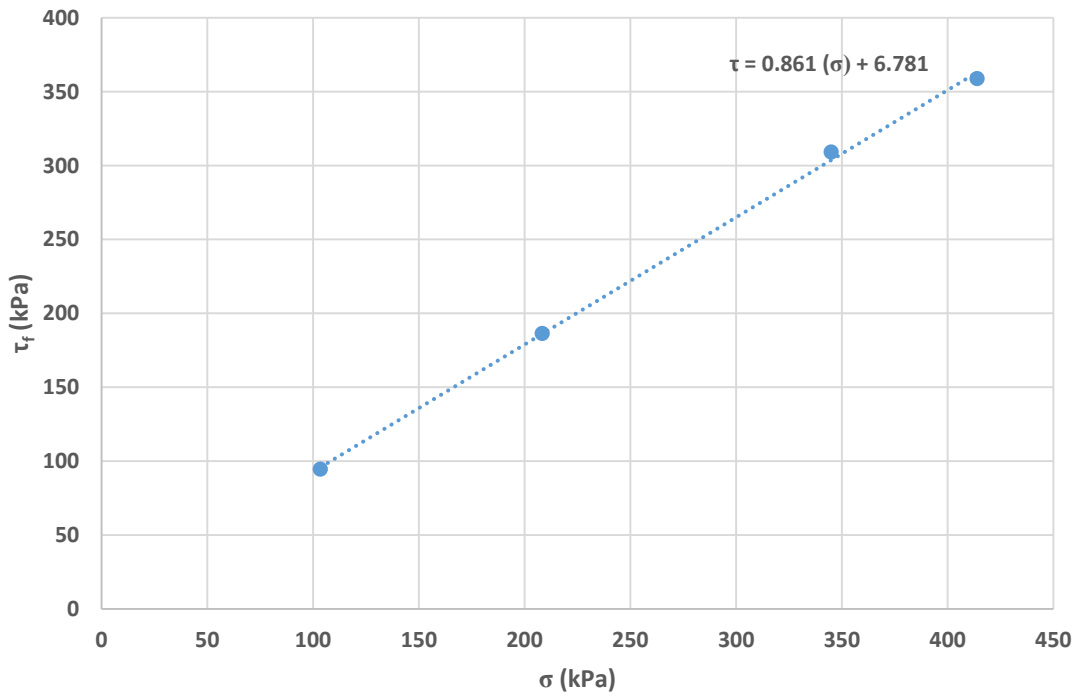


Figure 5.5 Plot of  $\tau_f$  versus  $\sigma$  for 40% gypsum (dry).

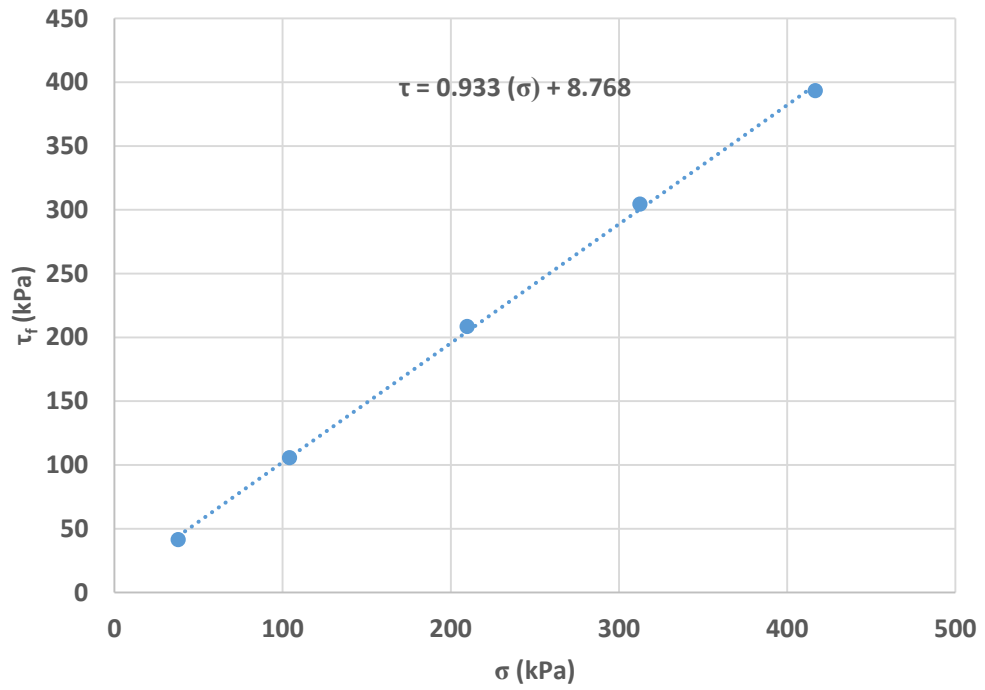


Figure 5.6 Plot of  $\tau_f$  versus  $\sigma$  for 60% gypsum (dry)

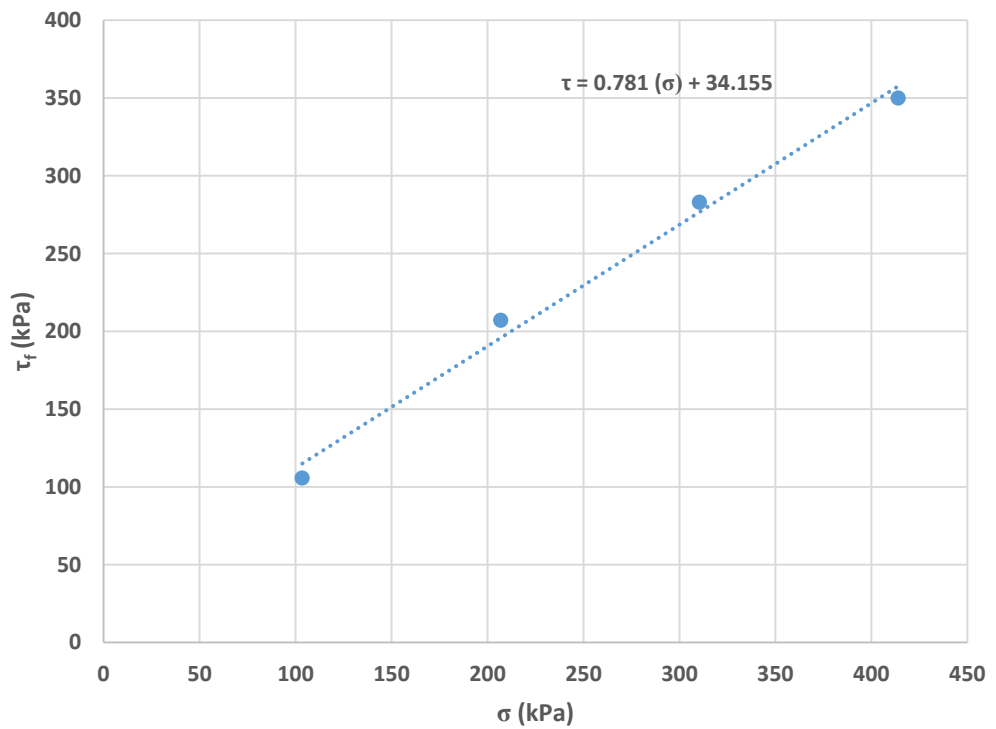


Figure 5.7 Plot of  $\tau_f$  versus  $\sigma$  for 10% gypsum (cemented).

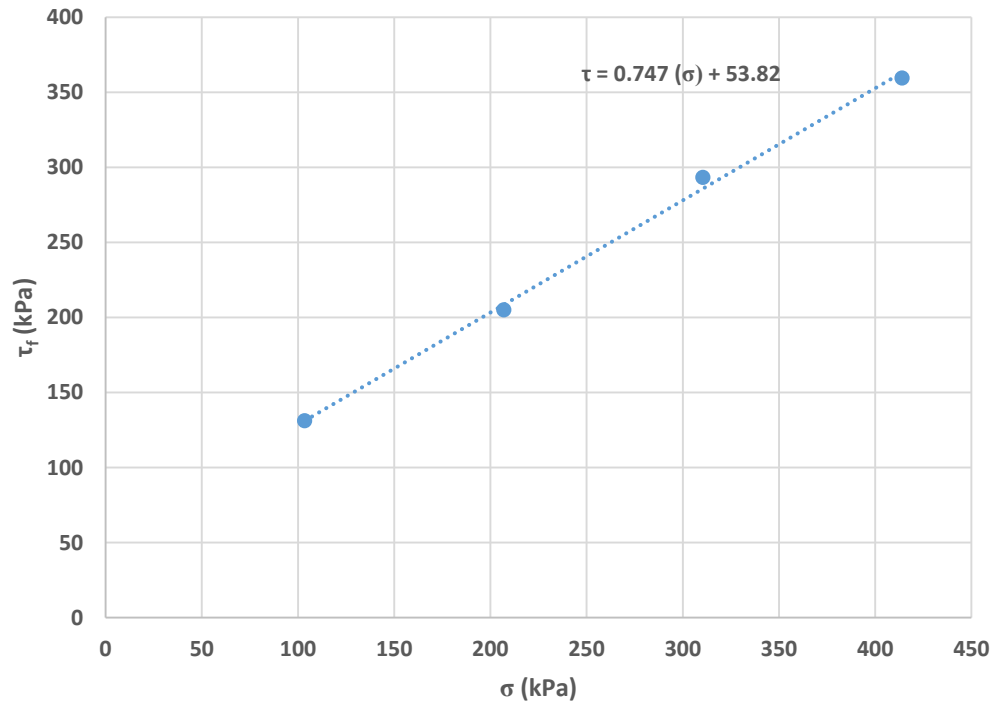


Figure 5.8 Plot of  $\tau_f$  versus  $\sigma$  for 20% gypsum (cemented).

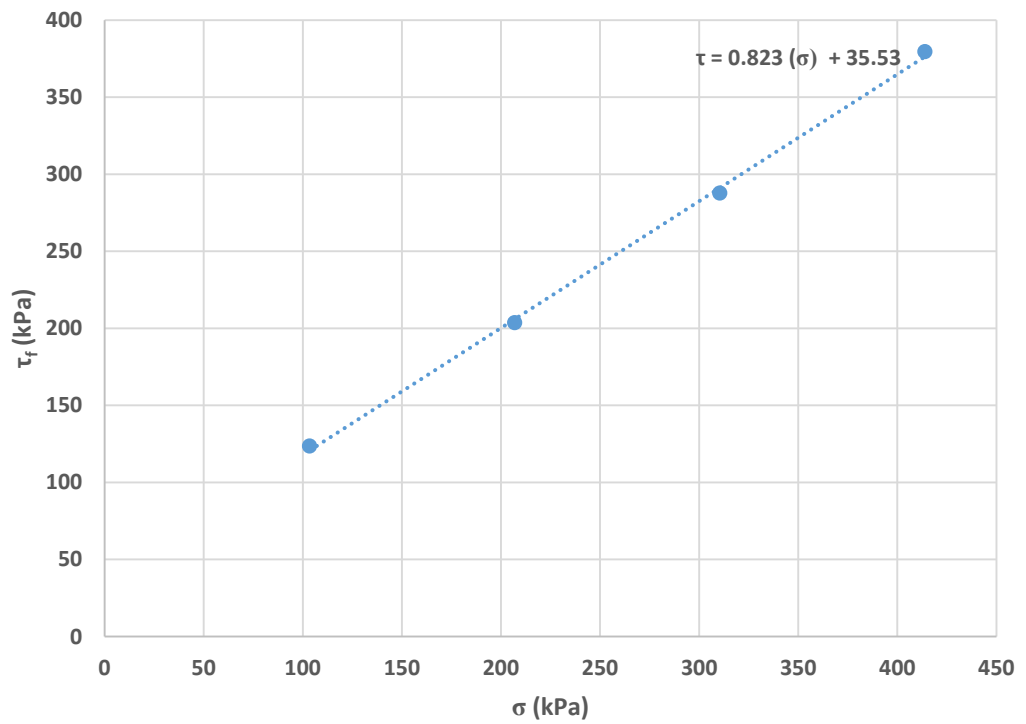


Figure 5.9 Plot of  $\tau_f$  versus  $\sigma$  for 40% gypsum (cemented).

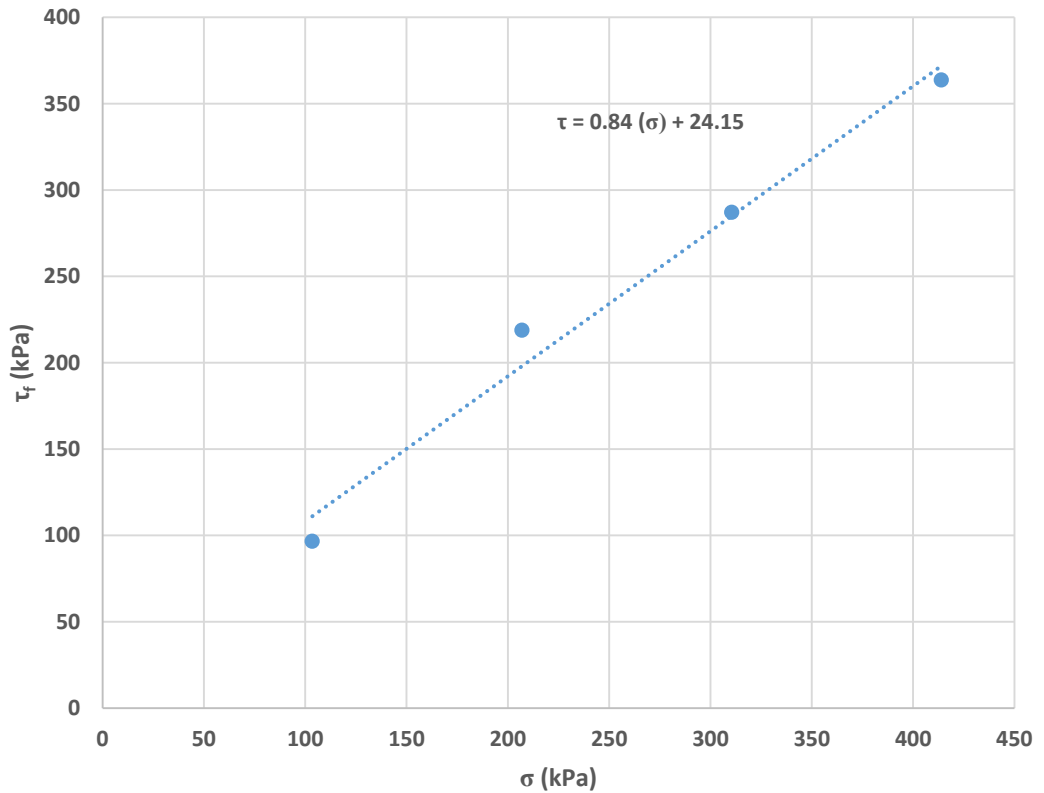


Figure 5.10 Plot of  $\tau_f$  versus  $\sigma$  for 60% gypsum (cemented).

Some distinct trends were observed from these plots. First, for the dry soils, the friction angle  $\phi$  increases with the increase in gypsum content. Friction angle is found by measuring the tangent inverse of the slope of failure envelope. It increases from  $36^\circ$  for 10% gypsum to  $44^\circ$  for 60% gypsum (Figure 5.11). Cohesion is very small, consistent with the nature of granular soils.

For the cemented soils, however, the behavior was slightly different. While  $\phi$  showed an increase with increase in gypsum content, cohesion intercept showed a distinct variation. Figure 5.11 shows the change in friction angle with gypsum. Cohesion for these soils was much higher than those of dry soils and the value peaked at 20% gypsum content

thereafter decreasing with gypsum. Figure 5.12 shows the cohesion intercept plotted against gypsum content in the cemented and uncemented sands.

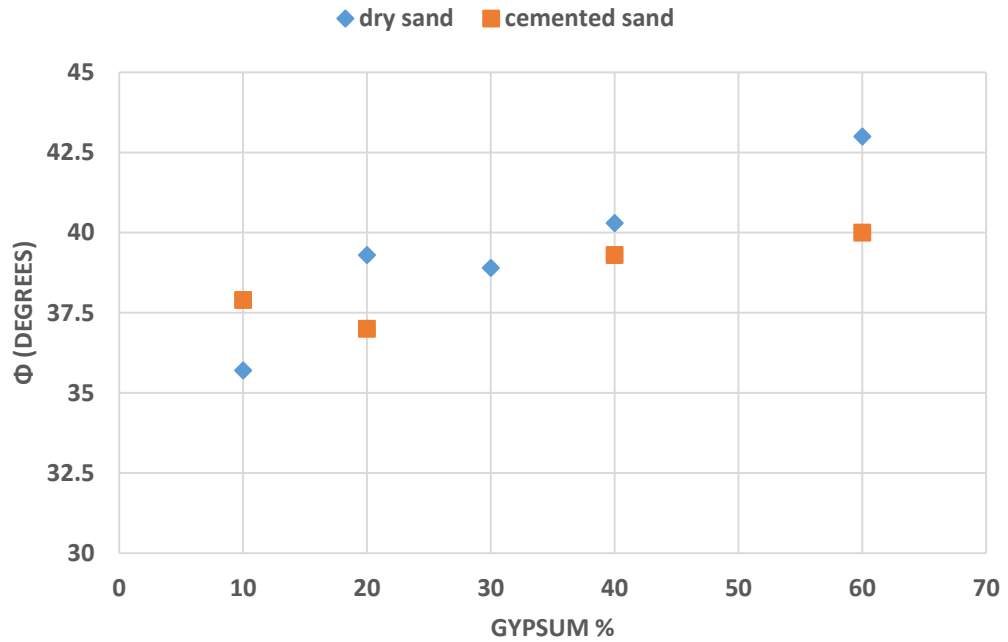


Figure 5.11 Friction angle versus gypsum content for the specimens tested

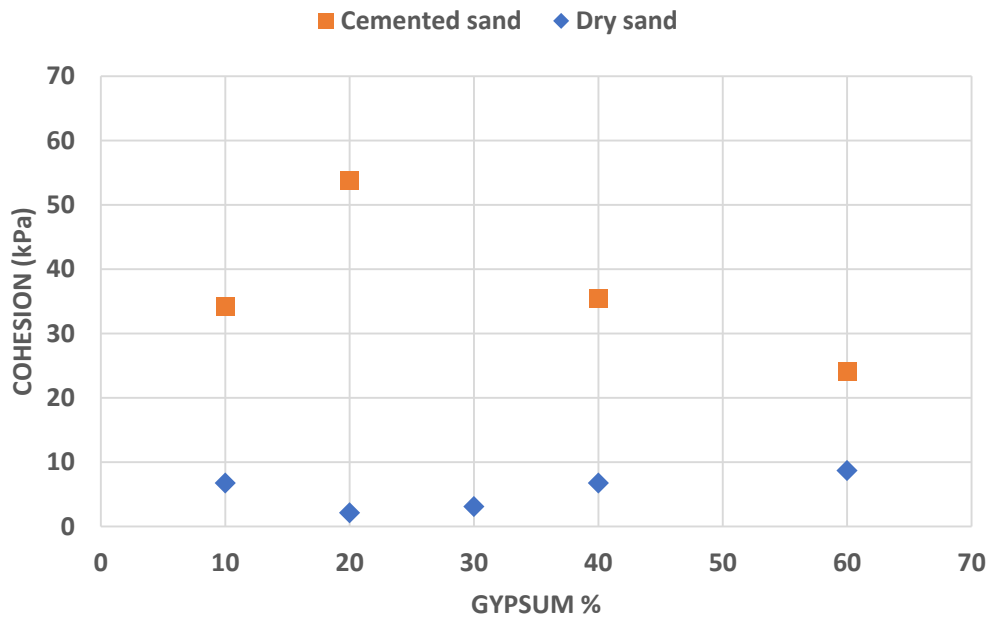


Figure 5.12 Cohesion versus gypsum content for the specimens tested

## 5.4 Inferences

The amount of gypsum in the sand affects both the friction angle and cohesion. The increase in  $\phi$  can be interpreted from two viewpoints. Introduction of gypsum into the sand matrix causes an increase in angularity and filling up of the void spaces, thereby increasing  $\phi$ . Gypsum, being a soft material, can be easily crushed under high loads. As such, the more gypsum in the soil, the more vertical consolidation the soil can undergo. In this process it attains a much denser configuration in comparison to soils with smaller gypsum content. As the void ratio is lower in a denser configuration,  $\phi$  is correspondingly higher. The relationship between gypsum content and consolidation is not exactly precise. This aspect would be described in detail in the next chapter on consolidation and collapse. Figure 5.13 shows the void ratio versus stress plot for two gypsum-sand samples. Void ratio was calculated from the height of consolidation in test, before the shearing step was performed. It can be seen that the soil with more gypsum tends to consolidate more.

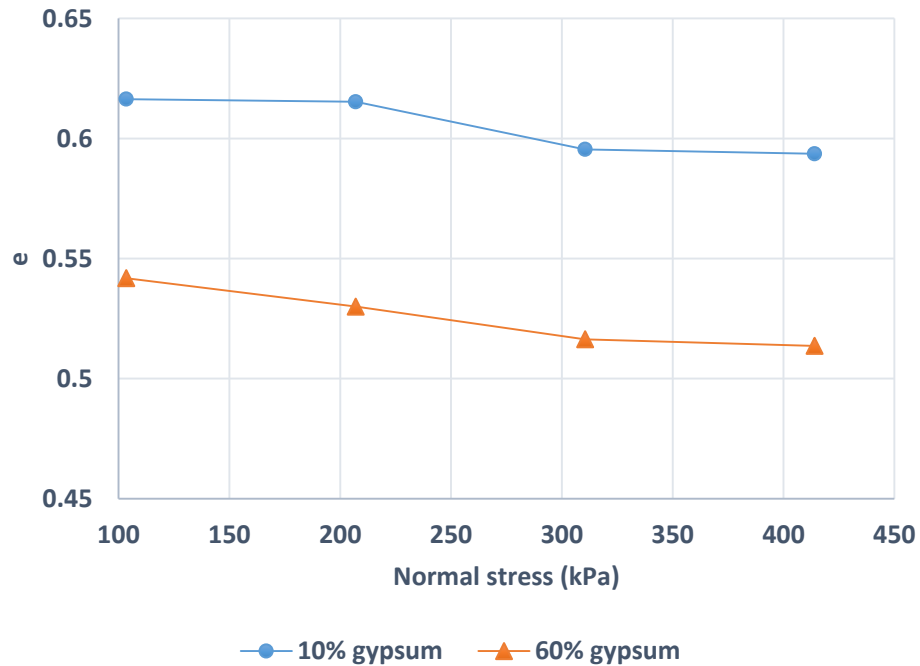


Figure 5.13 Void ratio versus normal stress

The cohesion of the soils is not significant under dry conditions and likewise has no relationship with the amount of gypsum. But the soaked soil samples show a significant amount of cementation and also exhibit the maximum amount of cementation when the gypsum content is 20%. This could be explained on the basis of gypsum acting as a filler material at lower concentrations affecting the structure of the soil fabric. After a certain critical concentration, gypsum starts to act as a dispersing agent and reduces the cohesion in the soil.

Bolan et al. (1991) found that soil surface acts as a sink for calcium and sulphate ions liberated from the dissolution of gypsum. They also noted that the gypsum dissolution was faster in soil than in water and followed first order kinetics. From prior electrical resistivity and salinity tests on gypsum soils, it was found that conductivity and salinity are



maximum at a gypsum concentration of 20%. Gypsum is known to be a sparingly soluble salt and therefore attains saturation concentration in solution at fairly low amounts of gypsum. Increasing the gypsum in the solution would cause the excess gypsum to precipitate. At this concentration, enough silica surface is available to act as a sink for the released ions, thereby promoting dissolution. When a good amount of calcium ions are released, sufficient cementation hydration reaction takes place enhancing the cohesive strength of the soil.

The results appear to be consistent with the findings of Al-Marsoumi et al. (2008), in which the cohesive strength of some gypsiferous soil samples collected in southern Iraq (with an average gypsum content of 15.5 %) was seen to be maximum when their gypsum content was increased by 20%. After 30% increase in gypsum content the cohesive strength started to decrease. The friction angle however showed a different trend. The friction angle generally increased with the addition of gypsum unlike the results of Al-Marsoumi et al. where it peaked at around 35% gypsum and subsequently reduced. The difference in results could be due to the differences in the tests conducted and also the variation in soil composition.

### 5.5 Specific gravity test (ASTM D854)

Gypsum rich soils are typically low density soils because of the low specific gravity of gypsum. While the specific gravity of quartz sand is close to 2.65, that of gypsum is around 2.32. In this regard, specific gravity of the soils was expected to decrease with increase in gypsum content. A series of specific gravity tests was performed on five soils with gypsum contents of 0%, 20%, 50%, 75% and 100%. Approximately 50 grams of each soil was used for testing and  $G_s$  was determined using a specific gravity flask, distilled water and a vacuum arrangement according to the ASTM D854 test specifications. Table 5.2 shows the  $G_s$  values of the five soils tested. Figure 5.14 shows the  $G_s$  of the soils plotted against their gypsum content.

Table 5.2 Measured specific gravity values of the soils

Soil type	$G_s$
0% gypsum	2.63
20% gypsum	2.56
50% gypsum	2.46
75% gypsum	2.38
100% gypsum	2.33

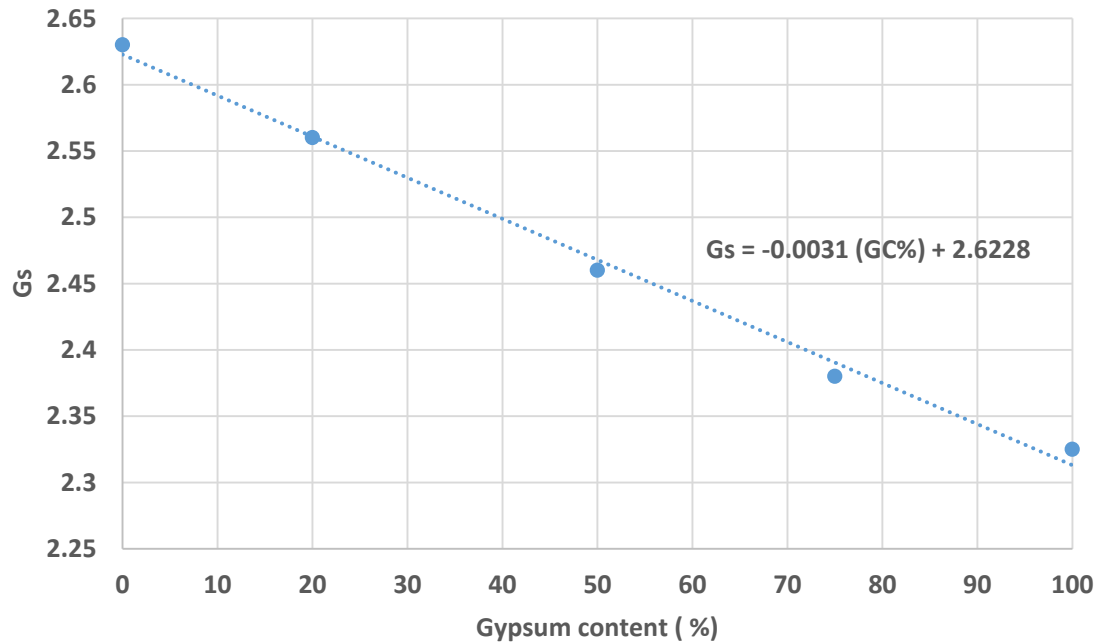


Figure 5.14 Specific gravity plotted against gypsum content

Specific gravity of the gypsum sand mixtures decreased with increase in gypsum content. It was seen that a good linear relationship existed between  $G_s$  and gypsum content (GC), with the former decreasing with increase in gypsum. Though the range of values over which  $G_s$  could vary was relatively narrow, it still shows a consistent trend. The relationship between  $G_s$  and gypsum content was:

$$G_s = -0.0031 (GC) + 2.6228 \quad (5.1)$$

## 5.6 Grain size analysis (ASTM D422)

Grain size analysis was performed on the quartz sand and gypsum used in the research to estimate the grain size distribution of these materials. The information derived from this test helps classifying the soils and estimating their engineering characteristics. Since coarse grained soil was used, mechanical sieve analysis (ASTM D422) was deemed suitable to develop gradation curves for the quartz and gypsum samples. Six sieves with sizes shown in Table 5.3 were used for the test. Approximately 750 grams of each material was chosen for the analysis. Mechanical sieving was performed for five minutes and the mass of the material retained on each sieve as used to determine the grain size distribution. Figure 5.15 shows the gradation curve for the quartz and gypsum samples.

Table 5.3 Sieve sizes used in grain size analysis of quartz and gypsum

Sieve number	Opening (mm)
10	2.0
40	0.425
60	0.25
100	0.15
140	0.105
200	0.075
pan	-

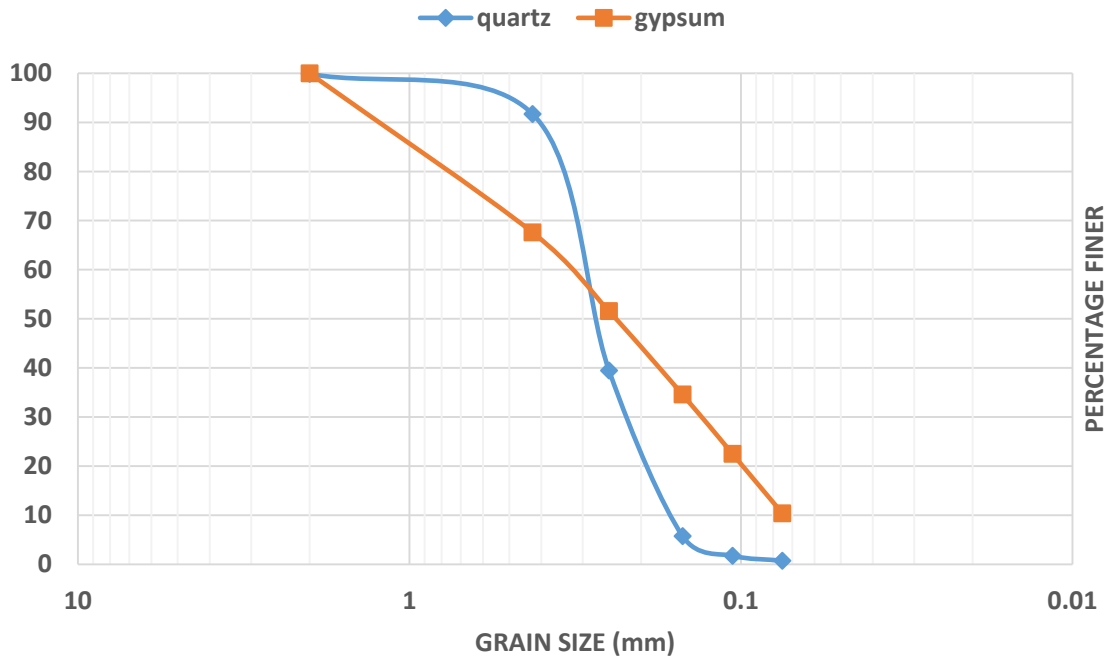


Figure 5.15 Gradation curves for quartz sand and gypsum

From the gradation curves it was found that the quartz sand was poorly graded and was classified as SP according to USCS ( $C_u = 1.76$  and  $C_c = 1.04$ ). More than 70% of the grain sizes were within the range 0.2 mm -0.4 mm. It could also be classified as clean sand since the percentage of fines was less than 2%. Gypsum on the other hand had a wider range of particle sizes varying from 0.075 mm to 2.0 mm ( $C_u = 4.66$  and  $C_c = 0.86$ ). The gradation curve showed that the gypsum sample had about 10% fines. Since the gypsum was non-plastic, it was assumed that the fine-grained fraction was silty. Therefore gypsum was classified as SP-SM according to the USCS.

## 5.7 Conclusion

Some samples of reconstituted gypsiferous sands were tested for their geotechnical properties. The effect of gypsum on the cohesive strength and friction angle was of particular interest. Direct shear strength testing was performed on the soils under dry and soaked conditions, the latter assumed to bring about cementation. Mohr-Coulomb failure envelopes were plotted for each soil type and their shear parameters were calculated from the failure envelopes. The tests revealed that for both the dry and wet samples, friction angle generally increases with increasing gypsum content. While the dry soils showed insignificant amount of cohesion and no relationship with gypsum content, the soaked samples had an appreciable amount of cohesion. Cohesion was particularly high for a soil sample with 20% gypsum content. It can be concluded that gypsum soil samples with a history of saturation exhibit a greater cohesion.

Specific gravity tests showed a decrease in  $G_s$  with increase in gypsum content. This aspect of gypsum soils is important, because  $G_s$  is directly associated with the unit weight of soils which is essential for all major geotechnical calculations. The resulting mechanical sieve analysis showed that both the quartz sand and gypsum were poorly graded, with gypsum having a wider range of particle size distribution. The knowledge of grain size helps in the determination of geotechnical and geophysical soil parameters like cohesion, friction angle, hydraulic conductivity, stiffness and electrical conductivity.

The results were cross-checked with electrical resistivity methods using Archie's law and also soil salinity and conductivity tests from soil water extracts. These aspects are described in the succeeding chapters. Apart from shear strength, the consolidation or collapse of gypsiferous soils is another major geotechnical parameter that has to be

investigated. All these parameters together have a great role to play in determining the safety and hazard potential of gypsiferous soils from an engineering viewpoint. The next chapter describes the collapse settlement of gypsiferous sands under varying conditions of gypsum concentration, moisture content and also the effect of time and dissolution on collapse.

## **6. Consolidation and Collapse Potential Testing of Gypsum Soils**

### **6.1 Introduction**

Collapse settlement is one of the most severe problems associated with gypsiferous soils around the world. These soils are characterized by low density and loose structure with gypsum often acting as a moderate cementing or binding agent. Gypsum is a material of low specific gravity of about 2.32 and a solubility of 2.1-2.5 g/L. Under natural conditions these soils are fairly stable and act as good foundation material but the soils undergo rapid settlement and loss of volume upon the introduction of water. This behavior is also known as hydro-compression settlement. Addition of water contributes to the loss of cementing material through leaching and dissolution processes which in turn lead to decrease in strength and stability of the soils. Clemence and Finbarr (1981) defined collapsible soils as “any unsaturated soils which goes through a radical rearrangement of particles and great loss of volume upon wetting with or without additional loading”.

Underground water pipelines, irrigation canals, dams, construction activities and sudden changes in water table elevations are some of the causes of collapse hazards in gypsiferous soil regions. Over the years, several researchers developed guidelines and criteria to quantify collapsible soils based on their physical properties. The double oedometer test and single collapse test are two widely used laboratory methods for determining collapse (Al-Rawas, 2000). The collapse settlement of a soil can be quantitatively estimated from a parameter called ‘collapse potential’, also referred to as CP.



To conduct a double oedometer test, two identical samples of soil are placed in an oedometer and progressively loaded up to the ultimate desired load. One of the samples is kept at its natural moisture content while the other sample is saturated. The difference in settlements ( $\Delta H$ ) of the dry and saturated specimens at 200 kPa is noted. This method was proposed by Jennings and Knight (1975). For a single collapse test, a sample of soil is put in an oedometer frame and gradually loaded to 200 kPa. At this point, the sample is suddenly flooded with water and left for 24 hours. The settlement during this period ( $\Delta H$ ) is noted and loading is continued till the final load. From either test, CP is expressed as:

$$CP = \Delta H/H_0 = [\Delta e / 1+e_0] * 100\% \quad (6.1)$$

Where  $\Delta H$  is the change in height of the specimen,  $H_0$  is the initial sample height,  $\Delta e$  is the change in void ratio and  $e_0$  is the initial void ratio of the sample (Al-Rawas, 2000). Figure 6.1 shows a typical plot from a collapse potential test.

Jennings and Knight (1975) also suggested a classification system to estimate the degree of severity of collapse settlement on the basis of CP. This classification is shown in Table 6.1 (Al-Rawas, 2000).

Table 6.1 Severity of collapse based on CP values

Collapse Potential (%)	Severity
0-1	No problem
1-5	Moderate trouble
5-10	Trouble
10-20	Severe trouble
>20	Very severe trouble

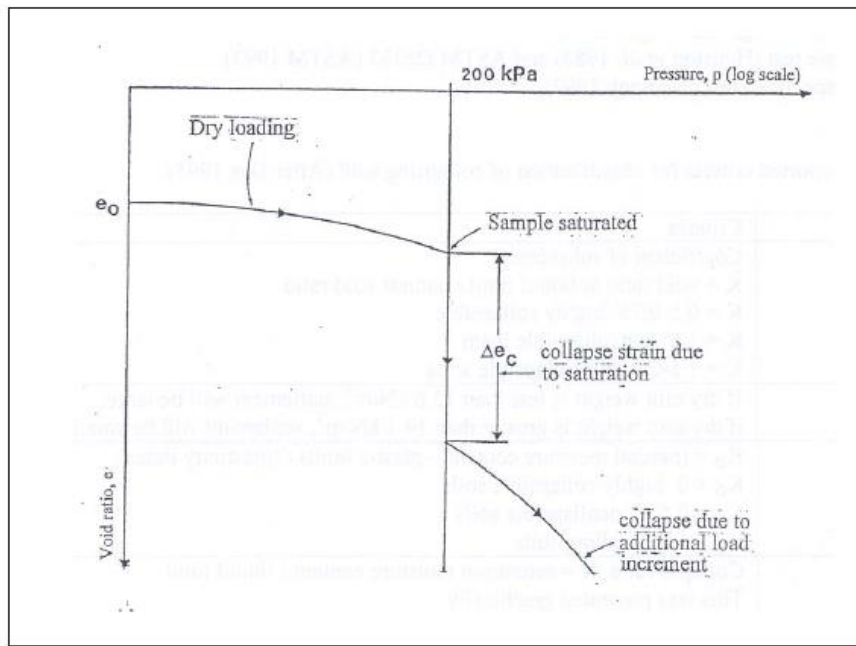


Figure 6.1. Plot showing the typical result from a CP test (Al-Rawas, 2000)

The collapse potential of gypsiferous soils has been studied by numerous researchers especially in the Middle East. Collapse potential is influenced by factors such as gypsum content, unit weight, initial moisture content, initial void ratio and soil plasticity. Fattah et al. (2011) used the computer program Settle3D to determine the hydrocompression settlement and collapse potential of gypsiferous soils in Iraq. They found that collapse potential increased with increasing gypsum content and increase in thickness of the collapsible layer but was not dependent on the footing dimensions. In another study using single collapse test and double oedometer test methods on Al-Tar region soils of Iraq, Fattah et al. (2008) discovered that collapse potential increases with increase in gypsum content. In an accompanying time-dependent study they observed that soils with low gypsum content showed a substantial decrease in collapse potential with time. Nashat (1990) found collapse potential to increase for a gypsum content of 20%-60% and decrease thereafter. However many other researchers in Iraq found minimal effect of gypsum content on collapse potential. Al-Ani and Seleam (1993), along with other researchers, found that increase in initial water decreases collapse potential (Seleam, 2006).

For this research, the collapse and consolidation behavior of gypsum-sands was studied using two methods. In the first method the collapsibility of soils was studied by varying the gypsum content, water content and time. The Geocomp direct shear machine (ShearTrac II) was used to bring about consolidation and a methodology similar to that of double oedometer test was applied. In the second method a consolidation load frame (Figure 6.2) was used and a single collapse test type of testing was performed on the gypsum soils by varying the gypsum content and time period. The testing procedures and results are described in the following sections.



Figure 6.2 Consolidation load frame

## 6.2. Collapsibility tests using Geocomp direct shear machine

When a sample of soil is set for shear strength testing in the shear machine, the sample is first consolidated under the required normal pressure. Considering the soil used for the study was sandy gypsum soil, this technique could be used to consolidate the soil and thus provide the required data to estimate collapse potential. An approach similar to that of the DOT test was adopted in which two identical samples were tested one after another at 200 kPa. The first one was tested under natural moisture content and the second sample was saturated. Strain was calculated using the relation  $\varepsilon = \Delta H/H$ , where  $\Delta H$  was

the change in height (inches) and  $H$  was the initial height (1.1”). The difference in strains between these two samples was regarded as the collapse potential (CP).

The soil is first poured into the shear box and the box is put in the direct shear machine. The samples were all predominantly loose soils with void ratios ( $e$ ) between 0.62-0.68 and a dry density of 1.48-1.60 g/cc. The sample dimensions and the physical properties of the soil and the load specifications are entered into the *SHEAR* software. Once the horizontal and vertical loads and deflections are initialized and set to zero, the soil is ready for testing. The test is then started and normal consolidation of the soil is allowed to occur under the load of 200 kPa. Since the soil is a fine grained sand, both the primary and secondary consolidation are almost complete within five to seven minutes. At this point, the test was terminated. Figure 6.3 shows a typical *SHEAR* consolidation plot. In a direct shear test, the next step would involve the shearing phase. The following sections discuss the tests conducted using this setup.

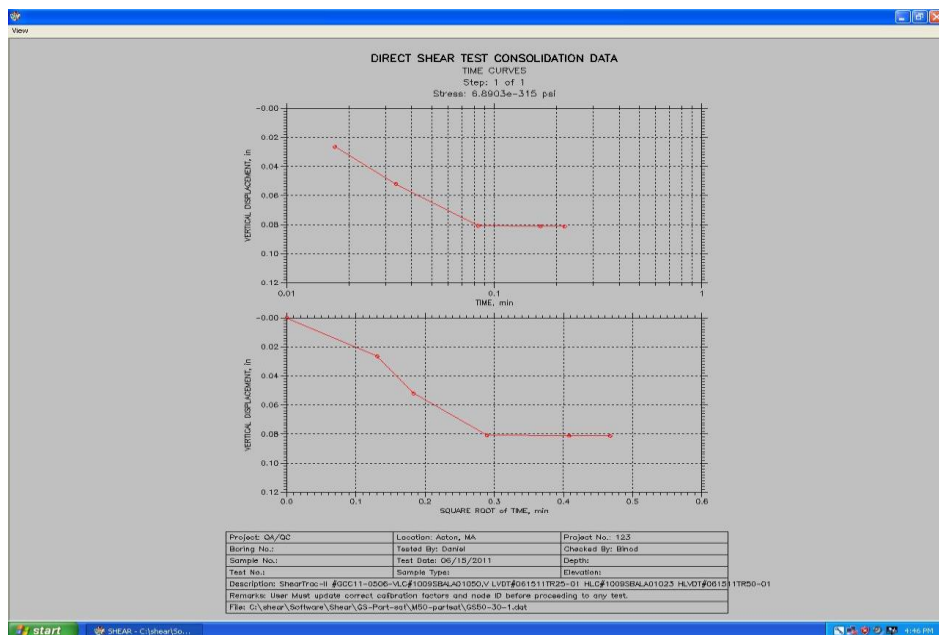


Figure 6.3 Consolidation versus time plot using SHEAR

### 6.2.1 Collapse potential with change in gypsum content

Seven different soil samples were taken with gypsum content ranging from 10% to 80%. Each sample was individually tested first dry then saturated. The samples were loaded to 200 kPa and consolidation was allowed to continue to the point where no further change in vertical displacement was visible. The difference in strains of the saturated and dry samples was the collapse potential. Figure 6.4 shows the plot for strains versus gypsum content for the soils tested under dry and saturated states. Figure 6.5 shows the plot of collapse potential versus gypsum content of the soils tested.

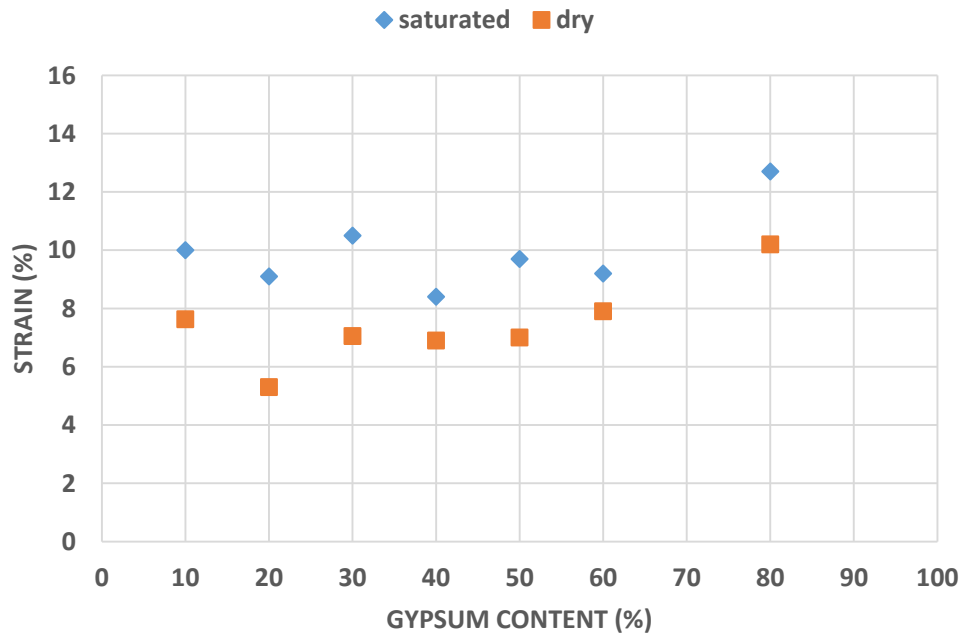


Figure 6.4 Vertical strain versus gypsum content at 200 kPa

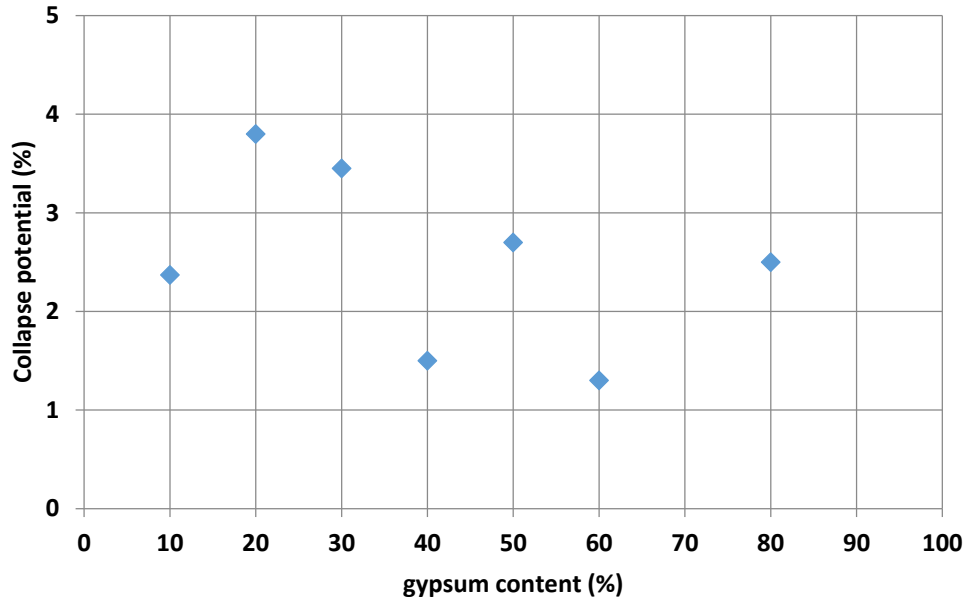


Figure 6.5 Collapse potential versus soil gypsum content at 200 kPa

From the tests, it was seen that collapse potential for the samples varied between 1.5% - 3.8 % . Using the Jennings and Knight (1975) classification criteria, the soils could be classified as moderately troublesome. The scatter in the data points also suggested that gypsum content did not seem to have any observable effect on the CP of the samples. This conclusion was in agreement with Seleam (2006) where CP of the tested soils varied in a narrow range 0.71% -1.45% and gypsum content showed little impact on it. In the next section, the impact of water content on collapse potential is described.

### 6.2.2 Vertical strain with change in water content

For conducting this test, the soil samples were put in the shear box and a certain amount of water was added to each sample. The water content was calculated using the relationship:

$$w\% = m_{\text{wat}} / m_{\text{soil}}. \quad (6.3)$$

Where  $m_{\text{wat}}$  is the mass of water added and  $m_{\text{soil}}$  is the weight of the soil in the box. The sample was allowed to sit for ten minutes to ensure uniform distribution of water through the soil. It was estimated that approximately 25 g of water would be required to saturate each sample. The box was then transferred to the shear machine and the consolidation test was conducted. Four different soils with gypsum content varying from 20%-70% were taken and several tests were conducted on each soil type. The data were plotted and averaged to find any trend between water content and strain. In some trial runs it was found that the value of collapse potential was negative. To avoid this discrepancy, vertical strains instead of collapse potential were plotted against water content. Figures 6.6 -6.10 show the plots for vertical strain versus initial moisture content for the different soils.



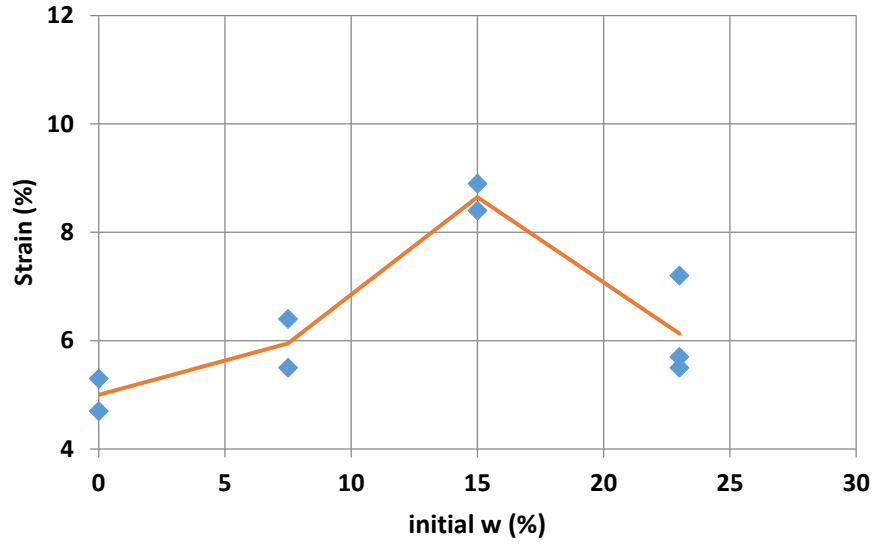


Figure 6.6 Strain versus initial w% for 20% gypsum at 200 kPa

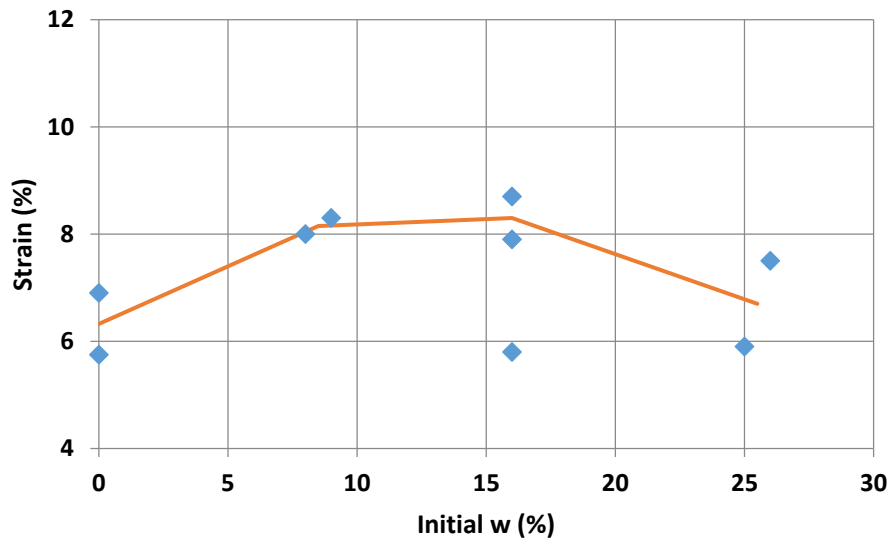


Figure 6.7 Strain versus initial w% for 30% gypsum at 200 kPa

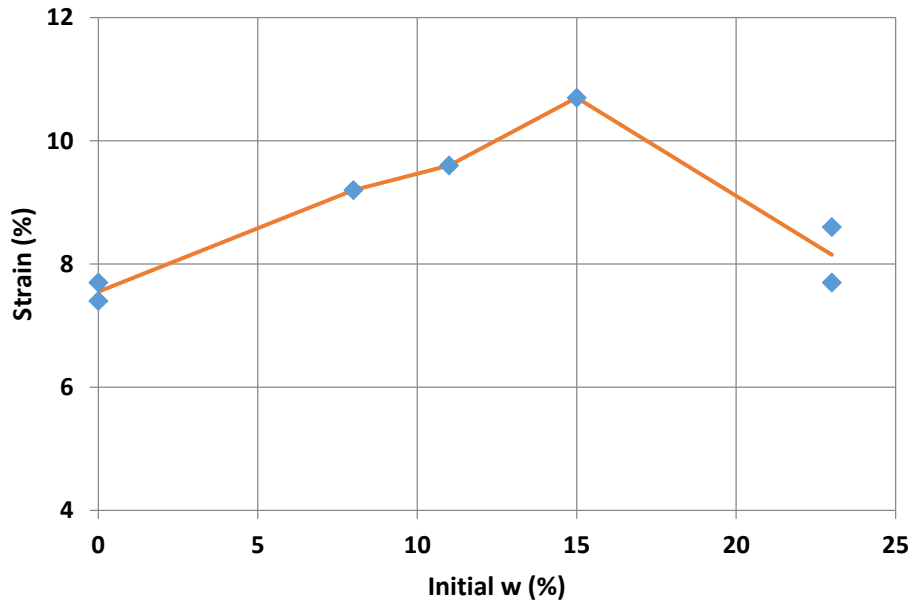


Figure 6.8 Strain versus initial w% for 50% gypsum at 200 kPa

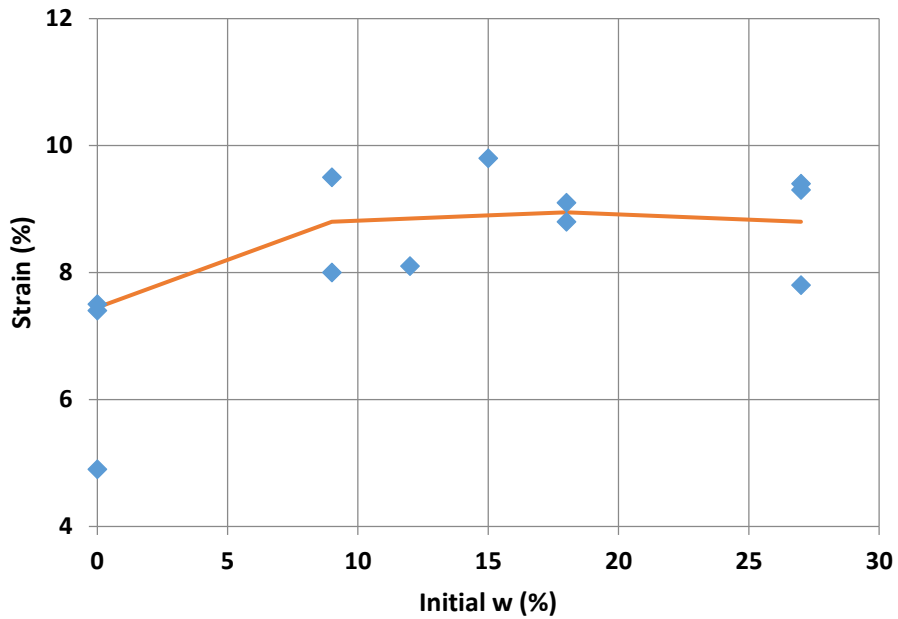


Figure 6.9 Strain versus initial w% for 70% gypsum at 200 kPa

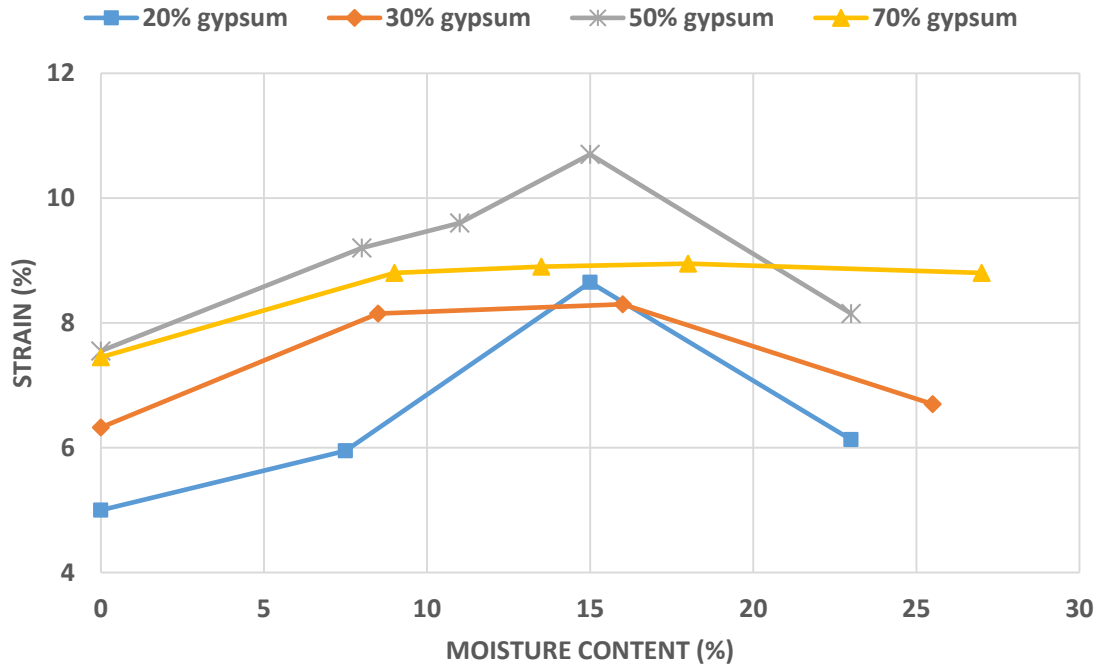


Figure 6.10 Strain versus initial w% plot for all soils tested

These plots revealed that vertical strain initially increases with moisture content to about 15%. This roughly corresponds to a degree of saturation of 60%. Beyond this point vertical strains appeared to decrease as water contents draws close to saturation.. This observation seems to be in agreement with Al-Rawas (2000) and Jennings and Knight (1975). The former states that collapse phenomenon will only occur up to a certain critical degree of saturation. Collapse mechanism is commonly known to occur in unsaturated soils. Jennings and Knight (1975), states that the critical degree of saturation is 50-60% for fine silty sands.

Another observation made from these tests was that, though collapse potential itself does not show any co-relation with gypsum content, the vertical strains for the four soils tested seemed to increase with increase in gypsum. Figure 6.11 shows the vertical strains

of the soils versus gypsum content. This led to the possibility of re-investigating the relationship between collapse potential and gypsum content using a different method of testing.

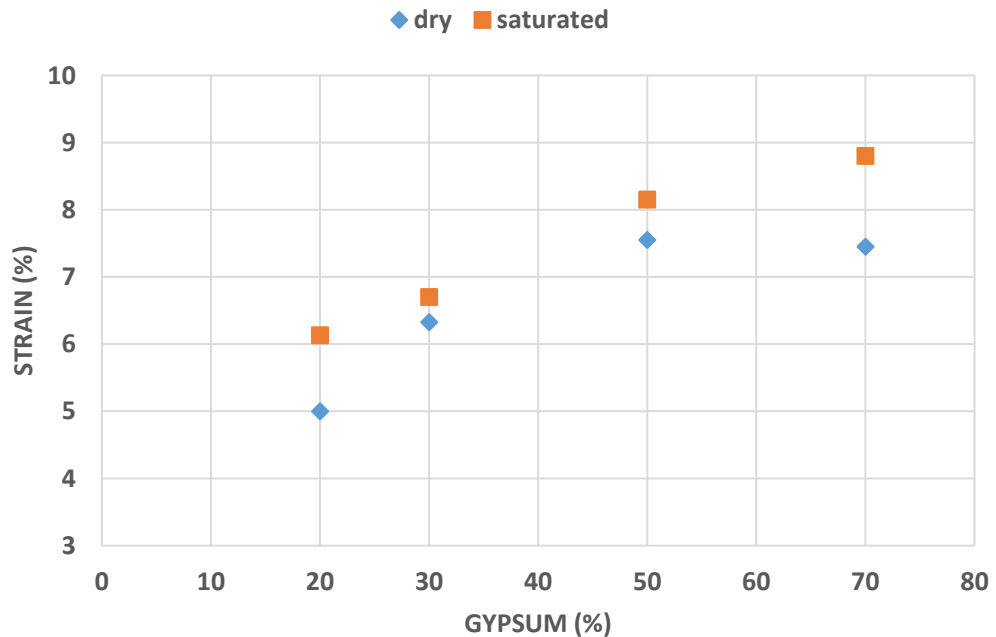


Figure 6.11 strain versus gypsum content at 200 kPa

### 6.2.3 Vertical strain with dissolution and time

In this section, the effect of time on gypsum dissolution and vertical strain was studied. Two soils with 30% and 50% gypsum content respectively were used for the tests and they were each put in a shear box. The box was mounted on a small tripod stand and placed inside a trough. The whole assembly was put in underneath a water tank from which water drops were allowed to trickle at a very small rate (Fig. 6.12). This configuration was used to ensure that the sample remained fully saturated throughout the experiment. It also served the purpose of leaching gypsum out of the soil. The excess water that would drain from the bottom of the shear box was collected in the trough. The electrical conductivity

( $\mu\text{S}/\text{cm}$ ) and Salinity (ppm) of the effluent were measured using the Extech 400 conductivity meter (Fig. 6.13).

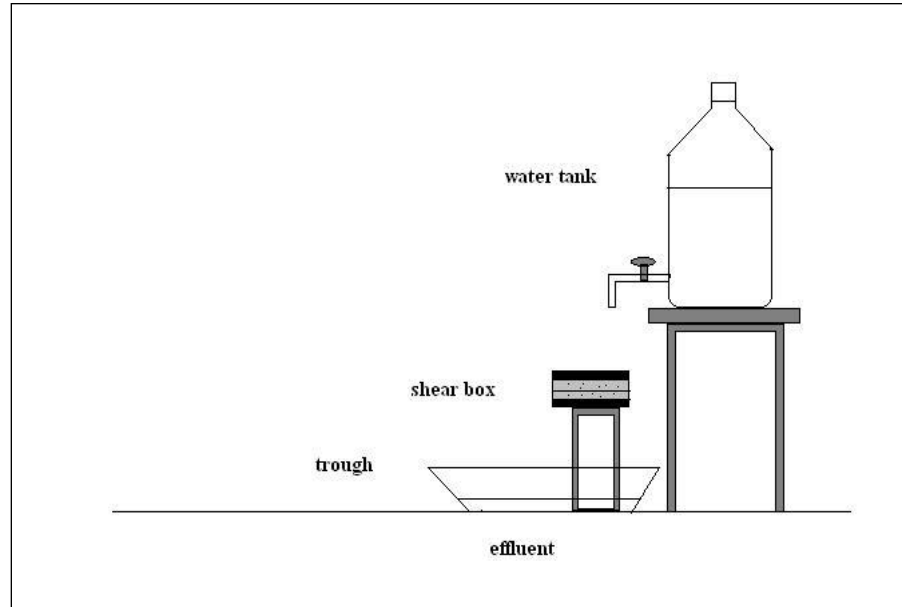


Figure 6.12 test arrangement for gypsum dissolution



Figure 6.13. The Extech 400 conductivity meter in use

The two soil samples were set in this arrangement for periods of 10 minutes, 1020 minutes (17 hours) and 2700 minutes (2 days). After the designated time, the shear box was taken to the direct shear machine and consolidated under a vertical load of 30 psi (200 kPa). Figure 6.14 shows the vertical strain versus soaking time for the two soils on a semi-log scale.

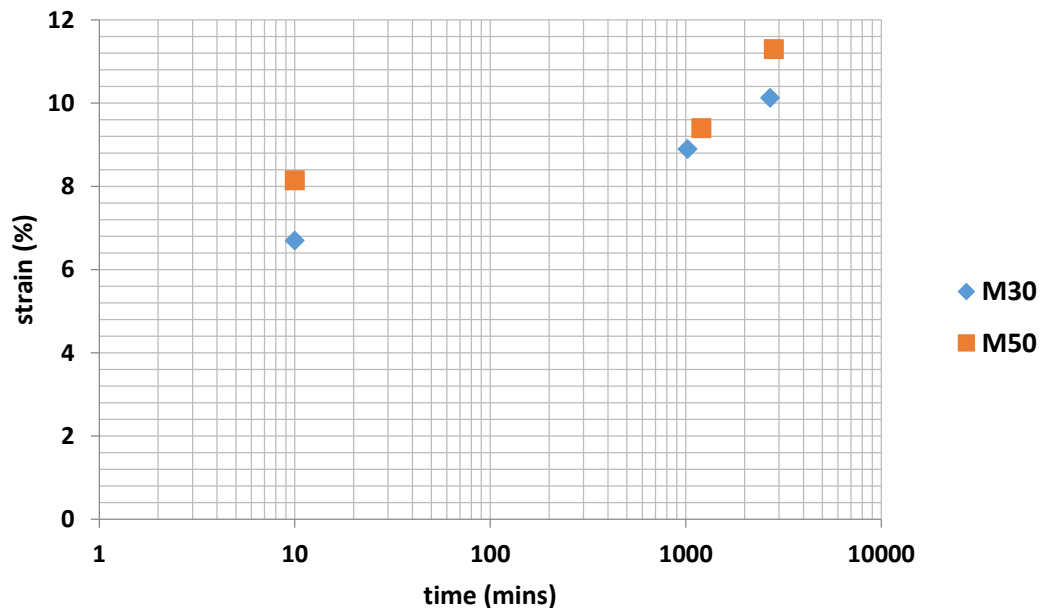


Figure 6.14 Vertical strain versus soaking time at 200 kPa

Both samples showed an increase in vertical strain with increasing soaking time. As water was percolated through the soil samples, gypsum was continuously leached. Therefore if the sample is leached for a longer time, more gypsum is lost, making the soil more collapsible in the process. The effluent water that was collected in the trough was transferred to a beaker. The electrical conductivity and salinity of the effluent collected at each time interval was measured (Table 6.2). Measurements were taken at temperature of 21° C.

Table 6.2 Electrical conductivity and salinity of effluent water

<b>Time (Minutes)</b>	<b>30% gypsum Conductivity (<math>\mu\text{S/cm}</math>)</b>	<b>30% gypsum Salinity (ppm)</b>	<b>50% gypsum Conductivity (<math>\mu\text{S/cm}</math>)</b>	<b>50% gypsum Salinity (ppm)</b>
10	4010	2160	3400	1820
1020	3460	1840	3270	1750
2700	3290	1740	3290	1740

Gypsum is a sparingly soluble salt and both EC and salinity are indicators of solubility. From the table, it is seen that for both the soils EC and salinity either remains fairly constant with time. This means that while water continuously leaches gypsum from the soil, the concentration of gypsum itself in the effluent is relatively unchanged. The water was most likely saturated with gypsum at concentrations of approx. 2.5 g/L.

### 6.3 Collapsibility tests using consolidation load frame

Investigation of collapsibility using the previous method yielded information about the effect of water content, time and dissolution on collapse but no significant relationship with gypsum content of the soils. The vertical strain profiles of the soils showed an increase in strain with increase in gypsum under both dry and saturated conditions. It was therefore decided that collapse potential would be re-investigated using a different method. The use of a one-dimensional consolidation load frame was considered. The ASTM D2435 test configuration for one-dimensional consolidation testing of cohesive soils was used. The same setup could also be used to determine the long-term deformation of the soils (creep).

The principle of SCT proposed by Knight (1963) was used in this test. The dimensions of the sample are given in Table 6.3. All the sample had a void ratios in the range of 0.56 -0.64. The samples was gradually loaded up to 200 kPa and the corresponding deformation at each load was recorded. At 200 kPa, the sample was inundated with water and left for 24 hours. Then it was further loaded till the final load. The different loading steps are shown in Table 6.4.

Table 6.3 Dimensions of a test sample

<b>Sample detail</b>	<b>units</b>
diameter	6.35 cm
depth	1.88 cm
volume	59 cm <sup>3</sup>



Table 6.4 loading steps in the collapse potential test

Step	Load (kPa)	Condition
1	48	Dry
2	96	Dry
3	200	Dry
4	200 (Inundation)	Inundated
5	312	Inundated

### 6.3.1 Collapse potential with gypsum content

A series of tests were initially conducted with a 1 hour time period between the loading steps. Eight soil samples were tested with gypsum content ranging from 5% to 75%. The tests were primarily conducted to assess the feasibility of the study using the consolidation frame setup. Figure 6.15 shows the deflection versus load plot for three soils. Unlike the collapse tests using the direct shear machine, the CP values from this test setup showed a well-defined relationship with gypsum content.

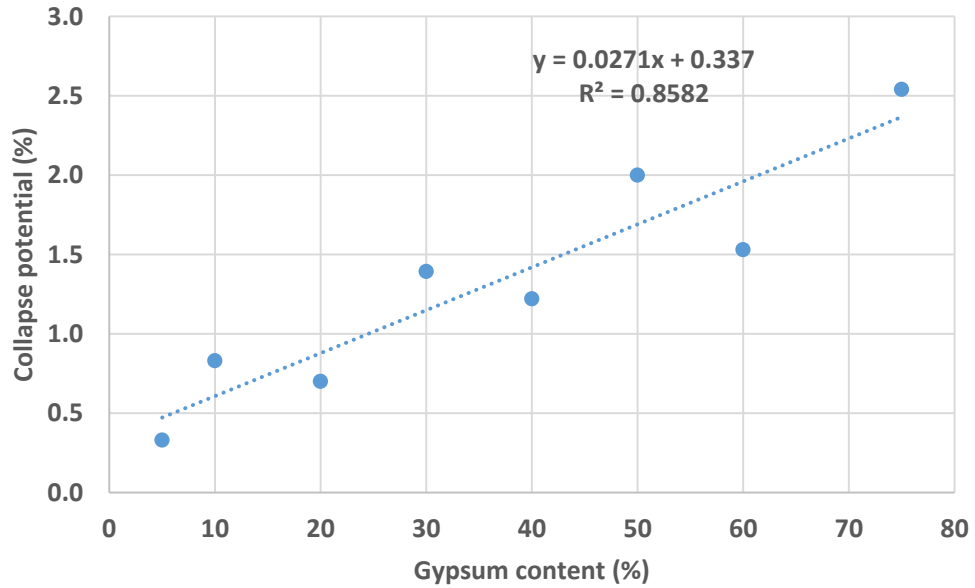


Figure 6.15 Collapse potential versus gypsum content (1 hour collapse step)

All these tests indicated that collapsibility (or strain) increases with increase in gypsum content. To confirm this behavior another set of collapse potential tests were performed on five soil samples with gypsum content ranging from 5%-75%. The actual single collapse test methodology was followed where the collapse loading step (at 200 kPa) was performed for 24 hours. The results from this were more representative of an actual oedometer test (Fig. 6.16). The collapse potential values were also greater because of 24 hours of consolidation as opposed to 1 hour. The tests showed a good linear relationship between collapse potential and gypsum content. Figure 6.17 shows the vertical strain versus load plots for the five soils tested.

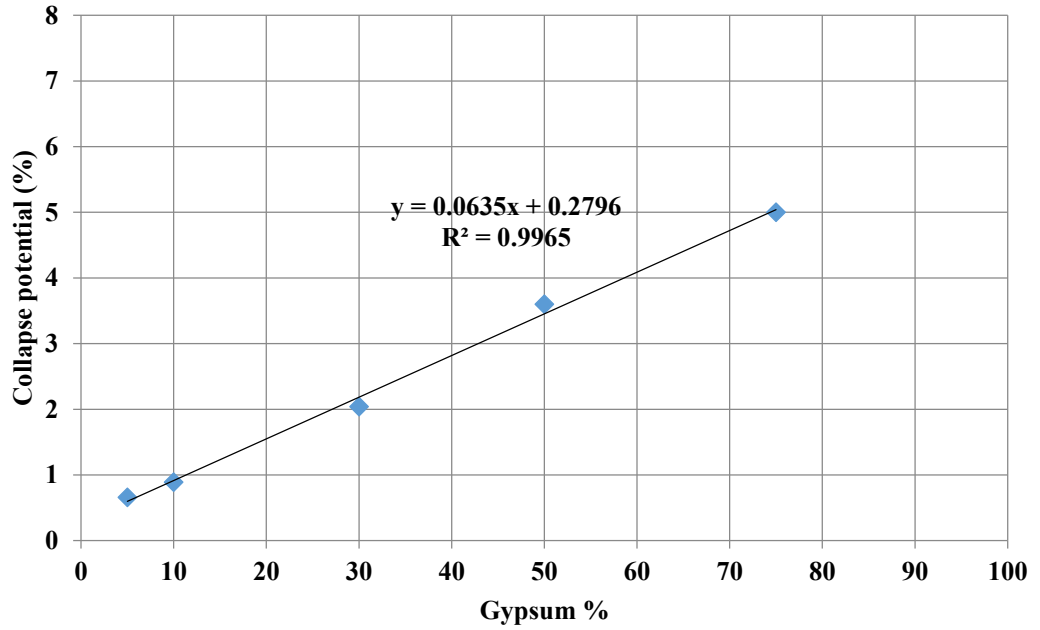


Figure 6.16 Collapse potential versus gypsum content (24 hours collapse step)

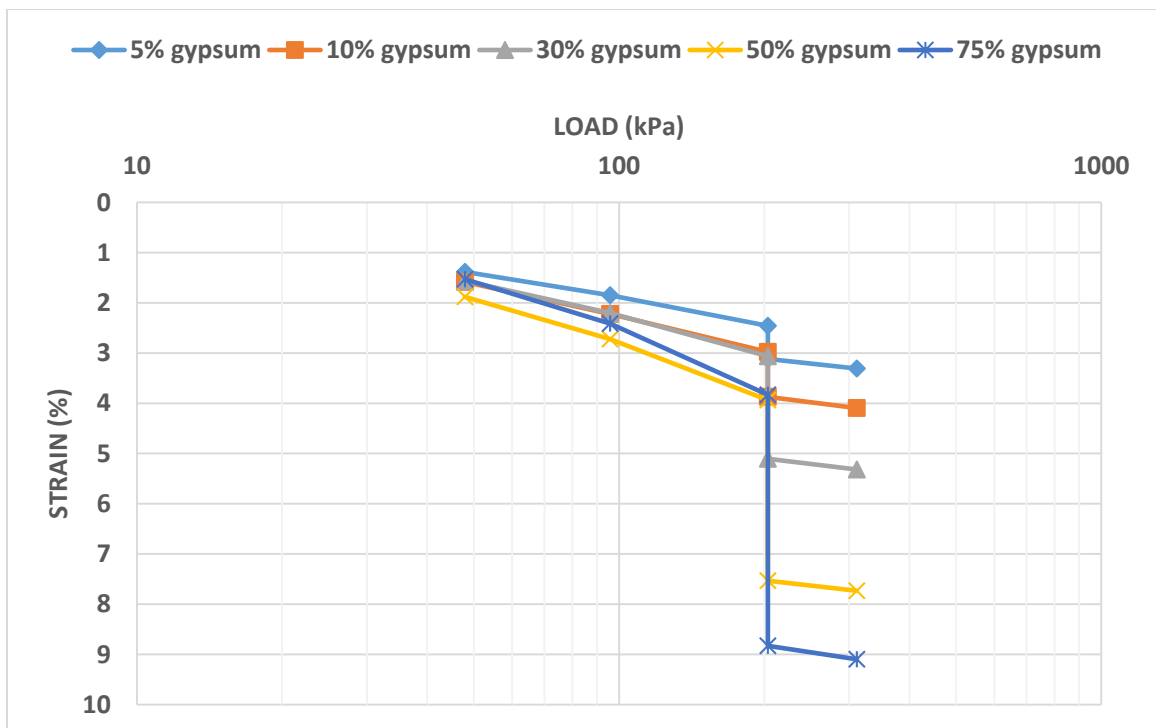


Figure 6.17 strain versus vertical load for all the soils tested

### 6.3.2 Collapse potential with time

This test was performed as a continuation to the 1 hour collapse step tests in order to examine the effect of long term loading on gypsum soil settlement (creep). After the final load (312 kPa) was applied a deflection reading was taken after 1 hour and the load was left on the load frame. The creep tests were performed on three samples with 10%, 30% and 60% gypsum contents by allowing the loading in the final step to continue for 72 hours (Figure 6.18). Measurements were taken every 24 hours, for three days. The plots showed that the long term settlement of the soil samples increased with gypsum content.

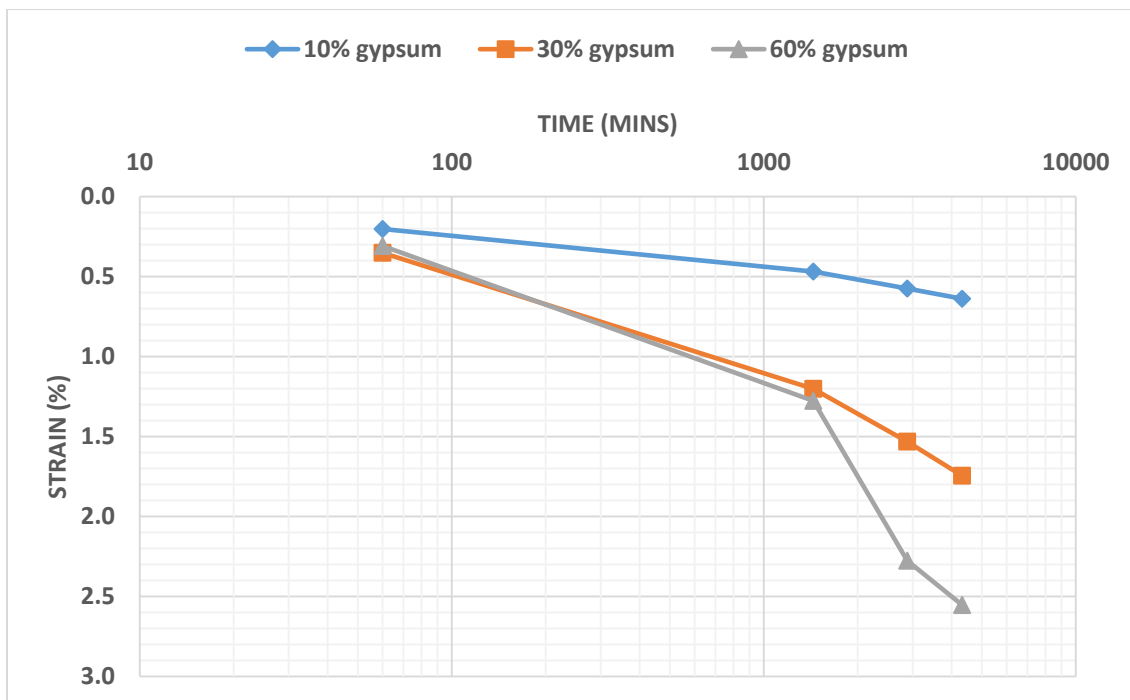


Figure 6.18 Creep deformation of three soil samples over 72 hours

#### **6.4 Inferences and conclusion**

Vertical strain and collapse potential were measured for different gypsum sand samples subjected to normal loading. The consolidation tests were performed by varying the gypsum content, initial water content and time. Data from the collapse test were collected and plotted. Though there was a small amount of scatter in the data, all the results indicate that collapse potential increases with increasing gypsum content of the soils. This behavior is attributed to the dissolution of gypsum in water and also its softness. The gypsum in the sand acts as a weak cementing agent and the soils have a fairly good amount of strength. When these soils are loaded under dry conditions, they compress under the loads. The sudden addition of water however causes a partial loss of cementing material through dissolution, crushing and re-arrangement. This results in an increase in settlement over time. The tests involving the use of consolidation load frame yielded more accurate results. Based on the Jennings and Knight (1975) criteria, soil samples with less than 10% gypsum could be classified under 'no trouble' category and soils with 10%-70% gypsum could be classified under 'moderate trouble' category.

The collapse settlement is also dependent on the moisture content of the soil, increasing with increase in moisture content. It is also dependent on the soil grain size and peaks at around a degree of saturation of 50-60 % for fine grained sands. The tests involving collapse versus time showed that long term settlement increased with time and gypsum content. This was because of the dissolution and leaching of gypsum. Dissolution of gypsum was determined by measuring the electrical conductivity and salinity of the effluent. The electrical conductivity ( $\mu\text{S}/\text{cm}$ ) and salinity (ppm) values remained fairly constant with time because of the sparing solubility of gypsum.

The results discussed here appear to be in agreement with the work of Fattah et al. (2008) and Fattah et al. (2011) wherein the hydrocompression behavior of gypsum sands in Iraq was studied using single and double oedometer tests and the computer program Settle3D. In the two studies conducted, it was found that the collapse potential of the soils used for footings increased with increasing gypsum content. For the double oedometer test and creep test, they chose three soil samples with gypsum content varying from 14% to 66%. The three samples were designated N1, N2 and N3 with their gypsum contents being 66%, 44% and 14.8 % respectively. The collapse potential plot of the three soils is shown in Figure 6.20. The long term deformation of the soils is also associated with their gypsum content. Soils with lower gypsum went through lesser creep deformation.

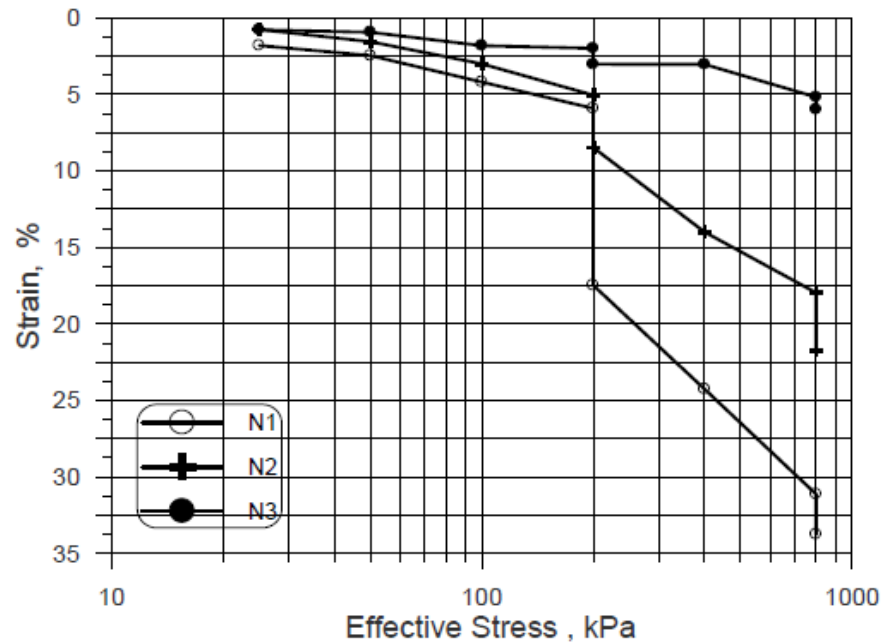


Figure 6.20 Collapse potential test results of three soil samples (Fattah et al., 2011)

Researchers also studied the effect of relative density and initial void ratio on collapse potential of gypsiferous soils. In most of the studies, collapse potential was found to increase with increasing initial void ratio (Seleam, 2006). These tests however could not be successfully conducted and verified in the lab because of the small specimen size. For both the test setups (consolidation load frame and direct shear machine), the sample volume was at best 90 cm<sup>3</sup> and as such it was difficult to compact the specimen to void ratios lower than 0.6. For almost all the collapse tests conducted in this research, the void ratio of the sample was in the range of 0.62-0.68.

In this research, the collapse tests were conducted at a normal stress of approximately 200 kPa. However the collapse potential could also be studied at different normal stresses depending on the requirements. An empirical equation has been presented by Seleam (2006) which can be used to convert collapse potential at any given pressure to collapse potential at 200 kPa:

$$CP_{200} = 140.25 * (CP_{pressure})^{0.0135} * (200 / pressure) - 139.05 \quad (6.4)$$

There is ample scope for further research in the area of collapsibility of gypsum soils. The effect of various physical and chemical parameters on collapsibility should be studied within any region known to have a history of collapsibility. It is also essential to develop different testing schemes which can be used to indirectly assess the collapse potential of soils without significantly disturbing the soils. Geophysical surveys, GPR, remote sensing and GIS are some examples of alternate means of testing that can be used to assess collapsibility of gypsum soils.

## **7. Statistical analysis of test results and estimation of gypsum content**

### **7.1 Introduction**

Electrical resistivity and free-free resonant column tests were conducted on reconstituted gypsum rich soil specimens to observe any variability in physical parameters that could be reflected by the variations in resistivity and shear wave velocity trends. The important properties of gypsum soils that control their physical and chemical behavior are gypsum content, moisture content, void ratio, dry unit weight and fines content. Geophysical tests to measure  $v_s$  and electrical resistivity were conducted by varying one or more of these parameters and while keeping the others constant. In the field, however, these variables could change spatially and temporally. Likewise, the knowledge of  $v_s$  and electrical resistivity data at a site could help estimate the physical conditions of the soil. These estimates could only be made if we have some design guidelines or statistical trends that relate  $v_s$  or resistivity with the physical or chemical properties of the soil. To address these aspect, statistical analysis was performed on the tests data using tools such as multiple regression analysis. In a similar manner, statistical analysis was also performed on the geotechnical tests such as collapsibility tests and direct shear strength tests, to estimate how the soil properties varied with changes in one or more physical parameters. Regression analysis also indicated which factors had a relatively higher impact on the variability of  $v_s$ , resistivity, collapse potential and shear strength. Based on these results, statistical design equations were created to correlate the different geotechnical and geophysical parameters.



## 7.2 Regression Analysis

Regression analysis is one of the most widely used statistical tools by engineers to establish relationships between dependent and independent variables. Statistical analysis also helps in developing predictive relationships, wherein the knowledge of one or more variables can help estimate the value of an unknown variable. Empirical equations are then developed to relate soil data with available geophysical information collected at a site. For this research, data analysis features of EXCEL were used to perform statistical analysis of soil variables. Multiple linear regression analyses can be performed to model the variability of a dependent variable with respect to one or more independent variables for a chosen level of confidence. The typical outputs gathered from regression analysis are: coefficient of determination ( $R^2$ ), standard deviation ( $\sigma$ ), significance level  $F$ ,  $p$ -values of independent variables and residuals. These values help us assess the significance of a regression and the relative impact of the different independent variables on the dependent variable. Non-linear regression was used to assess the validity of a relationship between a dependent and independent variable, wherever deemed suitable.

Free-free resonant column testing was performed on reconstituted gypsum soils to measure  $v_s$  by varying effective stress, moisture content and gypsum content. Electrical resistivity tests were conducted by varying gypsum content, moisture content and dry density.

Collapse potential of a soil can be influenced by a number of factors such as gypsum content, initial void ratio, dry unit weight, effective stress, moisture content, percentage fines and Atterberg limits of the soil. A reasonable estimate of some of these parameters

can shed light on the collapse potential of soil. It could also provide information about the shear strength properties of soil ( $c$  and  $\phi$ ).

### **7.3 Statistical analysis of shear wave velocity data**

Several tests were conducted on gypsum soil specimens to measure  $v_s$ . The first set of tests was conducted on dry soils by varying gypsum content and effective stress. The next set of tests was conducted on moist soils by varying gypsum content and degree of saturation while keeping the effective stress constant. Data points from all of these tests were collected in such a way that, the range of all three variables, gypsum content, effective stress and degree of saturation were covered. It was shown in Chapter 3 that  $v_s$  had a very good correlation with effective stress. In this context, multiple variable regression analysis was used to see if  $v_s$  could be reasonably correlated with gypsum content and water content as well. A 95% confidence level was chosen for the analysis. Appendix B shows the data considered for this regression.

The analysis revealed a very poor correlation of  $v_s$  with the three parameters. The summary output of the analysis is shown in Table 7.1. The complete analysis along with the ANOVA table is shown in Appendix B. The very high  $p$ -values of the individual variables shows that they play a very insignificant role in the regression, which was performed for a 95% confidence level ( $\alpha = 0.05$ ). The significance level  $F$  and adjusted  $R^2$  values were also extremely low indicating that there is a very low correlation between the dependent and independent variables. Because of these aspects, the regression was considered insignificant.

Table 7.1 Regression outputs of  $v_s$  modeled as a function of GC,  $\sigma'$  and  $w$  %.

<b>Regression parameter</b>	<b>Value</b>
R-square	0.077
Adjusted R-square	-0.022
Standard deviation	33.06
Number of observations	32
Significance F	0.517

Further interpretation of the variables revealed that, the influence of water content on the stiffness of gypsum soils varied in a very non-linear fashion. The impact of water content on the soil stiffness also varied with soil gypsum content. While in general,  $v_s$  increased with decrease in degree of saturation, matric suction and cementation affects influence stiffness below a certain degree of saturation. In soils with  $GC < 30\%$ , matric suction caused a sharp increase in  $v_s$  between  $S = 10\%$ - $20\%$ . In soils with  $GC > 40\%$ , the effect of matric suction was outweighed by cementation, causing  $v_s$  to plateau below  $S = 40\%$ . Due to these qualitative material variations, the linear regression model could not be used to explain the variability of  $v_s$  with using  $GC\%$ ,  $\sigma'$  and  $S\%$  as the dependent variables.

Another statistical analysis was performed using only two variables,  $GC\%$  and  $\sigma'$  as the dependent variables. To perform this regression, only the data points from the tests with cell pressure were taken as most of these tests were performed at zero degree of saturation. The confidence level was again chosen as 95%. Appendix B shows the detailed output of the regression analysis.

This analysis showed a much better correlation between  $v_s$  and the two variables. The key outputs from the regression analysis are shown in table 7.2. The significance  $F$  of the regression,  $R^2$  value as well as the individual  $p$ -values of the independent variables

point towards a good overall significance of the model. The y-intercept and the coefficients of GC and  $\sigma'$  are used to generate the linear regression equation.

$$v_s = 140.2 - 0.348 (GC) + 0.328(\sigma') \quad (7.1)$$

This equation predicts  $v_s$  as a linear function of GC and  $\sigma'$ . The predicted and actual values of  $v_s$  are shown in Figure 7.1. There was some scatter in the data, but it still had a well-defined trend. Among the two variables, effective stress has a more significant impact on  $v_s$ . the standard deviation of the predicted data is 15.18. The values are fairly well predicted around the mid-range but are somewhat scattered around the ends.

Table 7.2 Regression outputs of  $v_s$  modeled as a function of GC and  $\sigma'$

Regression parameter	Value
R-square	0.77
Adjusted R-square	0.74
Standard deviation	15.18
Number of observations	18
Significance F	1.54 E-05

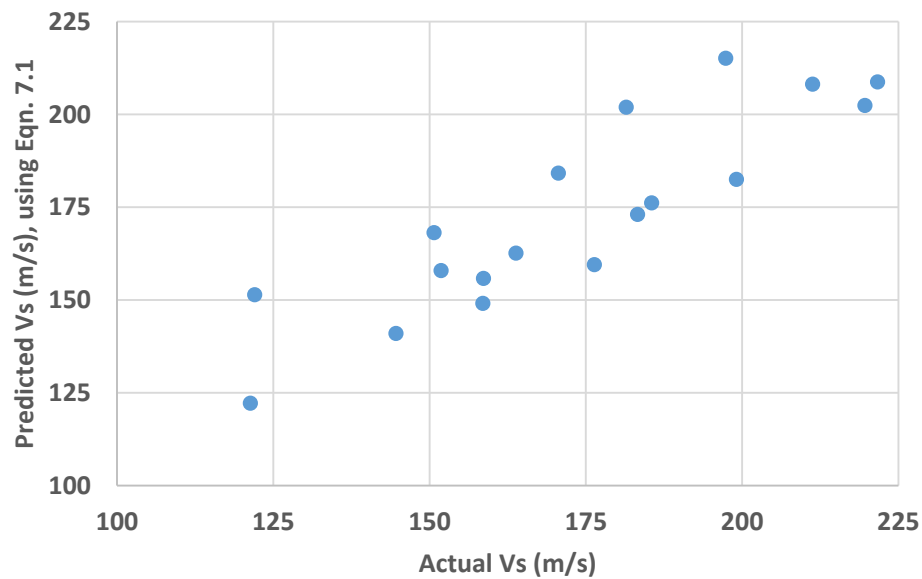


Figure 7.1 Comparison of predicted vs actual shear wave velocities

It was shown in Chapter 3 that when  $v_s$  varied approximately with the fourth root of effective stress according to the expression  $v_s = C \sigma^n$ . The average value of the exponential term 'n' was calculated and was recorded as 0.233. Figure 7.2 shows the  $C$  values of the specimens plotted against their gypsum content. The plot shows that the values of  $C$  range from 44 to 56 and are higher for M20 and M30.

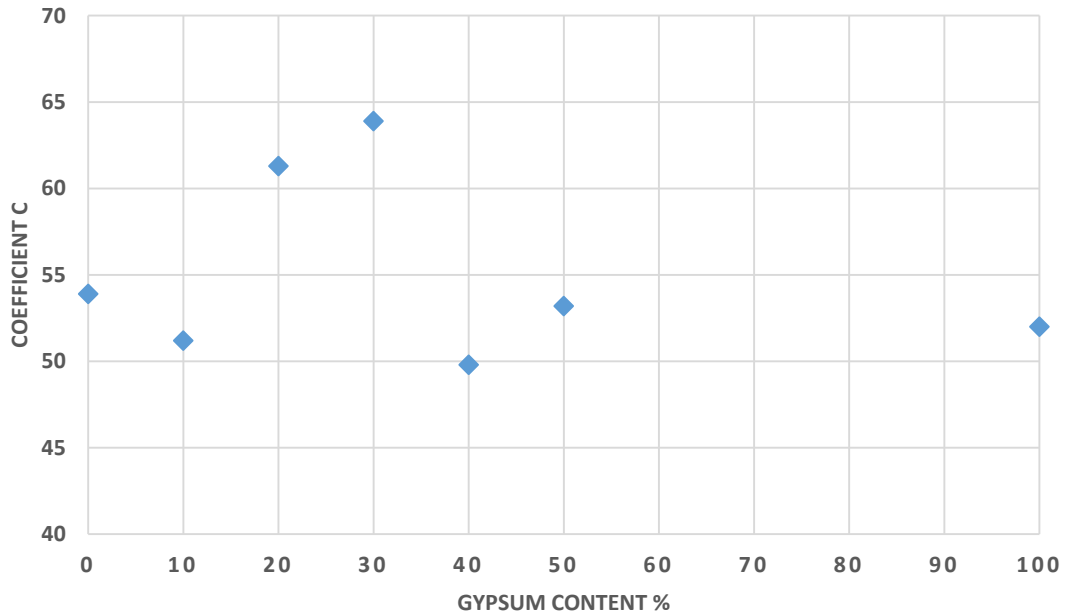


Figure 7.2 regression coefficient C vs gypsum content

Shear wave velocities measured in all the tests using cell pressure were normalised with their corresponding effective stresses raised to the power of 0.233. These normalised  $v_s$  values were plotted against gypsum content. The plot is shown in Figure 7.3. It is seen that normalised  $v_s$  is maximum when GC is between 10%-20%. This shows that the stiffness of dry gypsiferous soils is maximum at gypsum contents of 10%-20%. To be able to better estimate the gypsum content from normalized  $v_s$ , a portion of data from the above plot was excluded. Normalized  $v_s$  was plotted for specimens with gypsum content less than

50%. A second order polynomial curve was fitted through the data points (Figure 7.4). The curve showed a good fit with an  $R^2$  value of 0.92. Since soil stiffness increased up to 20 % gypsum content and decreased thereafter, a second order equation could help estimate the different possible gypsum contents that could be associated with a normalized  $v_s$  value. The equation of the curve was:

$$v_s' = -0.0277 (GC)^2 + 0.9134(GC) + 54.53 \quad (7.2)$$

Where  $v_s'$  is the normalized shear wave velocity and GC is the gypsum content. This model is however applicable to only soils with less than 50% gypsum and zero degree of saturation.

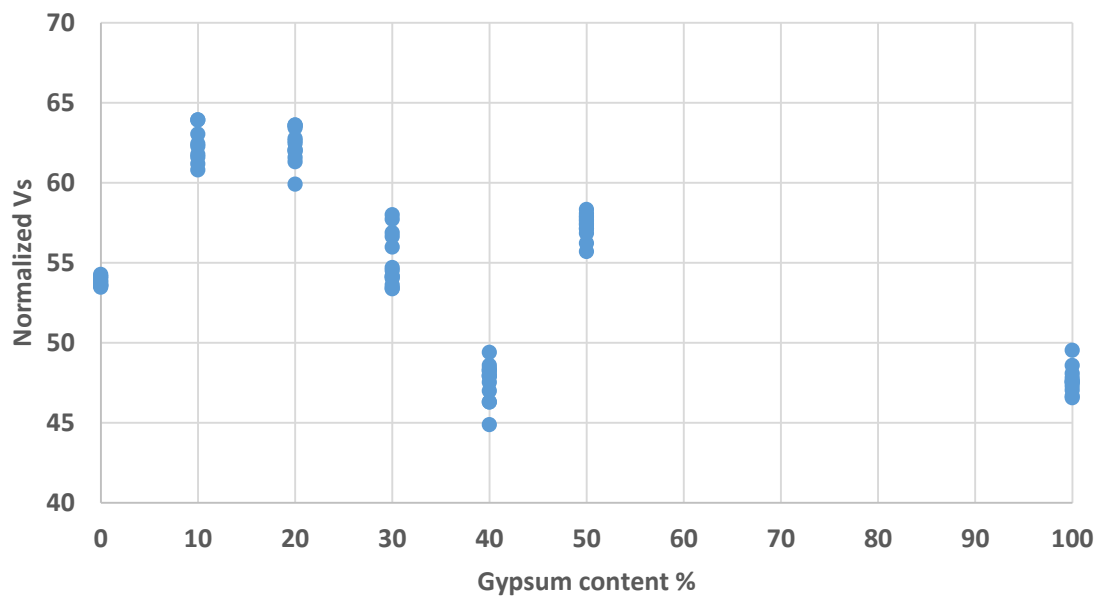


Figure 7.3 Normalised shear wave velocity versus soil gypsum content

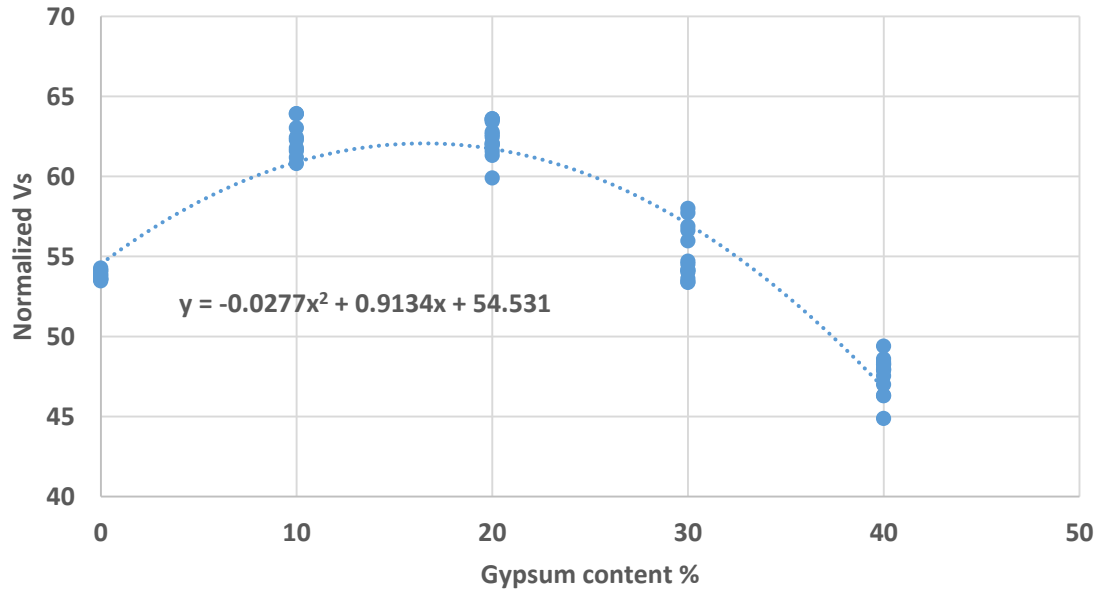


Figure 7.4. Normalised shear wave velocity versus gypsum content for specimens with less than 50% gypsum

To validate the observed trend, another set of FFRC tests were performed on dry gypsum sand mixtures, without the use of cell pressure. Five soil specimens with gypsum contents of 0%, 20%, 30%, 50% and 75% were tested. Shear wave velocities of the specimens were plotted against the effective stress. As no cell-pressure was used, only vacuum contributed to the effective stress and the maximum value attained was 24 in. (81 kPa). The average value of the exponential term ‘n’ in the expression  $v_s = C \sigma^n$  was 0.25. Shear wave velocities were again normalized with their effective stresses raised to the power of 0.25 and plotted against gypsum content (Fig. 7.5). It was seen that normalized  $v_s$  values were highest between gypsum contents of 20%-30%. The values then decreased and almost stabilized at higher gypsum contents. The data from 75% gypsum specimen was excluded and a second order polynomial curve was fitted through the remaining data

points (Fig 7.6). The curve was similar to the one reported above and had an  $R^2$  of about 0.85. The equation of the curve is shown below:

$$v_s' = -0.0099 (GC)^2 + 0.43(GC) + 61.67 \quad (7.3)$$

This lead to the conclusion that the gypsum content of a gypsiferous soil sample with up to 50% gypsum can be estimated from shear wave velocity measurements using a second order polynomial approximation.

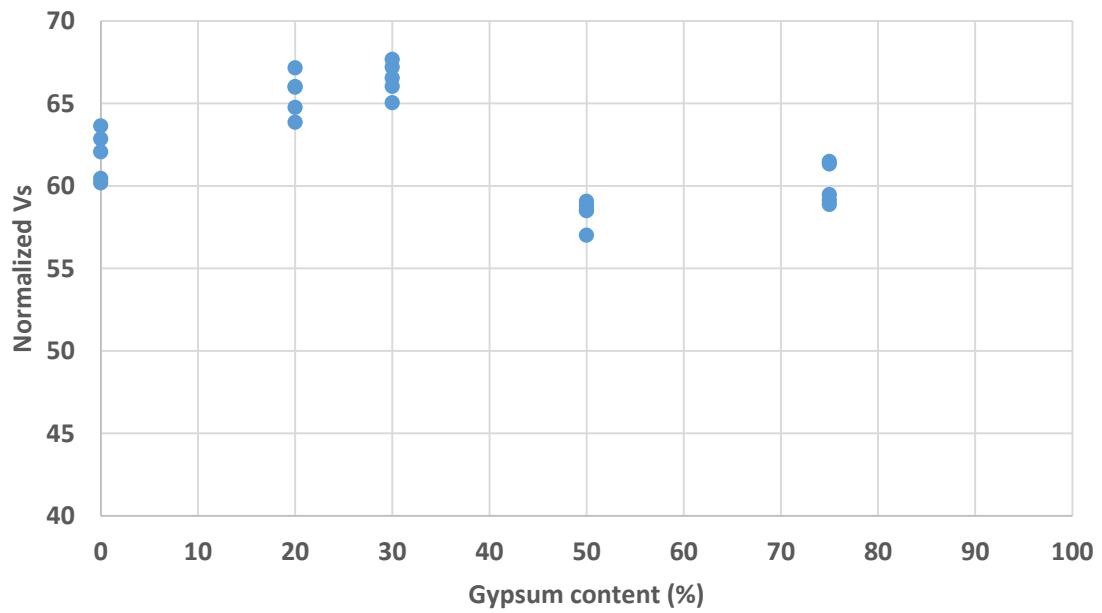


Figure 7.5 Normalised shear wave velocity versus soil gypsum content ( tested without cell pressure)



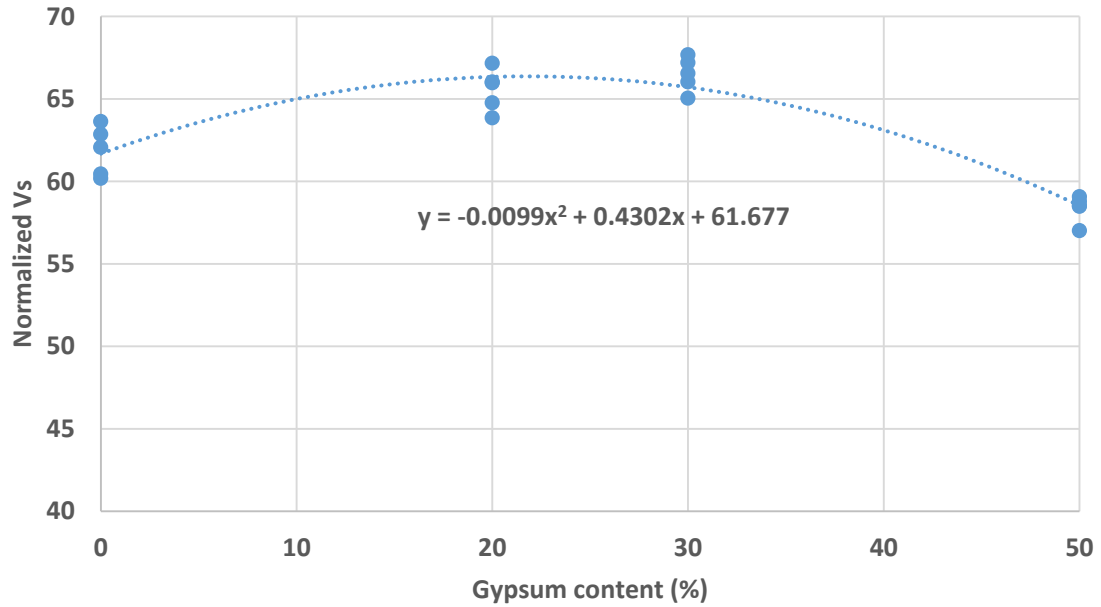


Figure 7.6 Normalised shear wave velocity versus gypsum content for specimens containing up to 50% gypsum (tested without cell pressure)

Normalised  $v_s$  values measured from the tests with moist samples were plotted against degree of saturation (Figure 7.7). Forty three different data points were considered over a range of gypsum content, S% and effective stress. This plot also again showed a peak in normalized  $v_s$  values between S= 10%-20% and an overall increase in stiffness with decrease in saturation. This increase in stiffness is due to cementation and matric suction. At lower gypsum content, matric suction causes an increase in stiffness whereas cementation causes an increase in stiffness at higher gypsum content. The results could not be fit into a mathematical model because of the more qualitative variation in stiffness based on gypsum content. The plot is in agreement with the results reported in Chapter 4. Section 7.7 of this chapter describes how this information can be used to estimate the gypsum content of soil.

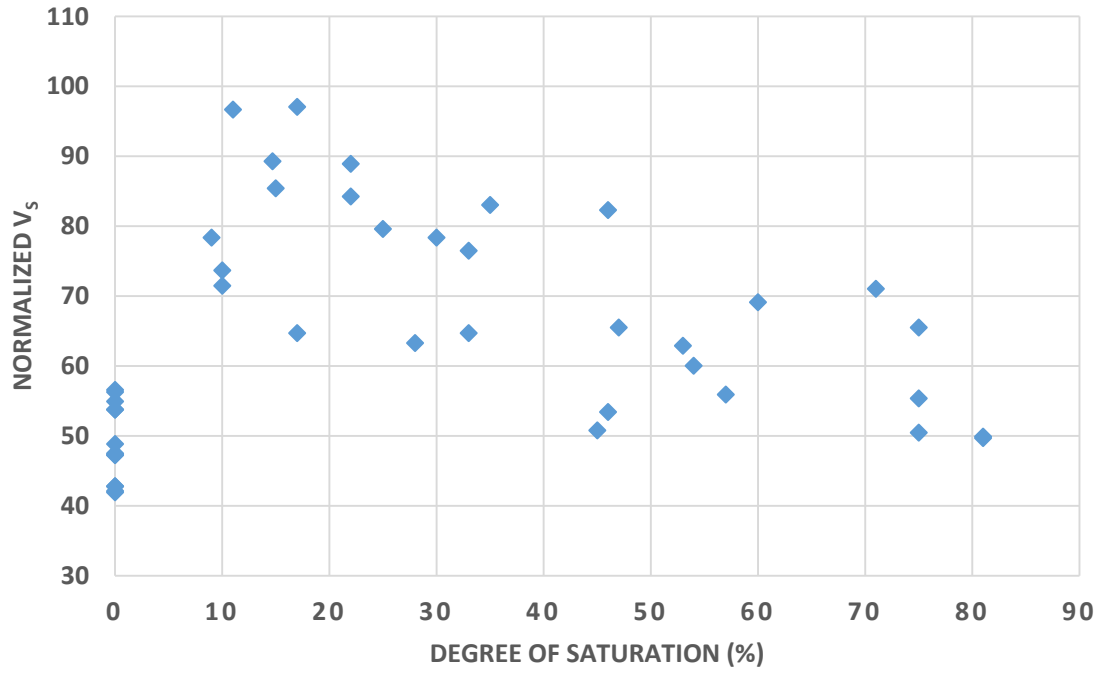


Figure 7.7. Normalised shear wave velocity versus degree of saturation

#### 7.4 Statistical analysis of electrical resistivity data

Electrical resistivity tests were performed on several gypsum soil samples using the four-electrode box resistivity method (ASTM G57). Tests were performed to observe changes in soil resistivity by varying moisture content, gypsum content and dry density. These tests and their results were described in chapter 3. Resistivity was found to vary with all the three variables under consideration. However, when performing resistivity measurements in the field, the spatial variability of all of these parameters must be considered. To address this aspect, statistical analysis was performed on the datasets to model resistivity as a function of gypsum content, moisture content and dry density. Multiple linear regression analysis was again chosen as the modeling tool to assess if any relationship could be established between resistivity and the three variables mentioned.

Pore-water resistivity measurements of the different soil samples showed that the values were comparable for all gypsum bearing soils. All the measurements were conducted at 22° C. However the soil sample with 0% gypsum had a much higher pore-water resistivity. Table 7.3 lists the soil specimens and their pore water resistivity. The resistivity measurements by varying the soil moisture content were normalized with their respective pore-water resistivity values to yield a parameter named normalized resistivity ( $R'$ ). The resulting plot is shown in Figure 7.8. The plot shows that normalized electrical resistivity ( $R'$ ) is comparable for all soils containing gypsum, irrespective of their gypsum content. When the soil has no gypsum, the normalized resistivity is lower than that of gypsiferous soils. This information could be used to estimate the moisture content of a gypsiferous soil sample from electrical resistivity data.

Table 7.3 Pore water resistivity of gypsum soil specimens

Specimen	Pore-water resistivity (Ohm-m)
0% gypsum	9.30
10% gypsum	2.85
20% gypsum	2.70
40% gypsum	3.32
60% gypsum	3.03

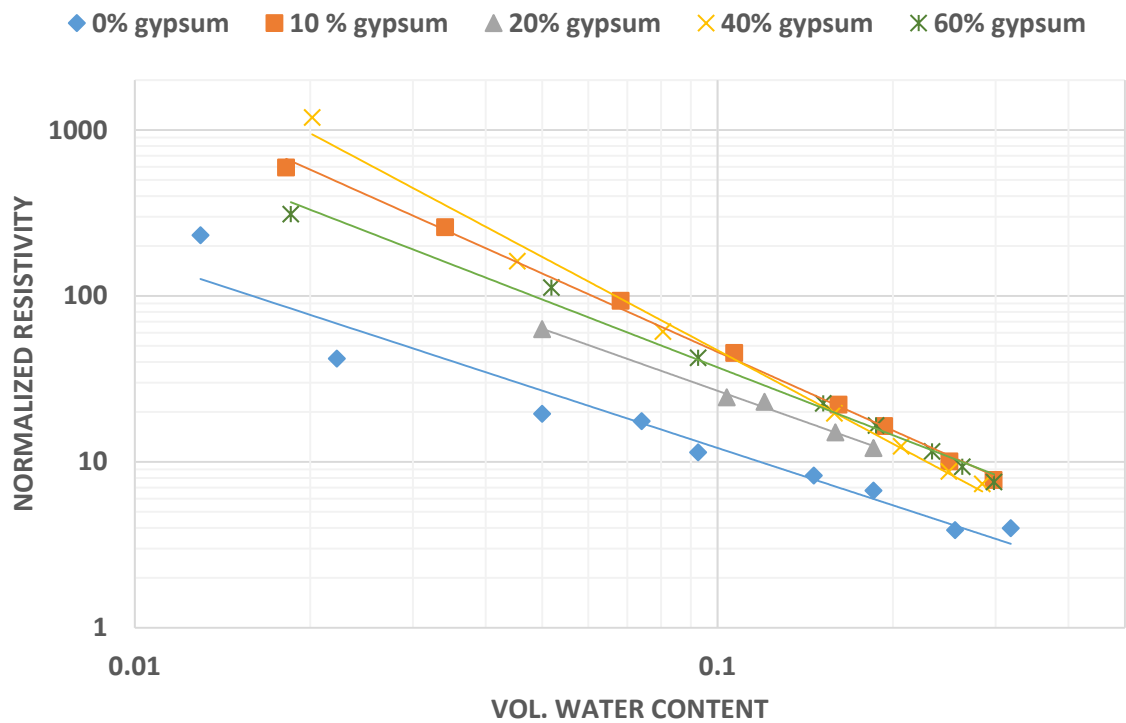


Figure 7.8 Normalized electrical resistivity versus volumetric water content

Resistivity was also found to vary with dry density of the specimen. Resistivity measurements were performed on saturated soil specimens over a range of dry densities and normalized with their respective pore-water resistivity. The resulting plot is shown in Figure 7.9. Normalized resistivity had a good linear correlation with the sample dry density. The coefficient of determination was 0.899 indicating a good regression between the two variables. It could be used to determine dry density of gypsiferous soils by measuring resistivity. There were however some limitations to this model. It was difficult to achieve dry densities lower than 1.45 g/cc or higher than 1.85 g/cc under the given testing conditions. The range of normalized electrical resistivity values were between 5 to 10 which was also a fairly narrow range.

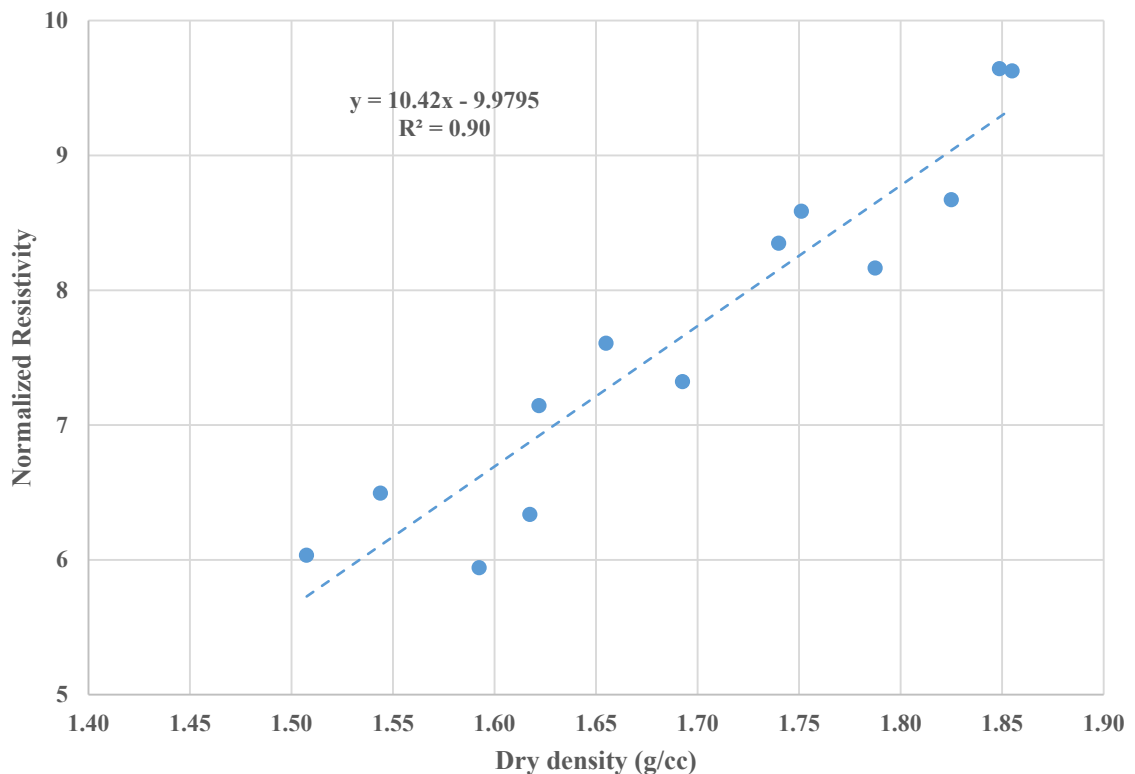


Figure 7.9 Normalized electrical resistivity vs dry density

Next, a multiple linear regression analysis was performed on the resistivity test data. Twenty two data points were chosen in such a way that they were representative of the range of GC%, volumetric moisture content, and dry density. Specimen M0 (with 0 % gypsum) was not considered for the analysis because non-gypsiferous soil showed much different resistivity measurements than gypsiferous soils. The confidence level was chosen at 95% ( $\alpha = 0.05$ ). The complete regression output along with the ANOVA table is shown in Appendix B. The key outputs from the regression are shown in Table 7.4. The analysis showed a good overall relationship between resistivity and the three variables. This was seen from an  $R^2$  value of 0.756 and a significance F level of 9.30 E-06 (much smaller than  $\alpha$ ). On a closer inspection, it was found that volumetric moisture content was the only significant variable contributing to the regression. Gypsum content and dry density yielded  $p$ -values much larger than  $\alpha$  rendering them insignificant from the regression point of view. As it was seen previously, resistivity varied only over a very narrow range with dry density, but it had a much broader range of variation with moisture content.

Table 7.4 Regression outputs of resistivity modeled as a function of GC%, vol. water content and dry density

<b>Regression parameter</b>	<b>Value</b>
R-square	0.756
Adjusted R-square	0.715
Standard deviation	4.84
Number of observations	22
Significance F	9.36 E-06

Due to the relative insignificance of GC% and dry density on the output range of electrical resistivity, the two variables were eliminated and normalized electrical resistivity for all gypsiferous soils was modeled solely as a function of volumetric moisture content. Thirty three datasets were chosen from the resistivity versus moisture tests on soils M10, M20, M40 and M60. The plot showed a good exponential relationship between resistivity and moisture content. The value of  $R^2$  of 0.94 was also comparatively higher for this model. This regression was accurate for a volumetric water content of 0.05 to 0.30. For water content below 0.05, the resistivity values increase sharply in no defined order.

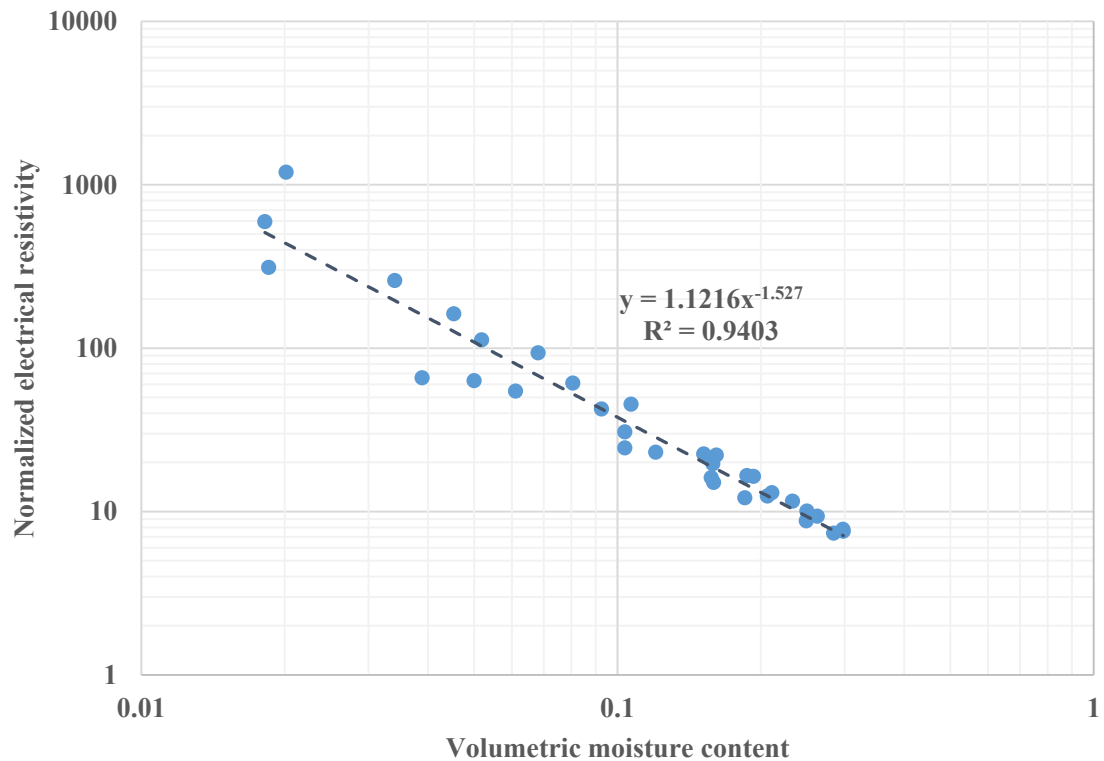


Figure 7.10 Normalized resistivity versus volumetric water content

This relationship between normalized resistivity and volumetric water content can be used to model the latter. Substituting  $y$  and  $x$  with resistivity and volumetric water content respectively, the equation is:

$$R' = 1.1216 \theta^{-1.527} \quad (7.4)$$

where  $R'$  is the normalized resistivity. By re-arranging the terms of the equation,  $\theta$  can be expressed as a function of  $R'$  as shown in Equation 7.4. Volumetric moisture content can be estimated from resistivity measurements using this expression.

$$\theta = \exp (0.075 - 0.655 \ln R') \quad (7.5)$$



## 7.5 Statistical analysis of direct shear strength test data

Direct shear strength tests were conducted using the Geocomp Shear Trac II direct shear machine to study the shear strength parameters  $c$  and  $\phi$  of gypsum soils. The tests were conducted on dry soil specimens and saturated soil specimens. Mohr-coulomb failure envelopes were plotted for each soil type for the test results. For both the soil types it was found that friction angle  $\phi$  increased with gypsum content. Cohesion was very small for the dry soils and the mean value of cohesion for all the soil types was 0.69 psi (4.7 kPa). Cohesion was higher and more significant for the saturated specimens because of the cementation action of gypsum. While there was no relationship with gypsum content, the average cohesion value measured for the saturated specimens was 5.35 psi (37 kPa).

Five gypsum-sand mixtures were tested under dry conditions and four mixtures were tested in saturated conditions. Accordingly, more data were available to perform a regression analysis on the dry direct shear strength datasets. As mentioned above, the average value of cohesion  $c$  was very small and it did not show any distinct variation with gypsum content. A linear relationship was found between friction angle  $\phi$  (degrees) and gypsum content. The relationship is shown in figure. The  $R^2$  value for this regression was 0.89 indicating a fairly good relationship between the two variables. Friction angle is related to gypsum content through the linear relation:

$$\phi = 0.1295 (GC) + 35.297 \quad (7.6)$$

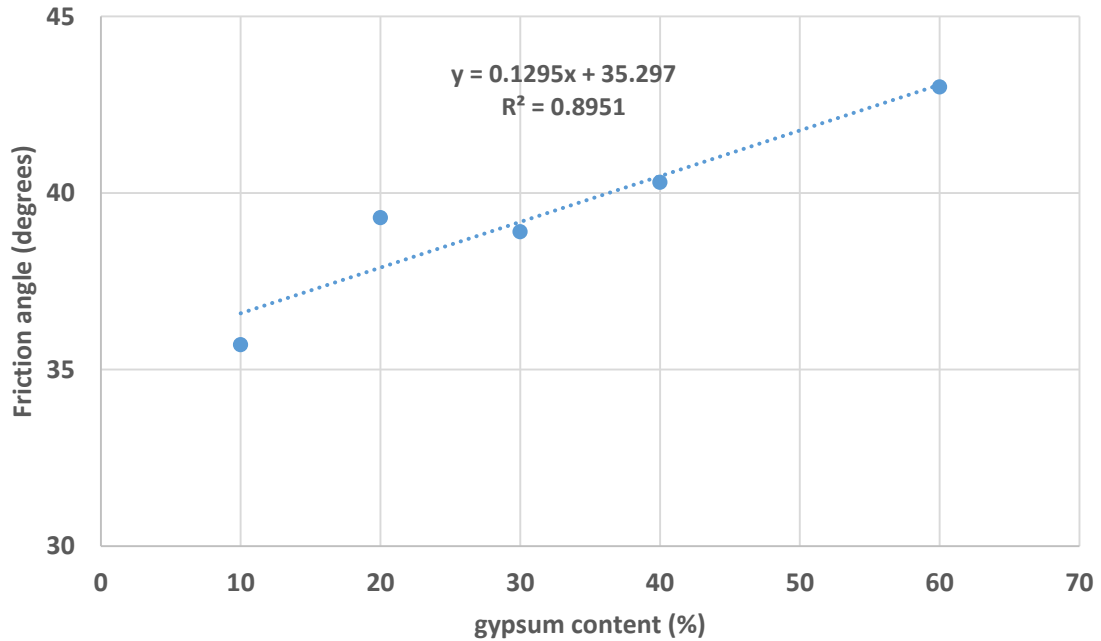


Figure 7.11 Friction angle versus gypsum content of dry gypsum sand mixtures

The drained shear strength of a soil is related to the normal stress through the relationship:

$$\tau' = c' + \sigma \tan (\varphi') \quad (7.7)$$

Where  $\tau'$ ,  $c'$  and  $\varphi'$  are the drained shear strength, drained cohesion and drained friction angle respectively. By substituting Eqn. 7.5 for drained friction angle and using the average cohesion value of 0.79 psi (5.47 kPa), the following regression equation was developed to predict the shear strength of a dry gypsum-sand for a given value normal stress:

$$\tau' = 5.47 + \sigma \tan [0.1295 (GC) + 35.297] \quad (7.8)$$

Equation 7.8 was used to predict the drained shear strength of 22 data points and the result was compared with actual shear strength values. Figure 7.12 shows the predicted versus the actual shear strength values. The predicted shear strength values compare favorably with the measured shear strength values. Equation 7.6 was developed based on

data from five soil samples. It can be further developed by testing more soil samples. The approach can also be extended to cemented soils by conducting more tests.

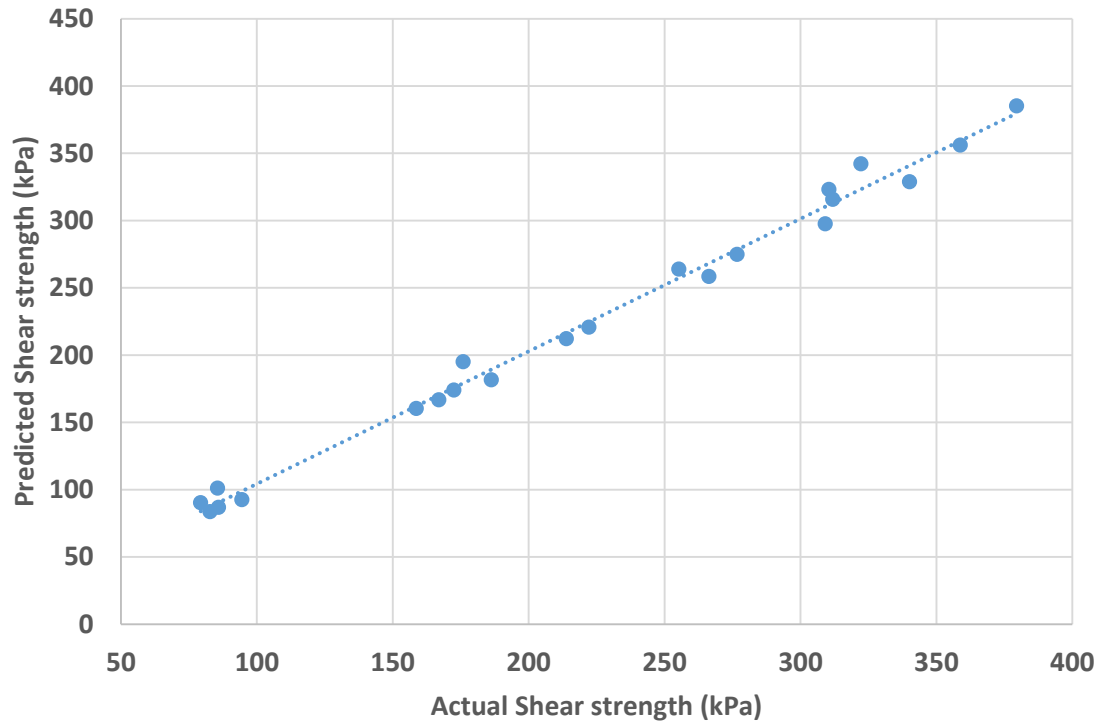


Figure 7.12 Predicted versus actual shear strength values of dry gypsum sand specimens

## 7.6 Statistical analysis of collapse potential data

One-dimensional consolidation test setups were used to measure collapse potential or vertical strain on gypsiferous soil samples. Tests were conducted on the soil samples by varying gypsum content and water content. The change in vertical strain of the samples was also measured with respect to time. As mentioned previously, the void ratios of the soil samples could not be varied significantly due to the small size of the test specimens and most of these tests were conducted at comparable initial void ratios (0.65 to 0.72). The outcomes of each of these tests are discussed here.

Collapse potential of soils was measured at a normal stress of 200 kPa according to Jennings and Knight (1975) and it was found to increase with increasing gypsum content. Soil samples with gypsum content ranging from 5% to 75% were tested. The variation of collapse potential with gypsum content had a linear relationship as shown in Figure 7.13. The  $R^2$  value of 0.996 indicated a good relationship between the two variables. The regression equation of the best fit line could therefore be used to correlate CP with GC%. The equation is shown as:

$$CP = 0.0635 (GC \%) + 0.0279 \quad (7.9)$$

The equation is developed by analyzing only five samples. A more reliable equation can possibly be developed by testing more gypsum soils samples. The plot shows that soils with less than 10% gypsum can be classified under 'no trouble' category and soils with 10%-70% gypsum can be classified under 'moderate trouble' category, according to Jennings and Knight (1975).

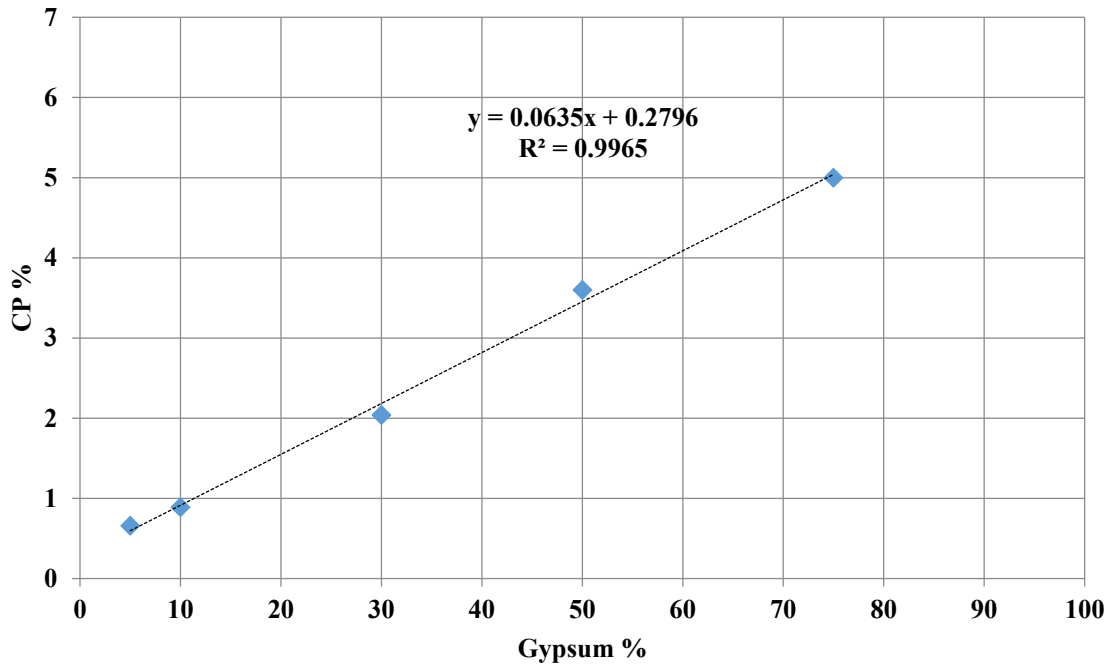


Figure 7.13 Collapse potential versus gypsum content

For the collapsibility tests under varying moisture contents, the measurable parameter was vertical strain. Soils specimens with gypsum content ranging from 20% to 70% were prepared and tested under different water contents. For an average sample void ratio of 0.67, most of the specimens were estimated to be saturated at a water content of about 27%. The change in vertical strain with moisture content was not linear. Vertical strain increased with water content, peaked approximately at 15% and would decrease thereafter (Figure 7.14). The results were in agreement Al-Rawas (2000) but variation was qualitative and could not be developed into a statistical model.

Likewise, the time-dependent collapse of gypsum soils was measured in terms of vertical strain. The long term deformation (creep) of the samples increased with time and also with gypsum content. The test results are shown in Figure 7.15.

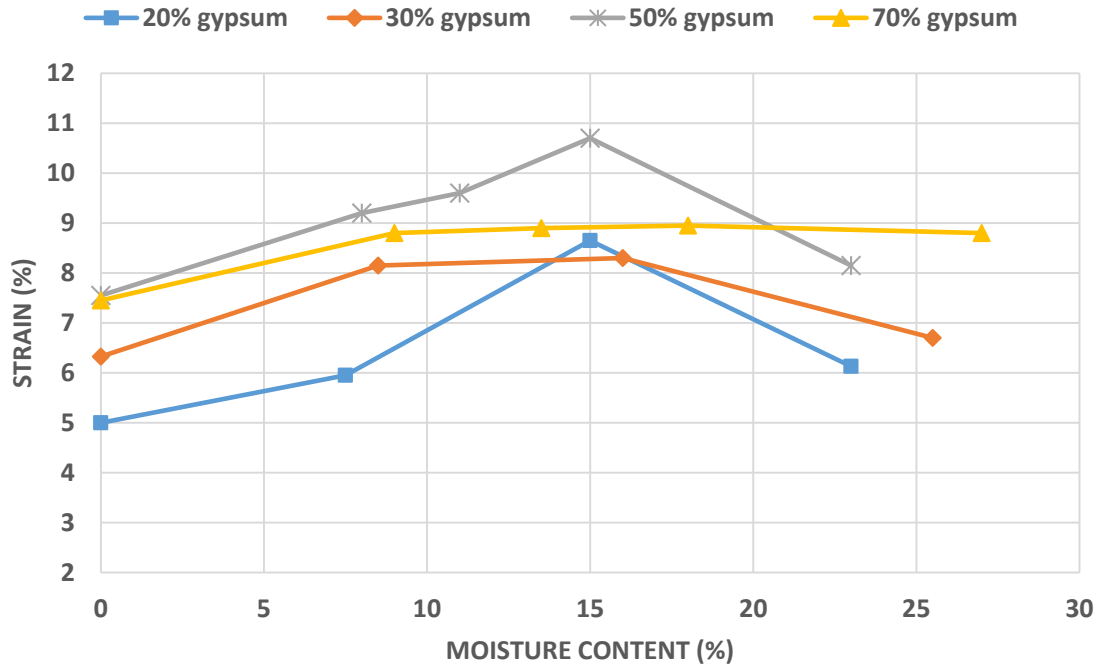


Figure 7.14 Vertical strain versus moisture content

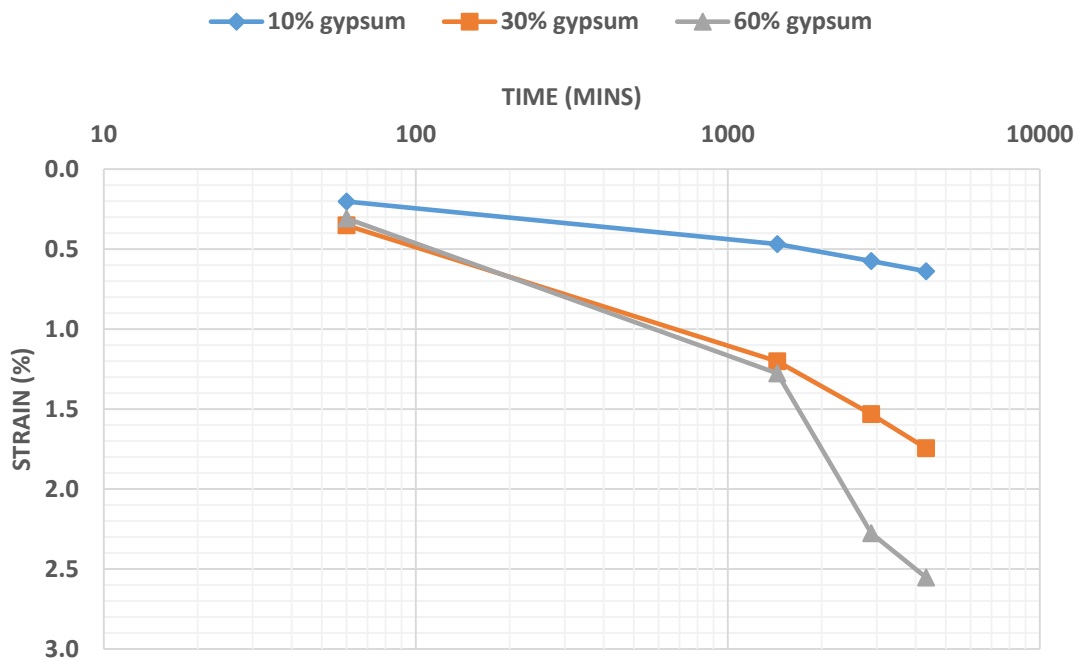


Figure 7.15 Collapse settlement of gypsum soils versus time

Multiple regression analysis was performed on the long term deformation data shown above, with vertical strain as the dependent variable and gypsum content and time (hours) as the independent variables. The confidence interval was again chosen at 95%. The analysis was performed on all the twelve data sets available. The main outputs from the analysis are shown in Table 7.5. The regression parameters indicate a statistically significant model. The ANOVA table for this regression is presented in Appendix B. The regression equation is shown below. In this expression, time, 't' is measured in minutes.

$$\varepsilon\% = 0.0219 (GC\%) + 0.000319 (t) - 0.0331 \quad (7.10)$$

Table 7.5 Regression outputs of strain modeled as a function of GC and time (mins.)

<b>Regression parameter</b>	<b>Value</b>
R-square	0.787
Adjusted R-square	0.740
Standard deviation	0.407
Number of observations	12
Significance F	9.4 E-04

## 7.7 Estimating gypsum content using geophysical methods

From the previous sections it was seen that shear-wave velocity varies with degree of saturation and gypsum content. At lower gypsum contents ( $< 20\%$ ),  $v_s$  increased sharply between S% of 10-25% owing to matric suction. On the other hand, the peak was gradually replaced by a plateau at higher gypsum contents due to the predominance of cementation effect. Figure 7.16 shows how the  $v_s$  of five soils with gypsum content ranging from 10%-60% varied between 10%-35% degree of saturation. Table 7.6 shows the average rate of decrease of  $v_s$  with S%, for the different specimens. This information about the rate of change of shear wave velocity between 10%-35% degrees of saturation can be used to estimate the gypsum content of soils.

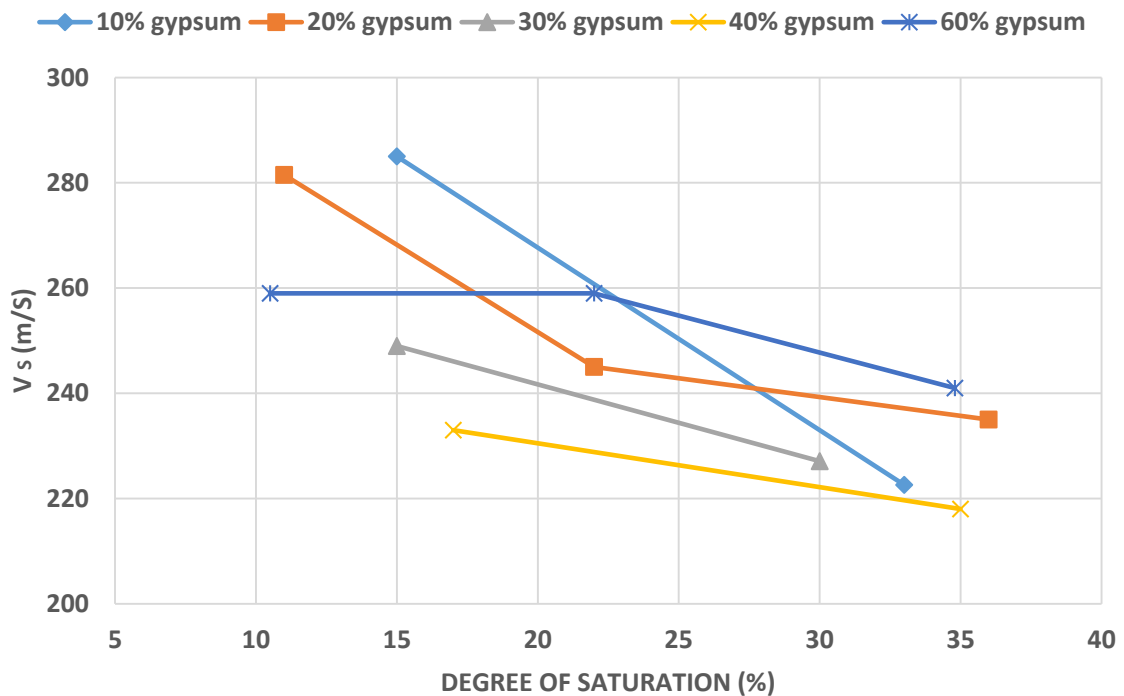


Figure 7.16. Shear-wave velocity versus degree of saturation for five gypsum soils



Table 7.6 Average rate of change of  $v_s$  between 10%-35% degree of saturation

Gypsum content	Average rate of change of $v_s$ (m/s/S %)
10	-3.46
20	-2.58
30	-1.46
40	-0.83
60	-0.74

The negative rate of change of  $v_s$  indicates that shear wave velocity decreases with increase in degree of saturation. It was shown using Eqn. 7.5, that normalized electrical resistivity can be used to predict the volumetric moisture content of gypsum soils.

Using Eqn. 7.5 and the information from table 7.6, an approach can be developed to predict the gypsum content of soils using geophysical methods. This approach presented here was developed for an effective stress of 58 kPa. For other effective stresses, it can be assumed that rate of change of  $v_s$  with S% would be proportional to the fourth root of effective stress. As such,  $v_s$  will only increase a little with an increase in effective stress. Also the tested specimens were loose to medium-dense sands with an average dry density of about 1.66 g/cc. Generally higher  $v_s$  values are obtained for dense soils.

As an example, if  $v_s$  for a gypsum soil at 58 kPa is 220 m/s, the  $v_s$  for the soil at 80 kPa for the same S% would be  $(80/58)^{0.25}$  times higher, which equates to 238 m/s. Considering this aspect, it can be assumed that for small increments of depth, the effect of overburden stress on  $v_s$  would be minimal and the main reasons for changes in  $v_s$  would be cementation and matric suction. For convenience, the rate of change of  $v_s$  with S% can be defined using a variable called 'M' value, with units of m/s/S%.

Using a combination of electrical resistivity data and shear-wave velocity data, the gypsum content of a soil layer in the field can be estimated. The different steps used in this process are described below:

- i) Conduct ER measurements and normalize the resistivity values with respect to pore water resistivity of gypsum soils.
- ii) The normalized electrical resistivity values can be used to estimate the volumetric moisture content of the soil along a vertical section, using Eqn. 7.5.
- iii) Next the volumetric moisture content should be converted to degree of saturation.
- iv) Shear wave velocity measurements should be conducted along the vertical section, with small increments of depth (about 1.5 m).
- v) The rate of change of  $v_s$  with respect to degree of saturation should be noted using the ' $M$ ' value described above.
- vi) If  $M$  is greater than 2.0 m/s/S%, then the soil contains 20% or less gypsum. If  $M$  is between 1.0-2.0 m/s/S%, then the soil has an intermediate gypsum content, ranging from 20%-40%. Finally, if  $M$  is less than 1.0 m/s/S%, the soil has a significant fraction of gypsum (40% or more).
- vii) Further estimation of gypsum content can be done using a quadratic relationship like Eqn. 7.2 and use of engineering judgement.
- viii) Using the value of gypsum content, collapse potential of the soil can be estimated using Eqn. 7.9.

These eight steps to estimating gypsum content and collapse potential can be shown in the form of a flowchart (Fig. 7.17). It should be noted that the approach is hypothetical and works only over a small range of S% and under the assumptions that the soil layer is homogeneous and gypsum is uniformly distributed in the layer.

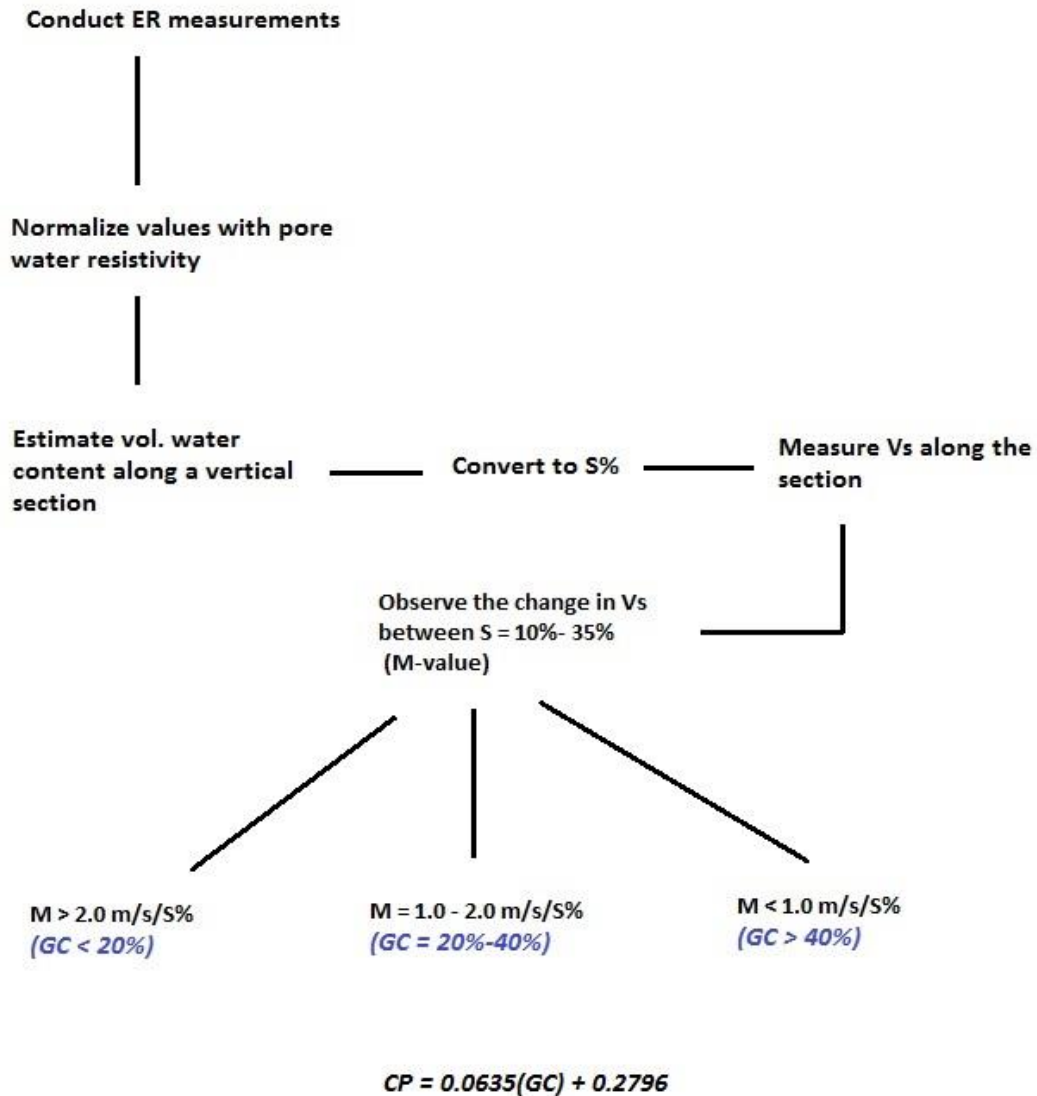


Figure 7.17. An approach to estimating gypsum content and collapse potential of soil using geophysical methods.

## 7.8 Conclusion

Statistical analysis was performed on the geophysical test data to develop equations or relationships to predict the geotechnical parameters that effect the collapsibility of gypsum soils. Equations 7.1 and 7.2 are predictive equations based on shear wave velocity data. They can be used to estimate gypsum content of soils and also the effective stresses. These expressions were developed using soils tested under zero degree of saturation. Even though water content also significantly affects the soil stiffness, the change is influenced by factors like cementation effect and matric suction making it difficult to lay down a predictive model.

Electrical resistivity data can be used to predict the soil moisture content and dry density. Moisture content has a much greater influence on resistivity while dry density values have a lesser influence. The latter can be used over a fairly small range of dry density and electrical resistivity. The variation of resistivity with gypsum content is marginal. Equation 7.5 can be used to predict volumetric moisture content from normalized electrical resistivity measurement. The equation works well for a volumetric content range of 0.05 to 0.30.

Data from direct shear testing of dry gypsum sand mixtures was used to model drained friction angle as a linear function of gypsum content (Eq. 7.6). The mean value of cohesion was chosen and Eqn. 7.8 was developed to estimate the drained shear strength of gypsum soils for given values of normal stress. The equation predicted the shear strength of soils with a fair level of accuracy. The approach could also be used to predict the shear strength of cemented or saturated soils by conducting more tests.

Statistical analysis was also performed on the collapsibility tests data. The knowledge of soil gypsum content and the time of saturation can be used to predict the collapse potential and vertical settlement of soils. This has been shown using equations 7.9 and 7.10. Collapse potential increases linearly with gypsum content. Figure 7.14 shows the variation in vertical settlement of gypsum soils with respect to water content. The relatively small size of test specimens made it difficult to bring about a significant change in the initial void ratios or dry densities of the specimens. Soil moisture content, dry density and gypsum content can be obtained from the geophysical test results.

The results from electrical resistivity testing and free-free resonant column testing were used to develop an approach to predict the gypsum content of soils in the field. It is based on the premise that for different gypsum soils, shear wave velocity changes with degree of saturation. The approach can work over a limited range of moisture contents, for loose to medium-dense gypsum soils. The knowledge of gypsum content helps in predicting the geotechnical soil parameters like collapse potential and shear strength.

The accuracy of the statistical analysis and models could be further improved if more test data was available. In the laboratory setup, the geophysical and geotechnical tests had some limitations and not all variables could be controlled and tested. The limited range of void ratios attainable is one such example. The analysis could also be improved by using non-linear multiple variable analysis tools. Multiple linear regression is not always the best tool to analyze variability of dependent and independent parameters. The use of statistical software packages such as MINITAB or SPSS could also assist developing more precise models. In spite of these limitations the analyses presented offer an approach as to how the

geophysical tests could be used to estimate the parameters that effect collapsibility of gypsum soils.

## **8. Conclusion**

### **8.1 Summary**

The objective of this research was to characterize gypsum rich soils in a laboratory setup, using geophysical and geotechnical investigation methods. The information gathered from these tests could be used in estimating the collapse potential and engineering hazards that could be associated with the soils. Shear wave velocity  $v_s$ , and electrical resistivity were the geophysical parameters that were used for characterizing the soils. Free-free resonant column testing was used to measure the  $v_s$  of the specimens. Electrical resistivity tests were conducted using the 2 and 4 electrode soil box resistivity methods. The geotechnical investigations consisted of determination of friction angle, cohesion, consolidation settlement and specific gravity of the soil specimens. The tests were conducted using the direct shear testing machine and the one-dimensional consolidation load frame.

Statistical analyses were performed on the test results using single and multiple variable regression analysis, in order to develop co-relations and design equations. The relationships and analysis performed on the geophysical test data was used to determine the factors that significantly affect the collapse potential of gypsum rich soils. An empirical method was developed to estimate the gypsum content of soils from electrical resistivity and shear wave velocity data collected at a site. The approaches described in this research could be further developed and used in site investigations in places known to contain gypsum soils. The following section provides a summary of the main outcomes and findings of this research. The later sections describe some of limitations that were encountered during the research and ideas for further research.

## 8.2 Observations and Inferences

- Shear wave velocity of gypsum soils varies with effective confining stress. It also varies with the gypsum content of the soils, though the variation is not linear. Stiffness of the soils is maximum at gypsum content around 20%. The differences are appreciable at higher confining stresses. A second order polynomial equation was developed to represent this variation in stiffness with respect to gypsum content for soils with up to 50% gypsum. This equation can be solved to estimate gypsum contents corresponding to a particular normalized  $v_s$  value.
- Shear wave velocity of gypsum soils also varies the soil moisture content. Stiffness of soils increases with a decrease in degree of saturation. At degrees of saturation below 40%, two mechanisms lead to an increase in soil stiffness. For soils with more than 30% gypsum, cementation occurs between quartz and gypsum particles leading to an increase in stiffness. For soils with less than 30% gypsum, matric suction leads to an increase in effective stress at lower degrees of saturation. This result is consistent with the findings of Qian et al. (2008). The effect of cementation is not appreciable at low gypsum contents. Both these mechanisms can be seen when  $v_s$  is plotted against degree of saturation. Matric suction causes a sharp increase in stiffness between  $S = 10\%$ - $20\%$ , while cementation leads to an increase and a subsequent plateau in  $v_s$  below  $S = 40\%$ . The rate of change of  $v_s$  with  $S\%$  can be used to characterize the soils based on their gypsum content and an empirical method has been proposed for the same.

Both matric suction and cementation lead to a substantial increase in stiffness of soils. Soil specimens previously subjected to saturation showed a



greater stiffness as compared to freshly prepared gypsum-quartz mixtures. These type of soils could be more representative of soils in situ.

- Electrical resistivity of gypsum soils increases with decrease in moisture content. The relationship between resistivity and volumetric water content can be estimated using an exponential curve. The electrical conductivity of the soil is primarily because of the pore water and the dissociated calcium and sulphate ions in the pore water. The pore water resistivity is comparable for all gypsum soils, regardless of gypsum content.
- The relatively small variation in pore water resistivity with respect to gypsum content is attributed to gypsum belonging to the class of sparingly soluble salts. This causes the solution to attain saturation at low salt concentrations. Increasing the gypsum concentration in the soil does not increase the ion concentration in the pore water and the excess gypsum precipitates on to the soil.
- The resistivity of soils with no gypsum is higher due to the absence of calcium and sulphate ions. Electrical resistivity increases with gypsum up to 20% and stabilizes with further increase in gypsum content.
- Electrical resistivity of gypsum soils increases with increase in dry density. Within a fairly small range, the relationship between resistivity and dry density is linear. The variation was in accordance with Archie's law. Since the conductivity of the soil is mainly due to pore water, decrease in soil porosity leads to increase in resistivity. Dry density however had a smaller impact on resistivity as compared to volumetric moisture content.

- Specific gravity ( $G_s$ ) of the soil specimens decreases with increase in gypsum. This is because of the lower  $G_s$  of gypsum (2.32) in comparison to quartz (2.65). The more the proportion of gypsum in the soil, the lower its specific gravity. This also causes dry unit weights of soil specimens to decrease with gypsum content.
- From consolidation testing, it was found that vertical deformation of the soil specimens increases with increase in gypsum content. Gypsum being a very soft mineral gets crushed under the application of normal load. Increasing the gypsum content of the soil leads to the crushing of gypsum particles and moving the soil into increasingly denser configurations.
- The drained friction angle of soil ( $\phi$ ) increases with gypsum content, because consolidation of the test specimen increased with gypsum. This increase in density led to a rise in friction angle. The increase was less pronounced in case of saturated (cemented) specimens. The Mohr-coulomb failure envelopes of different gypsum-sand specimens showed that cemented specimens had a significant amount of cohesion ( $c$ ) in comparison to dry (uncemented) specimens. This result was comparable to resonant column test results, wherein cemented specimens higher stiffness ( $v_s$ ) than uncemented specimens.
- The Collapse potential of gypsum soils increases linearly with gypsum content. These results are in agreement with the findings of Fattah et al. (2008). The severity of collapse of a soil specimen is estimated by the criteria defined by Jennings and Knight (1975). Based on this criteria, soils with more than 10% gypsum were classified into 'moderate trouble' category based on the severity of collapse

potential. Likewise, specimens with more than 70% gypsum came under ‘trouble’ category.

### **8.3 Limitations of the research**

The research was conducted using reconstituted gypsum-sand mixtures in a laboratory setting. Therefore there were limitations on the tests that were conducted and the conditions that could be created in the setting. Some of these aspects are described in this section.

- The physical properties of gypsum and quartz such as electrical conductivity and stiffness are not drastically different. Therefore the geotechnical and geophysical tests yield results that vary in a fairly narrow range. It as such becomes necessary to repeat the tests several times in order to derive meaningful conclusions.
- Most of the geophysical tests have non-unique results. Shear wave velocity and electrical resistivity do not show a well-defined variation with gypsum content. This is unlike geotechnical test data such as friction angle ( $\phi$ ) and collapse potential which increase linearly with gypsum content. As result, it is difficult to develop design equations using regression analysis to model gypsum content from the available geophysical data.
- There was no standardized compaction procedure used for specimen preparation. Fine grained soils are generally compacted using the standard or modified proctor methods. These methods could not be used since the soil specimens being tested were coarse grained.
- Because of the small size of the specimens used in consolidation tests, direct shear testing and electrical resistivity testing, it was difficult to achieve a wide range of

void ratios. All the tested specimens had a roughly uniform void ratio. Since the geotechnical and geophysical soil properties known to vary significantly with dry unit weight, this aspect was a major limitation on the tests and the spectrum of results that could be generated.

- The soils used in the research are simple mixtures of quartz and ground gypsum. It does not contain a significant amount of fines nor does it represent the macroscopic field conditions and heterogeneities. Seismic and electrical resistivity tests performed in the field might yield results much different from those of laboratory results. Electrical resistivity data could be different by orders of magnitude in clayey and silty soils. The presence of cavities or discontinuities in the subsurface also alter resistivity and shear wave velocity.

#### **8.4 Suggestions for future research**

This research study provides an insight into the behavior of gypsum soils under varying physical conditions. This information derived from this research could be used in establishing the geotechnical parameters that play a role in the collapsibility of gypsum soils and classifying the soils in terms of severity of collapse. There is however ample scope for further research in this field. More tests could be performed on the soils and the data could be used to predict and develop better relationships between the test parameters. Some of the following ideas could be tried and implemented in testing gypsiferous soils in order to estimate their engineering hazard potential.

- Free-free resonant column tests can be carried out using cell pressure at different moisture contents. This would provide more information about the variation in stiffness of moist gypsum soils especially at higher effective stresses. Soils with a history of saturation are stiffer than freshly prepared soil samples because of cementation between gypsum and quartz. A comparative analysis could be performed to estimate the increase in stiffness due to cementation. Alternatively, previously saturated and dried soil samples can be setup for resonant column testing to estimate the stiffness.
- Gypsum soils in arid regions mostly contain coarse grained soil fractions, but they could also contain up to 15% fines (Alphen & Rios Romero, 1971). The presence of fines might have a marked effect on soil electrical conductivity, shear strength and collapsibility. It is therefore essential to investigate the soils including some percentage fines. These soils could be more representative of field soils. Likewise, the effect of grain size of gypsum soils on stiffness and collapsibility could be studied.
- Laboratory data should be compared with field measurements. Shear wave velocity measurements and resistivity measurements should be conducted at sites containing gypsiferous soils. The measurements may vary by orders of magnitude, especially for electrical resistivity testing. Appropriate correlations can then be made between lab and field measurements and empirical equations can be developed to estimate the geotechnical soil parameters than are known to be responsible for collapsibility.

- Computer models (2- and 3-dimensional) can be used to simulate field soil conditions and estimate collapsibility at any given site. Computer models could also be used to simulate shear wave velocities and electrical resistivity profiles. Remote sensing and GIS analysis can be used along with the available geotechnical or geophysical information to characterize sites and estimate any engineering hazard that might be associated with them.
- Geochemical methods are widely used to estimate gypsum content of soils. Gypsum content is estimated by measuring the concentration of  $\text{Ca}^{2+}$  and  $\text{SO}_4^{2-}$  ions dissolved in water and precipitating them with chemicals of known concentrations. The use of barium chloride ( $\text{BaCl}$ ) solution to detect sulfate ions is well known (Porta, 1998). These methods could be used to supplement the available geophysical data.
- Thermogravimetric methods and X-ray diffraction are also popular tools used to determine the gypsum content in soils (Porta, 1998) . These methods can be used in addition to geotechnical and geophysical tests.

**Appendix A. Using the Function Generator and Dynamic Signal Analyzer in the  
Free-Free Resonant Column testing**

**A.1 Function Generator and Amplifier**

In the Free-Free resonant column testing, a Ledex 500 rotary solenoid is used to provide torsional excitation to the specimen. The solenoid is powered by a HP 3314A function generator, which imparts a transient voltage pulse to the former (Fig. A.1). The parameters of the function generator are set to those shown in Table A.1. After setting up these parameters, pressing the manual trigger button causes a 25-ms half-sinusoidal energy pulse with a 2.0 volts peak amplitude to be generated. The output of the function generator is sent to a PYLE PRO PZR 3000 amplifier which amplifies the voltage pulse by a factor of 8 (Fig A.2). The amplified output signal can be transmitted to the solenoid through either channel 1 or channel 2. The output levels on either channels are controlled by the respective knobs, which can be rotated clockwise to increase the level.

Table A.1 Input parameters for the HP 3314A function generator (Kalinski, 1998)

<b>Parameter</b>	<b>Value</b>
Mode	N Cycle
Frequency	20 Hz
Amplitude	1.0 V
Offset	-0.52V
Symmetry	50%
Phase	90 degrees
N	1
Function (sine, square, triangle)	Sine wave
Trigger	Manual



Figure A.1. HP 3314A Function generator



Figure A.2. PYLE PRO PZR 3000 amplifier



## A.2 Dynamic Signal Analyzer and EDM software

The Coco-80 dynamic signal analyzer (Crystal Instruments) was used to measure the response of the soil specimen to the torsional excitation. The strain response of the soil specimen is detected by the accelerometers. The output from the accelerometers is passed through PCB signal conditioner before being transmitted to the signal analyzer. The response is measured in the form of time history or frequency spectra. The analyzer has eight different input channels. In order to conduct these measurements the dynamic signal analyzer must be set to the following configurations.

After switching on the signal analyzer, the start screen is displayed with the list of available projects. To conduct the free-free resonant column test we need to load the auto-power spectra (APS) analysis function for a particular input channel. This is done by pressing the setup – CSA application group – linear and power spectra. By pressing enter, the analysis function is loaded. The acquisition mode is set to free-run to enable the capturing of random or irregular signals.

Windows should be loaded to measure the time history and power spectra. This is done by clicking on the ‘Traces’ menu and clicking ‘trace and window settings’. From the menu we select ‘add window’ (Figure A.3). If the input from the accelerometers is connected to channel1, we select:

Window 1: ch1 - to measure time history

Window 2: APS (ch1) – to measure power spectra

In the ‘Param’ menu, the input parameters should be set to those shown in Table A.2.

Table A.2. Input parameters of the signal analyzer for a Free-Free resonant column test (Kalinski, 1998)

Parameter	Value
Frequency	1.8432 kHz
Block size/Line	1024/450
Window type	Uniform
Average mode	Linear
Average number	128

Once the test is started, we click ‘start’ to perform the time history measurements. Upon the completion of the test, the resonant frequency  $f_n$  is identified from the APS window (Figure A.4). Pressing the ‘save’ button twice will save the time-domain and frequency-domain records. To access the recorded time block and APS, we must press File - Enter (select) - View file (Figure A.5).

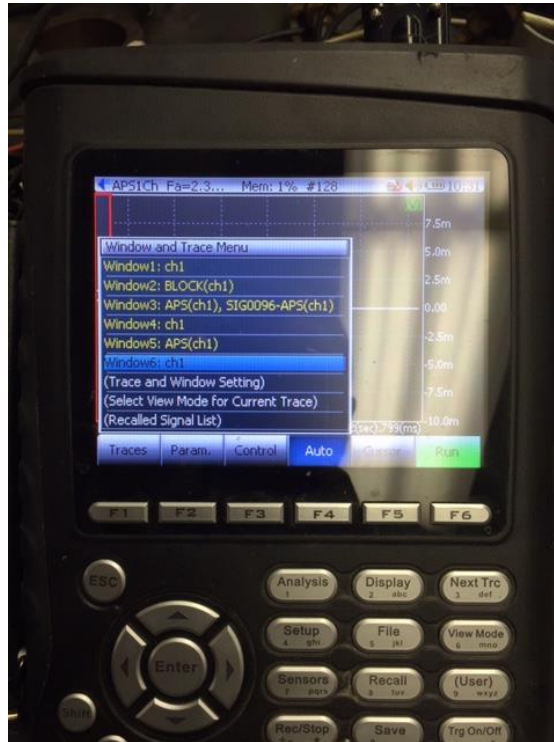


Figure A.3 Loading the time and APS trace windows

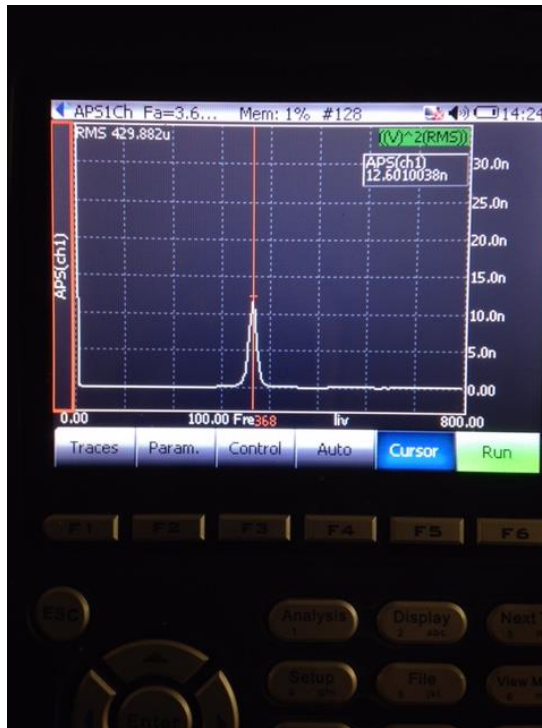


Figure A.4 APS window for measuring the resonant frequency  $f_n$



Figure A.5 viewing a saved file

The saved files can be downloaded to a computer using the engineering data management (EDM) software. The software comes with the Coco-80 signal analyzer and is loaded and activated on a computer using the License Key. Data can be transferred from Coco-80 to the computer using a USB cable, Ethernet or a wireless SD card. For this research, data was transferred to the computer using a USB cable. This mode of connection offers the advantage that the IP settings of the computer need not be adjusted to read the signal analyzer. Once the connection is established, the software detects the data files, which include time stream records, saved signals and CSA projects. Both the Coco-80 and the EDM software use ASAM ODS format for the data, which have a suffix ATFX (CI, 2008). The required files can be selected and downloaded to the computer.

The EDM software facilitates the viewing, exporting and searching of data. The data can be exported to other formats such as ASCII and UFF. It also contains tools for analyzing the data files. The time and frequency characteristics of the signals can be studied in detail using operations such as zooming and panning. Relative comparisons can be made between different signals. Additionally, important information such as peak and harmonic frequencies can be identified using cursors. Figures A.6 and A.7 show the time-stream and APS windows in the EDM software.

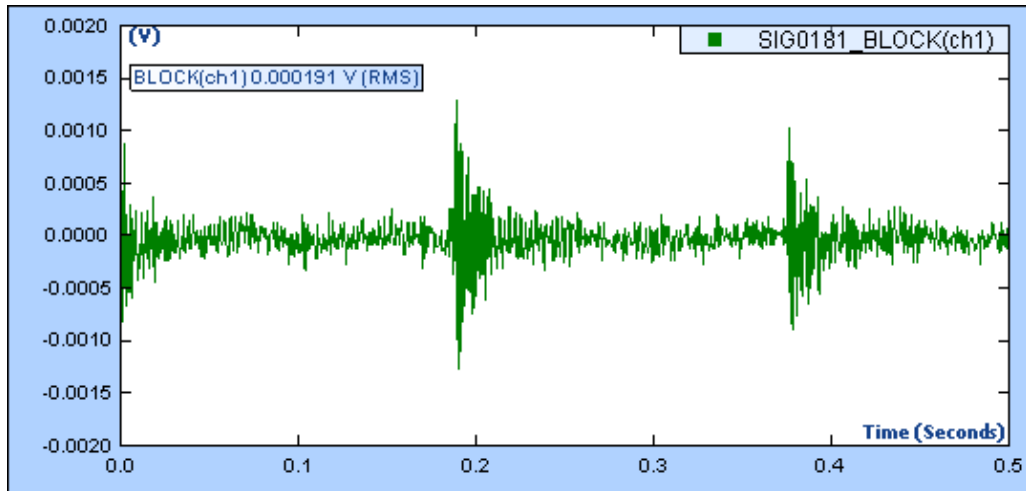


Figure A.6 Time domain window in the EDM software

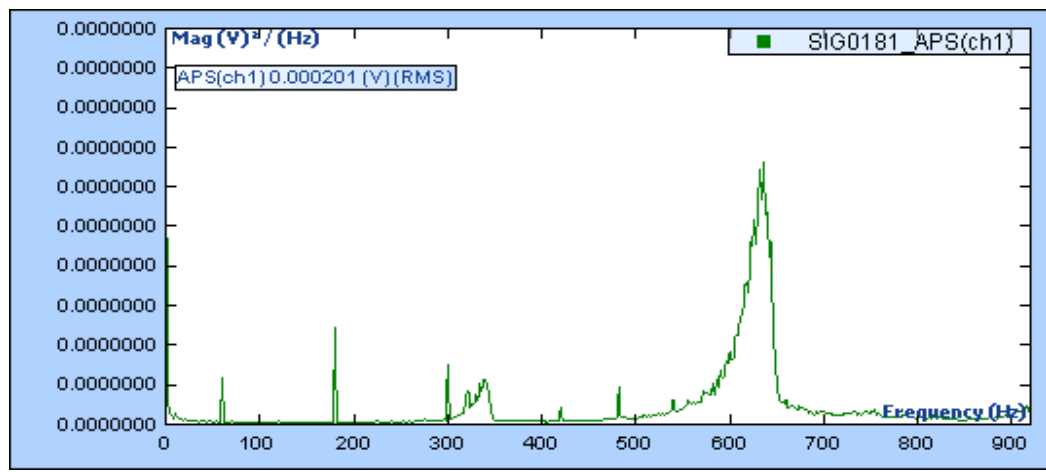


Figure A.7 APS window in the EDM software

## Appendix B. Multiple variable regression Outputs

### B.1 Shear wave velocity as a function of gypsum content, effective stress and degree of saturation

SUMMARY OUTPUT								
<i>Regression Statistics</i>								
Multiple R	0.277102883							
R Square	0.076786008							
Adjusted R Square	-0.022129777							
Standard Error	33.06626669							
Observations	32							
<i>ANOVA</i>								
	<i>df</i>	<i>SS</i>	<i>MS</i>	<i>F</i>	<i>Significance F</i>			
Regression	3	2546.291196	848.7637322	0.77627658	0.5171081			
Residual	28	30614.5838	1093.377993					
Total	31	33160.875						
	<i>Coefficients</i>	<i>Standard Error</i>	<i>t Stat</i>	<i>P-value</i>	<i>Lower 95%</i>	<i>Upper 95%</i>	<i>Lower 95.0%</i>	<i>Upper 95.0%</i>
Intercept	183.1778069	18.7714011	9.758344938	1.6471E-10	144.72633	221.6293	144.7263348	221.629279
X Variable 1	-0.30577233	0.217520772	-1.405715542	0.17080866	-0.7513434	0.139799	-0.751343432	0.13979877
X Variable 2	-0.030118363	0.111333383	-0.270524102	0.78874123	-0.2581745	0.197938	-0.258174461	0.19793773
X Variable 3	-0.241112025	0.253438538	-0.95136291	0.34956082	-0.7602573	0.278033	-0.760257336	0.27803329

In this regression the dependent variable (Y) is shear wave velocity ( $v_s$ ). The different independent variables are:

X Variable 1: gypsum content (GC)

X Variable 2: effective stress ( $\sigma'$ )

X Variable 3: degree of saturation (S%)

The regression equation is:

$$v_s = -0.305 (GC) - 0.030(\sigma') -0.241 (S\%) + 183.18 \quad (\text{B.1})$$

## B.2 Shear wave velocity as a function of gypsum content and effective stress

SUMMARY OUTPUT								
<i>Regression Statistics</i>								
Multiple R	0.878468							
R Square	0.771706							
Adjusted R Square	0.741267							
Standard Error	15.18729							
Observations	18							
<i>ANOVA</i>								
	<i>df</i>	<i>SS</i>	<i>MS</i>	<i>F</i>	<i>Significance F</i>			
Regression	2	11695.24586	5847.623	25.35238	1.54422E-05			
Residual	15	3459.807074	230.6538					
Total	17	15155.05294						
	<i>Coefficients</i>	<i>Standard Error</i>	<i>t Stat</i>	<i>P-value</i>	<i>Lower 95%</i>	<i>Upper 95%</i>	<i>Lower 95.0%</i>	<i>Upper 95.0%</i>
Intercept	140.1668	7.932859703	17.66914	1.885E-11	123.2583537	157.07533	123.258354	157.075334
X Variable 1	-0.34827	0.10994573	-3.16764	0.0063722	-0.582612107	-0.113925	-0.5826121	-0.11392455
X Variable 2	0.328087	0.04808306	6.823346	5.76E-06	0.225600721	0.430574	0.22560072	0.43057395

In this regression the dependent variable (Y) is shear wave velocity ( $v_s$ ). The different independent variables are:

X Variable 1: gypsum content (GC)

X Variable 2: effective stress ( $\sigma'$ )

The regression equation is:

$$v_s = -0.348(GC) + 0.328(\sigma') + 140.16 \quad (\text{B.2})$$

### B.3 Electrical resistivity as a function of gypsum content, volumetric water content and dry density

SUMMARY OUTPUT								
<i>Regression Statistics</i>								
Multiple R	0.86978531							
R Square	0.75652649							
Adjusted R Square	0.71594757							
Standard Error	4.8414025							
Observations	22							
<i>ANOVA</i>								
	<i>df</i>	<i>SS</i>	<i>MS</i>	<i>F</i>	<i>Significance F</i>			
Regression	3	1310.95358	436.984526	18.6433382	9.36143E-06			
Residual	18	421.905207	23.4391782					
Total	21	1732.85879						
	<i>Coefficients</i>	<i>Standard Error</i>	<i>t Stat</i>	<i>P-value</i>	<i>Lower 95%</i>	<i>Upper 95%</i>	<i>Lower 95.0%</i>	<i>Upper 95.0%</i>
Intercept	16.4965156	14.7745947	1.11654607	0.27887197	-14.543756	47.53678726	-14.543756	47.5367873
X Variable 1	0.04073945	0.06066485	0.67154951	0.51039805	-0.08671267	0.168191573	-0.086712671	0.16819157
X Variable 2	-84.162207	12.401408	-6.7865042	2.345E-06	-110.216599	-58.107816	-110.2165987	-58.107816
X Variable 3	4.60439834	10.0931458	0.45619061	0.6537091	-16.600514	25.80931071	-16.60051403	25.8093107

In this regression the dependent variable (Y) is electrical resistivity (ER). The different independent variables are:

X Variable 1: gypsum content (GC)

X Variable 2: Volumetric water content ( $\theta$ )

X Variable 3: Dry density ( $\rho$ )

The regression equation is:

$$ER = 0.041 (GC) - 84.16 (\theta) + 4.6 (\rho) + 16.49 \quad (B.3)$$



## B.4 Vertical strain as a function of gypsum content and time

SUMMARY OUTPUT								
<b>Regression Statistics</b>								
Multiple R	0.887299							
R Square	0.787299							
Adjusted R Square	0.740032							
Standard Error	0.407365							
Observations	12							
<b>ANOVA</b>								
	<i>df</i>	<i>SS</i>	<i>MS</i>	<i>F</i>	<i>Significance F</i>			
Regression	2	5.52817235	2.764086	16.656482	0.000944			
Residual	9	1.49351921	0.165947					
Total	11	7.02169156						
	<i>Coefficients</i>	<i>Standard Error</i>	<i>t Stat</i>	<i>P-value</i>	<i>Lower 95%</i>	<i>Upper 95%</i>	<i>Lower 95.0%</i>	<i>Upper 95.0%</i>
Intercept	-0.33123	0.27586197	-1.20072	0.2605066	-0.955277	0.29280962	-0.955277	0.29280962
X Variable 1	0.021913	0.00572299	3.829029	0.0040337	0.0089672	0.0348598	0.0089672	0.0348598
X Variable 2	0.000319	7.3963E-05	4.318738	0.0019367	0.0001521	0.00048674	0.0001521	0.00048674

In this regression the dependent variable (Y) is vertical strain ( $\epsilon\%$ ). The different independent variables are:

X Variable 1: gypsum content (GC)

X Variable 2: Time (t)

The regression equation is:

$$\epsilon \% = 0.022 (GC) + 0.0003 (t) - 0.33 \quad (\text{B.4})$$

## **Appendix C. Alternative laboratory geophysical methods for soil investigation**

### **C.1. Bender Element Testing (Camacho-Tauta et al., 2012)**

Bender element testing is another popularly used small-strain method to measure the shear wave velocity in laboratory soil specimens (Fig C.1). A bender element (BE) consists of two piezoelectric materials bonded together. The application of a voltage pulse causes one of the piezoelectrics to expand while the other shrinks. This process causes the element to bend in one direction depending on the polarization. The piezoelectric material is such that a mechanical disturbance causes it to produce a voltage. The bending of the element generates a shear wave that propagates through the soil specimen. The BE at the other end responds to this shear disturbance and produces a voltage. Therefore a BE couple can be used as a source and a receiver. An oscilloscope measures the time difference between these two voltage pulses ( $t$ ). Shear wave velocity is then calculated as the distance between the bender elements ( $L$ ) divided by  $t$ :

$$v_s = L / t \quad (C.1)$$

Small strain shear modulus can again be estimate using Eqn. C.1.

Bender element testing offers the advantage of easy coupling with other geotechnical test setups. It is commonly used along with triaxial tests, direct shear tests and oedometer tests. The test is easy to conduct but the interpretation of arrival time is often difficult and subjective.

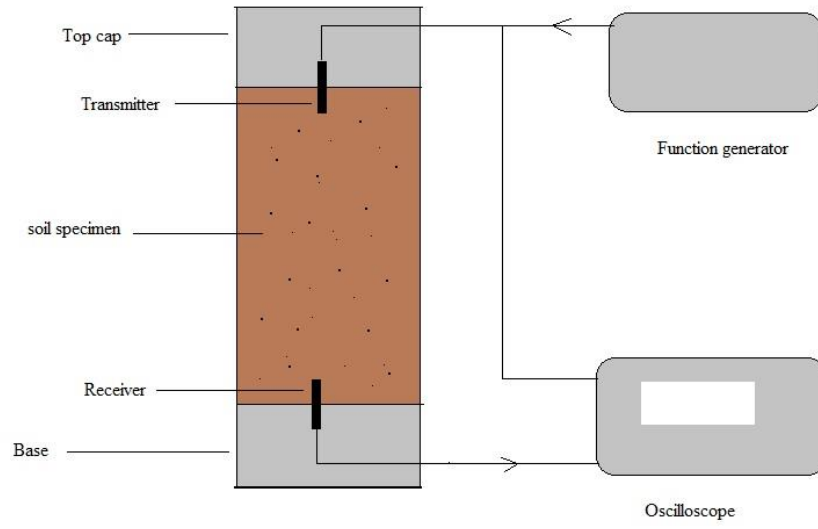


Figure C.1. Block diagram showing the setup of a BE test

## C.2. Four-probe resistivity cell (Kalinski & Kelly, 1993)

This test is an alternative to the Miller soil box method to measure the electrical resistivity of soil. While the Miller box is easy to use and does not necessitate the calculation of calibration factors between measured resistance and resistivity, it has the limitations of offering very little control on water content and pore-water resistivity. Also the Miller box allows resistivity to be measured only in one path and small scale heterogeneities cannot be accounted for. The four-probe resistivity cell (Fig. C.2) addresses these issues. Both disturbed and undisturbed soil specimens can be tested using this setup.

In this method a circular cell constructed of non-conducting material is used, kept open at both sides. It has eight electrodes spaced at equal intervals. For each measurement four adjacent electrodes are used at a time. The two outer electrodes are the current electrodes and the inner electrodes measure the potential drop. Eight such resistivity measurements are taken and the resistivity of the soil is calculated from the average value derived from the measurements. For a specimen with average measured resistance  $R$ , resistivity is calculated using the expression:

$$\rho_o = f(Rk_1 + k_2) \quad (C.2)$$

Where  $f$  is the temperature correction factor and  $k_1$  (m) and  $k_2$  (Ohm-m) are cell constants. In order to derive the cell constants, a solution of known resistivity is used and several resistance measurements are made. Relationships between measured resistance and known resistivity are derived, thus helping establish the values of cell constants. Laboratory measurements are standardized to a temperature of 20° C and thus for measurements made at this temperature, the temperature correction factor becomes unity.

The test has the advantage of being used along with a pressure membrane apparatus, which can be used to vary the moisture content in fine grained soils. A porous plate apparatus is used for the same purpose for granular soils. These features also enable the measurement of pore-water resistivity. The specimen should be held with a plastic cap or a filter paper since the cell is open from both the sides. Another major advantage of this test is that the resistivity of soil derived from averaging eight measurements gives a very representative value. However the derivation of cell constants from each cell using a standard solution is a tedious and complex process.

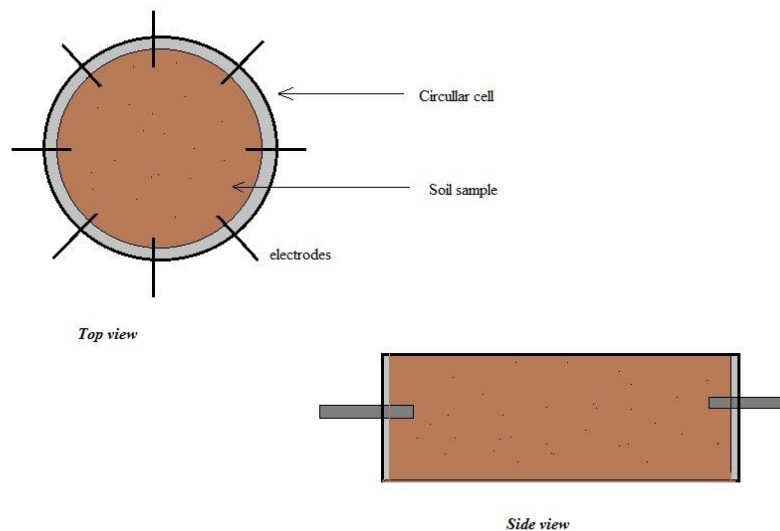


Figure C.2 Four-probe resistivity cell

## References

- Adiku, S., Renger, M., & Roth, C. (1992). A Simple Model for Extrapolating the Electrical Conductivity Data of Gypsum Containing Soils from Reference Soil Extract Data. *Agricultural Water Management*, 21, 235-246.
- Al-Amoudi, O., & Abduljawad, S. N. (1994). Modified Oedometer For Arid, Saline Soils. *Journal of Geotechnical Engineering*, 120(10), 1892-1897.
- Al-Ani, M. M., & Seleam, S. N. (1993). Effects of Initial Water Content and Soaking Pressure on the Geotechnical Properties of Gypseous Soils. *Journal of Al-Muhandis*, 116.
- Al-Marsoumi, A. M., Kadhum, M. J., & Kadhum, S. K. (2006). Geotechnical Properties of Tel-Afar Gypseous Soils. *Basrah Journal of Science*, 24, 19-31.
- Al-Marsoumi, A. M., Kadhum, M. J., & Kadhum, S. K. (2008). Some Mechanical Properties of Sandy Gypsiferous Soils in Rumaila-Khor Al-Zubair Area, Southern Iraq. *Marina Mesopotamica*, 23, 333-347.
- Alphen, J. G., & Rios Romero, F. D. (1971). *Gypsiferous Soils: Notes on Their Characteristics and Management*. Wageningen: International Institute for Land Reclamation and Improvement.
- Al-Rawas, A. A. (2000). State-of-the-Art Review of Collapsible Soils. *Science and Technology, Special Review*, 115-135.
- Al-Saoudi, N. K., Al-Khafaji, A. N., & Al-Mosawi, M. J. (2013). Challenging Problems of Gypseous Soils in Iraq. *Proceedings of the 18th International Conference on Soil Mechanics and Geotechnical Engineering*, (pp. 479-482). Paris.
- Archie, G. E. (1942). The Electrical Resistivity Log as an Aid in Determining Some Reservoir Characteristics. *Amercian Institute of Mining, Metallurgical and Petroleum Engineers*, 146, 54-62.
- Awadh, S. M., & Abdallah, H. H. (2009). Mineralogical, Geochemical and Geotechnical evaluavtion of Al-Sowera Soil for Building Bricks Industry in Iraq. *Journal of Geology and Mining Research*, 1, 118-125.
- Azam, S. (2000). Collapse and Compressibility Behavior of arid Calcereous Soil Formations. *Bulleton of Engieering Geology and the Environment*, 59, 211-217.
- Azam, S. (2003). Influence of Mineralogy on Swelling and consolidation of Soils in Eastern Saudi Arabia. *Canadian Geotechncial Journal*, 40, 964-975.
- Bell, F. G. (2007). *Engineering Geology*. Burlington: Butterworth-Heinemann.

- Bhatt, S., & Jain, P. K. (2014). Correlation Between Electrical Resistivity and Water Content of Sand- A Statistical Approach. *Amercian Internationla Journal of Research in Science, technology, Engineering & Mathematics*, 6, 115-121.
- Bolan, N. S., Syers, J. K., & Summers, M. E. (1991). Dissolution of various Sources of Gypsum in Aqueous Solutions and Soil. *Journal of the Science of Food and Agriculture*, 57, 527-541.
- Burger, H. R., Sheehan, A. F., & Jones, C. H. (2006). *Introduction to Applied Geophysics: Exploring the Shallow Subsurface*. New York: W.W. Norton & Company.
- Camacho-Tauta, J., Alvarez, J., & Reyes-Ortiz, O. (2012). A Procedure to Calibrate and Perform the Bender Element Test. *DYNA*, 79, 10-18.
- Cha, M., & Cho., G. (2007). Shear Strength Estimation of Sandy Soils Using Shear Wave Velocity. *Geotechnical Testing Journal*, 30.
- CI. (2008). *Coco-80 User Manual: Dynamic Signal Analyzer Mode*. Crystal Instruments.
- Clemence, S. P., & Finbarr, A. O. (1981). Design Considerations for Collapsible Soils. *Journal of Geotechnical Engineering*, 107, 305-317.
- Cooper, A. H., & Calow, R. C. (1998). *Avoiding Gypsum Geohazards: Guidance For Planning And Construction*. Nottingham: British Geological Society.
- Das, B. M. (2002). *Principles of Geotechncial Engineering*. Thomson Learning Inc. .
- Engler, T. W. (2012, Spring). *Chapter 2: Electrical Properties of Rocks*. Retrieved from [www.researchgate.net](http://www.researchgate.net):  
<https://www.researchgate.net/file.PostFileLoader.html?id...assetKey...>
- Fattah, M. Y., Aswad, M. F., & Majeed, Q. G. (2011). Hydro Compression and Settlement and Collapse of Gypseous Soils.
- Fattah, M. Y., Yousif, J., & Huda, N. (2008). Long-Term Deformation Of Some Gypseous Soils. *Engineering and Technology Journal, Iraq*, 26.
- Fisher, M. (2011, November). Amending Soils with Gypsum. *Crops & Soils Magazine*, pp. 4-9.
- Founie, A. (2007). *2006 Minerals Yearbook*. USGS.
- Guinea, A., Playa, E., Rivero, L., Himi, M., & Bosch, R. (2010). Geoelectrical Classification of Gypsum Rocks. *Surveys in Geophysics*, 31, 557-580.
- Gupta, S. C., & Hanks, R. J. (1972). Influence of Water on Electrical Conductivity of the Soil. *Soil Science Society of America Proceedings*, 36(2), 855-857.

- Haeri, S. M., Hamidi, A., & Tabatabaee, N. (2005). The Effect of Gypsum Cementation on the Mechanical Behavior of Gravelly Sands. *Geotechnical Testing Journal*, 28.
- Hamidi, A., & Haeri, S. M. (2008). Stiffness and Deformation Characteristics of a Cemented Gravelly Sand. *International Journal of Civil Engineering*, 6, 159-173.
- Hanchey, N. (2016, May). *The Mosul Dam's Impending Doom*. Retrieved from <https://www.theodysseyonline.com/mosul-dams-impending-doom>
- Harris, P., Scullion, T., & Sebesta, S. (2004). *Hydrated Lime Stabilization of Sulfate-Bearing Soils in Texas*. College Station: Texas Transportation Institute.
- Herrero, J., & Porta, J. (2000). The terminology and the concepts of gypsum-rich soils. *Geoderma*, 96, 47-61.
- Jennings, J. E., & Knight, K. (1975). A Guide to Construction on or with Materials Exhibiting Additional Settlement Due to Collapse of Grain Structure. *Proceedings of 6th Regional Conference on Soil Mechanics and Foundation Engineering*, (pp. 99-105). Durban, South Africa.
- Jones, C. E. (2013, April). *Gypsum and Halite: Evaporite Minerals*. Retrieved from [www.pitt.edu: http://www.pitt.edu/~cejones/GeoImages/1Minerals/2SedimentaryMineralz/Gypsum.html](http://www.pitt.edu/~cejones/GeoImages/1Minerals/2SedimentaryMineralz/Gypsum.html)
- Kalinski, M. E. (1998). *Determination of In Situ Vs and Gmax Using Surface Measurements in Cased and Uncased Boreholes*. Austin.
- Kalinski, M. E. (2006). *Soil Mechanics Lab Manual*. John Wiley and Sons, Inc.
- Kalinski, M. E., & Thummaluru, M. S. (2005). A New Free-Free Resonant Column device for Measurement of Gmax and Dmin at Higher Confining Stresses. *Geotechnical Testing Journal*, 28(2).
- Kalinski, M. E., & Vemuri, S. C. (2005). A Geophysical Approach to Construction Quality Assurance Testing of Compacted Soils Using Electrical Conductivity Measurements. *Geotechnical Special Publication No. 133*. American Society of Civil Engineers.
- Kalinski, R. J., & Kelly, W. E. (1993). Estimating Water Content of Soils from Electrical Resistivity. *Geotechnical Testing Journal*, 16(3), 323-329.
- Knight, K. (1963). The origin and Occurrence of Collapsing Soils. *Proceedings of 3rd Regional Conference of Africa on Soil Mechanics and Foundation Engineering*, 1, 127-130.
- Kramer, S. L. (1996). *Geotechnical Earthquake Engineering*. Singapore: Pearson Education.



- Little, D. S., & Nair, S. (2009). *Recommended Practice for Stabilization of Sulfate Rich Subgrade Soils*. College Station: National Cooperative Highway Research Program.
- Martin, P. (2016, April). *Fearing a flood*. Retrieved from The Globe and Mail: <http://www.theglobeandmail.com/news/mosul-dam-could-breach-any-minute-as-kill-as-many-as-15-millioniraqis/article29569107/>
- Muckel, G. B. (2004). *Understanding Soil Risks and Hazards: Using Soil Surveys to Identify Areas With Risks and hazards to Human Life and Property*. Lincoln: United States Department of Agriculture, Natural Resources Conservation Service, National Soil Survey Center.
- Mulvey, W. E. (1992). *Soil and Rock Causing Engineering Geological Problems in Utah*. Salt Lake City: Utah Geological Survey.
- Nashat, I. H. (1990). *Engineering Characteristics of Some Gypseous Soils in Iraq*. Ph.D. Thesis, College of Engineering, University of Baghdad, Department of Civil Engineering.
- Papadopolos, Z., Kolaiti, L., & Mourtzas, N. (1994). The Effect of Crystal Size on the Geotechnical Properties of Neogene Gypsum in Crete. *Quarterly Journal Engineering Geology*, 27, 267-273.
- Porta, J. (1998). Methodologies for the Analysis and Characterization of Gypsum in Soils: A Review. *Geoderma*, 87, 31-46.
- Qian, X., Gray, D. H., & Woods, R. D. (1991). Resonant Column Tests on Partially Saturated Sands. *Geotechnical Testing Journal*, 14, 266-275.
- Rhoades, J. D., Kaddah, M. T., Halvorson, A. D., & Prather, R. J. (1977). Establishing Soil Electrical Conductivity-Salinity Calibrations Using Four-Electrode Cells Containing Undisturbed Soil Cores. *Soil Science*, 123(3), 137-141.
- Rhoades, J. D., Raats, P. A., & Prather, R. J. (1976). Effects of Liquid-Phase Electrical Conductivity, Water Content, and Surface Conductivity on Bulk Soil Electrical Conductivity. *Soil Science Society of America Journal*, 40, 651-655.
- Rogers, J. D. (2007). *Impacts of the 1928 St. Francis Dam Failure on Geology, Civil Engineering and America*. Los Angeles: Association of Environmental and Engineering Geologists.
- Samouelian, A., Cousins, I., Tabbagh, A., Bruand, A., & Richard, G. (2005). Electrical Resistivity Survey in Soil Science: a Review. *Soil and Tillage research*, 83(2), 173-193.
- SCDOT. (2008). *Geotechnical Design Manual, Chapter 12: Geotechnical Earthquake Engineering*. South Carolina Department of Transportation.

- Seleam, S. N. (2006). Evaluation of Collapsibility of Gypseous Soils in Iraq. *Journal of Engineering*, 13, 712-726.
- Shahid, S. A., & Abdelfattah, M. A. (2009). Gypsum Polymorphism in the Desert Environment of Abu Dhabi Emirate. *European Journal of Scientific Research*, 29, 237-248.
- Skinner, W. J. (1959, February). Experiments on the Compressive Strength of Anhydrite. *The Engineer*, 255-259,288-292.
- Waltham, T. (2008). Sinkhole Hazard Case Histories in Karst Terrains. *Quarterly Journal of Engineering Geology and Hydrogeology*, 41, 291-300.
- Yilmaz, I. (2001). Gypsum/Anhydrite: Some Engineering Problems. *Bulletion of Engineering Geology and the Environment*, 59, 227-230.

## Vita

**Author:** Raghava Aditya Bhamidipati

**Place of birth:** Nagarjunasagar, India

### **Education:**

- **Master of Science in Civil Engineering (MSCE),** May 2012  
University of Kentucky  
Lexington, KY
- **Bachelor of Technology (B.Tech) in Civil Engineering,** May 2010  
Maulana Azad National Institute of Technology  
Bhopal, India

### **Work Experience:**

- Ph.D. candidate, Department of Civil Engineering, University of Kentucky  
Worked on the use of laboratory geophysical and geotechnical investigation methods to characterize gypsum rich soils, August 2012- August 2016
- Laboratory Instructor and Teaching Assistant in the Department of Civil Engineering, University of Kentucky, January 2013- May 2016  
Courses taught: Soil Mechanics, Land Surveying and Environmental Engineering
- Member of technical staff at Kentucky Transportation Centre (KTC) on the seatbelt survey project, May -July 2013 and May-July 2014
- Research Assistant, Department of Civil Engineering, University of Kentucky  
Worked on a USEPA sponsored project, May 2011- May 2012.

### **Awards:**

- Recipient of the 'Deans Award for Outstanding Teaching Assistant', College of Engineering, University of Kentucky, April 2016

### **Society Memberships:**

- Member of the American Society of Civil Engineers (ASCE)